NASA CR-159333

AIRCRAFT NOISE PREDICTION PROGRAM VALIDATION

Final Report

Belur N. Shivashankara

Boeing Commercial Airplane Company
Seattle, Washington

Prepared for
Langley Research Center
under contract NAS1-15526

National Aeronautics and
Space Administration

1980

NASA CR-159333

AIRCRAFT NOISE PREDICTION PROGRAM VALIDATION

Final Report

Belur N. Shivashankara

Boeing Commercial Airplane Company
Seattle, Washington

Prepared for
Langley Research Center
under contract NAS1-15526

National Aeronautics and
Space Administration

1980

CONTENTS

CONTENTS (CONCLUDED)

FIGURES

FIGURES (CONCLUDED)

AIRCRAFT NOISE PREDICTION PROGRAM VALIDATION

Belur N. Shivashankara
Boeing Commercial Airplane Company

1.0 SUMMARY

NASA has developed a modular computer program (ANOPP) for predicting aircraft flyover and sideline noise. The program prediction methodology is to predict one-third octave band spectra at the source for the various significant components of the aircraft noise. The sound pressure levels (SPL's) are propagated to the observer before conversion to subjective units such as perceived noise.

Although the prediction methods in the program are considered to be the best available to NASA at this time, a number of uncertainties remain about the accuracy of the program for predicting the noise of actual aircraft. This has led to a number of NASA contracts to evaluate ANOPP against flight noise data of the current wide-body fleet.

The purpose of the validation study was to (1) assemble a high-quality flyover noise data base for aircraft that are representative of the U.S. commercial fleet, (2) determine the accuracy of ANOPP with respect to the data base, and (3) analyze the data for source and propagation effects in order to suggest improvements to the prediction methodology.

Ten test conditions were selected from an existing data base obtained during a Boeing 747 airplane noise test. The aircraft was powered by Pratt & Whitney Aircraft JT9D engines fitted with hardwall nacelles (no acoustic treatment); only the primary plug and sleeve downstream of the turbine were lined. These test conditions covered a range of 98.8% to 75.4% of the rated engine rpm. The acoustic data were measured during 122m (400 ft) level flyovers using 12 ground plane microphones placed in line under the flightpath. The airplane was flown in a clean configuration with 20° flaps and landing gear up. The data were analyzed using a 0.1-sec integration time and an ensemble averaging technique that established accurate spectra and well-defined directivities.

The noise predictions were made for each of the selected conditions for all the major components and the total noise. The predicted spectra, SPL and PNLT directivities, and effective perceived noise levels (EPNLs) were compared with corresponding measured data.

On a total airplane noise PNLT basis, ANOPP was found to overpredict in the forward arc and underpredict in the aft arc at all power settings 90% corrected rpm and higher. The magnitude of overprediction or underprediction was about 9 dB. At lower power settings such as approach (75.4% corrected rpm), PNLT was underpredicted by about 9 dB for all angles between 80° and 160°.

For all power settings 90% corrected rpm and higher, the overprediction in the forward arc was due to the buzzsaw noise component. At lower power settings (approach), the predicted buzzsaw levels are appreciably lower and total airplane PNLT is not overpredicted in the for-

ward arc. At aft angles underpredictions are obtained at all power settings. For high power, the aft angle underprediction is due to the jet noise component. At other aft angles, for all power settings, the underpredictions may be due to several components in addition to jet noise, including fan tones, core, and turbine noise.

On an EPNL basis, the prediction was by mere coincidence within 1 EPNdB of the measured value at high power. The close agreement was due to the overprediction of PNLT in the forward arc and the underprediction in the aft arc canceling each other. At approach power, the total airplane EPNL was underpredicted by about 5 EPNdB.

Based on preliminary estimates of the noise source components, it was found that the jet, fan, core, and turbine noise modules need significant modifications to improve their prediction accuracy of flyover noise for the 747 airplane with hardwall JT9D engines.

2.0 INTRODUCTION

The importance of accurate flight noise prediction for both present and future aircraft is achieving widespread recognition within the Government and aerospace industry. This need has led to the development of individual noise component (fan, jet, etc.) prediction methods. Flight noise prediction is the ultimate goal, although static-to-flight estimates are also relevant due to the need to run ground static tests for developmental engines.

NASA has developed a modular computer program called the Aircraft Noise Prediction Program (ANOPP) for predicting flyover and sideline noise from aircraft. The program prediction methodology is to predict one-third octave band spectra at the source for the various significant components of aircraft noise and to propagate these spectra to the observer before conversion to subjective units such as perceived noise.

Although the prediction methods in the program are considered to be the best available to NASA at this time, a number of uncertainties remain about the accuracy of the predictions for actual aircraft. Many of the prediction methods, such as jet noise, are based on model data. Full-scale predictions require a range of parameters, such as Strouhal number, that extends beyond the available model-scale data base. The prediction methods are based largely on static test data. Flight effects are added as a modification to the static predictions, usually through an oversimplified theoretical model such as a moving point source. Installation effects such as modification of flow fields around the source, wing and fuselage shielding of the sources, and interactions between the sources are not presently included within the program. These factors require that a study be made of the program's ability to predict noise from full-scale aircraft in flight.

The purpose of this study was to (1) assemble a high-quality flyover noise data base for aircraft that are representative of the U.S. commercial fleet, (2) determine the accuracy of ANOPP with respect to the data base, and (3) analyze the data for source and propagation effects in order to suggest improvements to the prediction methodology.

3.0 FLIGHT TEST DESCRIPTION

3.1 GENERAL

The full-scale data base on which noise prediction methods are based or by which they are confirmed has, historically, been inadequate. This has been true especially in the flight case, because the motion of the airplane introduces several measurement and data analysis problems. Two of the most important problems are:

1. The constantly changing position of the airplane with respect to the ground-based microphone during the integration time required to get a stable noise spectrum

2. Uncertainties in the position of the airplane relative to the ground-based microphone

A flight test program designed to minimize the above problems and to obtain high-quality noise data was conducted by the Boeing Commercial Airplane Company in 1977. These tests were performed with a "clean airplane configuration," that is, with gear up and minimum flaps (20°), to reduce airframe noise. The airplane was flown over a linear array of ground plane microphones at nominally constant altitude, attitude, and power setting. A wide range of power settings was tested, from flight idle to full-power takeoff. The following sections provide a detailed description of the test site, instrumentation, data acquisition, and data reduction procedures. The test program, as far as is known, is unique and is believed to provide data of high quality to be used in assessing the flight component noise levels for high bypass ratio engines.

3.2 TEST SITE

The flight test was conducted at Bayview Airport in the state of Washington. This airport was chosen since it met several requirements for the research flight test. The ambient noise levels at this airport are quite low because of very little traffic in and out of the airport. The airport is located in relatively flat terrain, enabling the airplane to get into the level flyover mode well ahead of the first target location and stay in that mode beyond the last target (the placing of targets will be discussed in sec. 3.5.2). The runway has a paved, hard, concrete surface that is ideally suited for ground microphone installation.

Further, the runway surface itself is virtually horizontal over its entire length, a desirable feature for level flyover acoustic measurements. The final and the most important consideration was the willingness of the airport authorities to allow one of their runways (designation 3/21) to be marked with targets and instrumented with microphones over much of the runway and its vicinity. During noise recordings, the traffic at the test site was monitored to assure that no extraneous noise sources were present.

3.3 TEST AIRPLANE AND ITS ENGINES

A Boeing 747-100 airplane equipped with four Pratt & Whitney Aircraft JT9D engines was utilized. The outlines of the airplane with major dimensions marked are presented in figure 1. Three of the four engines were of the JT9D-3A type. The fourth engine was a JT9D-7CN

trimmed to the -3A takeoff power setting. The JT9D-7CN engines are JT9D-3A engines that have been uprated to JT9D-7 ratings. The JT9D-3A engines are rated at a nominal static takeoff thrust of 193.5 kN (43 500 lb). They are twin-spool turbofan engines with a bypass ratio of 5 and were fitted with short fan duct nacelles. The engines have 2 high-pressure turbine stages, 4 low-pressure turbine stages, and 3 and 11 stages in the intermediate- and high-pressure compressors. The front fan has one stage with no inlet guide vanes. Some salient details of the JT9D-3A engine are provided in figure 2.

The nominal gross weight of the airplane was 272 230 (600 000 lb) at the beginning of the test. All engines utilized hardwall inlets and ducts, with acoustic treatment only on primary plug and sleeve downstream of the turbine.

3.4 FLIGHT TEST PROCEDURE

The airplane was flown over the runway at a nominally constant altitude of 122m (400 ft) with all engines set at the same nominal power setting. The landing gear was up and the flaps were set at 20°, thereby exposing only one slot out of the three-slot flap mechanism. The pitch angle was chosen to allow level flyover at the desired airspeed.

The desired power setting, airspeed, and altitude were maintained for about 6 to 7 sec before approaching the microphone array and for a total time of about 20 sec. This assured the airplane "on condition" for directivity angles ranging from 20° to 160° (re: engine inlet axis). The microphones were placed along the centerline of the runway, and the airplane was flown such that the projection of the flightpath on the runway would coincide with the runway centerline. The flight path relative to the microphone array is shown in figure 3.

3.5 INSTRUMENTATION

Both ground-based and airborne instruments were used. The ground-based instrumentation included microphones for noise and weather instrumentation. The onboard instrumentation monitored several engine and airplane parameters. The weather was also monitored using an instrumented light airplane. Detailed description of the instrumentation is provided in the following sections.

3.5.1 ACOUSTIC INSTRUMENTATION

Twelve ground microphones were placed along the centerline of the test range runway, with a 15.24m (50 ft) spacing between microphones (fig. 3). These microphones were all 13 mm (1/2 in.) in size and were mounted on their sides on 0.61 x 0.61m (2 ft x 2 ft) aluminum plates (fig. 4).

Time synchronization for all microphones was provided by the Inter Range Instrumentation Group (IRIG) time code, and standard calibration procedures were used. The time code generator on the ground was synchronized with the airborne time code generator.

3.5.2 AIRPLANE POSITION INSTRUMENTATION

Boeing Airplane Position and Attitude Camera System (APACS) was used for determination

of the airplane position relative to the microphones at any instant in time. This system (ref. 1) uses a 35-mm motion picture camera mounted in the belly of the airplane looking downward. The camera is synchronized with the IRIG time code generator and is operated at 5 or 10 frames/sec. The camera photographs the 1.2m square (4-ft square) targets that are marked in parallel lines on the ground directly below the flightpath. Adjacent targets are carefully positioned on lines perpendicular to the desired airplane flightpath and are about 15.2m (50 ft) apart. Typical target markings are shown in figure 5.

Following a flight test, the movie films are developed and read using a film reader, such as the Benson-Lehner Telereadex type 29E film reader. The reader converts the x and y coordinates of the targets on film and film frame time into punched cards for computer entry.

To calculate the airplane position in space from the film, it is necessary to know the airplane pitch and roll angles. The airplane attitude is obtained either by a flight test gyro system or by an inertial navigation system.

The punched card information, in combination with the pitch and roll data, is used to compute the attitude and off-center distance of the airplane from the runway centerline as well as the visual overhead time with respect to a given microphone.

For the present flight test, two APACS cameras were installed in the electronic door of the test airplane. Both were operated continuously during each flyover to photograph several positioning targets painted on the runway, as shown in figure 6. The targets were referenced to the U.S. Coast and Geodetic Survey Benchmark 82, located on the pavement on the approach end of runway 3. It can be seen that the targets cover a distance of 1651m (5417 ft) along the flightpath. The 12-microphone array occupies only 183m (600 ft) in the midportion of this target range (fig. 6(b)). The spread of the target locations on either side of the microphone array is necessary to obtain airplane position information for both low and high acoustic emission angles.

The IRIG time code was used for synchronization of aircraft, engine, and noise data.

3.5.3 ONBOARD PERFORMANCE INSTRUMENTATION

Several engine operating parameters were measured online by the onboard data acquisition system. Normal performance parameters for all engines were either monitored or generated by an engine performance program. The following are some of the parameters that were available for acoustic data analysis:

1. IRIG time
2. Primary and secondary jet velocities (ideal)
3. Fan, turbine, and nozzle pressure ratios
4. Fan rotor speed and fan tip relative Mach number
5. Combustor inlet pressure and temperature

6. Combustor exit temperature

7. Primary and secondary total temperatures

8. Primary and secondary mass flow rates

For NASA ANOPP predictions, average performance parameters were calculated for each flyover and used as inputs to the program. Since the variation of performance parameters over each flyover was reasonably small, use of an averaged set of performance parameters for each flyover was considered adequate.

3.5.4 WEATHER INSTRUMENTATION

Surface Measurements:

Surface weather instrumentation consisted of the following measurements at the indicated heights:

1. Ambient temperature: 1.22m (4 ft), 9.14m (30 ft)

2. Ambient relative humidity: 1.22m (4 ft), 9.14m (30 ft)

3. Ambient wind speed and direction: 9.14m (30 ft)

Vertical Measurements:

Vertical profiles of air temperatures, relative humidity, and wind speed and direction were obtained during each test period. The temperature and relative humidity measurements were performed by Meteorological Research, Inc., who used an instrumented light airplane. Wind profiles were obtained through a ground-based BIBAL station.

The entire test was conducted within the FAA FAR 36 weather window. The ambient temperature and relative humidity on the ground were nearly constant at 12.8° C (55° F) and 55% to 60% relative humidity during all flyovers. The vertical temperature from ground to 300m (984 ft) elevation was nearly constant (±1° C) and the relative humidity varied less than 10% in 300m.

3.6 TEST CONDITIONS

Test conditions were chosen to cover a wide range of engine power settings. The test cases used for this prediction validation contract are shown in table 1. Nominal gross weight of the airplane was 272 223 kg (600 000 lb) at the beginning of the test. All flyovers were flown at a nominal altitude of 122m (400 ft) with the aircraft in a relatively clean configuration (20° flaps, landing gear retracted). Pitch angle was determined by the airplane velocity and engine rpm chosen.

TABLE 1: TEST CASES

Case number	$\%N_{1c}$	Velocity of Airplane m/s (ft/s)
1	98.8	110.6 (363)
2	98.2	86.9 (285)
3	93.7	93.9 (308)
4	89.5	98.8 (324)
5	91.0	98.8 (324)
6	91.3	92.0 (302)
7	90.7	90.8 (298)
8	84.4	91.1 (299)
9	78.7	93.6 (307)
10	75.4	92.7 (304)

4.0 ACOUSTIC DATA REDUCTION AND ANALYSIS

The acoustic data reduction and analysis procedures were carefully chosen to eliminate as many data quality problems as possible. As a matter of fact, the instrumentation and flight test procedure were dictated by the data handling procedures selected.

4.1 DATA REDUCTION

The output from all 12 ground plane microphones were recorded simultaneously on analog magnetic tapes during the flyover test. From these tapes the microphone signals were reduced to one-third octave band spectra at the Boeing Noise Technology Laboratory.

Data reduction into one-third octave bands was done one microphone at a time, starting with the first microphone in the array. For each microphone, spectra were obtained at consecutive 0.10029 sec using an integration time of 0.1 sec. The difference between the consecutive spectra time interval and this integration time–0.00029 sec–is the time required for the computer to store the spectrum and restart the one-third octave band analyzer. The beginning and end of data reduction for each microphone was selected to cover at least 15° to 165° directivity angle based on the airplane position data. The one-third octave band spectra were stored on digital magnetic tape (DMT) to be used by the ensemble averaging program discussed in the next section.

A similar procedure was used for reducing the data into narrowband spectra. The microphone signals were processed to give 0- to 10-kHz narrowband spectra with a constant bandwidth of 37.5 Hz and an integration time of 0.1 sec. One spectrum was obtained every 0.12 sec. As before, the difference of 0.02 sec represents the time required by the computer to store the data and restart the FFT analyzer. The narrowband spectra were also stored on DMT for further processing. The airplane position camera pictures of the targets were reduced to provide tables of targets and microphone locations, time at which the airplane was optically overhead each target and microphone, the airplane altitude and pitch angle at that location.

4.2 ENSEMBLE AVERAGING PROGRAM AND DATA NORMALIZATION PROCEDURE

4.2.1 ENSEMBLE AVERAGING PROGRAM

The production of a spectrum from a microphone signal requires a finite time called the sampling time or integration time. In the flyover noise measurements, the airplane position is constantly changing relative to the stationary microphone on the ground during the integration time. This leads to a loss in spatial resolution or the ability to define a spectrum of a precise angle. For level flyovers the greatest loss of spatial resolution occurs at the overhead position. In the present flyover–at a level 122m (400 ft) altitude and 91 m/s (300 ft/s) speed –this loss of spatial resolution was calculated as ±10.6° for a standard 0.5 sec integration time. This uncertainty can be reduced to ±2.1° by choosing a smaller integration time of 0.1 sec, as was done in the present analysis.

The reduction of integration time from 0.5 to 0.1 sec, however, increases the statistical uncertainty in the spectral level estimates. To overcome this problem, the ensemble averaging technique is used. This technique is discussed in detail in section 3.3.3 of reference 1.

The ensemble averaging concept is illustrated in figure 7. A straight-line array of microphones is used. The separation distance between adjacent microphones is chosen such that it is larger than the distance traveled by the airplane, in level flyover, during the chosen integration time. For example, in the present case, at 91 m/s (300 ft/s) the airplane traveled 9.1m (30 ft) during the chosen integration time of 0.1 sec. The spacing between microphones was 15.24m (50 ft). This assures that the signals measured at the microphones are statistically independent. During a level flyover a 0.1-sec integration spectrum can be obtained at each microphone for any desired emission angle by choosing appropriate delayed signals. Since all these spectra correspond to the same range and emission angle, one could determine an average spectrum using the independent spectrum from each microphone. The net result is vastly improved statistically confidence. For the present case using a 12-microphone array, the effective integration time for the average spectrum is 0.1 x 12 = 1.2 sec. Thus, by the use of level flyover and the 12-microphone array, it was possible to increase the integration time from the standard 0.5 sec to 1.2 sec while reducing the spatial uncertainty from ±10.6° to ±2.1°. In figure 8, 0.1-sec spectra from several individual microphones are plotted along with the ensemble average of all 12 microphones. It can be seen that the data scatter has been greatly reduced by the ensemble averaging technique.

The ensemble averaging of the data is accomplished using a computer program. The inputs to the program are the one-third octave band (or narrowband) spectra with a 0.1-sec integration time on digital magnetic tape as described in section 4.1. The optical overhead times for the targets and microphones are provided in a tabular form along with the corresponding airplane altitude, pitch angle, and physical location of the targets and microphones.

4.2.2 DATA NORMALIZATION

The ensemble averaging program also normalized the data to the following:

- 122m (400 ft) altitude
- Zero engine angle to the horizontal
- Atmospheric propagation effects corrected to standard day, 25° C (77° F), 70% relative humidity using ANSI procedure (ref. 2) for tones
- No correction to ground microphone data to convert it to free field

The above data normalization is done prior to ensemble averaging, that is, on the raw data. This is a necessary step in the ensemble averaging technique since it removes small deviations of airplane altitude and attitude during a given flyover from the measurements made at each microphone and brings the SPL's at all the microphones in the array to a compatible basis.

4.3 TYPICAL AIRCRAFT NOISE RESULTS

4.3.1 SPECTRA AND DIRECTIVITIES

The ensemble averaged data for operation at nominal takeoff, cutback, and approach engine power conditions are presented in figures 9 and 10. These data are normalized as described in section 4.2.2, i.e., to 122m (400 ft) level flyover, zero pitch angle, standard day atmosphere, and as measured by ground plane microphones.

The spectra (fig. 9) show relatively smooth behavior in the lower frequency region for aft angles. This is achieved by the use of ground plane microphones which eliminate the ground interference modulations from the low-frequency region. Further, the use of the ensemble averaging technique reduces random error, thus contributing to even smoother spectrum shapes.

Directivities at selected frequencies are presented in figure 10 for the same three power conditions. Once again, the data show smooth behavior.

The discussions of data trends and separation of total noise into various components is included in section 6.0.

4.3.2 REPEATABILITY

The data repeatability was good. Spectra at the angles are compared in figure 11 for two consecutive runs. The data can be seen to repeat within ±1 dB at all frequencies up to 5000 Hz. For the 160° case, there is a wide variation at frequencies above 8000 Hz. This is believed to be due to large atmospheric attenuation corrections made to high-frequency data to correct from test day to standard day conditions. At shallow angles to the horizontal, the propagation path is large and when corrections are made to change the pitch angle to zero, the propagation distance corrections become appreciable. The change in propagation distance requires two corrections to be made to the SPL. The first—spherical divergence correction—is only about 1 dB for a pitch angle correction of 3° at 160° directivity. However, the second correction—to standard day atmospheric conditions—is substantial at frequencies greater than 5000 Hz. Due to inherent limitations of the atmospheric correction procedure, very erroneous corrected SPL's are occasionally obtained for shallow radiation angles and high frequencies.

5.0 COMPARISONS OF ANOPP PREDICTIONS WITH FLYOVER DATA

5.1 GENERAL

The NASA ANOPP was run to obtain predictions for total noise and several noise components. Comparisons of predictions with 747 flyover data were made every 10° between 20° and 160° for 10 cases. The predictions and data provided in the comparisons are for ground plane microphones on an acoustically hard surface, 122m (400 ft) level overhead flyover, engines, zero pitch angle, and standard day (25° C, 70% relative humidity) weather conditions. Comparisons are provided on a spectral basis followed by directivity comparisons. Comparisons are also provided for PNLT and EPNL.

5.2 MODULES AND OPTIONS

The NASA ANOPP has some alternative source modules. Further, within each module there are several user-selected options. The modules used and the options selected within each module are provided in table 2. The selections for the options were based on their appropriateness to the particular flight test situation.

5.3 SPECTRAL COMPARISONS

5.3.1 LOW-FREQUENCY REGION (50 to 200 Hz)

The total airplane noise in the low-frequency region is underpredicted at all power settings and angles (fig. 12, 13, and 14). The magnitude of underprediction varies from 5 to 15 dB. At high powers, the far aft angle (e.g., 150°) underprediction is due to the jet noise component. It will be shown in section 6.2 that at high power, jet noise may be underpredicted at all directivity angles. At low powers, the far aft angle underprediction is again mostly due to the jet noise component. However, at other angles, it may be due to underprediction of core noise and airframe noise components.

5.3.2 MIDFREQUENCY REGION (250 to 1000 Hz)

At high power (fig. 12 and 13), the total airplane noise in the midfrequency region of the spectrum is overpredicted at all angles. The maximum overprediction—of the order of 10 dB—is found in the forward arc. At approach power (fig. 14) SPL's in this frequency region are underpredicted by about 2 to 6 dB.

Examination of the component predictions shows that fan noise is responsible for the overprediction of the midfrequency region at high powers. The fan noise subcomponent expected at these frequencies is the buzzsaw noise. In the ANOPP FAN module, INCT = 1 includes the inlet combination tones (i.e., buzzsaw) and INCT = 0 excludes it. The effect of selecting INCT = 1 and 0 upon the fan noise prediction is examined in figure 15. If INCT = 1, large overprediction is obtained. If INCT = 0, large underprediction of fan noise in the midfrequencies is seen. Thus, it is clear that buzzsaw noise prediction is responsible for the overprediction of total noise in the midfrequencies at high engine power settings. At approach power, the buzzsaw is generally not expected to be dominant and the prediction also appears

TABLE 2: MODULES AND OPTIONS

NOISE COMPONENT	MODULE	OPTIONS SELECTED
JET	JRSJET	IOPT = 6
FAN		
a) Inlet Fan Noise	FAN	IDBB = 0 IDRS = 0 IGV = 0 INBB = 1 INCT = 1 INDIS = 0 INRS = 1
b) Aft Fan Noise	FAN	IDBB = 1 IDRS = 1 IGV = 0 INBB = 0 INCT = 0 INDIS = 0 INRS = 0
CORE	GECORE	None needed in this module
TURBINE	TUR	ITOPT = 2
AIRFRAME	AFM	N = 1 ITEWN = 1 ITEHTN = 1 ITEVTN = 1 ITEFN = 1 ILESN = 0 IMGN = 0 INGN = 0 ITYPW = 1

to lower the level of this component appreciably.

The underpredictions at low power in the midfrequency region could be due to core noise prediction being too low, at least in the aft quadrant. Other components, such as airframe noise and jet noise, may also be underpredicted.

5.3.3 HIGH-FREQUENCY REGION (1000 to 10 000 Hz)

At high powers the forward arc total noise is again too high due to erroneous buzzsaw noise component predictions.

At low power (approach), the forward arc is generally underpredicted except for the fan tones. From 90° aft, the entire high-frequency region is underpredicted by up to about 10 dB.

5.4 DIRECTIVITY COMPARISONS

Measured SPL directivities are compared with ANOPP predictions for total and component noise in figures 16, 17, and 18 at the takeoff, cutback, and approach power settings. Four representative frequencies are included in these comparisons. Directivity comparisons of fan tone first and second harmonics (F_1 and F_2) are presented in figures 19 and 20. These tones do not always occur in the same one-third octave band since Doppler frequency shift is experienced due to the motion of the airplane relative to the fixed microphones. In figures 19 and 20, the one-third octave band center frequencies at which F_1 and F_2 occur are also indicated.

The directivity comparisons show that at 63 and 160 Hz (fig. 16(a), 17(a), 18(a)), the total noise is underpredicted at all three power settings. At 400 and 1000 Hz, forward arc noise is overpredicted at takeoff and cutback powers. At approach power, the total noise is generally underpredicted at these frequencies for all directivity angles.

The directivity comparisons for fan first harmonic (fig. 19) show that at high powers the first harmonic is overpredicted in the forward arc and underpredicted in the aft arc. At approach power, the first harmonic is underpredicted for all angles greater than 50°. Similar results are obtained for the fan tone second harmonic, as shown in figure 20.

5.5 PNLT AND EPNL COMPARISONS

Predicted and measured PNLT's are compared in figures 21 and 22. The predictions include total noise and various components. Figures 21(b), (f), and (j) correspond to takeoff, cutback, and approach power settings, respectively.

At takeoff and cutback powers, the total noise PNLT is overpredicted from 30° to 70° and underpredicted for all directivity angles greater than 80°. The large overprediction in the forward arc is due entirely to the erroneous buzzsaw noise prediction. At approach power setting, the total PNLT is underpredicted at most angles.

The total noise PNLT's for both data and prediction are plotted as a function of corrected

rpm at five directivity angles in figure 22. In general, the agreement is poor, in particular at angles 90° and higher where PNLT's are underpredicted. In the forward arc, overpredictions are seen at all power settings 90% corrected rpm and higher.

Total and component noise EPNL's are compared with data as a function of corrected rpm in figure 23. In this plot, the predicted and measured EPNL's are in close agreement at all power settings except for two lower power settings where predicted values are low. If taken at face value this could lead to a rather deceptive conclusion regarding the accuracy of ANOPP for predicting EPNL. The close agreement at high power is due not to the accuracy of the prediction but to large overprediction of PNLT in the forward arc and underprediction in the aft arc. When combined, the underpredicted and overpredicted PNLT's compensate and a relatively accurate EPNL prediction results.

At approach power, the total airplane EPNL is underpredicted by about 5 EPNdB.

6.0 EVALUATION OF COMPONENT PREDICTIONS

The comparisons between measured data and ANOPP predictions indicate significant errors in the prediction of total noise of the 747 airplane. Since the predicted total noise is the sum of predictions for individual components, it is necessary to separate the measured total noise into various components before determining which of the component predictions need improvement. It is beyond the scope of this project to achieve a total separation of components from the measured total noise. Component separation for a limited range of frequencies and angles is attempted in order to provide some insight regarding the accuracy of ANOPP in predicting component noise levels.

6.1 COMPONENT SEPARATION TECHNIQUE

The separation of components from the flyover data is a very complex exercise. Components that dominate at certain angles and frequencies are relatively easy to identify. However, where several components contribute to comparable noise levels, it becomes difficult to accurately isolate them. In the present flyover data, for example, the fundamental fan tone F_1 can be identified at almost all angles and power settings without much difficulty. Also, jet noise can be detected at takeoff to approach power at angles greater than 130° for the low-frequency end (50 to 80 Hz) of the spectrum. However, at frequencies greater than 80 Hz and at angles less than 130°, the levels of jet noise are not clearly identifiable and additional analysis becomes necessary.

In the aft arc, between 100° and 130° there is an indication of a reasonably strong nonjet noise source even at takeoff power. This could be core noise or possibly aft-radiated fan noise. Again, more analysis is required to resolve this issue.

Inlet fan noise is another component that shows up as a rather dominant component in the flyover data. This is because hardwall nacelles were selected for this test. The buzzsaw noise or the inlet combination tones can be seen at several angles in the 250- to 1000-Hz range although not as clearly as the fan tone F_1.

There are no clearly defined paths to achieve source isolation and component separation. There are, however, a number of techniques that will permit a reasonable estimation of component noise levels to be made. They include the following:

1. Examine the flight spectra (several angles) and directivities (several frequencies) over a range of airplane/engine operating conditions, both on a one-third octave band and narrowband basis.

2. Plot flight data into various trend curves such as:
   - SPL (f,θ) vs Log V_P for jet noise (where V_P = primary jet velocity)
   - SPL-OASPL vs Log (Strouhal number) for jet noise
   - SPL (f,θ) vs Log V_a for airframe noise (where V_a = airplane velocity)
   - SPL (f,θ) vs Log (rpm) for fan noise
   - SPL vs relative tip Mach number for fan and buzzsaw noise

3. Compare data with component predictions. In the ideal case, the prediction's directivity or spectrum shapes will be correct such that only level adjustments as a function of power setting will be needed to get a good match between the data and prediction.

4. Compare model scale test results with the full-scale data. Boeing has model scale data for the JT9D jet noise, both static and with relative velocity.

5. Examine static engine spectra and directivities. Boeing has conducted static tests with the JT9D engine, acquiring data on several sidelines for a wide range of power conditions.

6. Study measured static source locations for the engine. For example, jet noise sources will be located downstream of nozzle exit stations. Source locations may be determined by the Boeing-developed multiple sideline technique (ref. 3) or microphone correlation techniques.

7. Determine static-to-flight effects. Comparison of flight data with extrapolated static data will provide clues regarding the nature of the source.

8. Use correlation techniques including internal-to-far-field cross-correlation and coherence function analysis (ref. 4, 5, and 6) and far-field correlations as suggested in reference 7.

The component separation effort for this study was limited to three power conditions representative of takeoff, cutback, and approach. Techniques 1 through 7 were used to varying degrees, with emphasis on the first three techniques.

In the following sections, the component separation and comparisons with ANOPP are discussed on a component-by-component basis.

6.2 JET NOISE COMPONENT

Typical comparisons between JT9D model jet noise spectra and the 747 flyover data are presented in figure 24. The model data were measured in a wind tunnel and have been scaled and extrapolated to the full-scale conditions. Good agreement is seen at 140° and 150° in the low- to intermediate-frequency region of the spectrum where jet noise is expected to dominate. At 120°, the model jet noise levels are lower than the total airplane levels indicating that sources other than jet noise either contribute to or dominate the airplane noise. It should be noted that the close agreement between wind tunnel model and full-scale flight data at 140° and 150° may have been somewhat fortuitous. The comparisons do, however, show that the spectral and directivity shapes obtained for model scale jet noise can be applied to full-scale flyover jet noise prediction. Carefully conducted model scale tests also provide static-to-flight effects and scaling laws for jet noise.

In figure 25, the difference between the SPL and OASPL (50 to 1000 Hz) is plotted as a function of a Strouhal number based on relative velocity. The relative velocity, in this figure, is the difference between the primary jet velocity and the airplane velocity. Under ideal conditions, all jet-noise-dominated portions of the spectra would collapse onto a single curve

since jet noise scales with Strouhal number. In figure 25, at 120° and 150°, the 98.2% N_{1C} (takeoff) and 91.3% (cutback) spectra appear to be reasonably close to each other at the low-frequency end. The 75.4% N_{1C}(approach) case, by this analysis, appears to be dominated by sources other than jet noise, even at the low-frequency end. This type of analysis was used by Blankenship, et al. (ref. 8) to separate the jet noise components from flyover data. Detailed analysis of this type appears to be useful in separating the jet noise component.

Another method is to examine the trend of data with selected airplane/engine parameters. In figure 26, OASPL (50 to 1000 Hz) is plotted as a function of primary jet velocity. Most probable jet-noise-dominated regions are indicated on the figure. SPL's at two frequencies are plotted as a function of log (V_P) in figure 27 for several directivity angles. Again, regions of probable jet noise domination are noted on the figure.

Using analysis techniques such as those illustrated in the previous paragraphs, levels of jet noise were deduced for the takeoff power condition. In figure 28, derived jet noise component SPL directivities are plotted along with the ANOPP predictions. The difference between the derived and predicted jet noise levels are also indicated in the figure.

The frequencies were limited to those identified as being clearly dominated by jet noise at aft arc angles. It is noted that judgments regarding ANOPP prediction accuracy will be more valid in the aft arc region (120° and above). At lower angles the flight jet noise levels are estimates and may change somewhat as more detailed analysis is accomplished.

In summary, the ANOPP prediction for jet noise is relatively inaccurate. The level is underpredicted at all angles and power settings (2 to 15 dB). The predicted SPL directivity shape is roughly similar to that of the derived jet.

6.3 FAN NOISE COMPONENT

6.3.1 FAN TONES

The SPL's at the blade passage frequency (F_1) and its second harmonic (F_2) are compared at three power conditions in figures 19 and 20. These figures indicate that neither the levels nor the directivity shapes are predicted correctly by ANOPP for the fan tone first harmonic. At certain power conditions and directivity angles, the turbine fundamental tone (T_1) also resides in the same one-third octave band as F_2. Based on the present analysis, separation of T_1 and F_2 does not appear to be possible. Source location studies using static full-scale test data may provide a way to separate these two components.

6.3.2 BUZZSAW AND FAN BROADBAND NOISE

The flight data shows regions where buzzsaw noise is dominant at higher power settings such as takeoff and cutback. To recognize this component, various frequencies were plotted against fan tip relative Mach number for several directivity angles, as shown in figure 29. A rather steep increase in noise level as the relative tip Mach number approaches 1.0 from the subsonic region is an indication of the "cut-on" of buzzsaw noise. In figure 29, this can clearly be seen at 630 and 1000 Hz.

In figures 30(a) and (b), data at takeoff power is compared with fan noise prediction at several frequencies typical of buzzsaw and broadband fan noise. An overprediction of 10 to 15 dB is seen in the forward arc. In the aft arc, the predictions agree reasonably with data at most frequencies. At cutback power similar results are obtained (figs. 30(c) and (d)). The overprediction in the forward arc has been shown in section 5.3 to be due to the buzzsaw noise component prediction. For broadband noise at approach power (figs. 30(e) and (f)), underpredictions of up to 10 to 20 dB are evident. However, at this power, the total noise at these frequencies may include significant noise from components other than fan. In summary, fan noise prediction appears to be generally inaccurate for tones, buzzsaw, and broadband fan noise subcomponents.

6.4 CORE NOISE COMPONENTS

The spectral comparisons at takeoff power (fig. 12) show a potentially significant contribution of nonjet noise components in the vicinity of 250 to 400 Hz at all angles between 60° and 120°. The directivity plots (fig. 16) show maxima at 60° and 100° for 400 Hz. Near-field sideline data for the complementary static test showed a very flat directivity at these frequencies, indicating widely separated sources of comparable strength. The preliminary assessment is that the spectrum in the vicinity of 250 to 400 Hz is dominated by inlet-radiated fan noise in the forward arc, which perhaps peaks around 60°. The aft arc is dominated by core noise at these frequencies, with a peak most probably between 110° to 130°.

At cutback power, the spectra of figures 13 and 17 show a similar result. At this power setting the levels of inlet fan noise in the forward arc are more pronounced than those for the takeoff case. Again, indications are that core noise dominates in the aft arc, peaking around 120° and in the frequency region near 250 to 400 Hz.

At approach power, spectra in figure 14 indicate a dominant component centered around 250 Hz. In figure 18, it is seen that 250 Hz peaks at 110°. Also, figure 18 shows that 400-Hz directivity has two maxima, one at 40° and the other at 120°. Again, this leads to the expectation of the prominence of fan noise in the forward arc and core noise in the aft arc.

The flyover data and core noise prediction at several frequencies are plotted against log V_p in figure 31. At 70°, 90°, and 120°, the data for the 250- and 315-Hz cases is close to that predicted for the core noise. This along with the observations made so far indicate possible core noise dominance in the 250- to 315-Hz and 90° to 120° regions at all power settings including takeoff power. Having recognized this, the effect of moving the entire predicted core noise spectrum to peak at a frequency one-third octave band lower and increasing its level by about 3 dB was examined using data shown in figure 12. This modification to the core noise prediction provided better data-to-prediction comparisons in the core-noise-dominated region.

6.5 TURBINE NOISE COMPONENT

The spectral comparisons at takeoff power shown in figure 12 indicate that at 150° through 120° the turbine tone can be easily recognized in the data. The turbine tone levels at takeoff power are underpredicted by 15 to 20 dB at 150° and by 10 to 12 dB at 120°. At cutback power at 150° (fig. 13), it is not straightforward to draw definite conclusions regarding the turbine tone since it happens to occur at the same one-third octave band (4000 Hz) as the fan

tone F_2. However, the measured level at 4000 Hz is about 5 dB greater than that for the fan fundamental blade passage frequency. The 4000 Hz may, therefore, be dominated by the turbine tone. If it is, then the prediction for turbine tone at 150° is low by about 20 dB. At other angles the separation of the turbine tone needs further analysis. At approach power, from figure 14, similar conclusions are reached at 150°. At 120° the turbine tone noise prediction may be about 5 to 7 dB lower than 747/JT9D flyover values.

The broadband turbine noise levels appear to be far below the total measured noise and, as such, no levels can be derived from data for this component. The predicted turbine tone level at aft arc angles is substantially lower than measured levels. Additive corrections are needed to improve the match between 747/JT9D flyover data and the ANOPP prediction.

6.6 AIRFRAME NOISE COMPONENT

For all test conditions reflected in this report, the airplane velocity (V_a) varied from 86.9 to 110.6 m/s (285 to 363 ft/s). Although this may appear to be a reasonable range of V_a variation to study airframe noise, the situation is not straightforward. This is because, as seen in table 1, the engine power settings were also varying simultaneously so observed SPL changes may be due to changes in either or both engine noise and airframe.

Four low-frequency SPL's are plotted as a function of primary jet velocity in figure 32. In this case primary jet velocity is used only as a parameter indicative of engine power setting. At 70° and 90°, the low-power data vary little with jet velocity (or engine power setting). Therefore, airframe noise may be important at low frequencies in the forward quadrant at or near approach power settings.

The SPL's are plotted as a function of airplane velocity in figure 33. In this figure, the prediction of ANOPP for airframe noise is shown. If the SPL is mainly due to airframe noise, then good collapse of data should be obtained when plotted as a function of airplane velocity. No such collapse is obvious in figure 33 and, therefore, no inferences can be drawn regarding the validity of the NASA ANOPP airframe noise predictions.

7.0 CONCLUDING REMARKS

NASA aircraft noise prediction program, ANOPP, was run to obtain predictions for 747 airplane total noise and the jet, core, turbine, fan, and airframe noise components. Program inputs corresponded to flyover noise test conditions of a Boeing 747 airplane fitted with four Pratt & Whitney Aircraft JT9D turbofan engines. The predictions were compared with measured noise data in several ways, including:

- One-third octave band spectra at 30°, 60°, 90°, 120°, and 150°
- Directivities at several frequencies
- Directivities for fan tone first and second harmonics
- Tone-corrected perceived noise level (PNLT) as a function of directivity angle
- Effective perceived noise level (EPNL) as a function of engine power setting

On a total airplane noise PNLT basis, ANOPP was found to overpredict in the forward arc and underpredict in the aft arc at all power settings 90% corrected rpm and higher. The magnitude of overprediction or underprediction was about 9 dB. At lower power settings such as approach (75.4% corrected rpm), PNLT was underpredicted by about 9 dB for all angles between 80° and 160°.

On an EPNL basis, the prediction was by mere coincidence within 1 EPNdB of the measured value at high power. The close EPNL agreement is the result of overpredictions of PNLT in the forward arc and underpredictions in the aft arc canceling each other. At approach power, the total airplane EPNL was underpredicted by about 5 EPNdB.

To enable identification of the source modules that need correction and the magnitude of the correction method, an attempt was made to separate the measured noise into various components predicted by ANOPP. The scope of the contract precluded a detailed investigation in this regard. In the beginning of the contract work it was hoped that the directivity shape and spectrum shape predicted by ANOPP would be generally correct. Under that circumstance, the flight component levels could be more easily identified. Improved predictions could be achieved by applying appropriate corrections to the current predictions such as ΔdB versus angle or ΔdB versus frequency.

For jet and fan noise, at least, neither the predicted spectrum shape nor the directivity shape was correct and, therefore, component separation proved to be very complicated. Based on preliminary estimate of the components, the following conclusions are drawn on the validity of the NASA ANOPP program:

1. The jet noise is underpredicted by a 3 to 7 dB in the aft arc (e.g., 150°) at the low-frequency end of the spectrum where it can be clearly identified in the data. The prediction of jet noise in the forward arc also appears too low although accurate separation of jet noise in this region is difficult.

2. The fan tones are overpredicted in the forward arc and underpredicted in the aft arc at takeoff and cutback power and underpredicted at most angles at approach power. The predicted directivity has two peaks, one in the aft arc and one in the forward arc whereas the data shows a prominent peak around 90°. At 90° underpredictions are of the order of 5 to 10 dB. The buzzsaw and broadband fan noise is overpredicted by 10 to 15 dB in the forward arc.

3. The core noise prediction will fit flyover data better for angles between 90° and 120° if about 3 dB is added to its power level and the entire spectrum is shifted to one-third octave band lower frequency at all power settings.

4. The turbine tone appears to be underpredicted in the far aft arc where it can be distinguished. Under several conditions, the turbine tone lies within the same one-third octave band as the fan tone second harmonic, making it difficult to separate the two components. The broadband turbine noise could not be distinguished in the data.

5. No comments are made on the airframe noise prediction since it was not possible to clearly distinguish this component.

To better assess the modifications required to improve the ANOPP prediction, accurate separation of components is essential. A detailed examination would be required of all available static and wind tunnel model data as well as static engine and flight test data. The study would include definition of model and engine source locations and static-to-flight effects. This should aid in the identification of jet and nonjet noise components at certain angles and frequencies. Correlation and coherence techniques may also prove useful. Combining various techniques will make it possible to separate components accurately. Once components are separated and evaluated from various data bases, prediction procedures can be improved.

APPENDIX

Spectral comparisons of data and ANOPP predictions at seven test conditions are provided in the appendix. These comparisons are in addition to those shown in figures 12, 13, and 14 corresponding to takeoff, cutback, and approach power settings. The engine power setting for each condition is identified on the figures. The modules and options used for ANOPP predictions are provided in table 2. For each condition, comparisons are shown at directivity angles of 30°, 60°, 90°, 120°, and 150°. The SPL's in these figures correspond to:

- 122m (400 ft) altitude
- Zero engine angle to the horizontal
- Standard atmosphere (25° C, 70% relative humidity)
- Ground plane microphones
- Four engines

REFERENCES

1.. Chun, K. S., Berman, C. B., and Cowan, S. J., "Effects of Motion on Jet Exhaust Noise From Aircraft." NASA CR-2701, 1976.

2. American National Standard Method for the Calculation of the Absorption of Sound by the Atmosphere. ANSI, S1.26, 1978.

3. Jaeck, C. L., "Static and Wind Tunnel Near Field/Far Field Jet Noise Measurements From Model Scale Single-Flow Baseline and Suppressor Nozzles--Summary Report," NASA CR-2841, 1977.

4. Shivashankara, B. N., "Gas Turbine Engine Core Noise Source Isolation by Internal-to-Far Field Correlations," *Journal of Aircraft*, vol. 15, No. 9, September 1978, pp. 597-600.

5. Karchmer, A., and Reshotko, M., "Core Noise Source Diagnostics on a Turbofan Engine Using Correlation and Coherence Techniques," NASA TMX-73535, 1976.

6. Wang, Hun En, "The Application of Coherence Function Techniques for Noise Source Identification," Ph.D. thesis, Purdue University, 1978.

7. Parthasarathy, S. P., Cuffel, R. F., and Massier, P. F., "Separation of Core Noise and Jet Noise," AIAA paper 79-0589, March 1979.

8. Blankenship, G. L.. Low, J. K. C., Watkins, J. A., and Merriman, J. E., "Effect of Forward Motion on Engine Noise," NASA CR-134954, 1977.

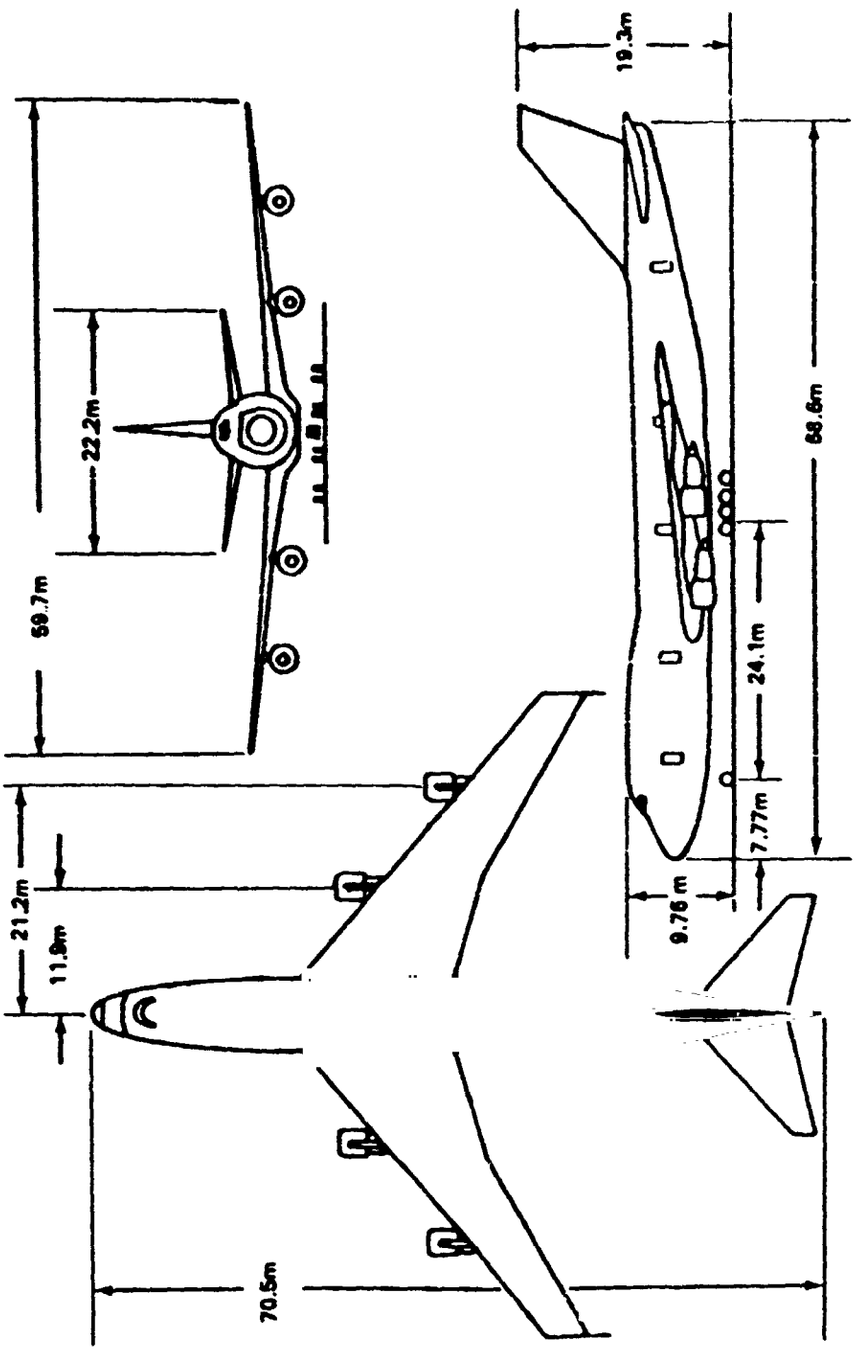

Figure 1.--Schematic Diagram of the Test Airplane--Boeing 747-100

TYPE	Turbofan, 2-shaft, bypass ratio 5.0.
INTAKE AND FRONT FAN	No inlet guide vanes, 1-stage fan, pressure ratio 1.51:1, and airflow 678 kg (1495 lb)/sec, at 3330 rpm.
COMPRESSOR (INTERMEDIATE)	3 rows of blades driven by low pressure turbine at 3330 rpm.
COMPRESSOR (HIGH-PRESSURE)	Variable inlet vanes, 3 rows of variable stator blades, 8 rows of fixed blades driven by high pressure turbine at 7415 rpm. Overall pressure ratio 22:1. Air mass flow 113 kg (250 lb)/sec at 7415 rpm.
COMBUSTOR	Annular. 20 fuel nozzles.
TURBINE	6 stages, 2 high pressure (7415 rpm) and 4 low pressure (3330 rpm).
RATING	193.5 kN (43,500 lbf)/7415 h.p. turbine rpm/static, dry.

Ref: Aircraft Engines of the World, Paul H. Wilkinson, Published by Paul H. Wilkinson, Washington, D.C. 20014

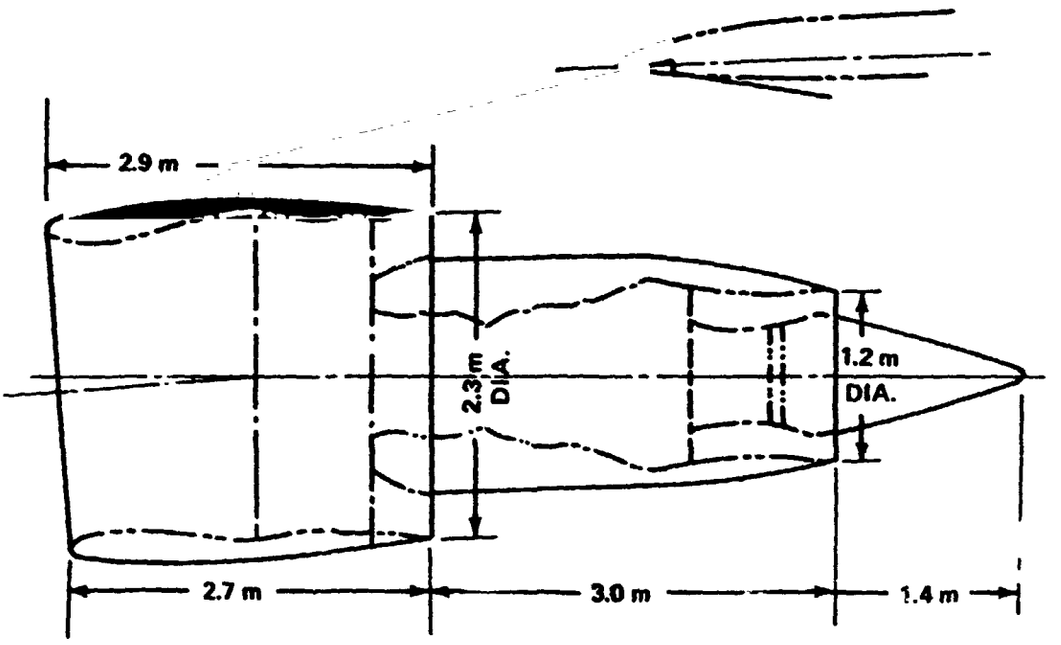

Figure 2.–Specifications of the Pratt & Whitney Aircraft JT9D Engine and the 747 Nacelle Schematic

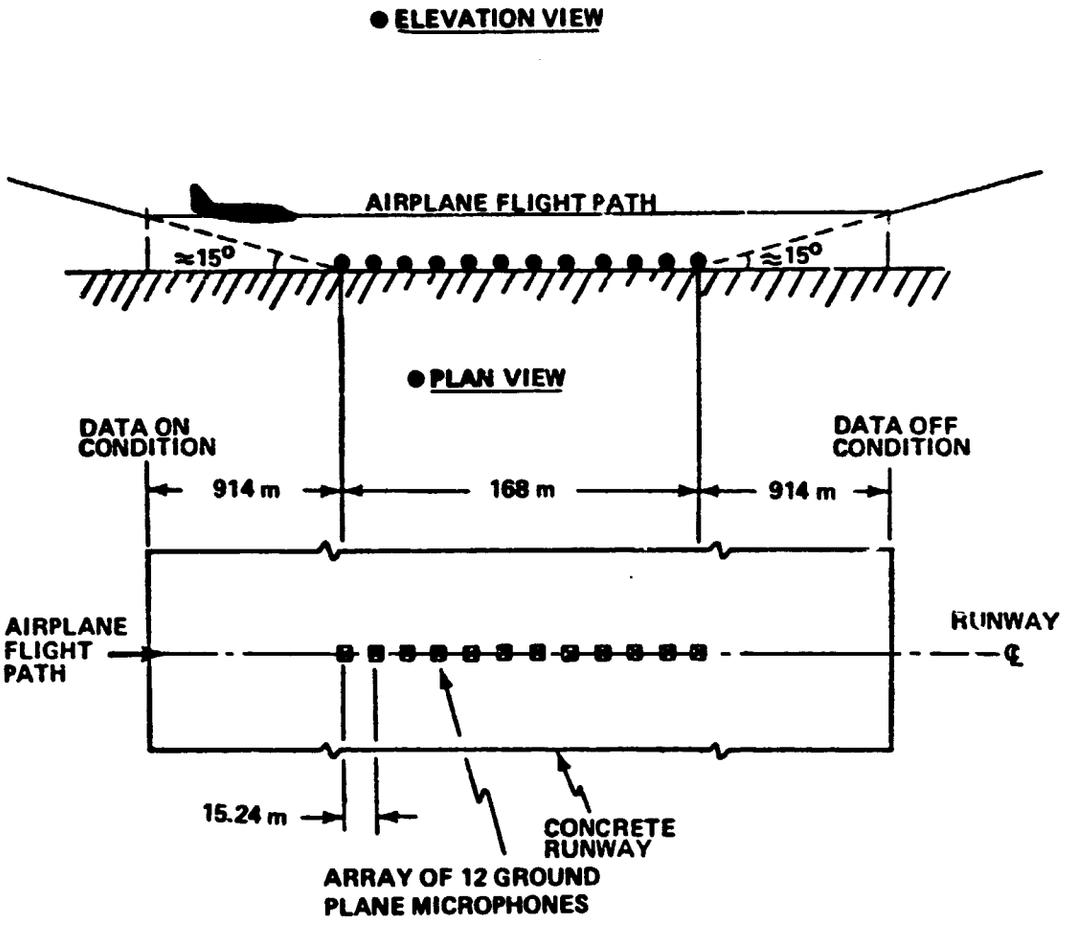

Figure 3.—General Layout of the Test Site

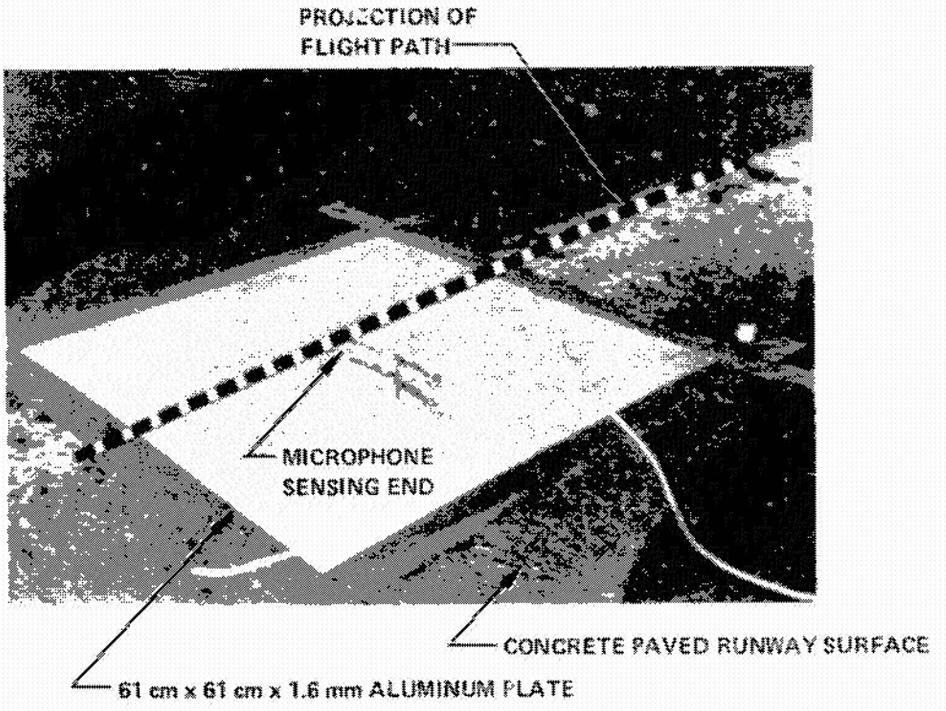

Figure 4.—Closeup View of the Ground Microphone Installation

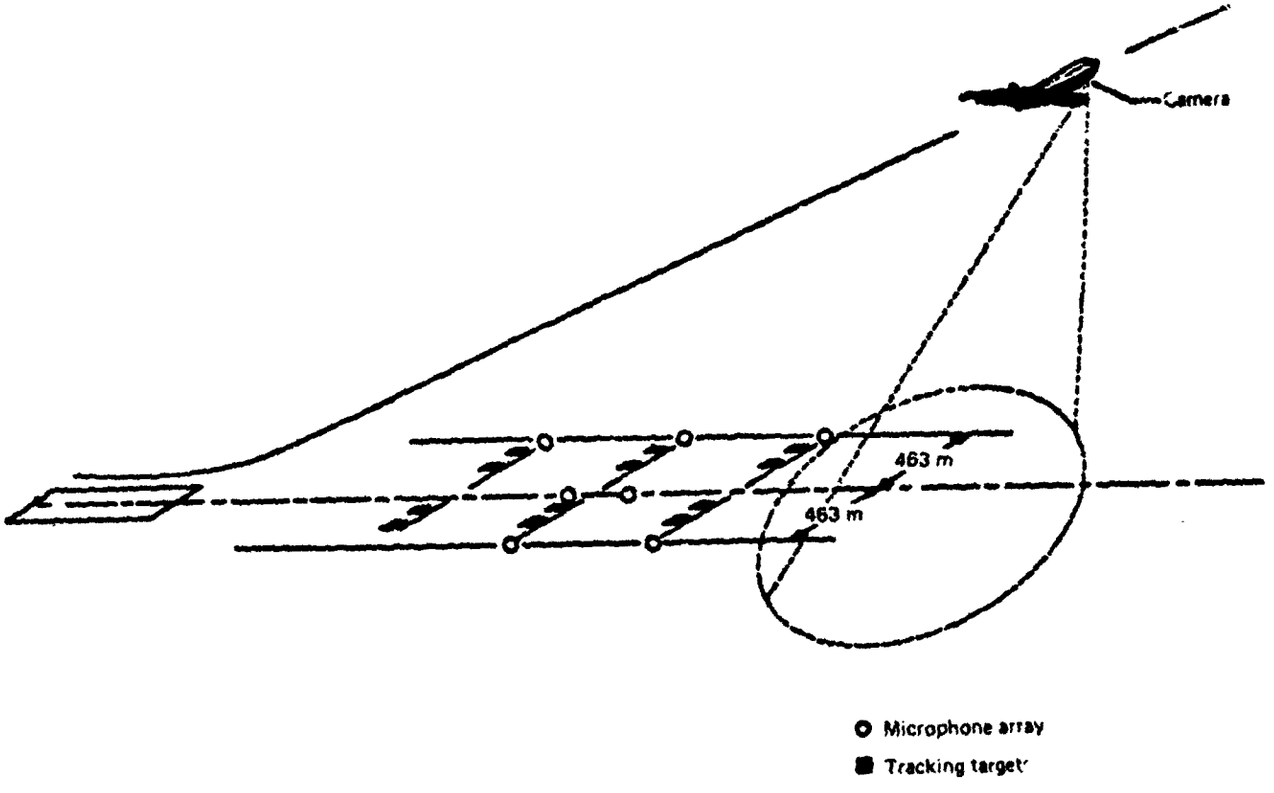

Figure 5.—Typical Markings for Boeing Airplane Position and Attitude Camera System (APACS)

Target Number	Station	Offset + So.	Elevation
0101	-500.00	-40.00	80.59
0102	-500.00	0.00	79.47
0103	-500.00	40.00	77.94
0201	400.00	-40.00	81.19
0202	400.00	0.00	80.79
0203	400.00	40.00	80.39
0301	1100.00	-40.00	79.40
0302	1100.00	0.00	79.00
0303	1100.00	40.00	78.60
0401	1800.00	-40.00	80.30
0402	1800.00	0.00	79.80
0403	1800.00	40.00	79.50
0501	2225.00	-40.00	81.40
0502	2225.00	0.00	80.93
0503	2225.00	40.00	80.55
0504	2225.00	80.00	80.08
0505	2225.00	120.00	79.70
0601	2600.00	-40.00	82.41
0602	2600.00	0.00	81.93
0603	2600.00	40.00	81.60
0604	2600.00	80.00	81.05
0605	2600.00	120.00	80.65
0701	3300.00	-40.00	85.29
0702	3300.00	0.00	84.81
0703	3300.00	40.00	84.41
0801	4000.00	-40.00	89.62
0802	4000.00	0.00	89.22
0803	4000.00	40.00	88.82
0901	4917.78	-40.00	93.84
0902	4917.78	0.00	92.81
0903	4917.78	40.00	92.68

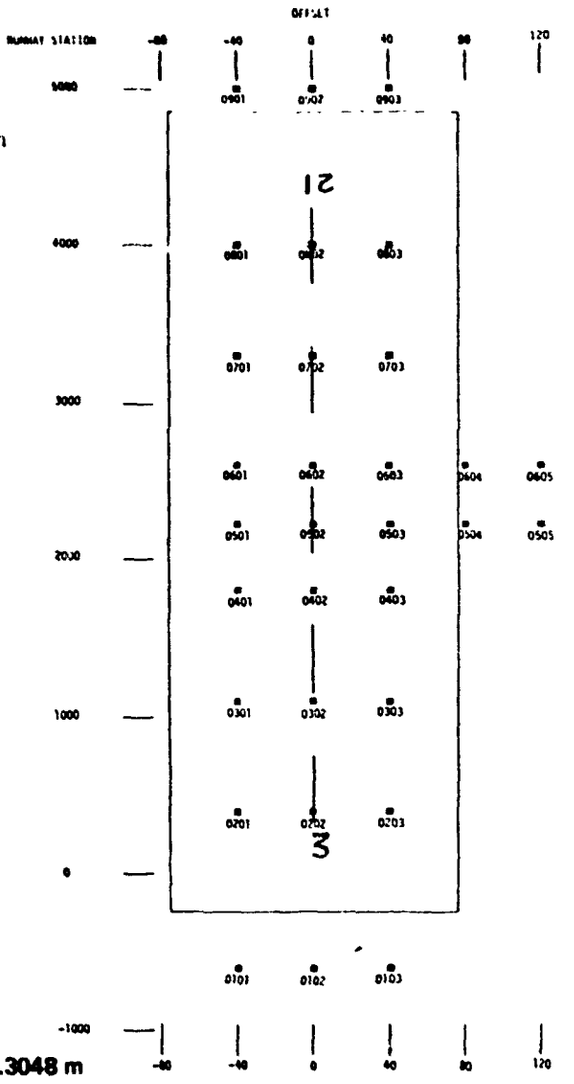

Dimensions for Station, Offset and Elevation are in 0.3048 m

(a) TARGET LAYOUT

Figure 6.—Target Markings for APACS and Details of Microphone Layout at Bayview Airport

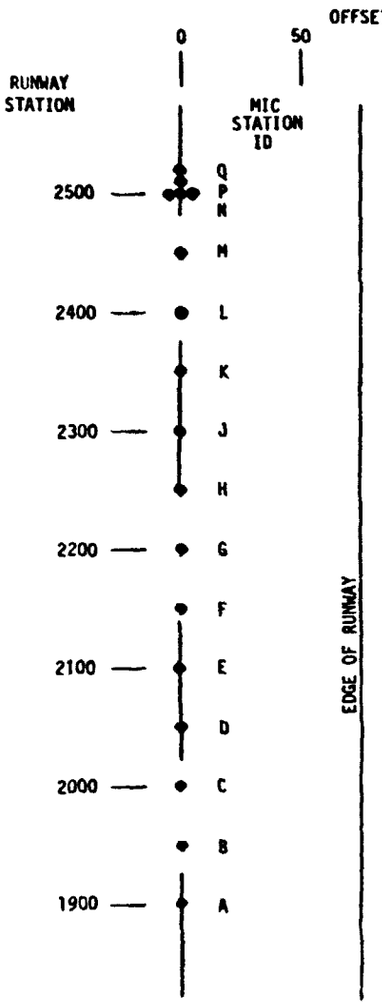

Microphone Station I.D.	Station	Elevation on Runway Centerline
A	1900.00	80.00
B	1950.00	80.10
C	2000.00	80.30
D	2050.00	80.40
E	2100.00	80.55
F	2150.00	80.75
G	2200.00	80.85
H	2250.00	80.99
J	2300.00	81.12
K	2350.00	81.23
L	2400.00	81.38
M	2450.00	81.53
N	2500.00	81.67
P	2510.00	81.71
Q	2520.00	81.73

Dimensions for Station and Elevation are in 0.3048 m

(b) MICROPHONE POSITIONS

Figure 6.—(Concluded)

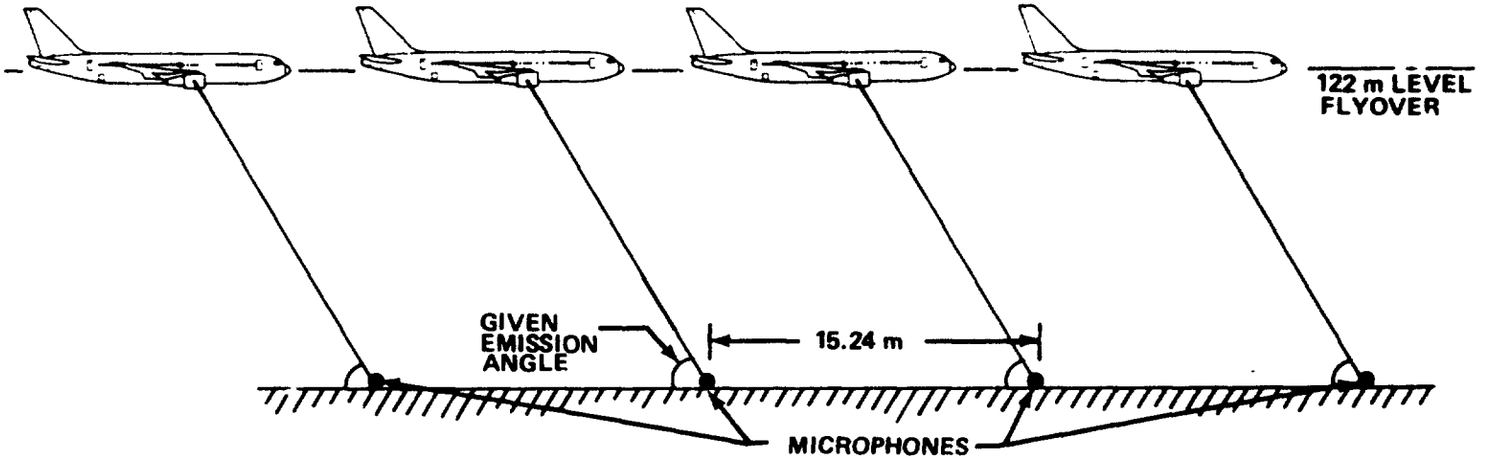

Figure 7.—Concept of the Ensemble Averaging Technique

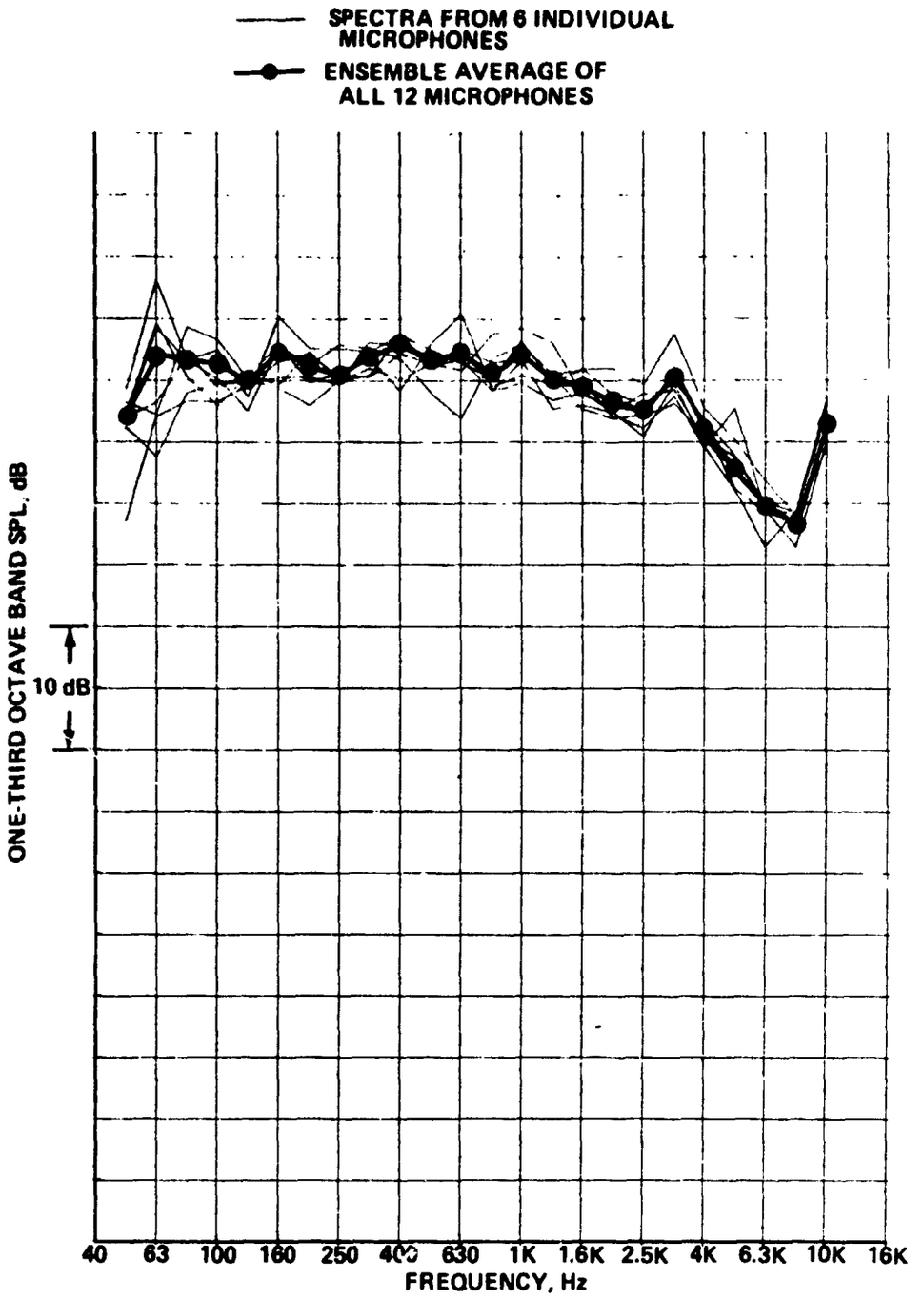

Figure 8.—Comparison Between Individual Microphone Spectra and the Ensemble Averaged Spectrum

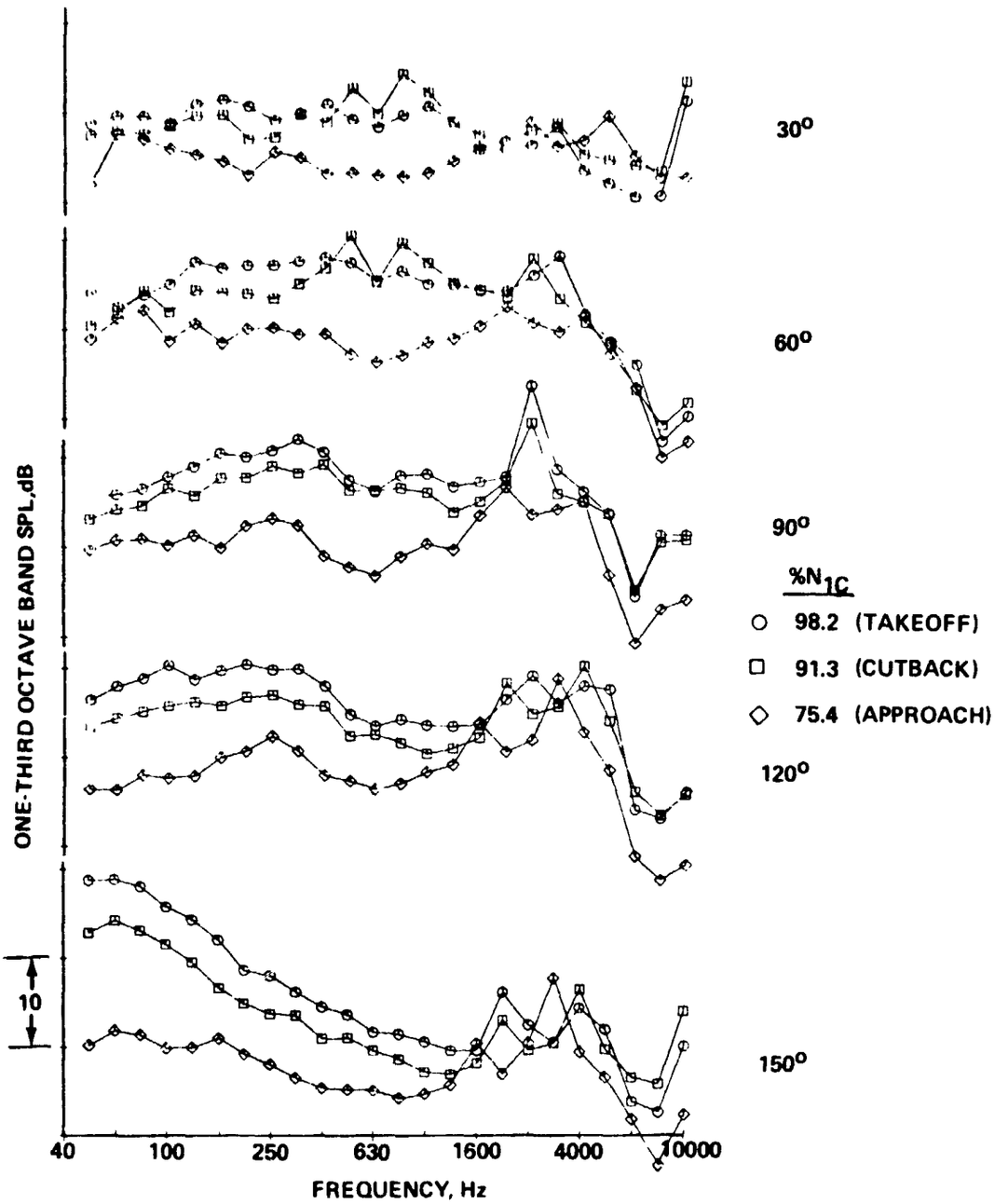

Figure 9.–Typical Flyover Noise Spectra at Several Angles for Takeoff, Cutback, and Approach Conditions

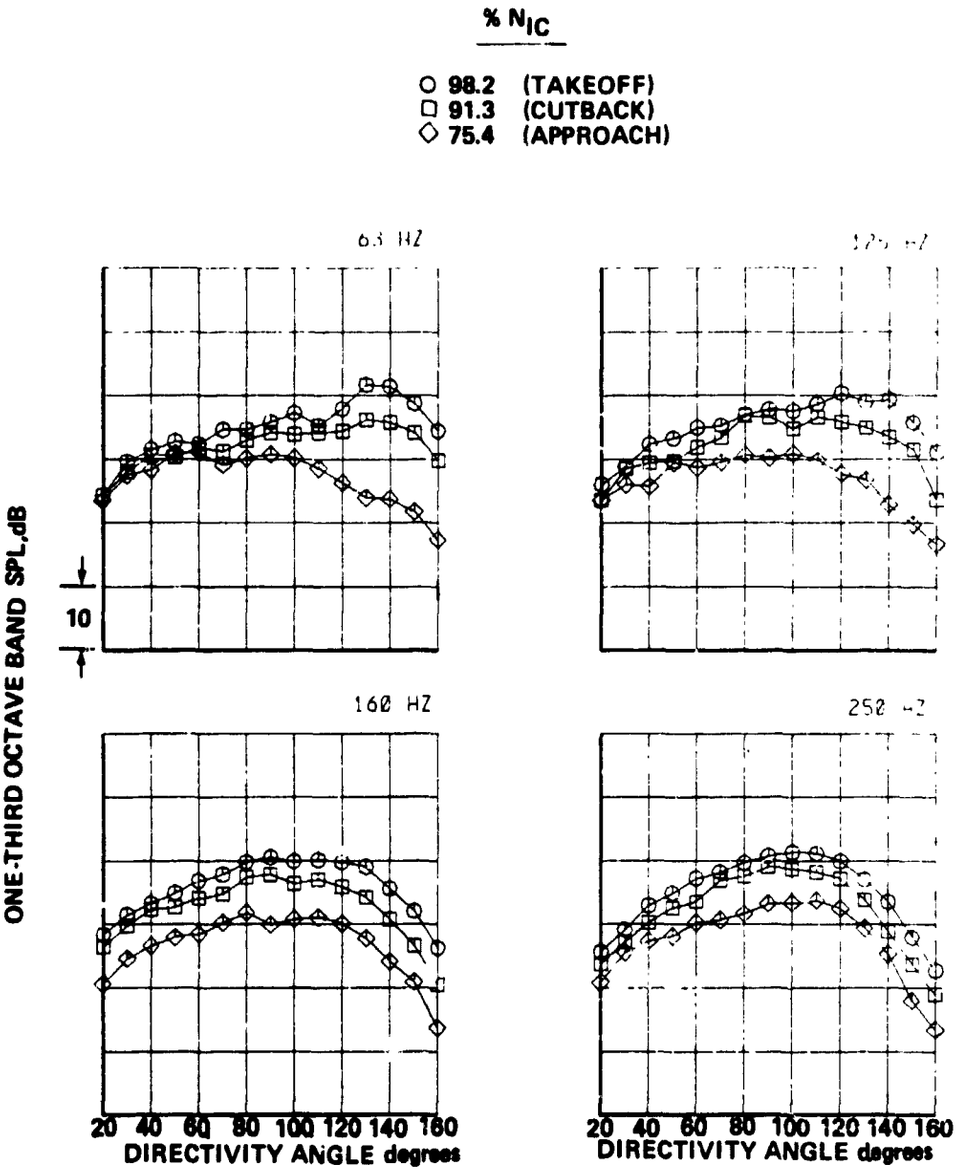

(a) FREQUENCY 63 TO 250 Hz

Figure 10.–Typical Flyover Noise Directivities at Various Frequencies for Takeoff, Cutback, and Approach Conditions

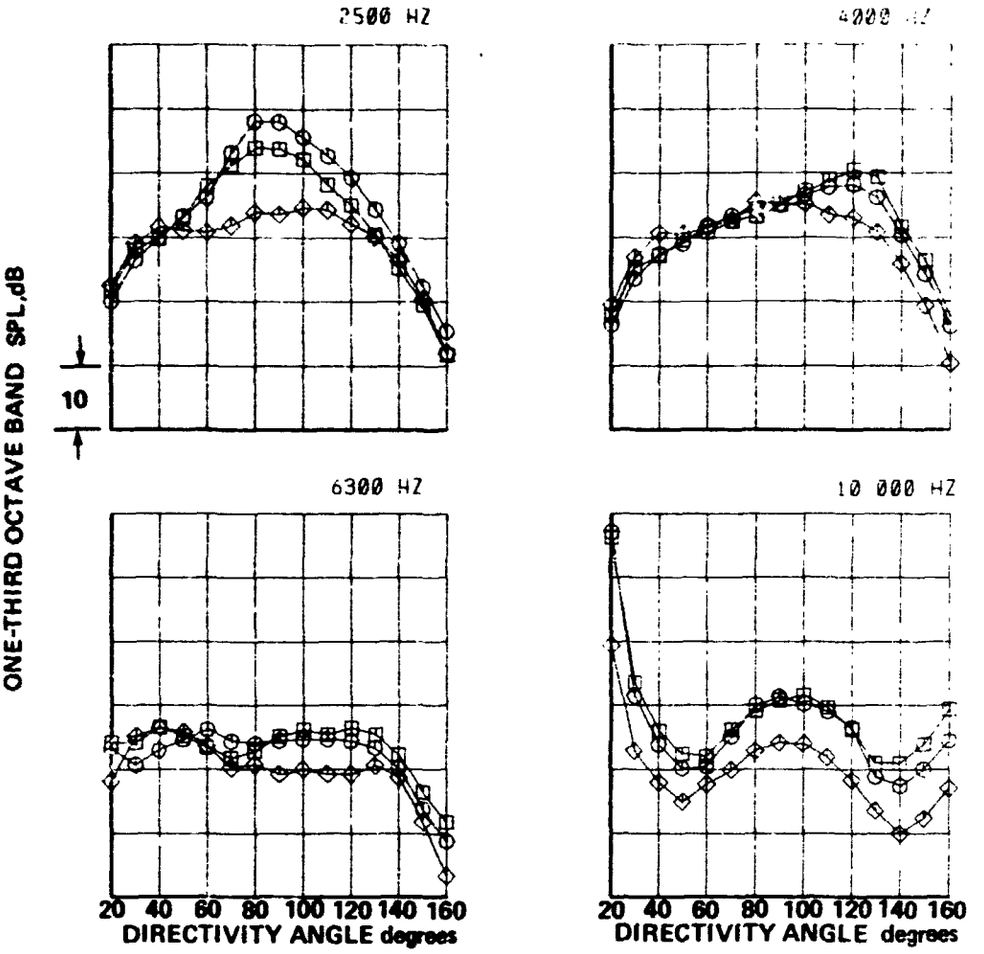

(b) FREQUENCY 400 TO 1600 Hz

Figure 10.--(Continued)

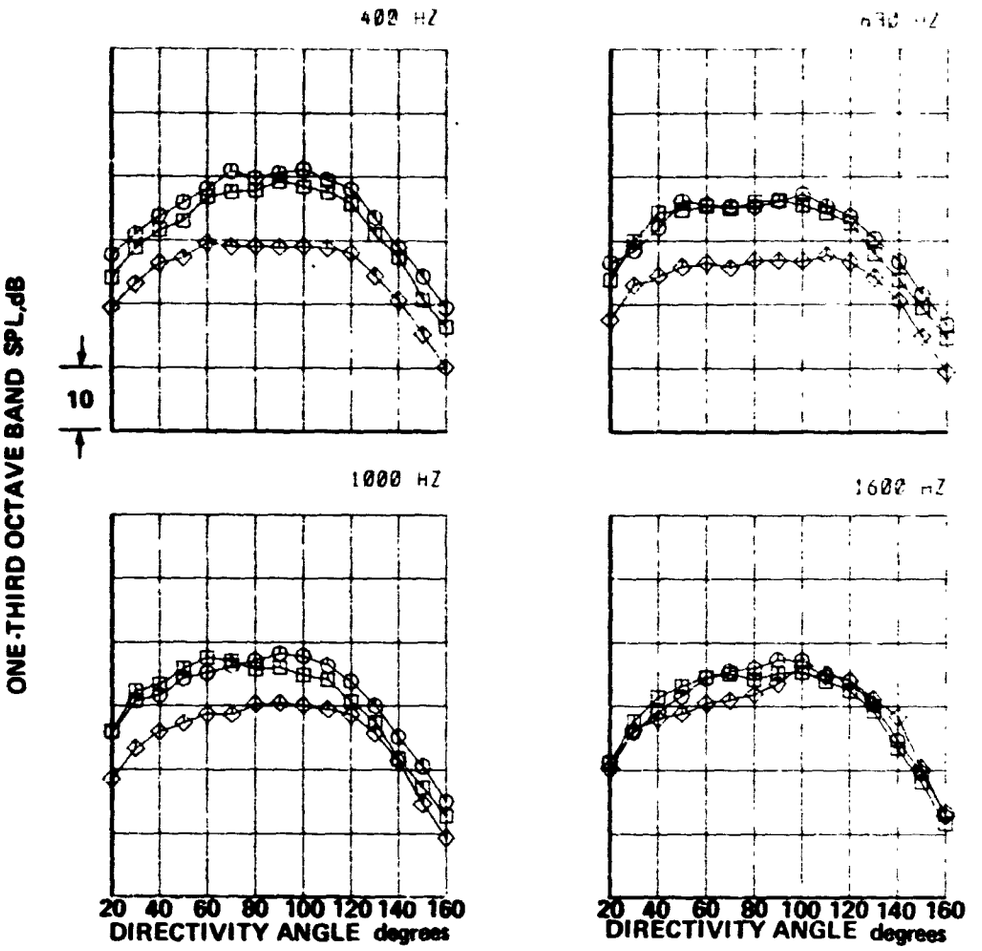

(c) FREQUENCY 2500 TO 10,000 Hz

Figure 10.—(Concluded)

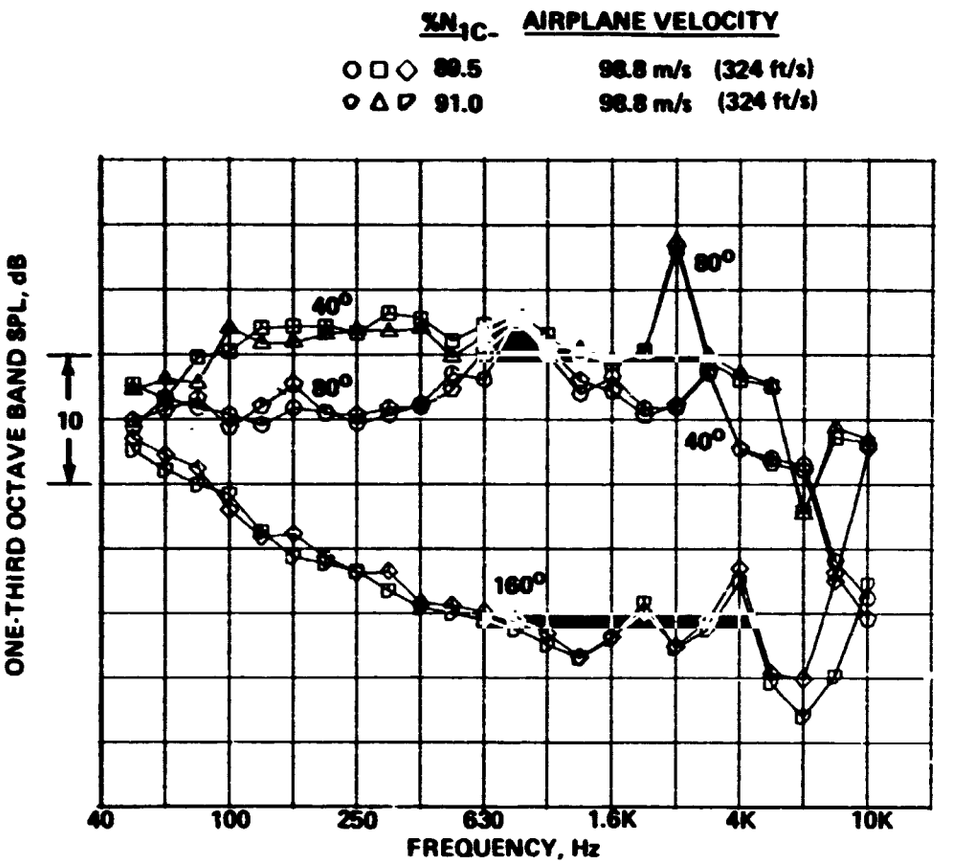

Figure 11.—Data Repeatability

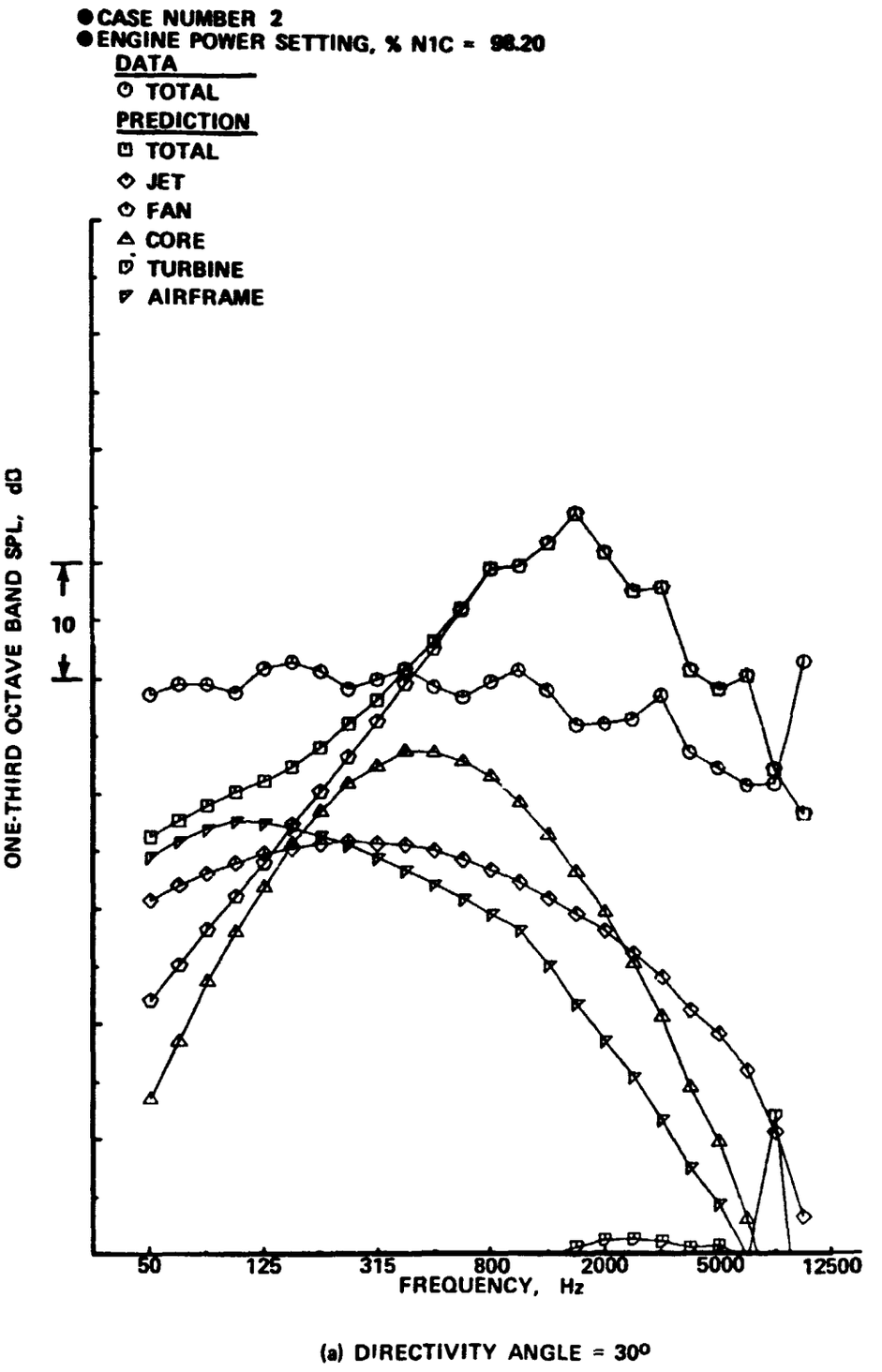

Figure 12. – Spectral Comparisons of Data and Prediction at Takeoff Power

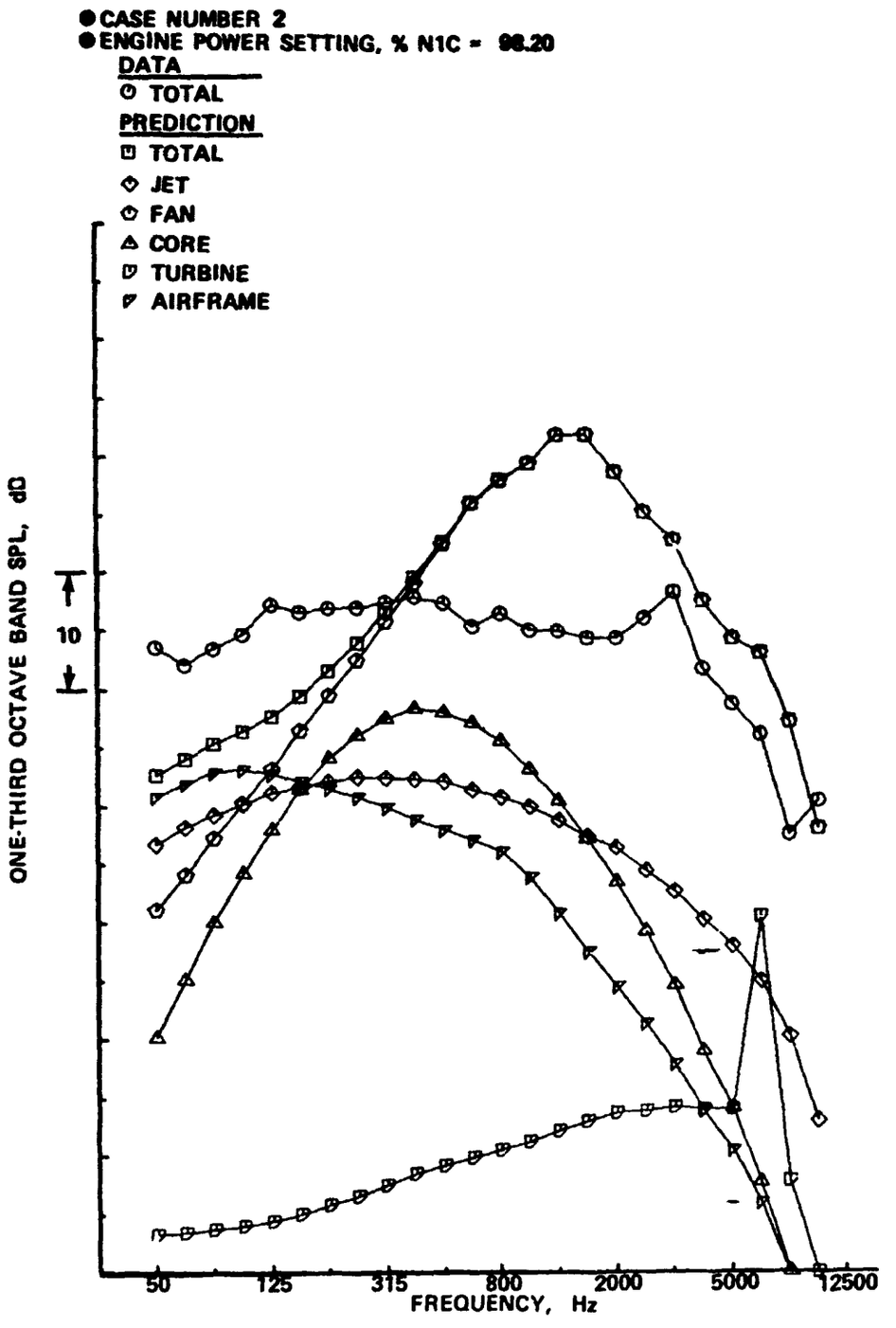

(b) DIRECTIVITY ANGLE = 60°

Figure 12. – (Continued)

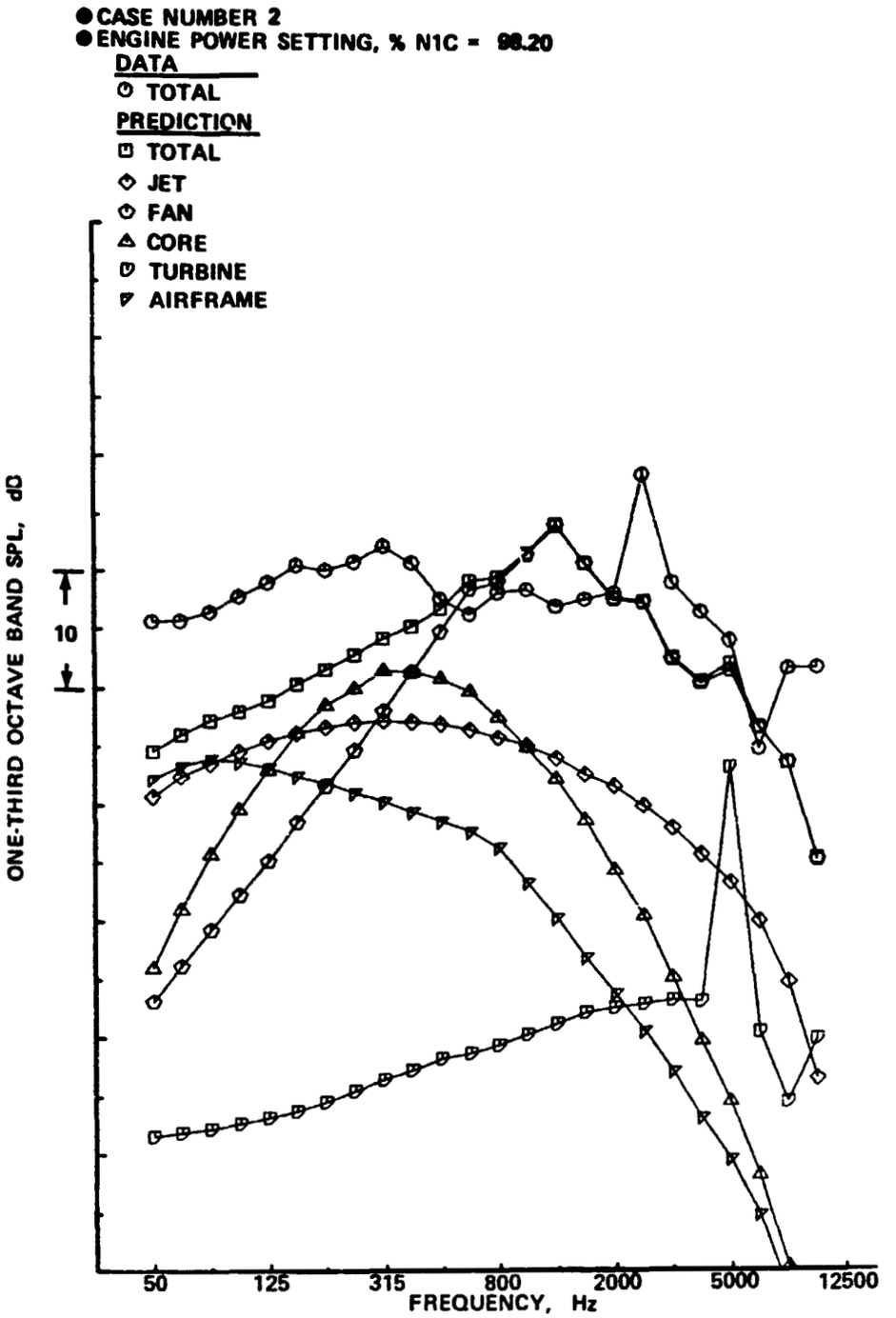

(c) DIRECTIVITY ANGLE = 90°

Figure 12. – (Continued)

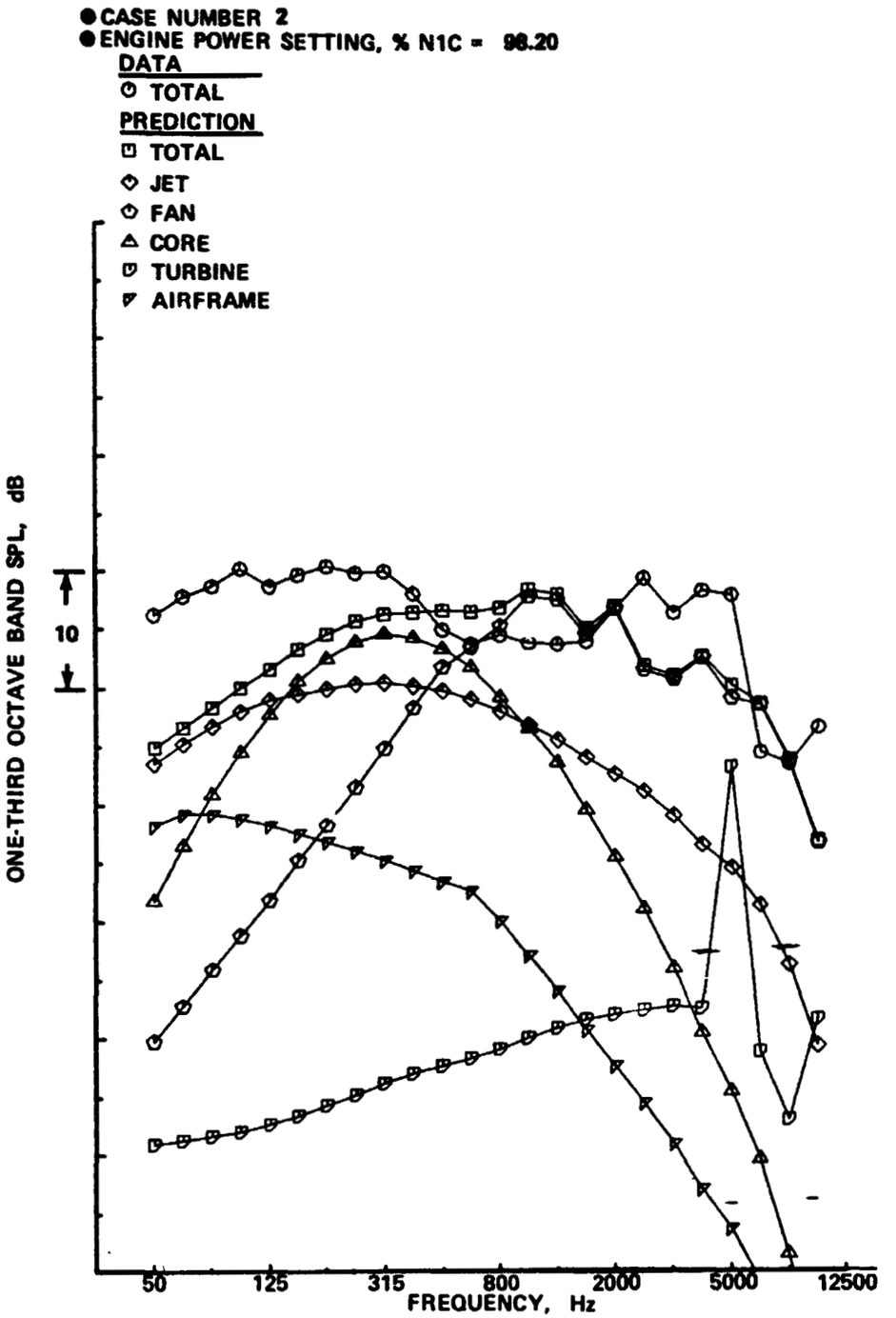

(d) DIRECTIVITY ANGLE = 120°

Figure 12. — (Continued)

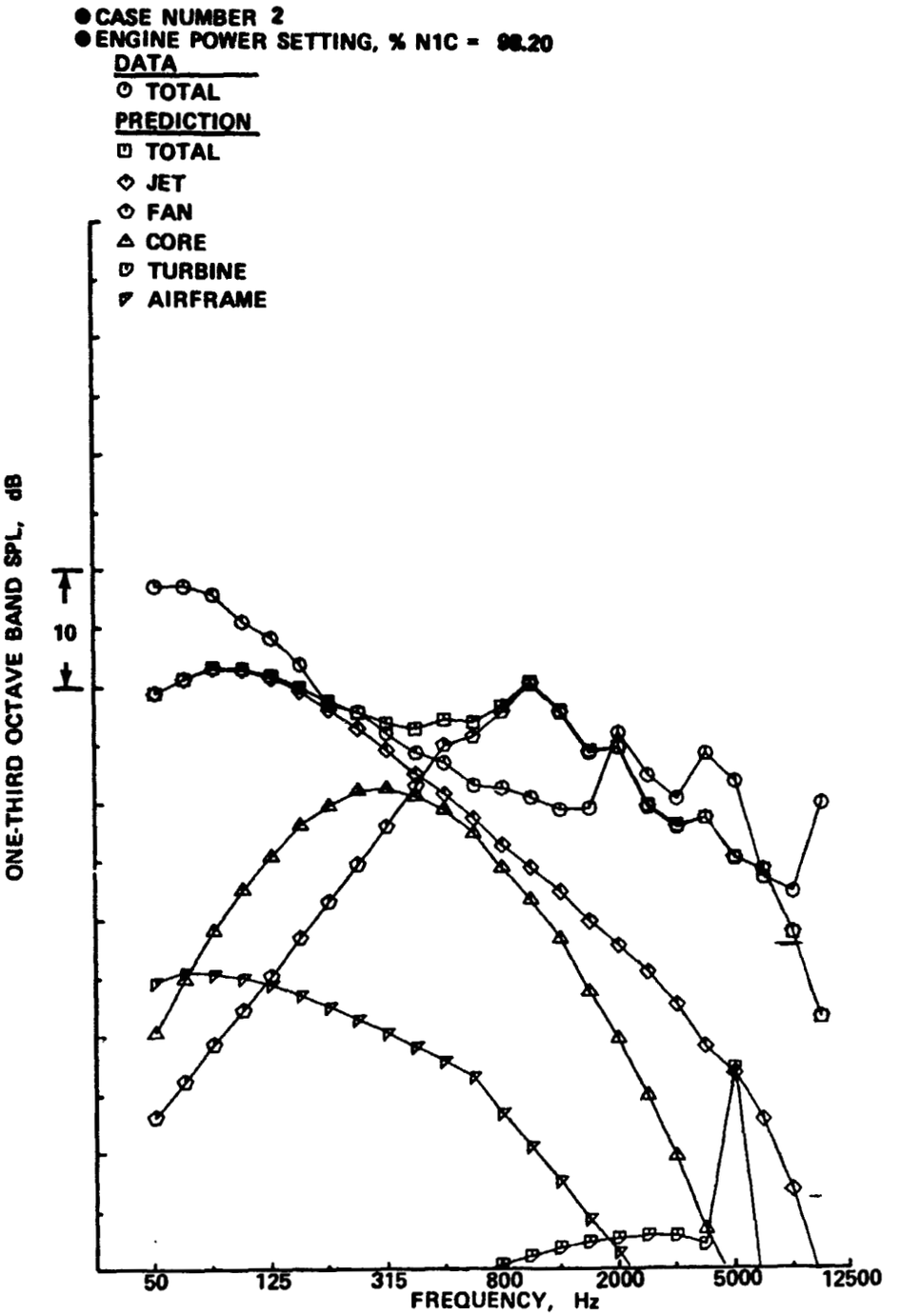

(e) DIRECTIVITY ANGLE = 150°

Figure 12. – (Concluded)

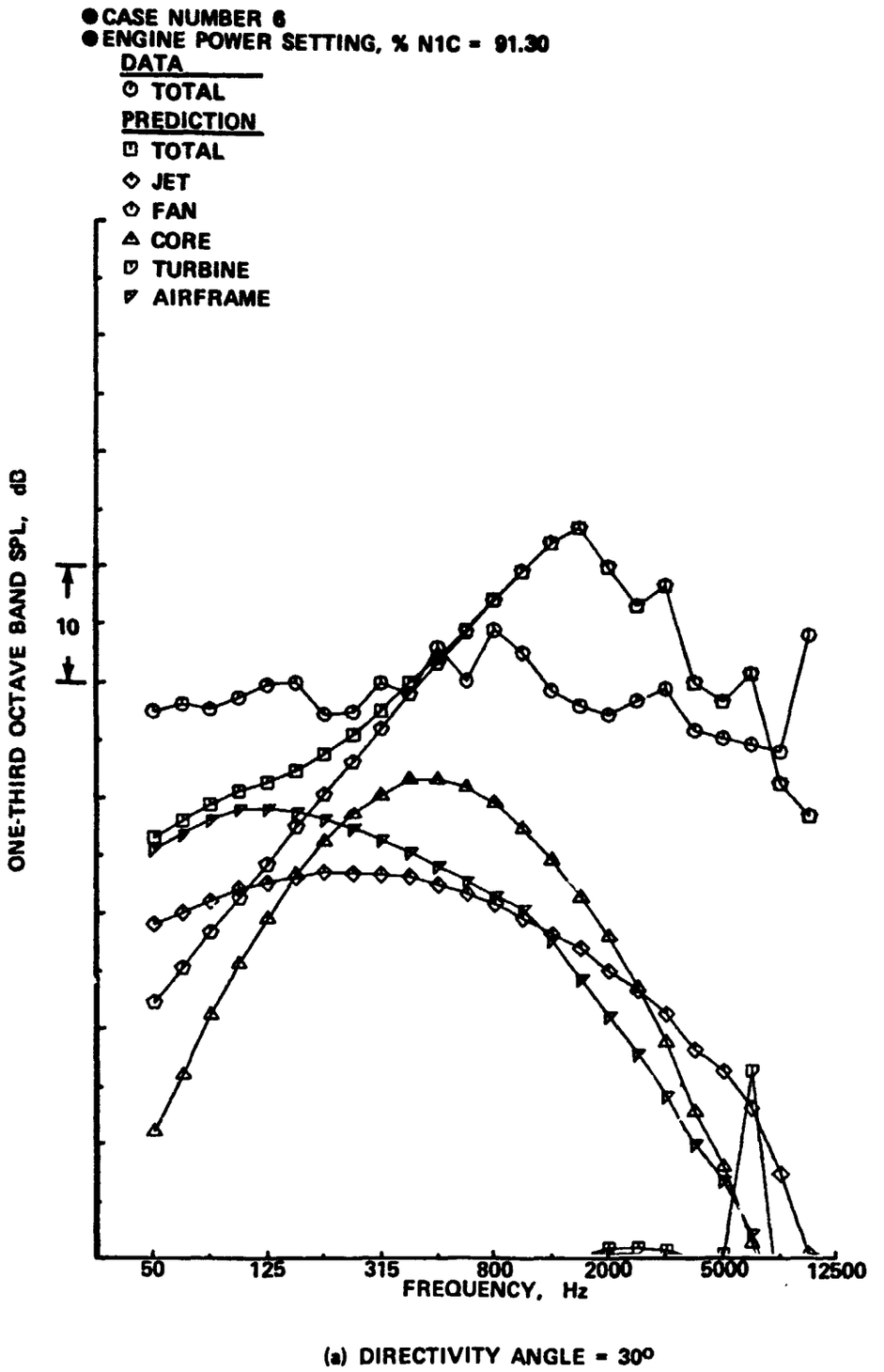

Figure 13. — Spectral Comparisons of Data and Predictions at Cutback Power

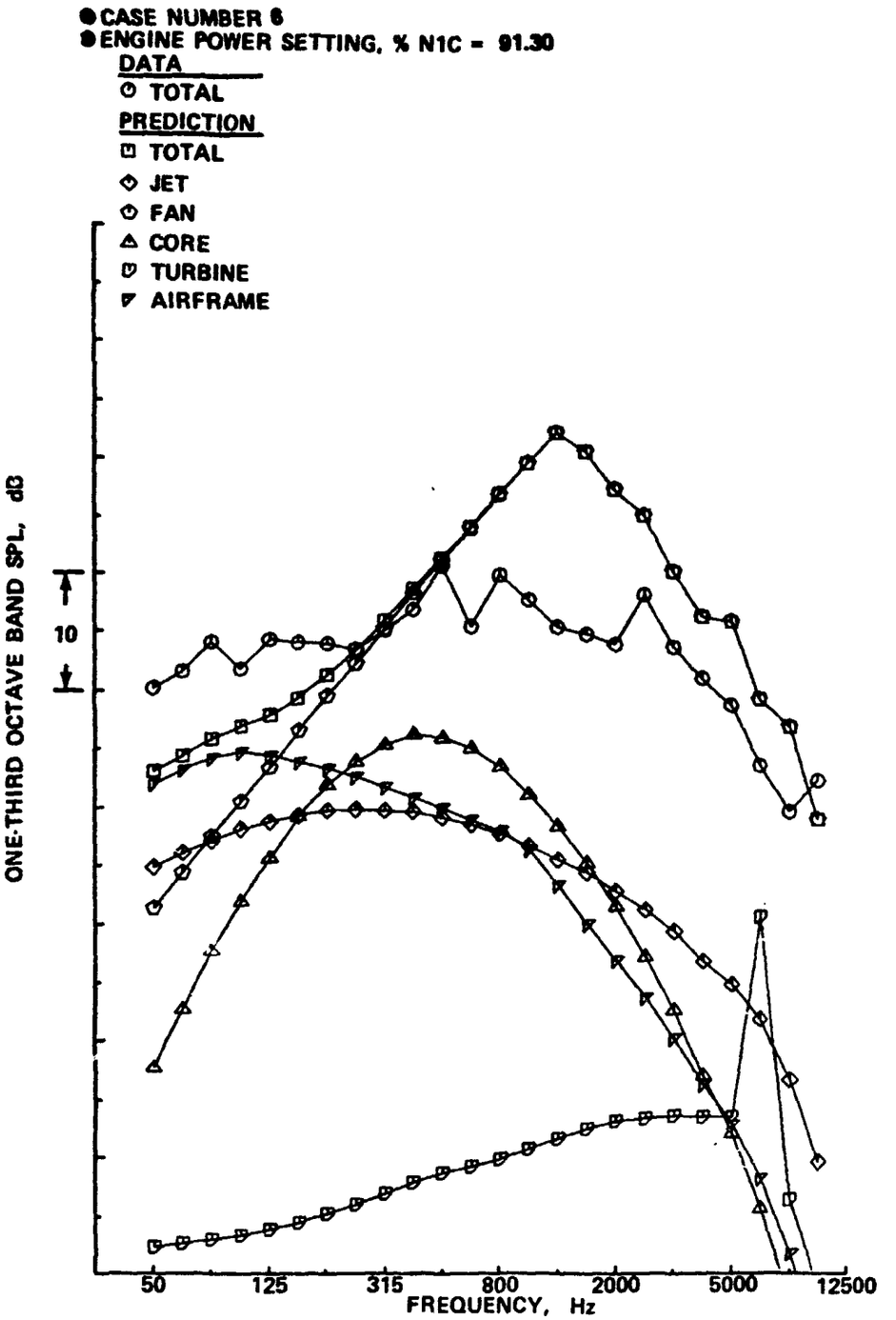

(b) DIRECTIVITY ANGLE = 60°

Figure 13. – (Continued)

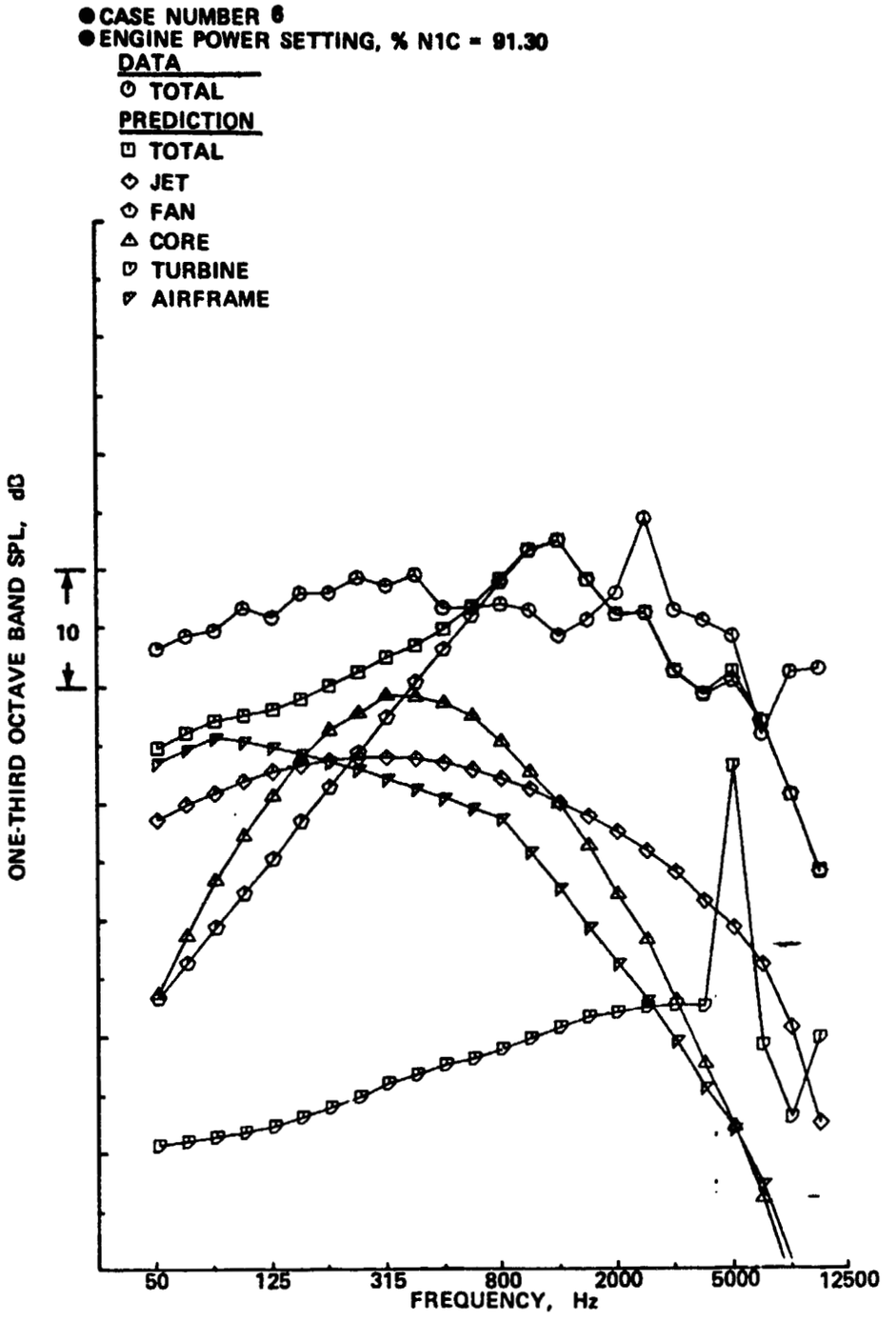

(c) DIRECTIVITY ANGLE = 90°

Figure 13. – (Continued)

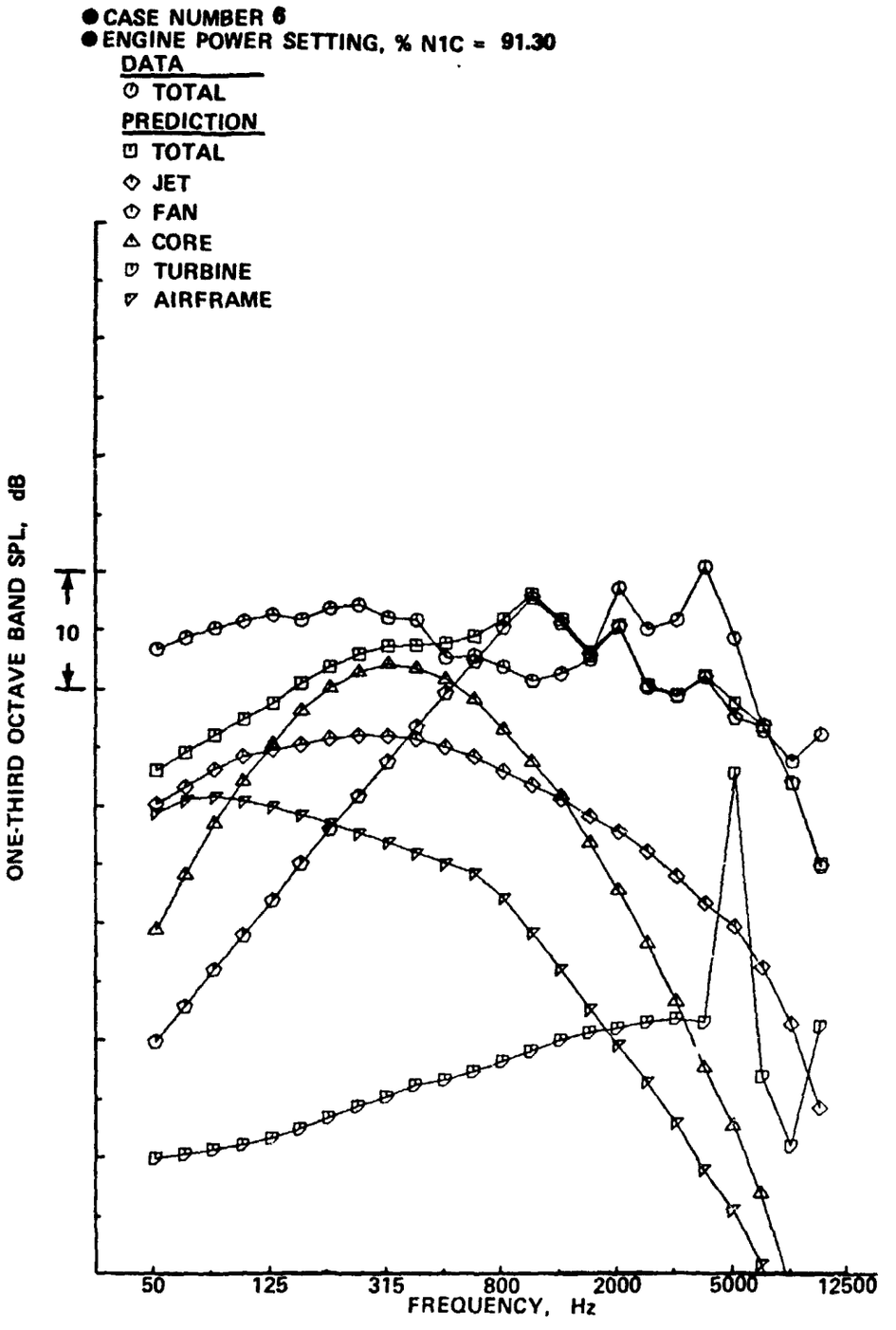

(d) DIRECTIVITY ANGLE = 120°

Figure 13. – (Continued)

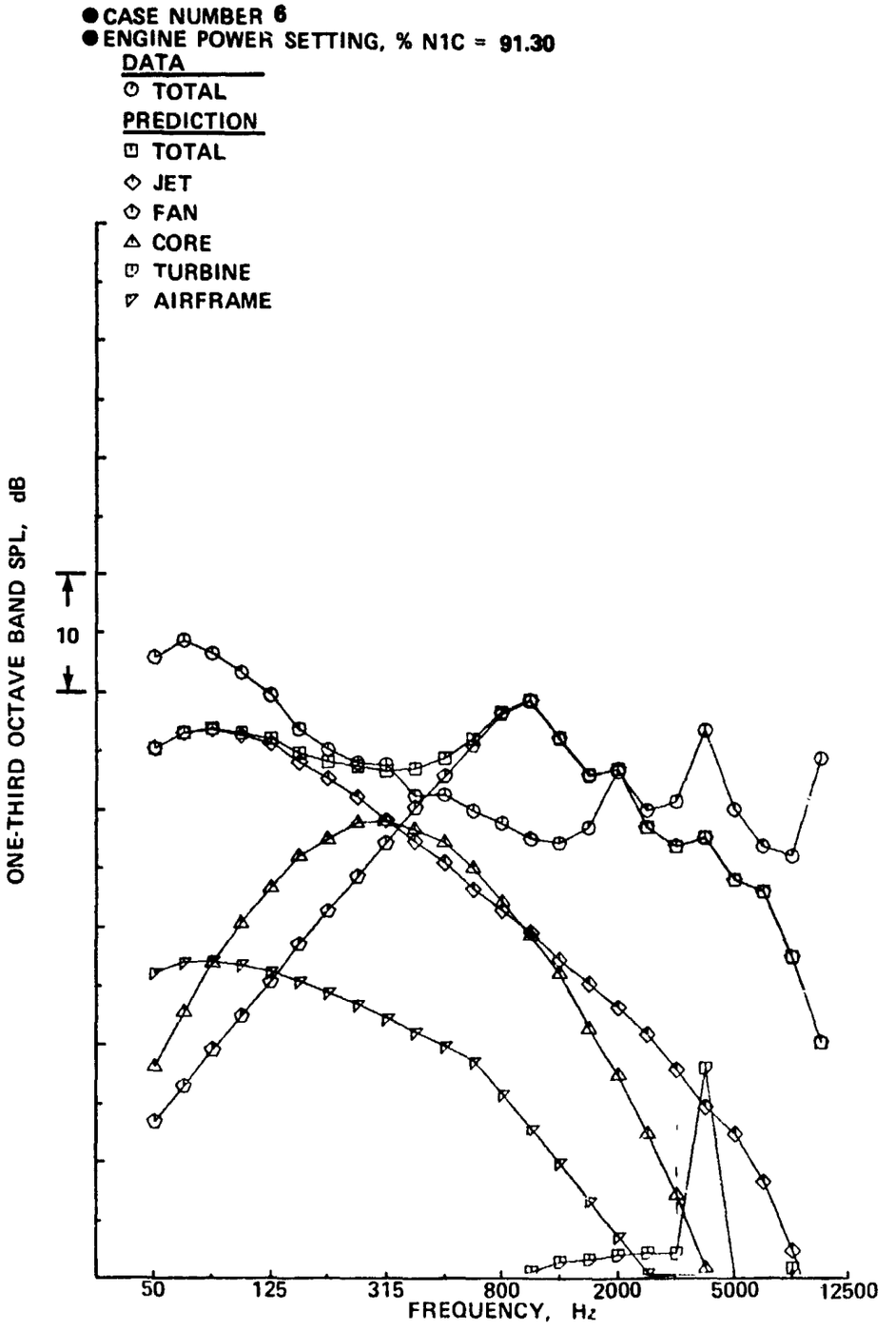

(e) DIRECTIVITY ANGLE = 150°

Figure 13. -- (Concluded)

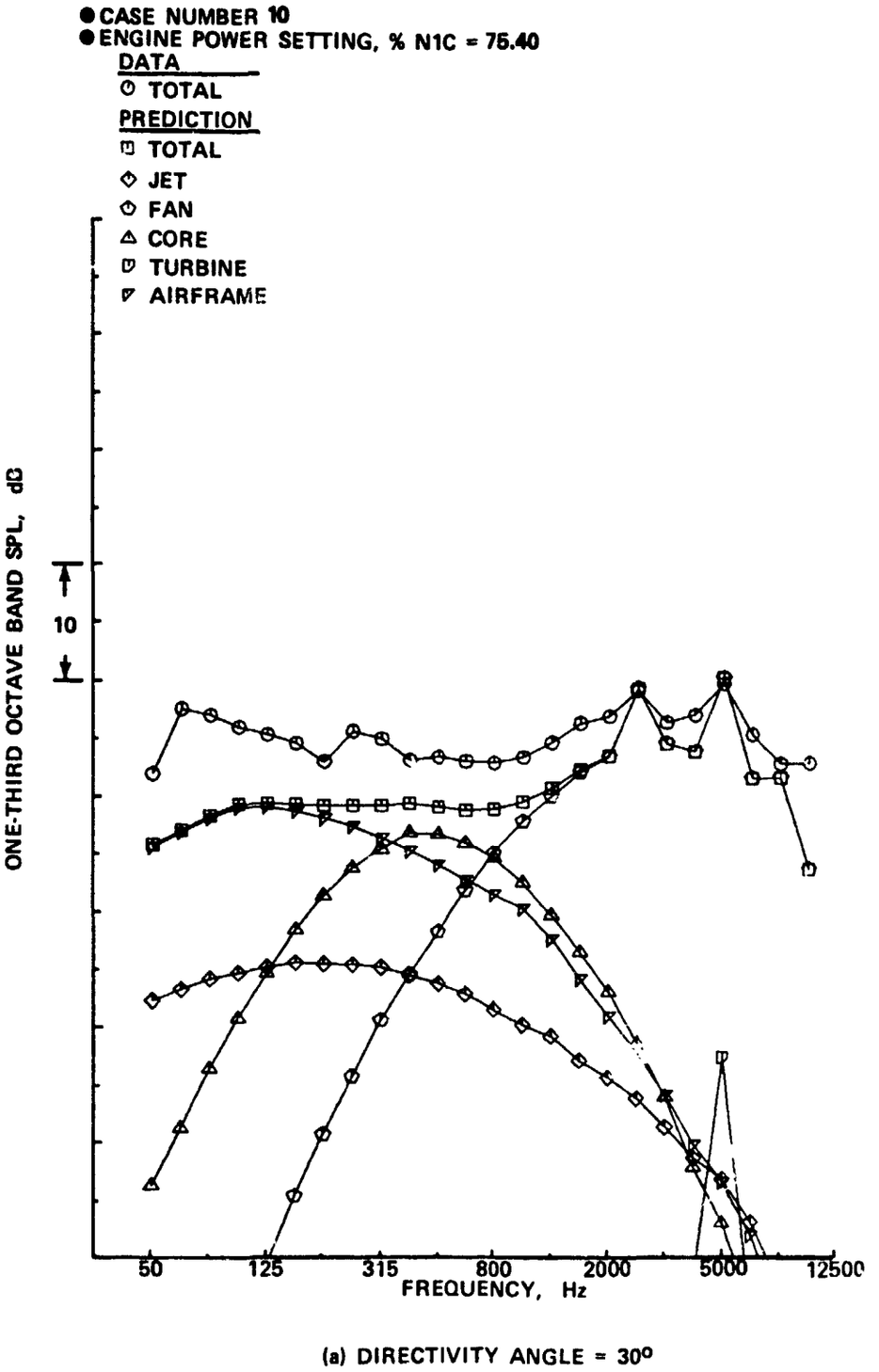

Figure 14. — Spectral Comparisons of Data and Predictions at Approach Power

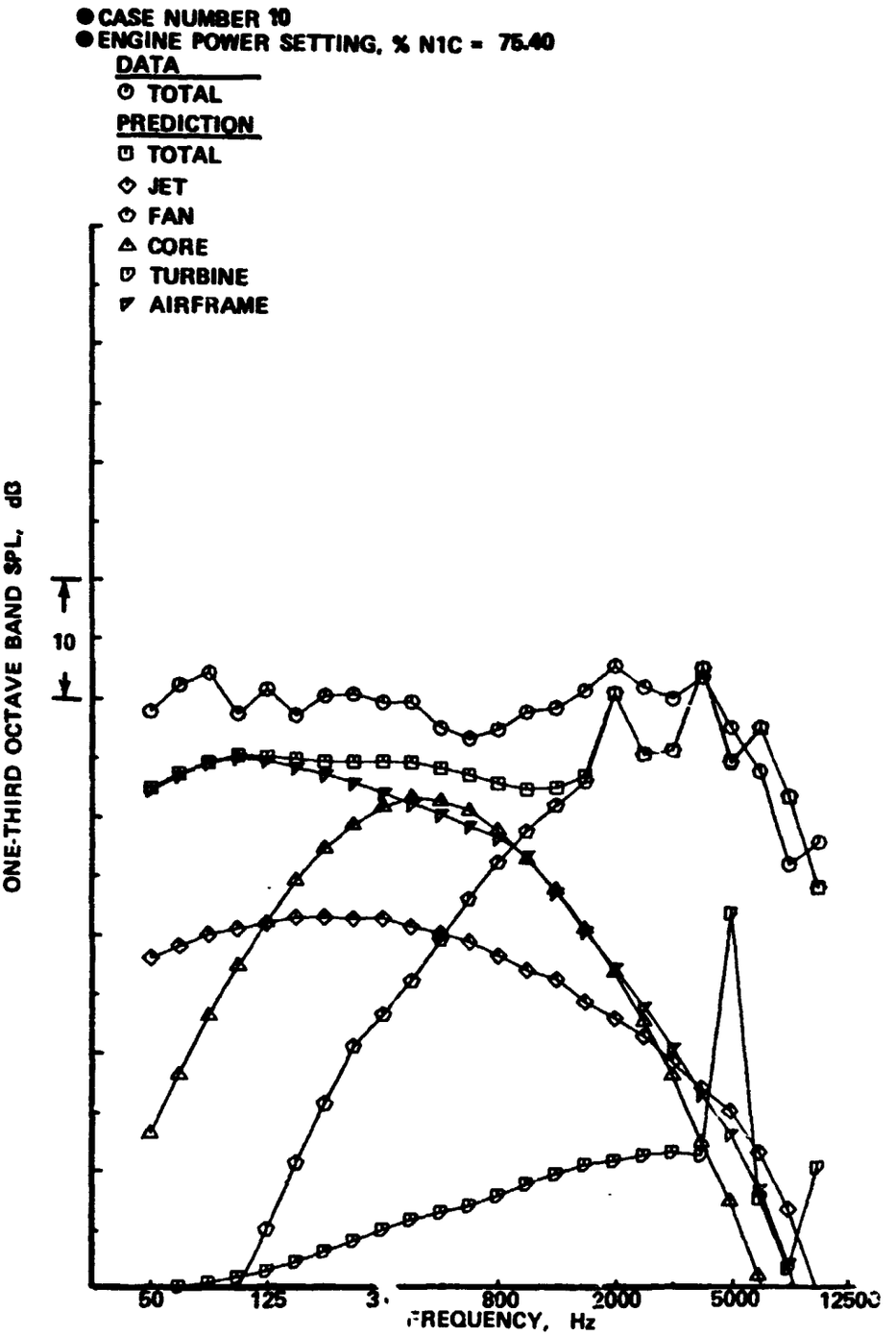

(b) DIRECTIVITY ANGLE = 60°

Figure 14. – (Continued)

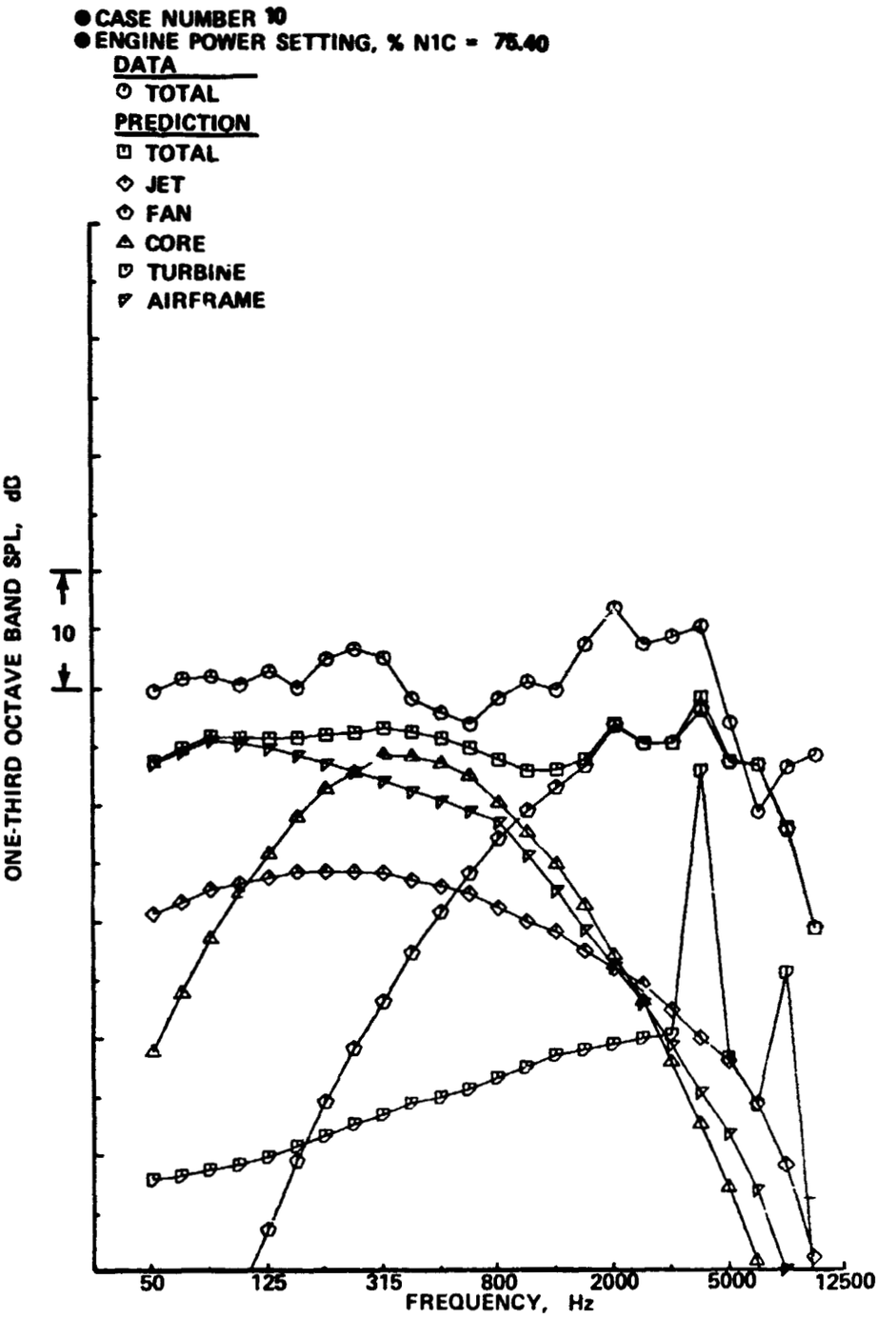

(c) DIRECTIVITY ANGLE = 90°

Figure 14. – (Continued)

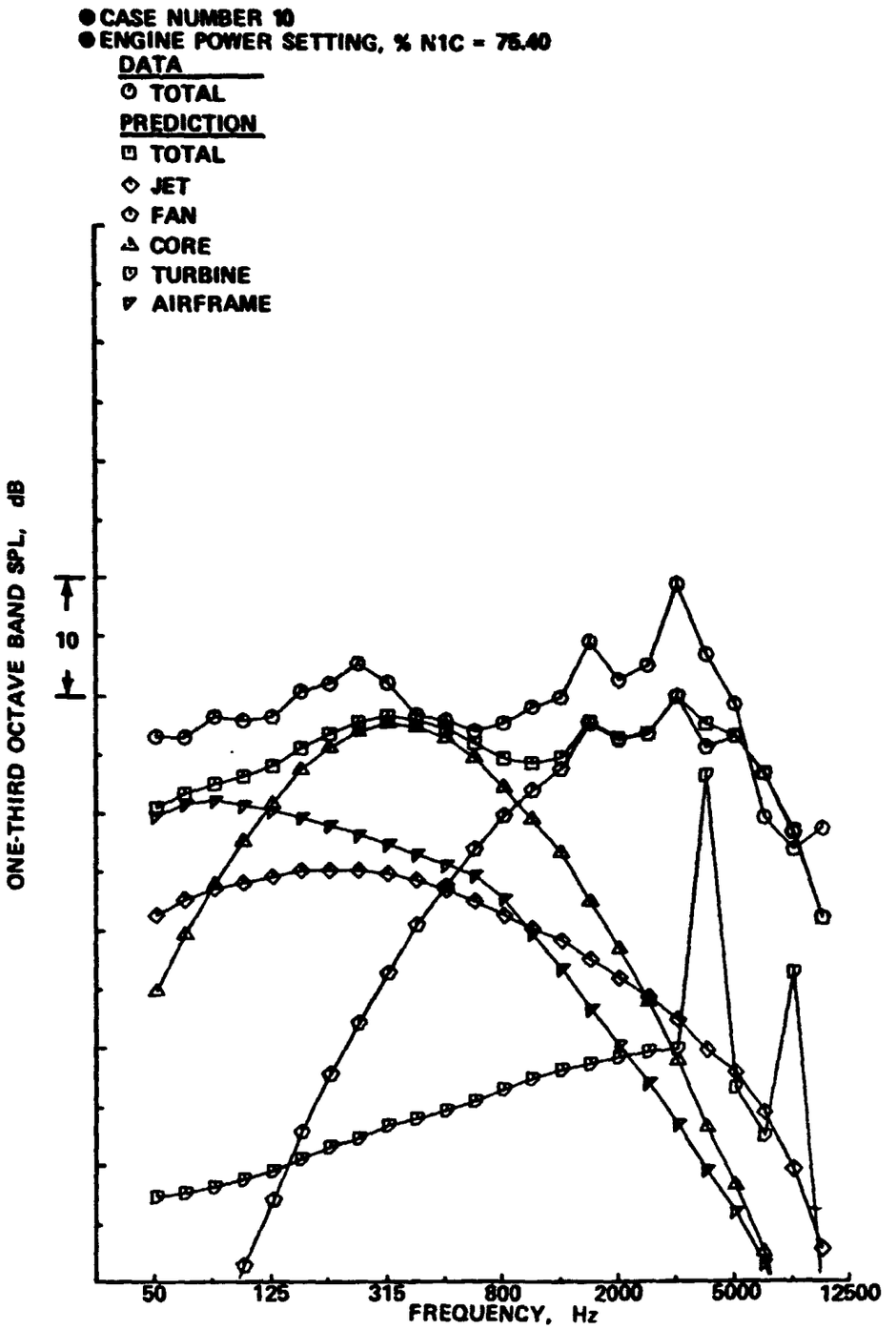

(d) DIRECTIVITY ANGLE = 120°

Figure 14. – (Continued)

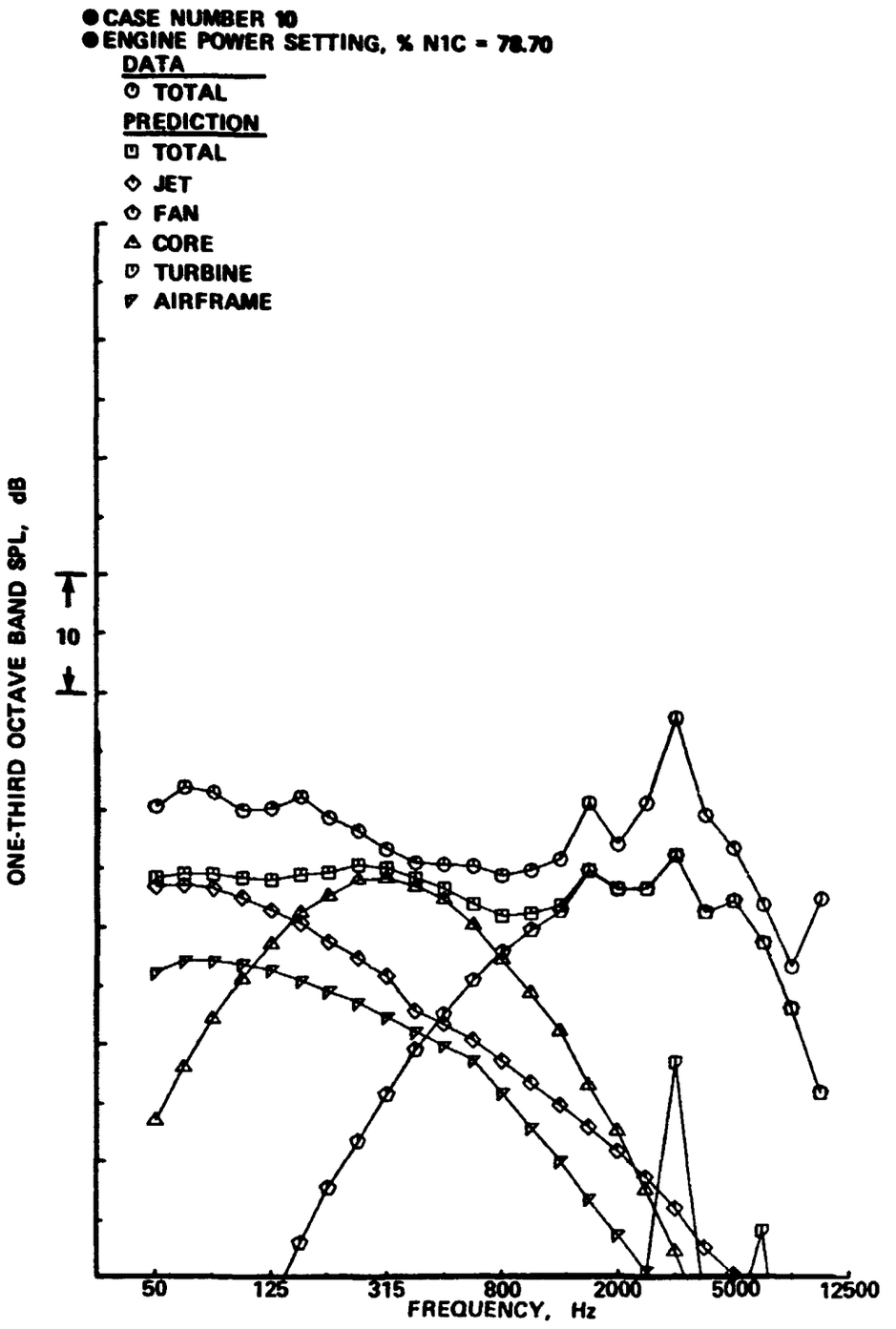

(e) DIRECTIVITY ANGLE = 150°

Figure 14. – (Concluded)

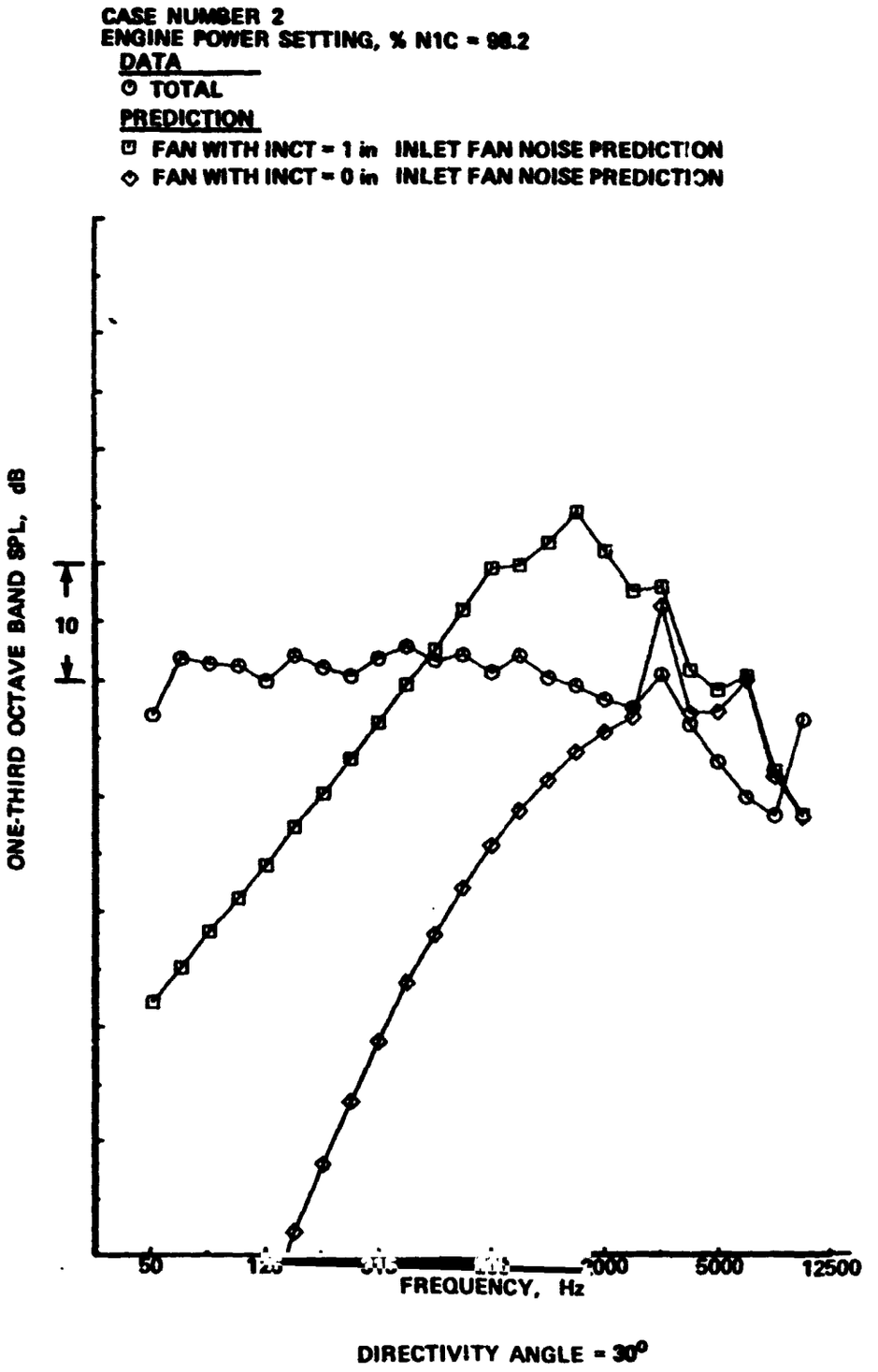

Figure 15. – Effect of INCT = 0 and 1 in Fan Noise Source Module on Data Prediction Spectral Comparisons

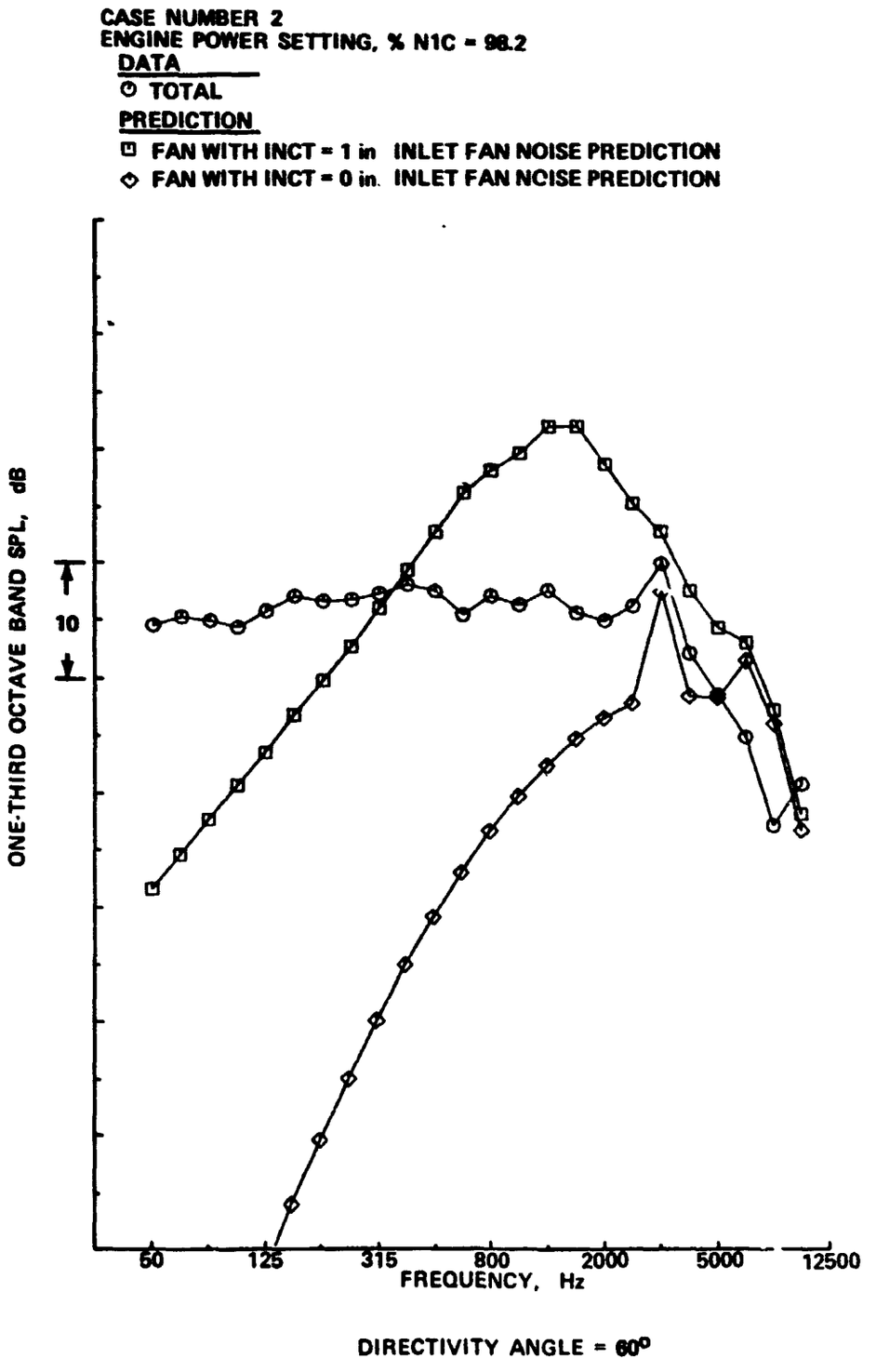

Figure 15. – (Continued)

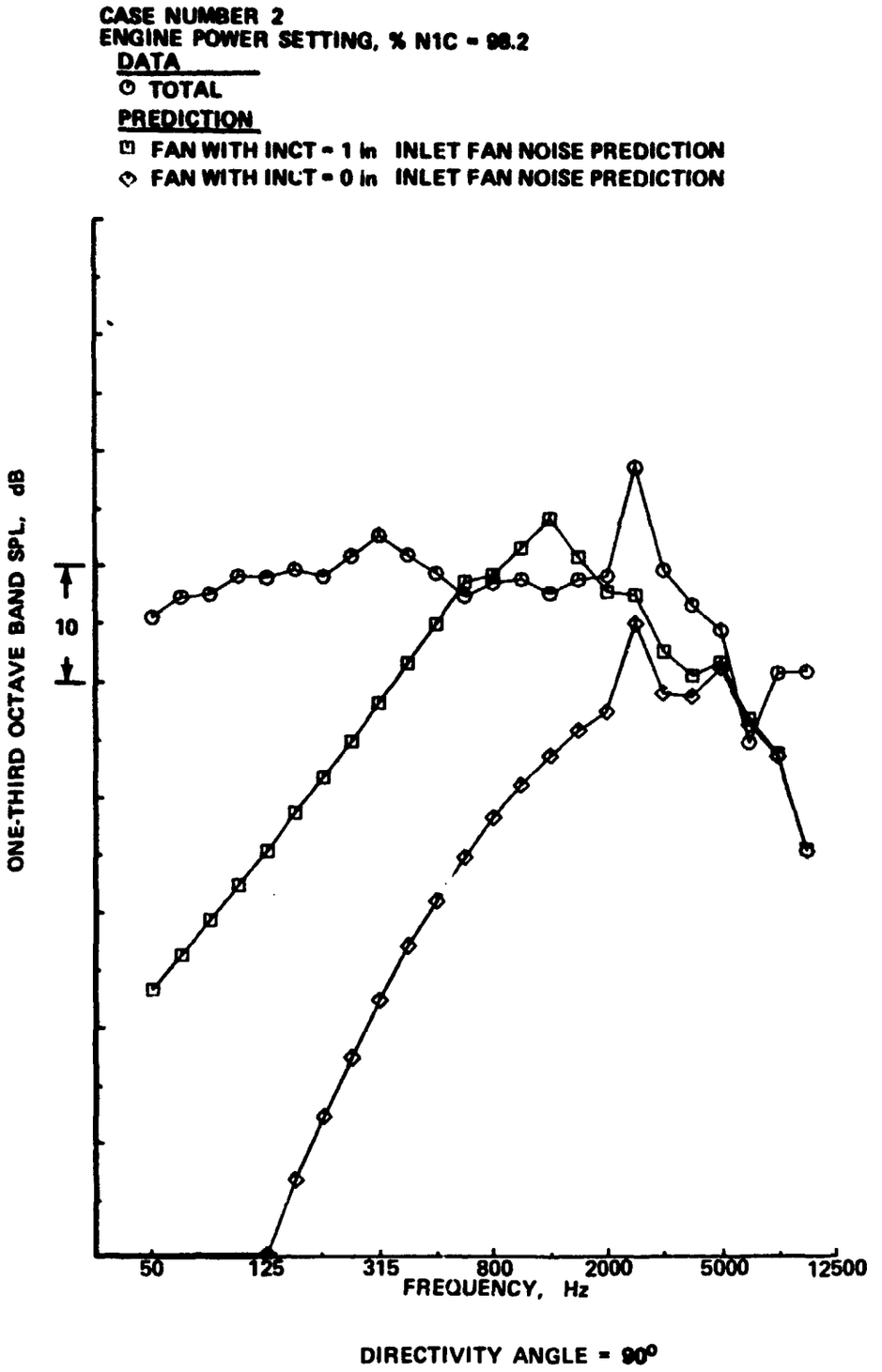

Figure 15. — (Continued)

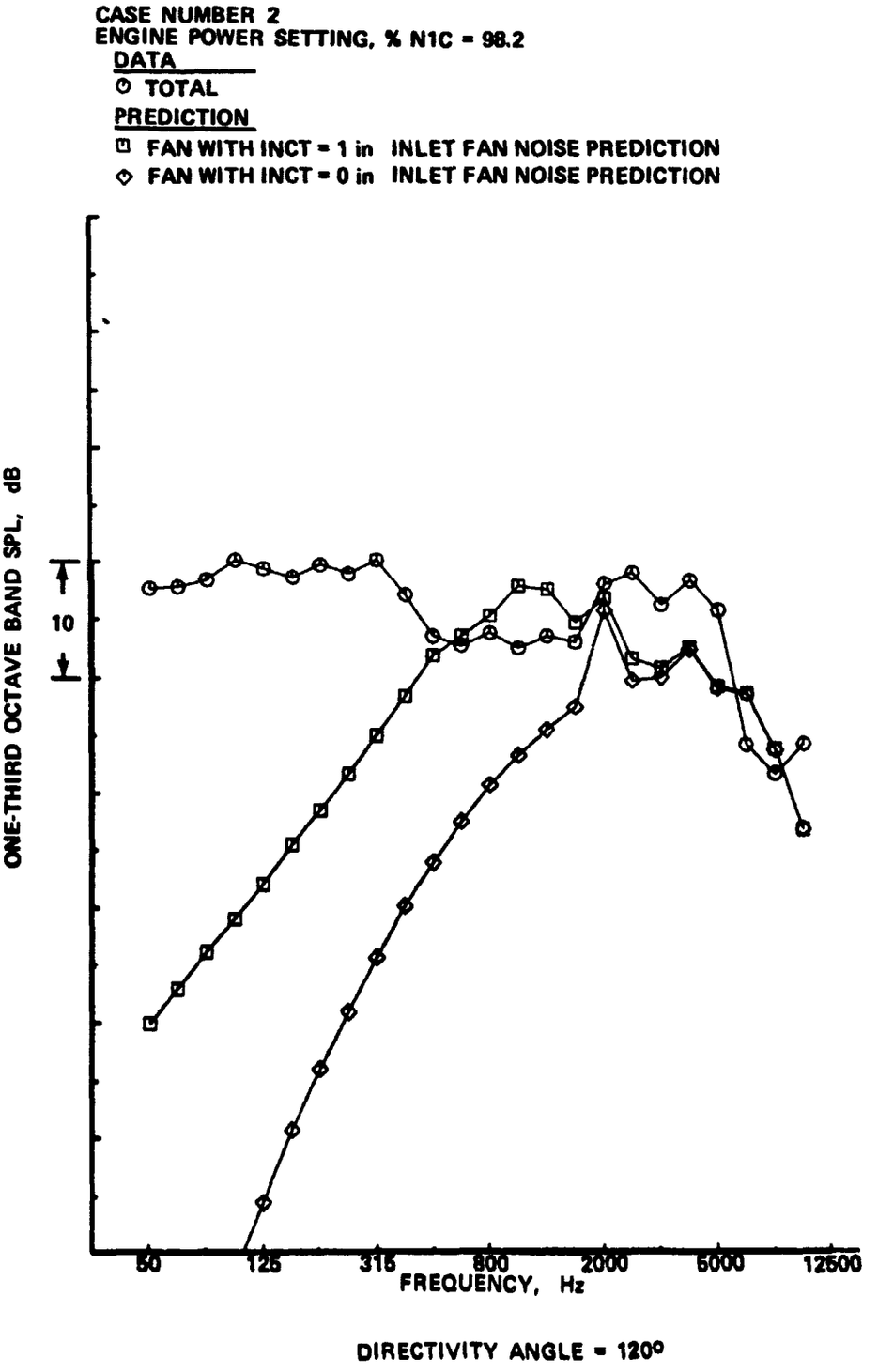

Figure 15. – (Continued)

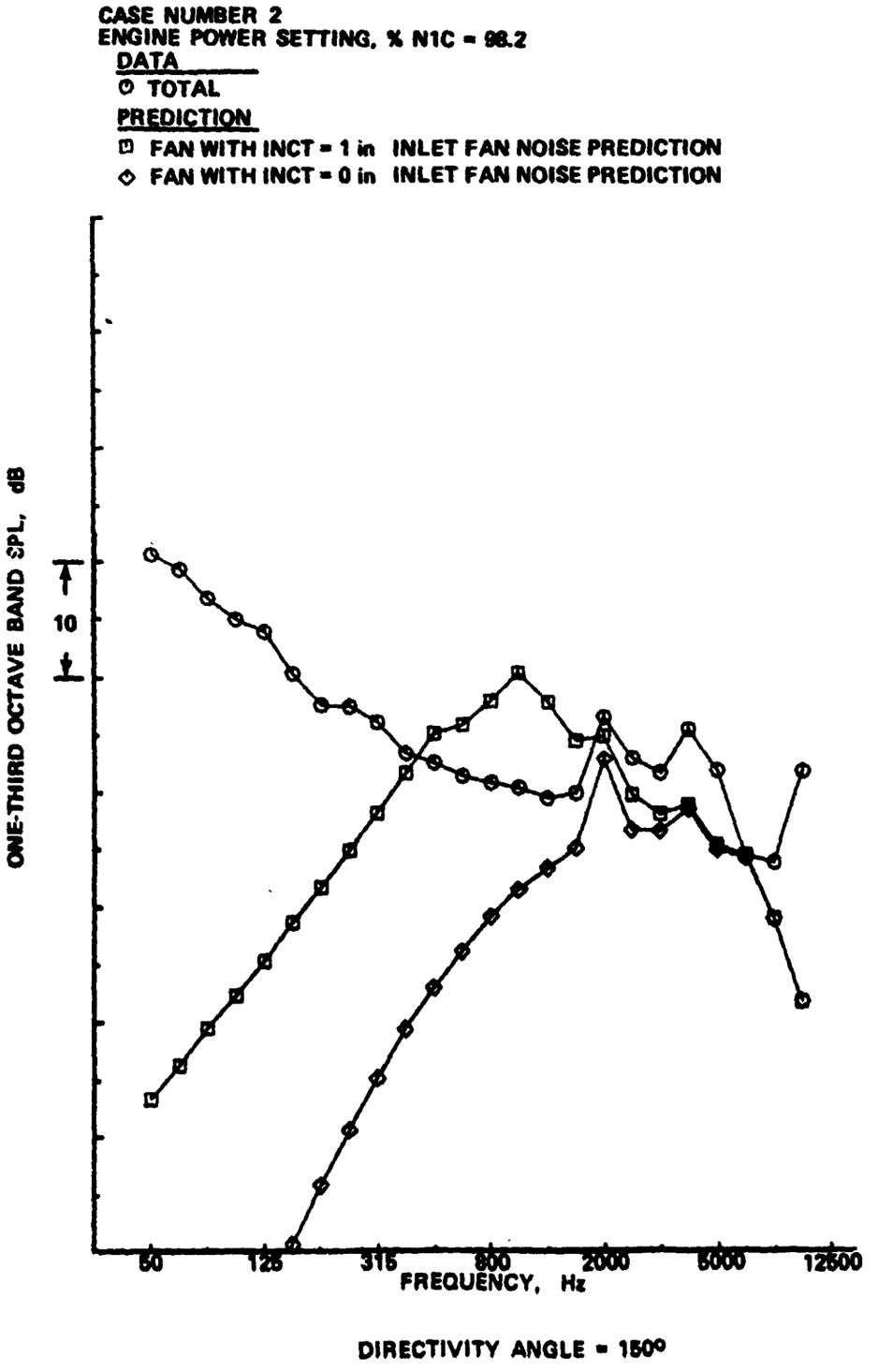

Figure 15. — (Concluded)

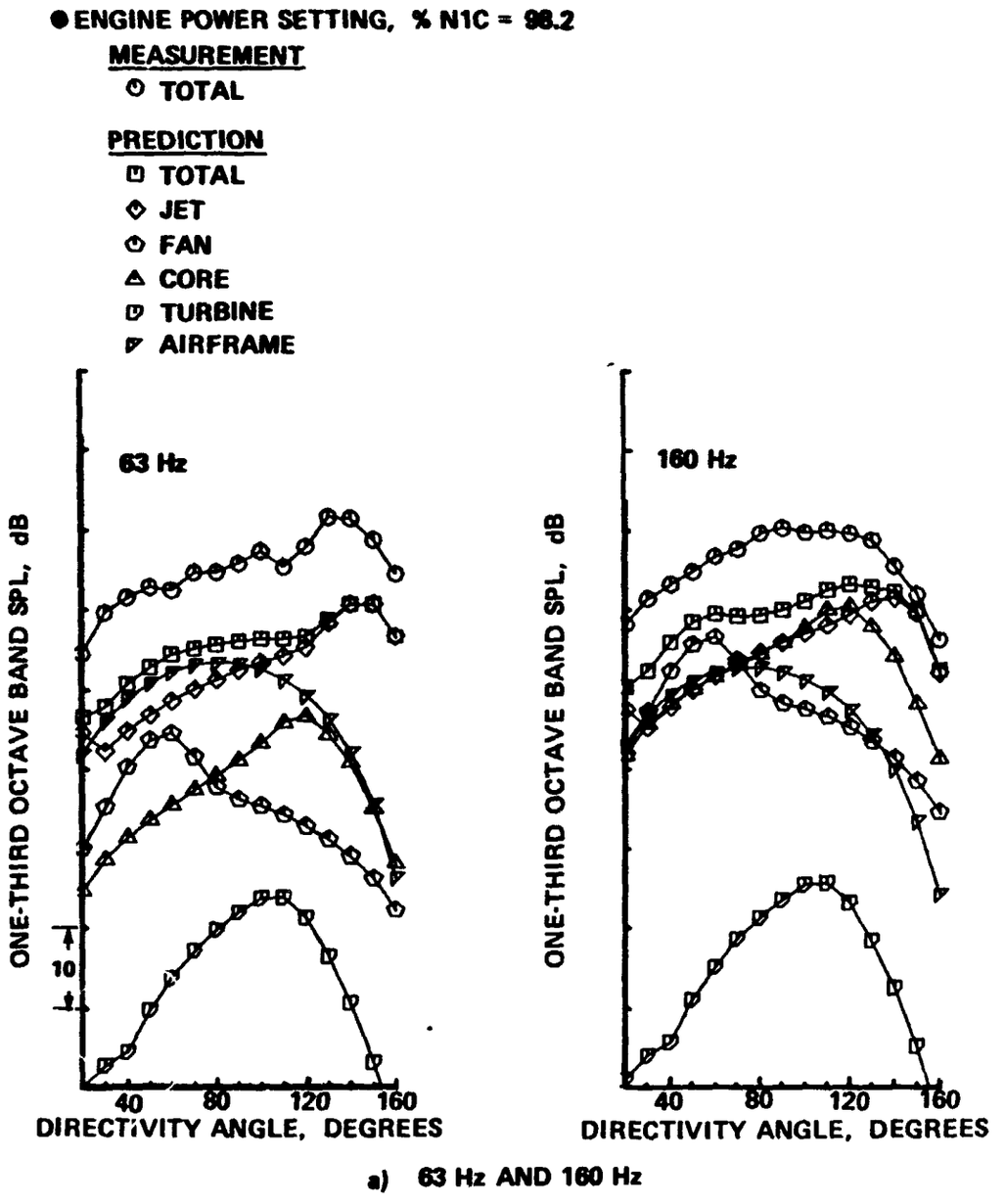

Figure 16. — SPL Directivity Comparisons of Data and Prediction at Takeoff Power

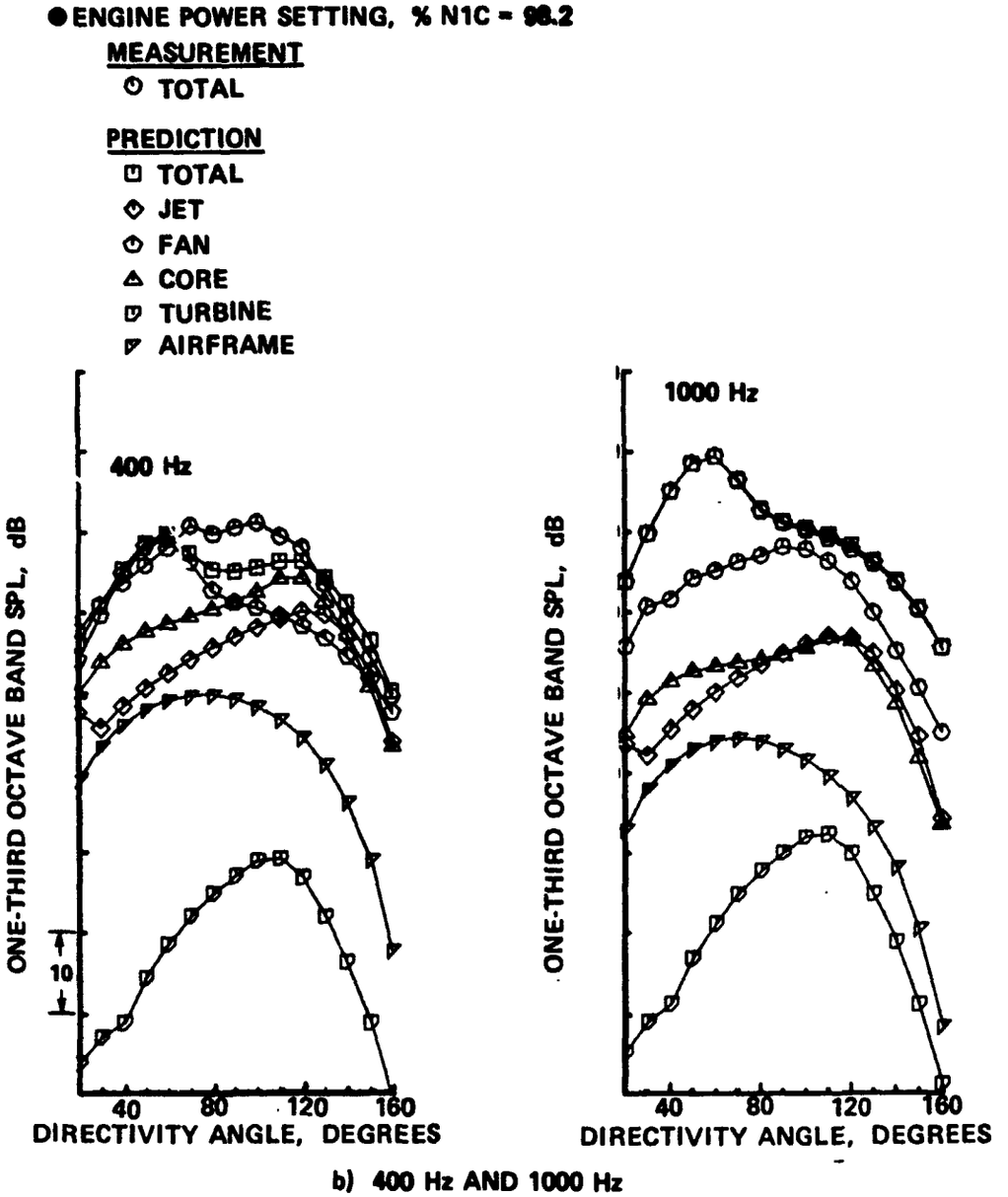

b) 400 Hz AND 1000 Hz

Figure 16. – (Concluded)

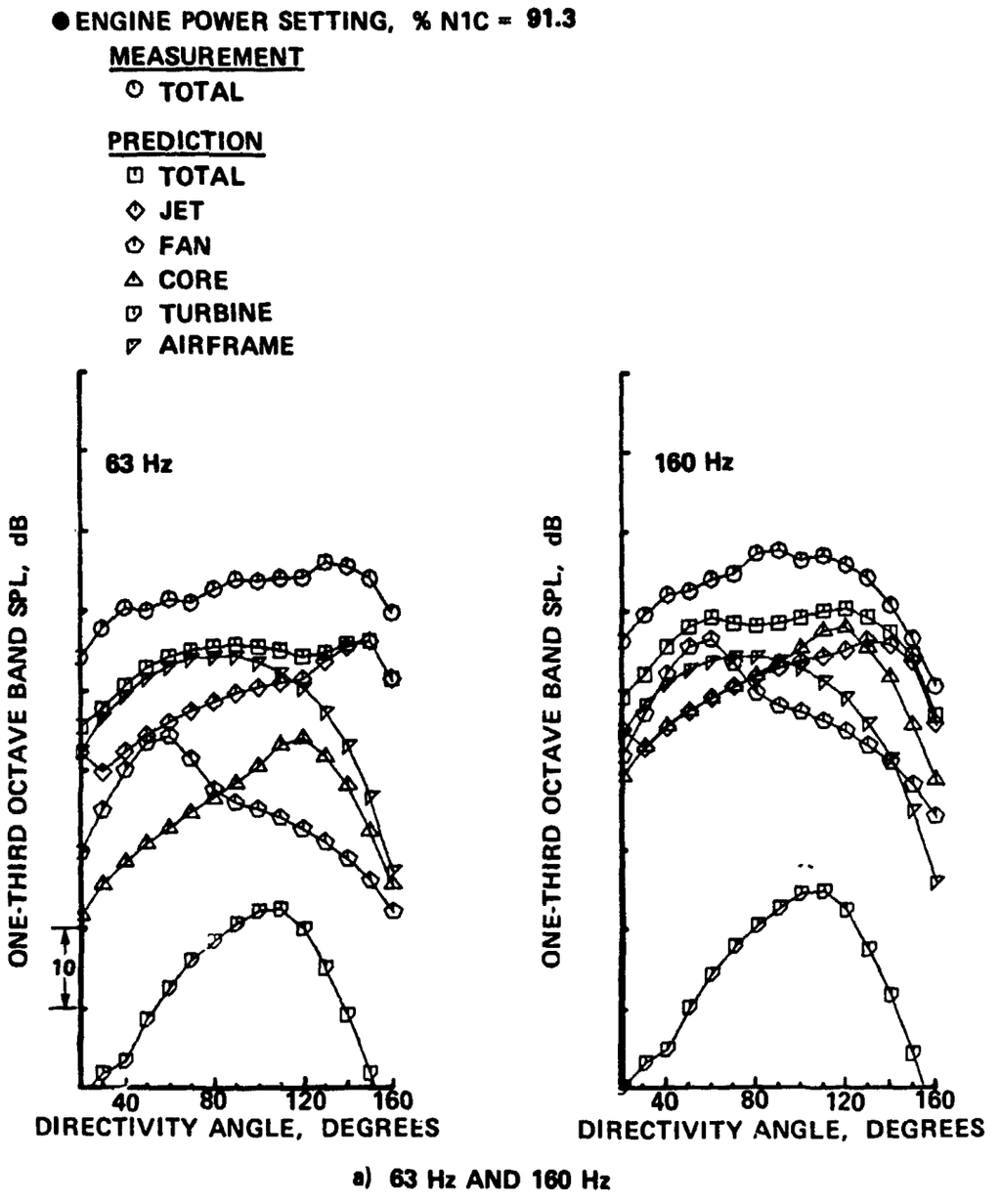

Figure 17. – SPL Directivity Comparisons of Data and Prediction at Cutback Power

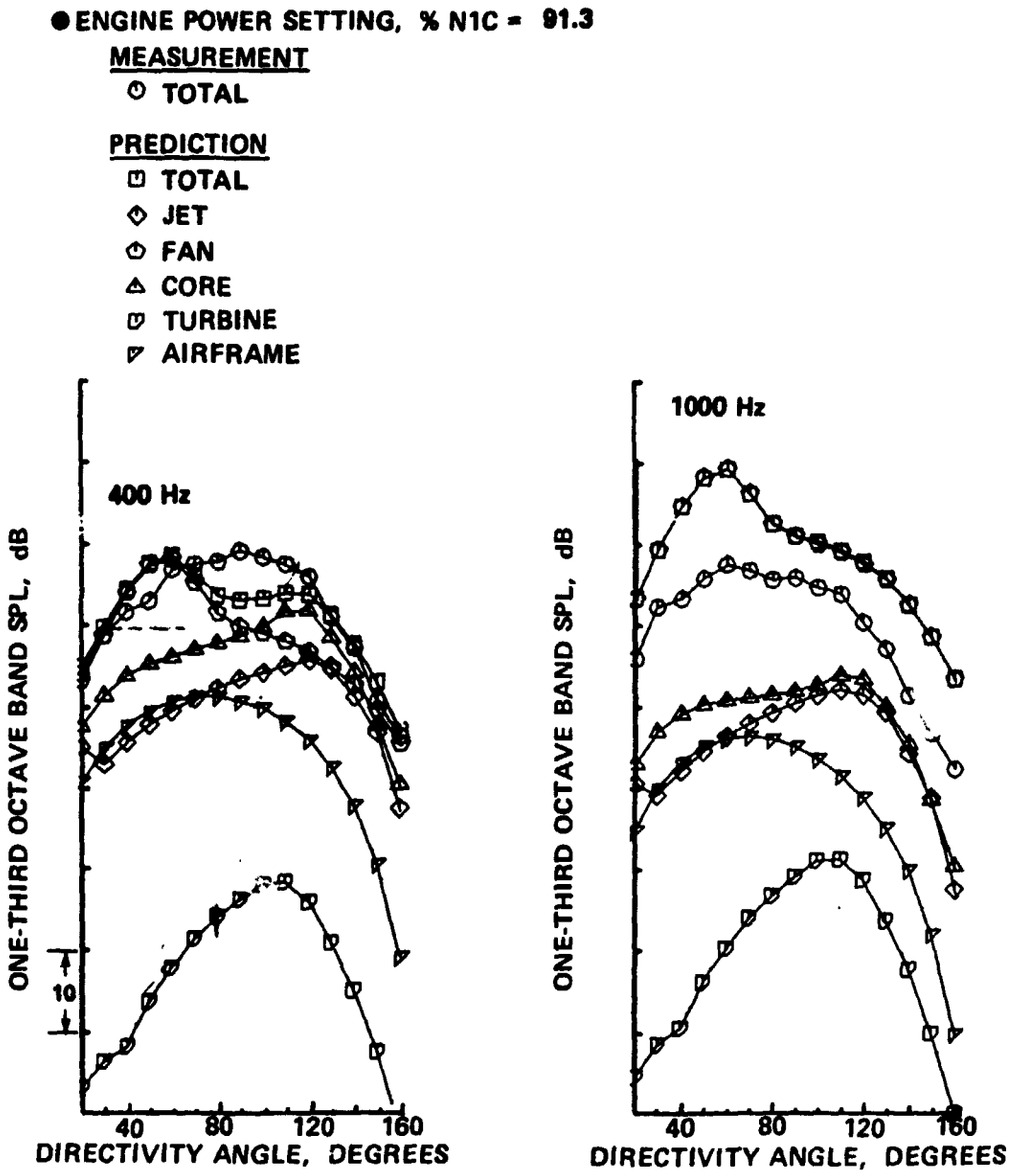

b) 400 Hz AND 1000 Hz

Figure 17. – (Concluded)

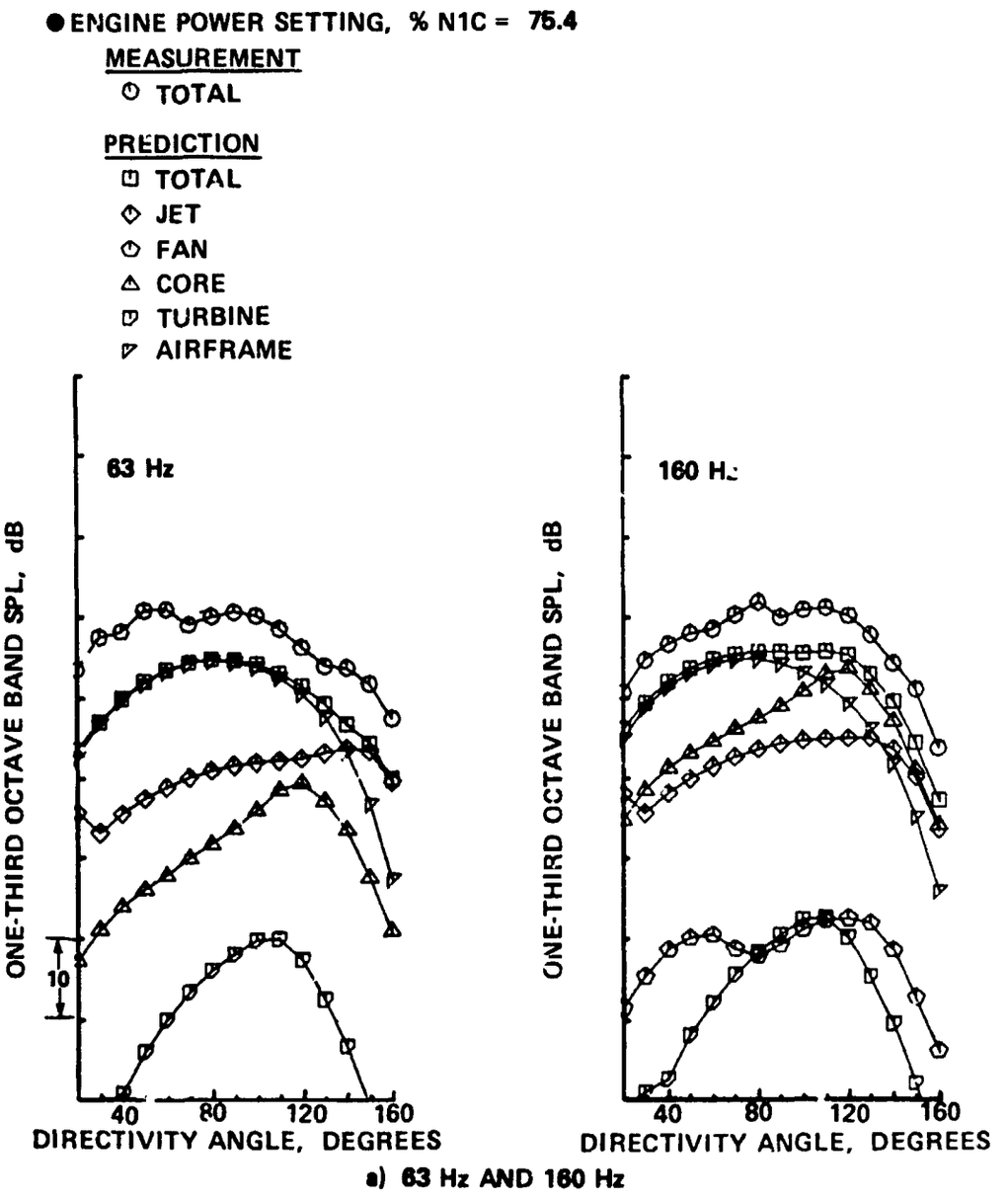

Figure 18. – SPL Directivity Comparisons of Data and Prediction at Approach Power

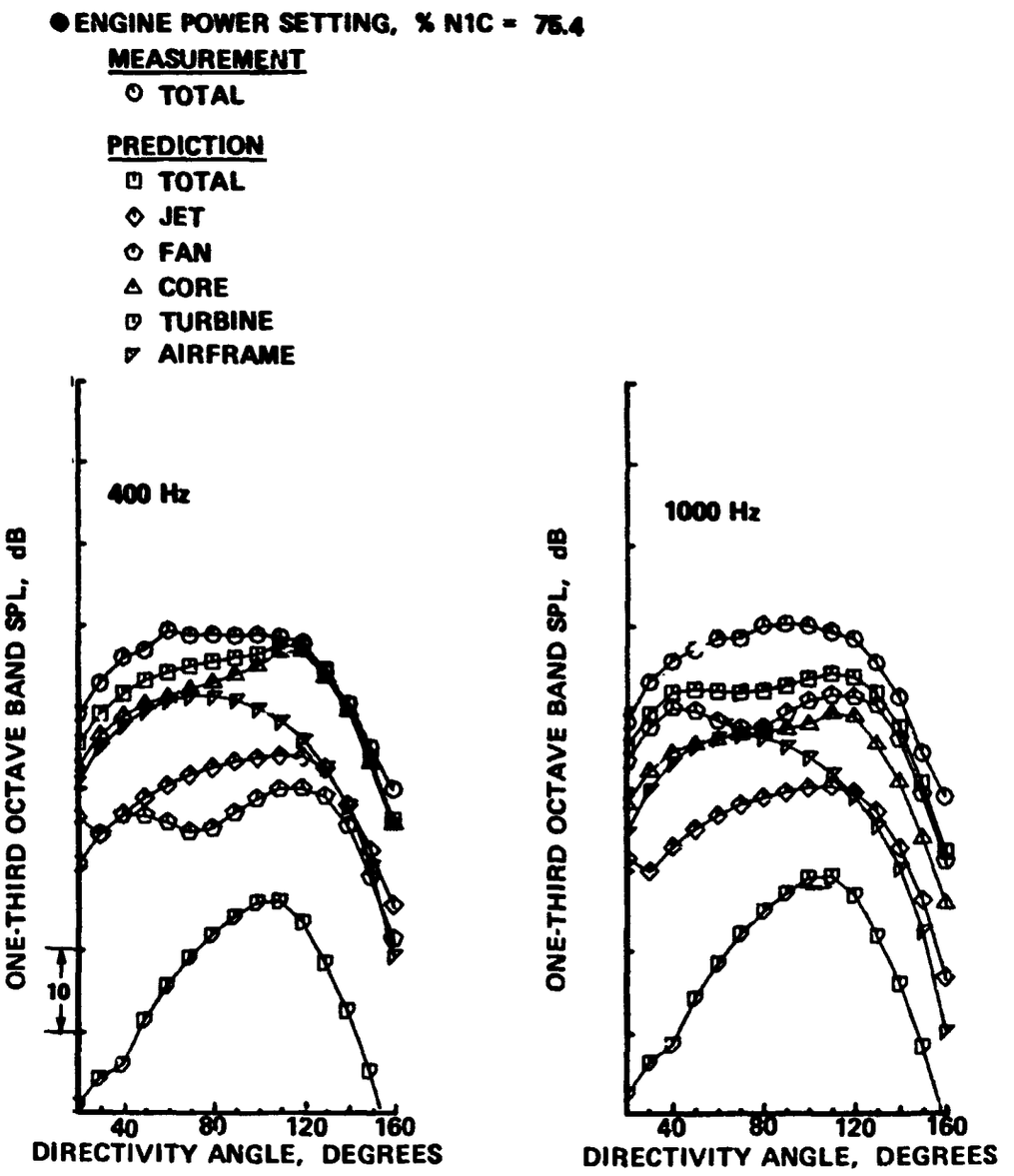

b) 400 Hz AND 1000 Hz

Figure 18. — (Concluded)

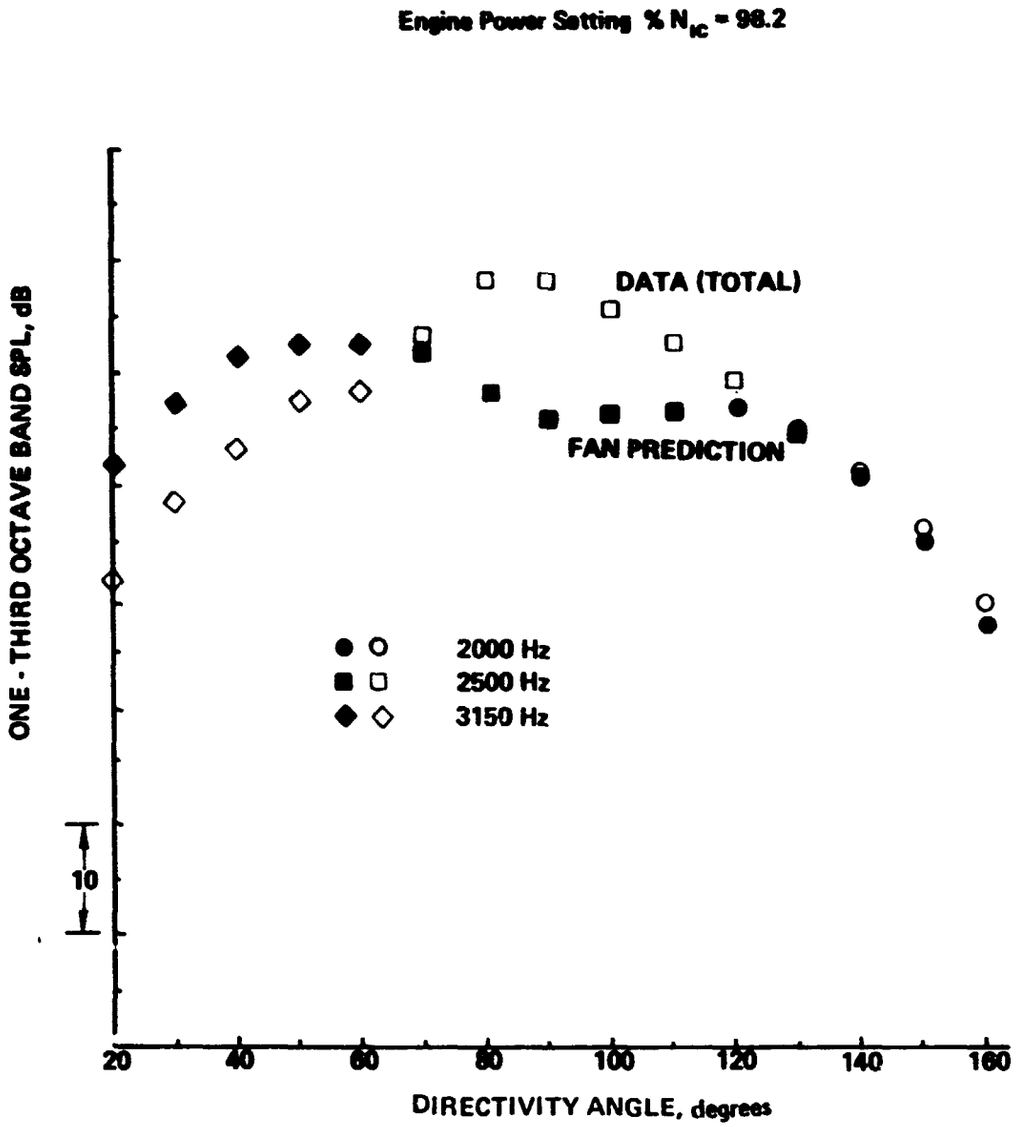

a) Takeoff Power

Figure 19. — Fundamental Fan Tone (F_1) Directivity Comparisons of Data and Prediction

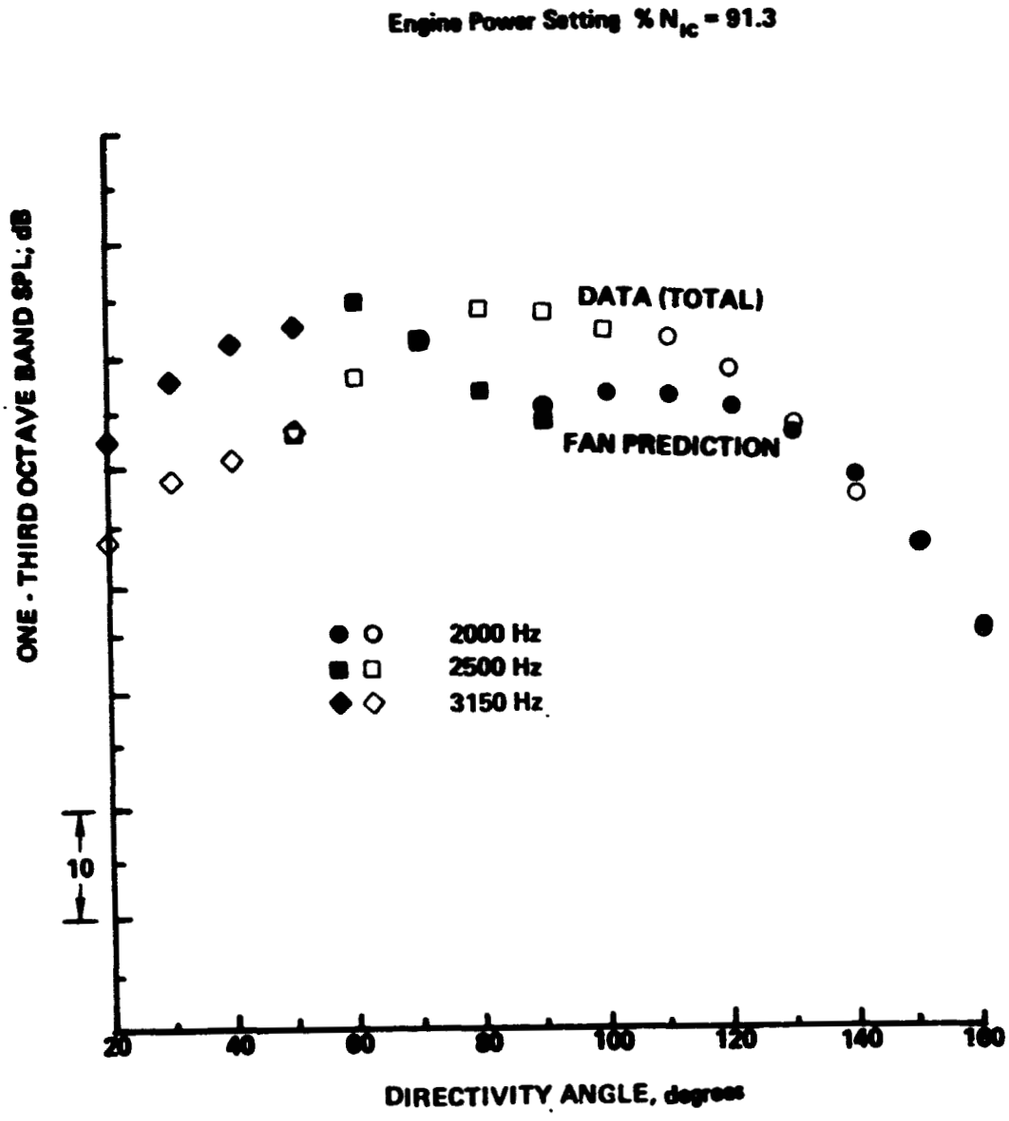

b) Cutback Power

Figure 19. — (Continued)

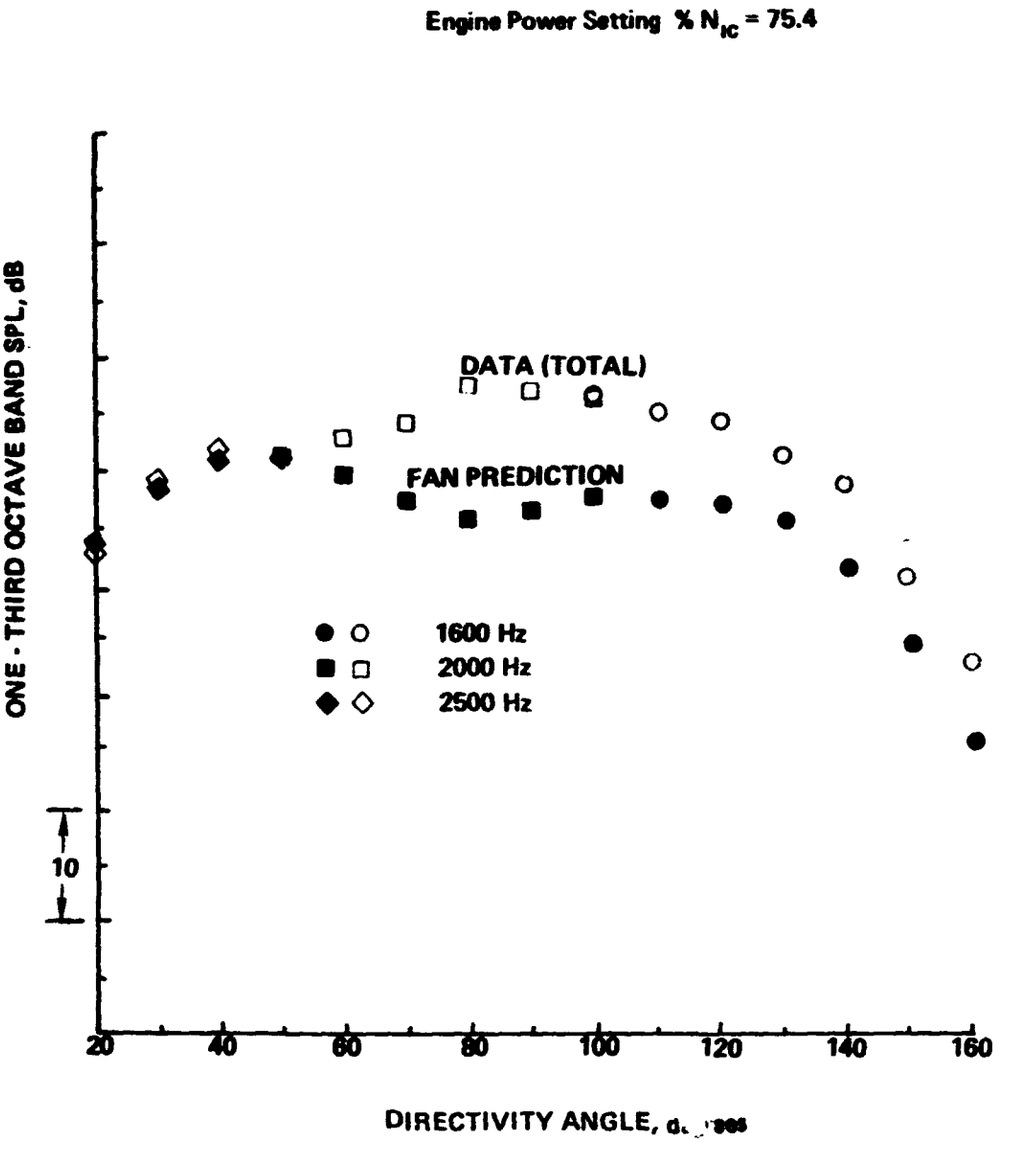

c) Approach Power

Figure 19. – (Concluded)

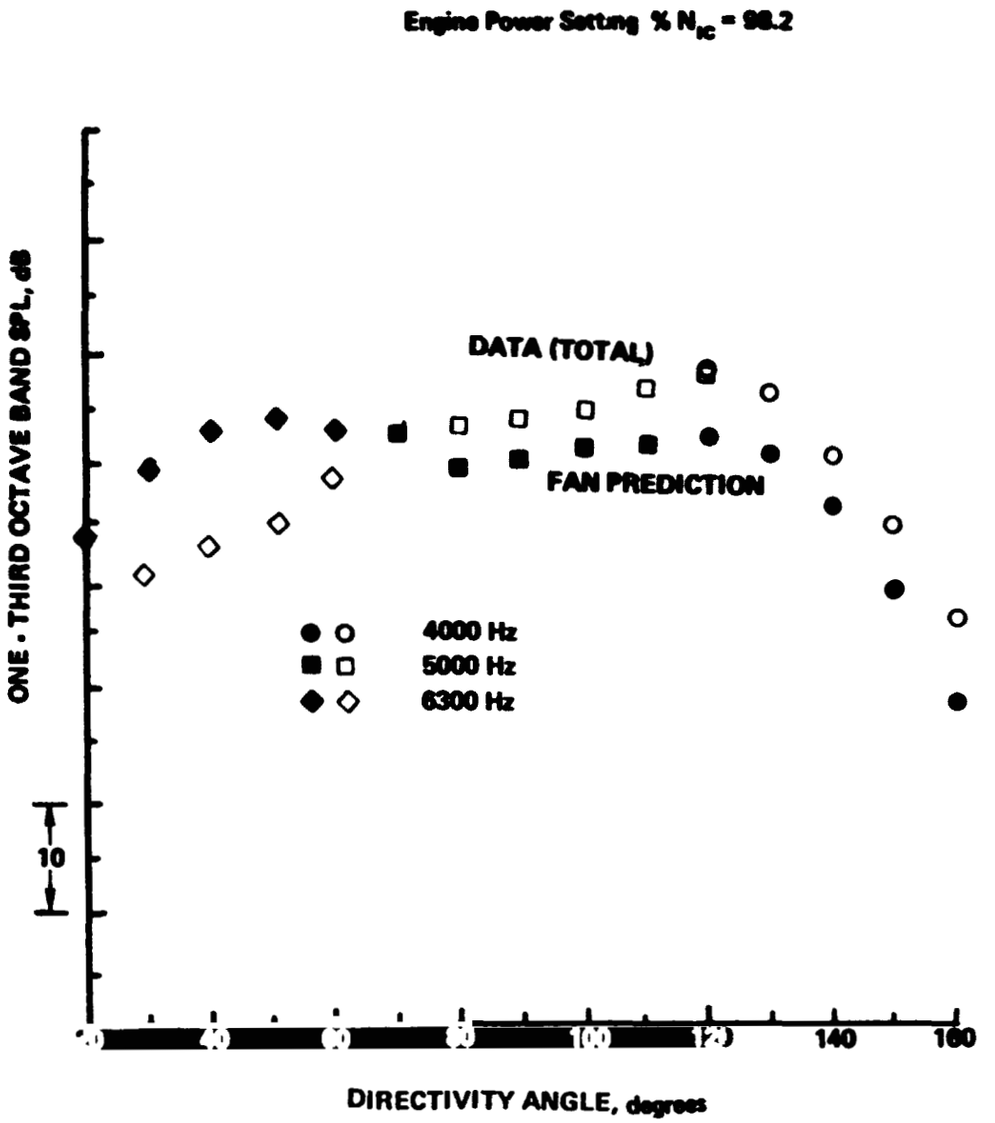

a) Takeoff Power

Figure 20. – Second Harmonic Fan Tone (F_2) Directivity Comparisons of Data and Prediction

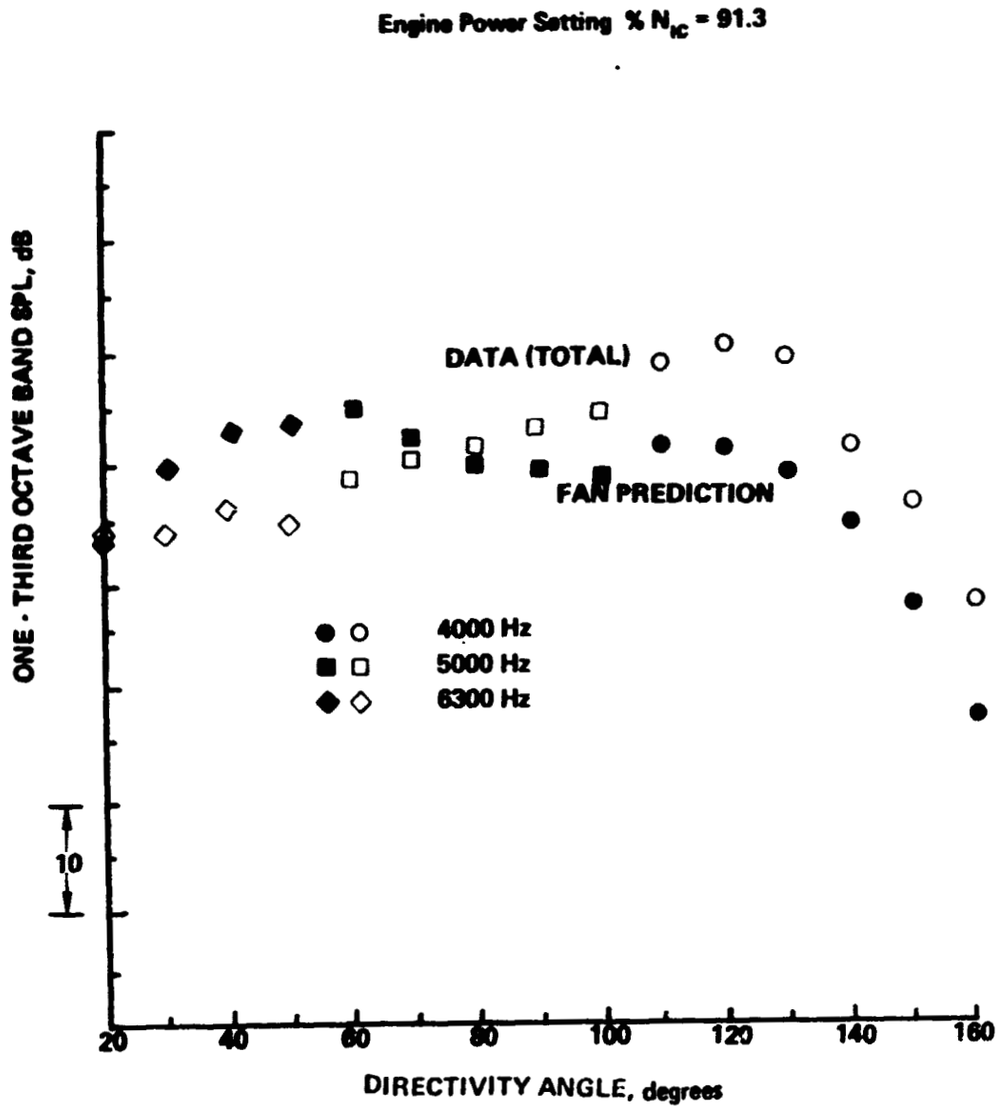

b) Cutback Power

Figure 20. – (Continued)

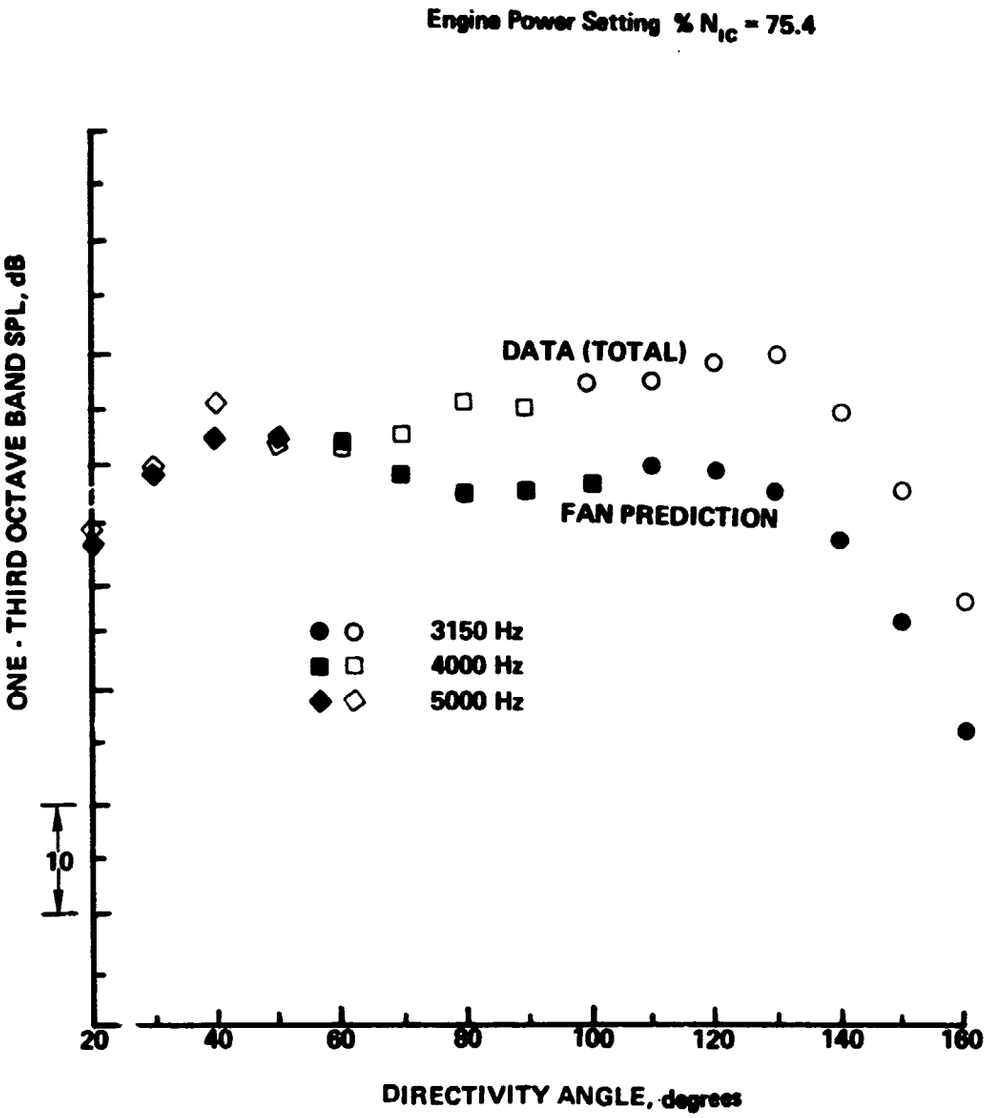

c) Approach Power

Figure 20. – (Concluded)

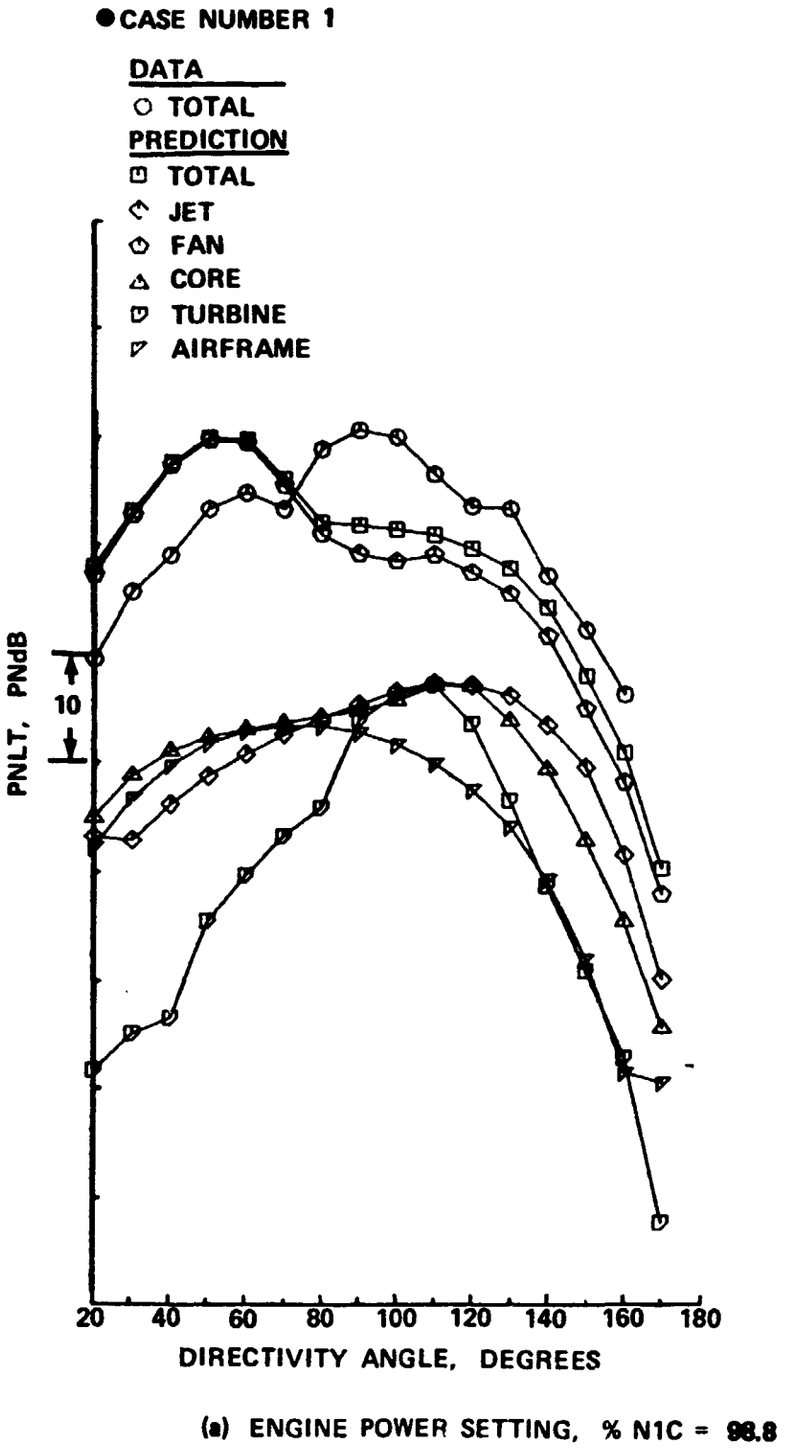

Figure 21. – PNLT Directivity Comparisons of Data and Prediction

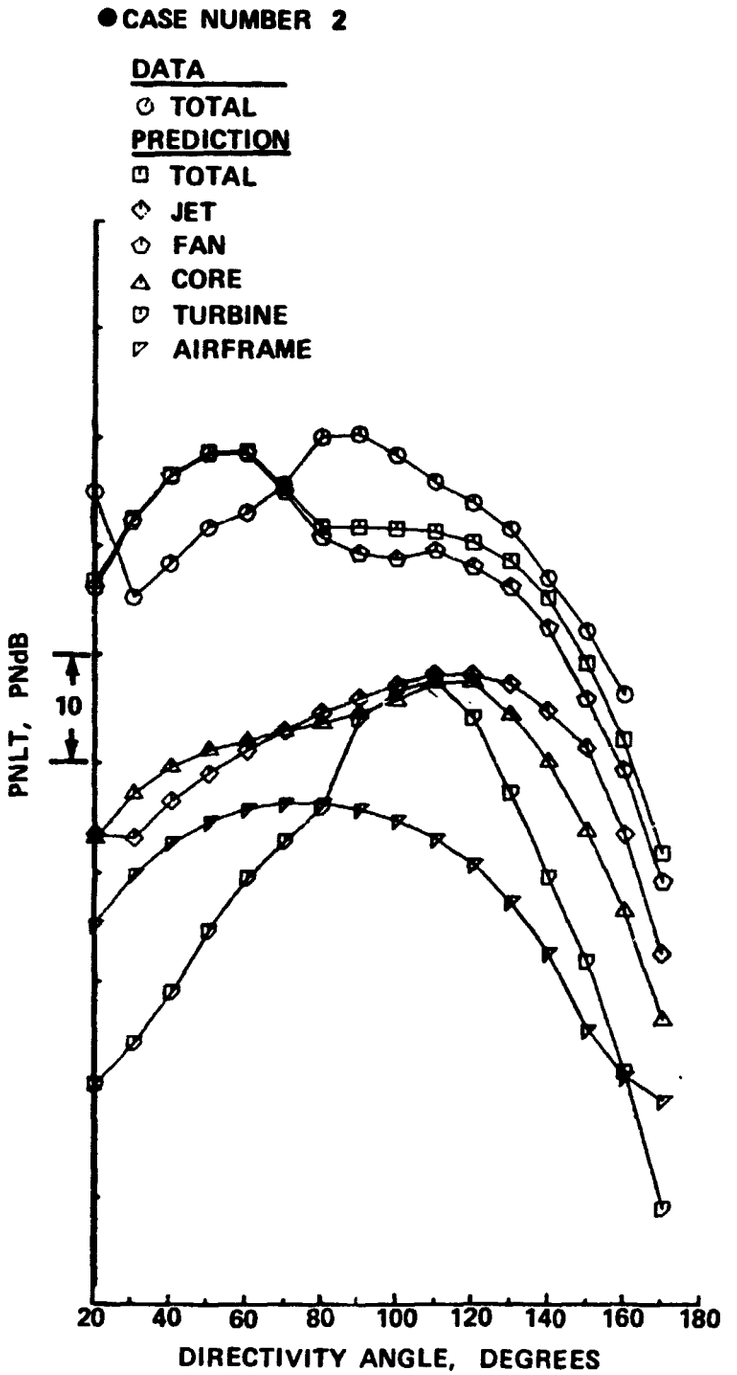

(b) ENGINE POWER SETTING, % N1C = 98.2

Figure 21. — (Continued)

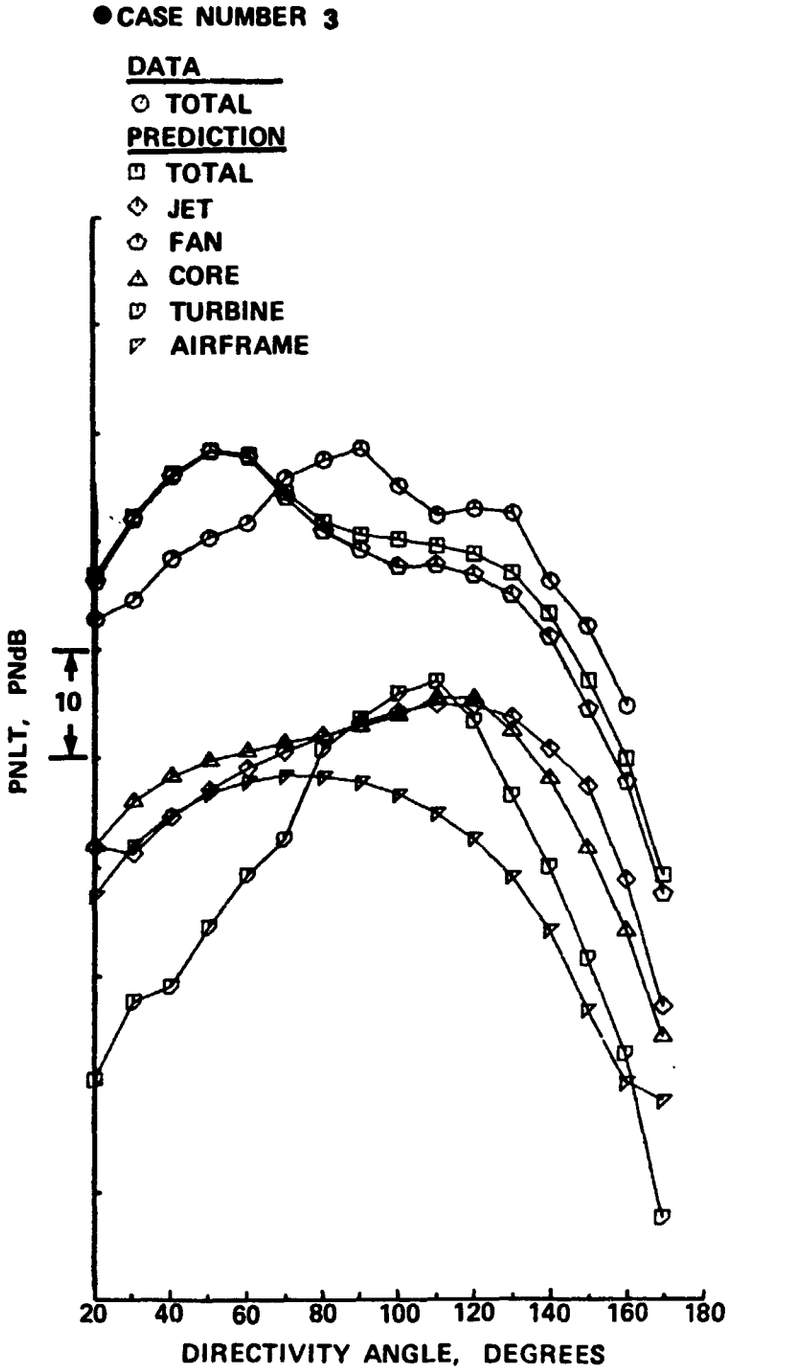

(c) ENGINE POWER SETTING, % N1C = 93.7

Figure 21. – (Continued)

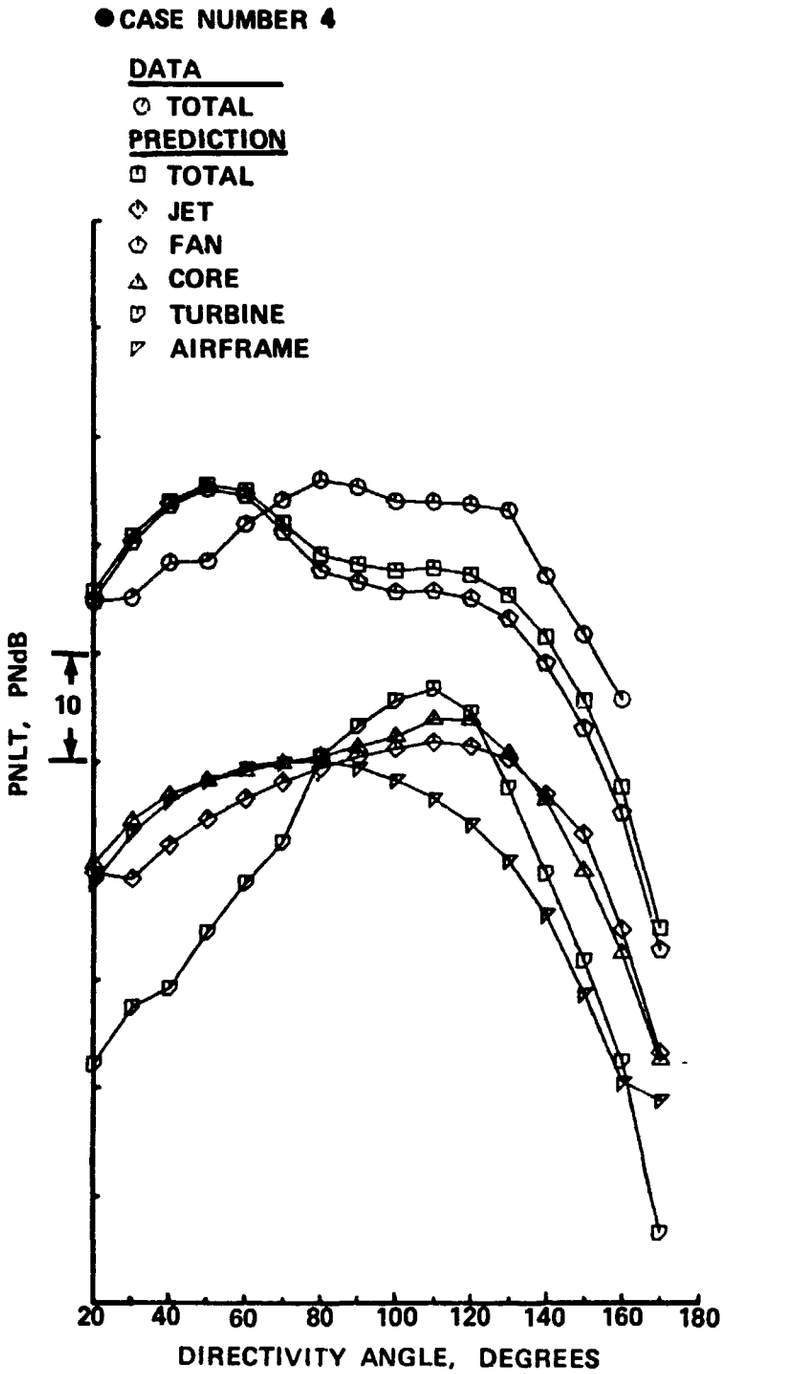

(d) ENGINE POWER SETTING, % N1C = 89.5

Figure 21. – (Continued)

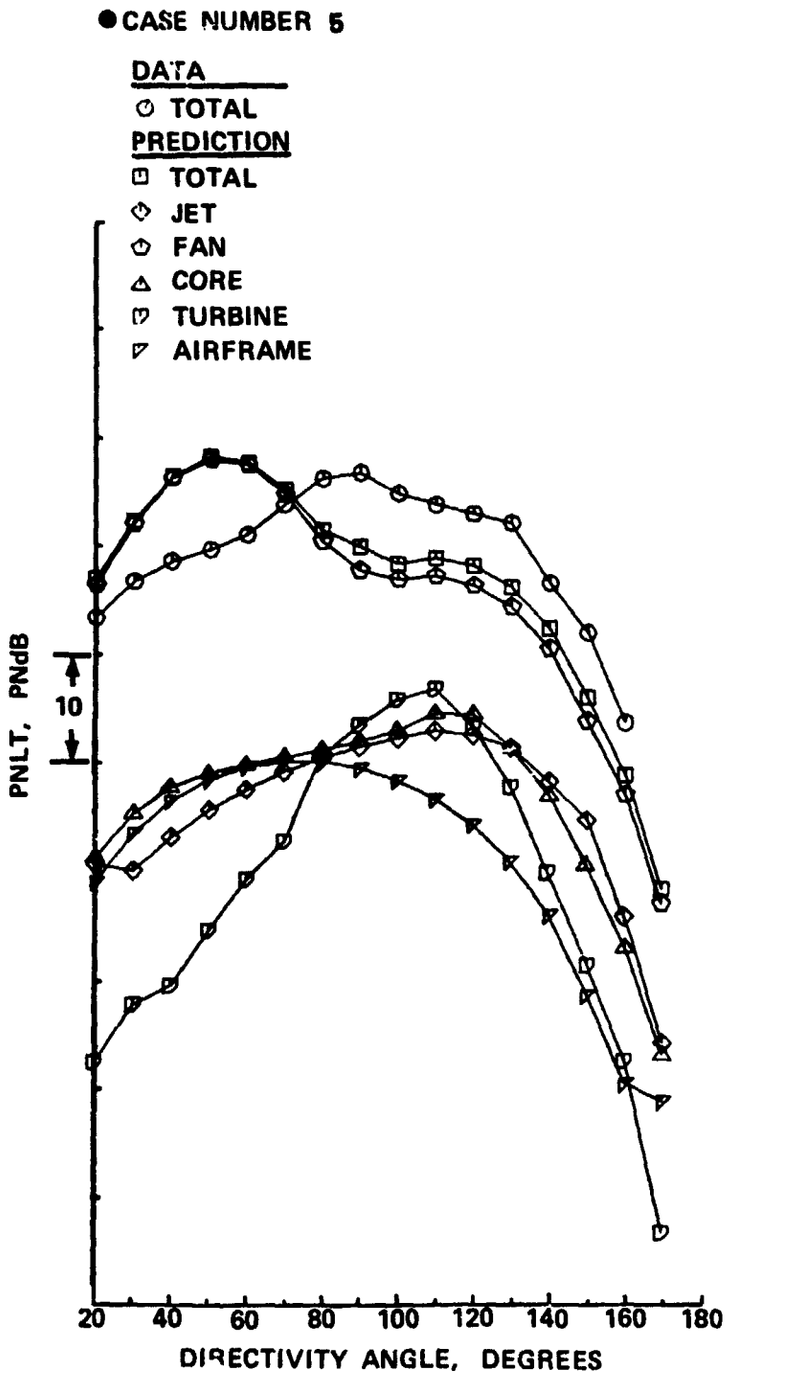

(e) ENGINE POWER SETTING, % N1C = 91.0

Figure 21. – (Continued)

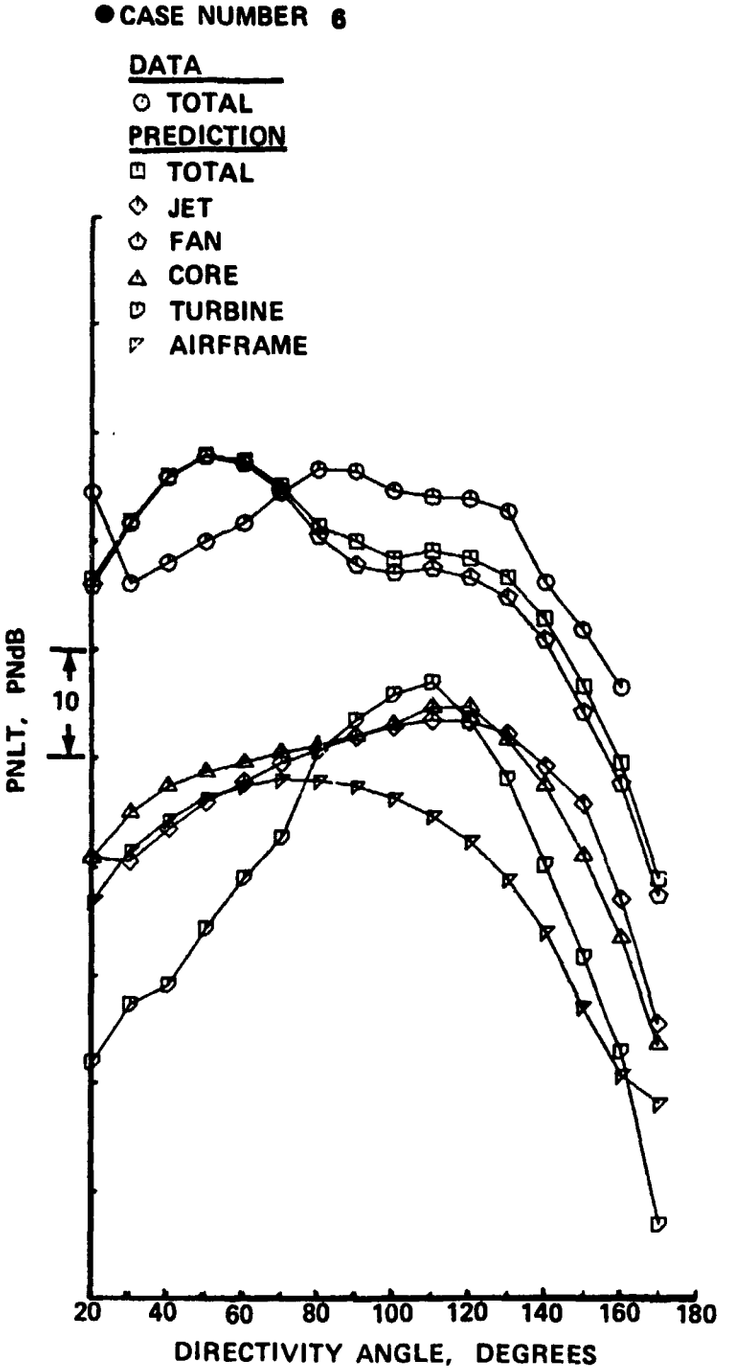

(f) ENGINE POWER SETTING, % N1C = 91.3

Figure 21. – (Continued)

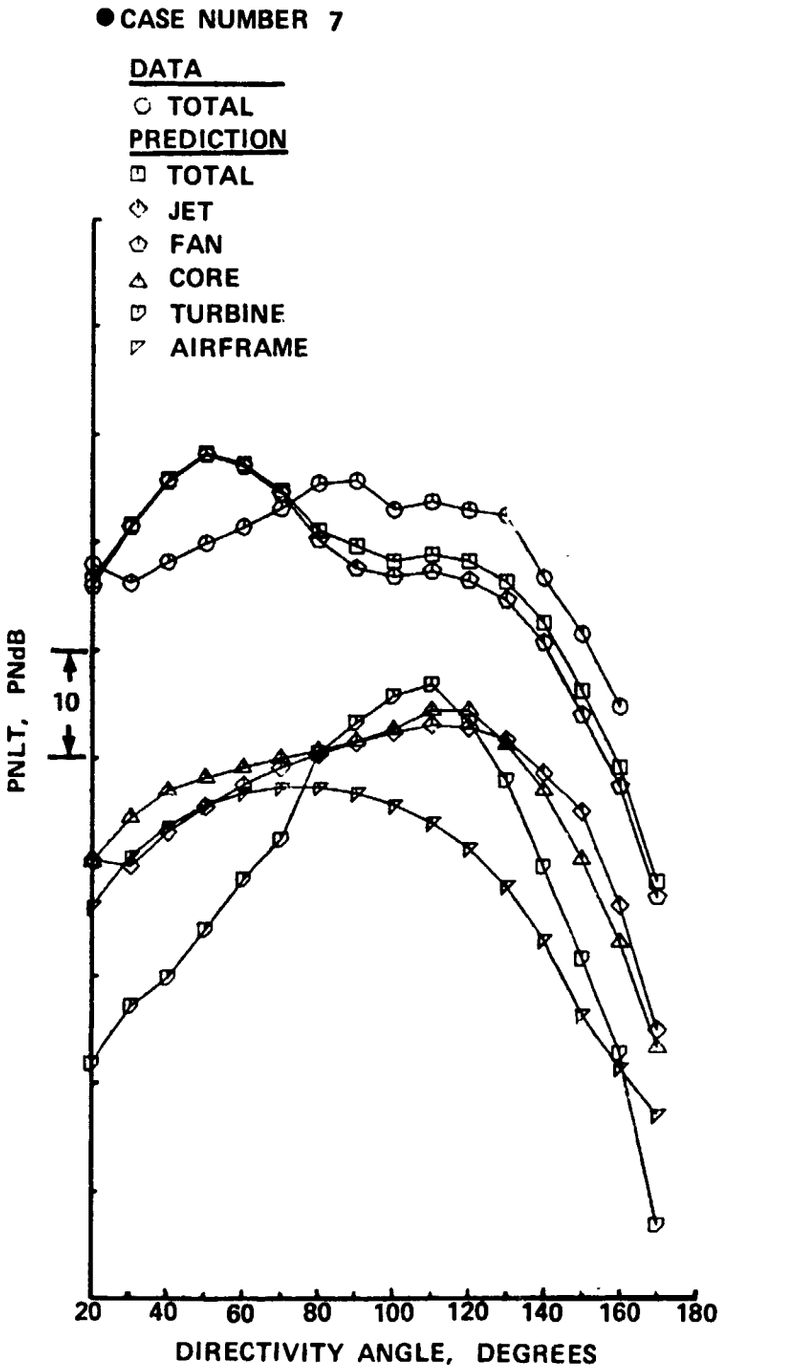

(g) ENGINE POWER SETTING, % N1C = 90.7

Figure 21. – (Continued)

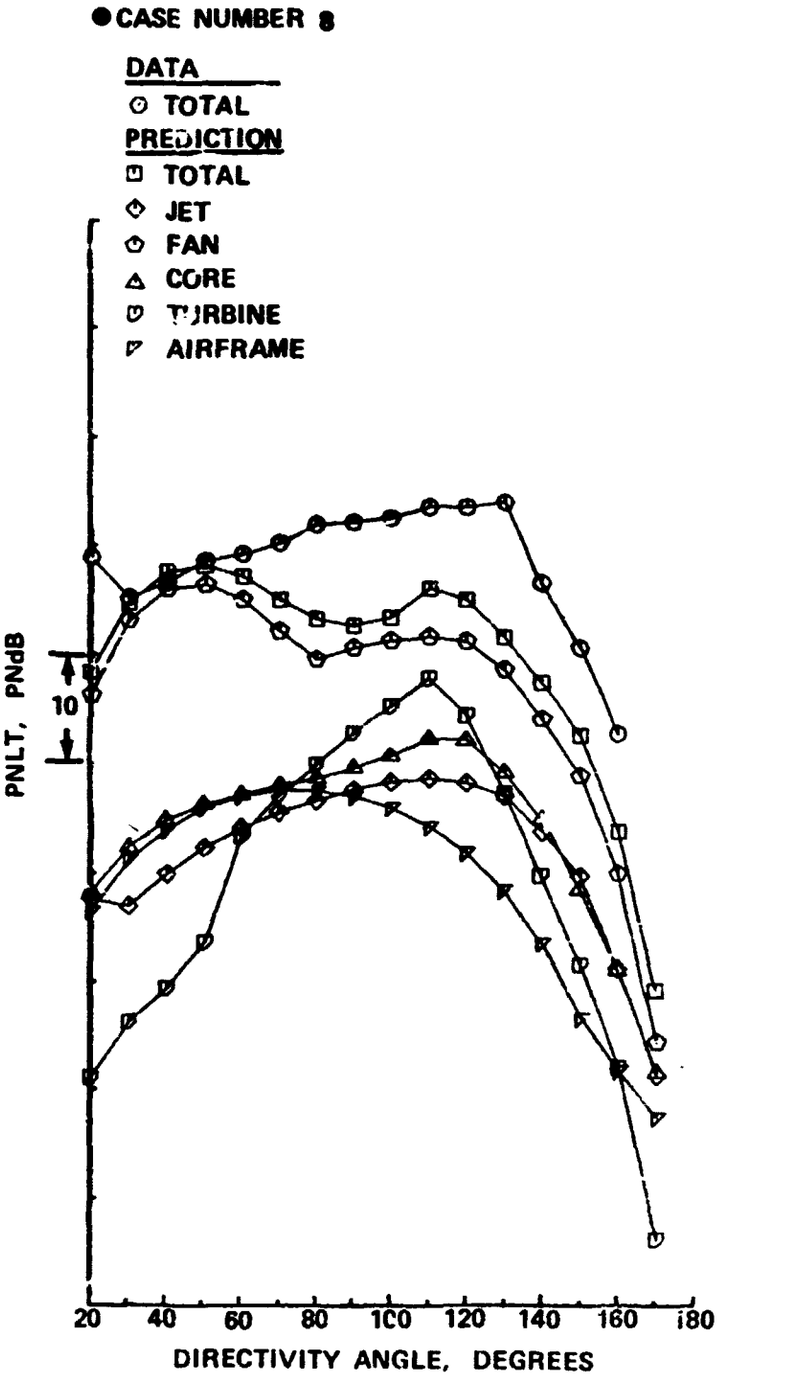

(h) ENGINE POWER SETTING, % N1C = 84.4

Figure 21. — (Continued)

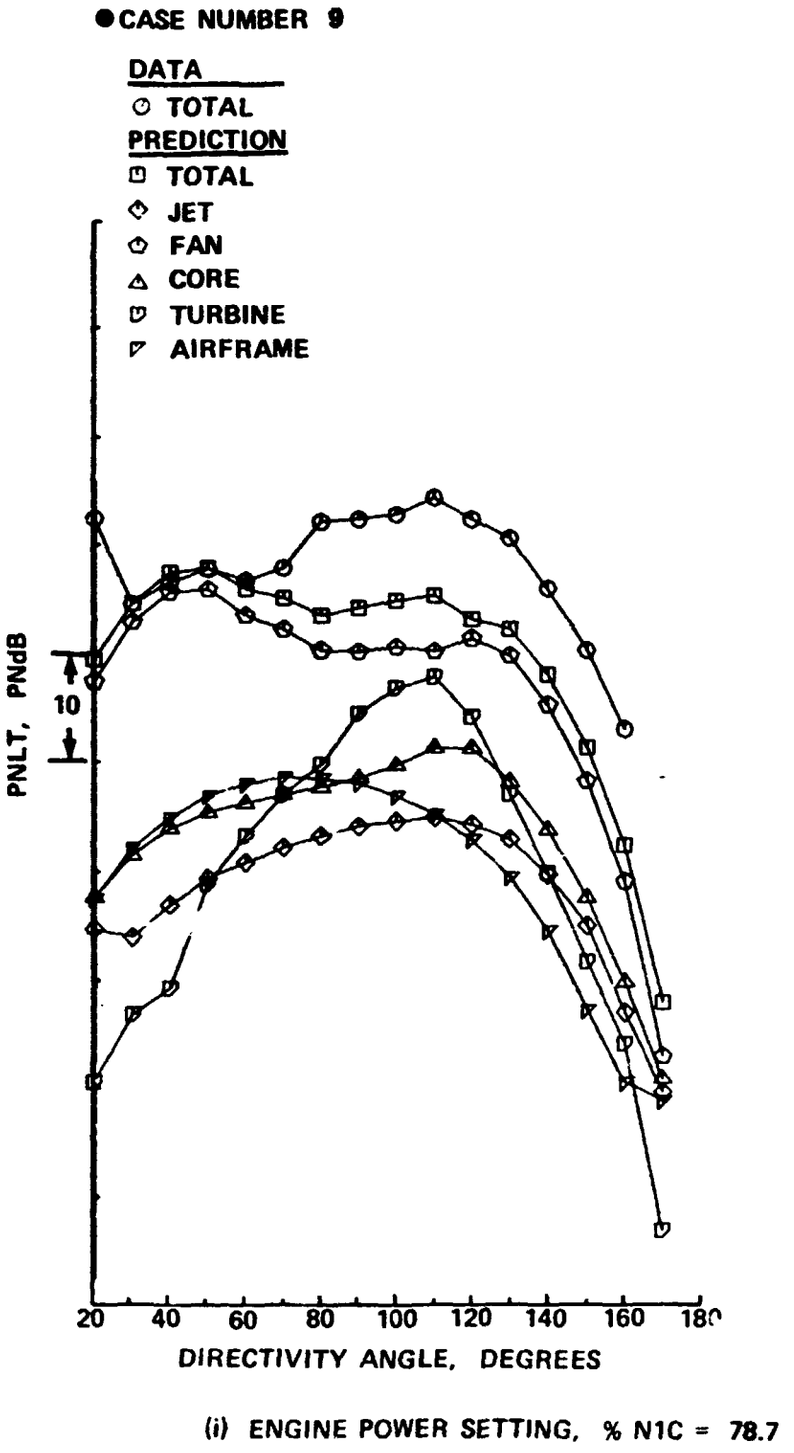

(i) ENGINE POWER SETTING, % N1C = 78.7

Figure 21. – (Continued)

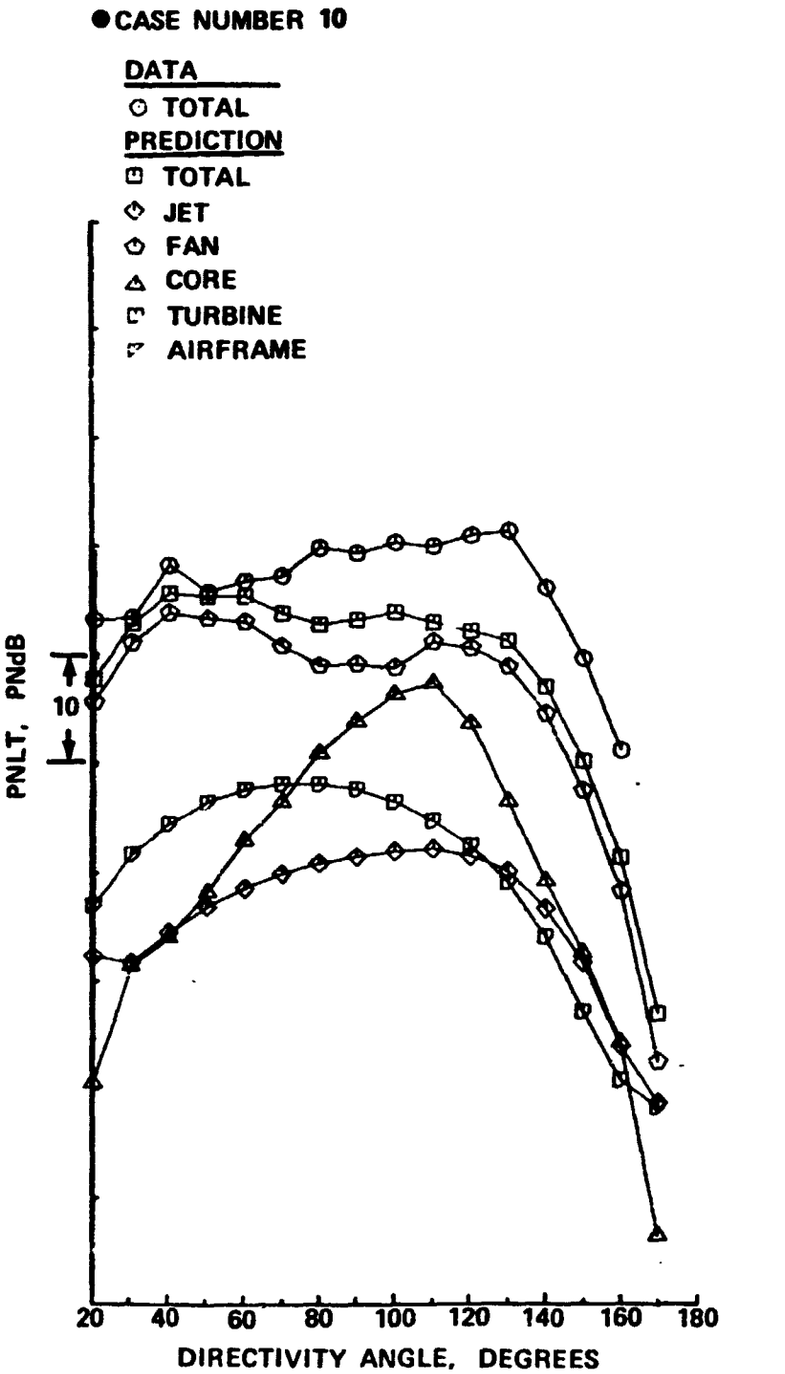

(j) ENGINE POWER SETTING, % N1C = 75.4

Figure 21. – (Concluded)

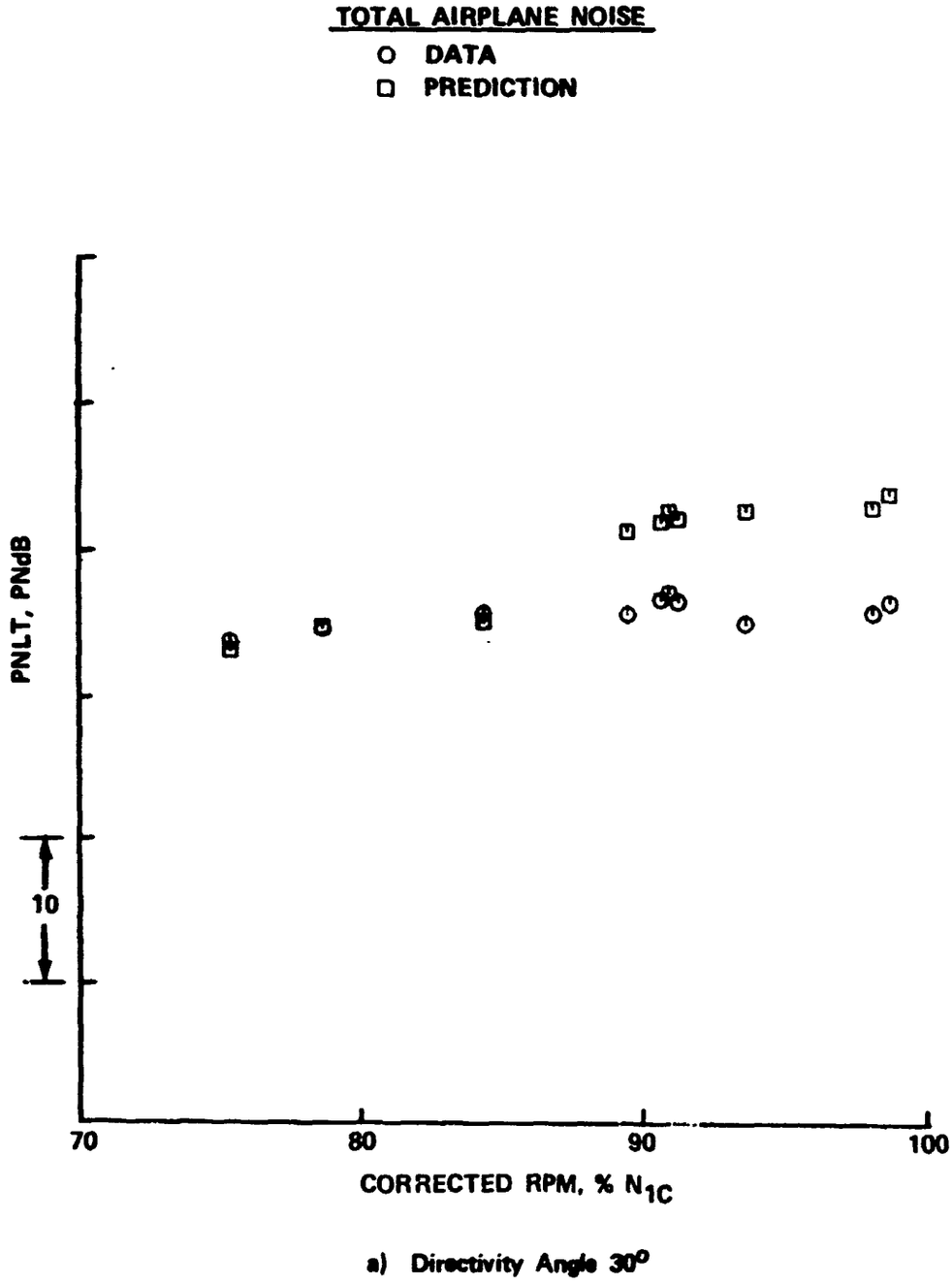

Figure 22. -- PNLT Comparisons as a Function of Corrected RPM

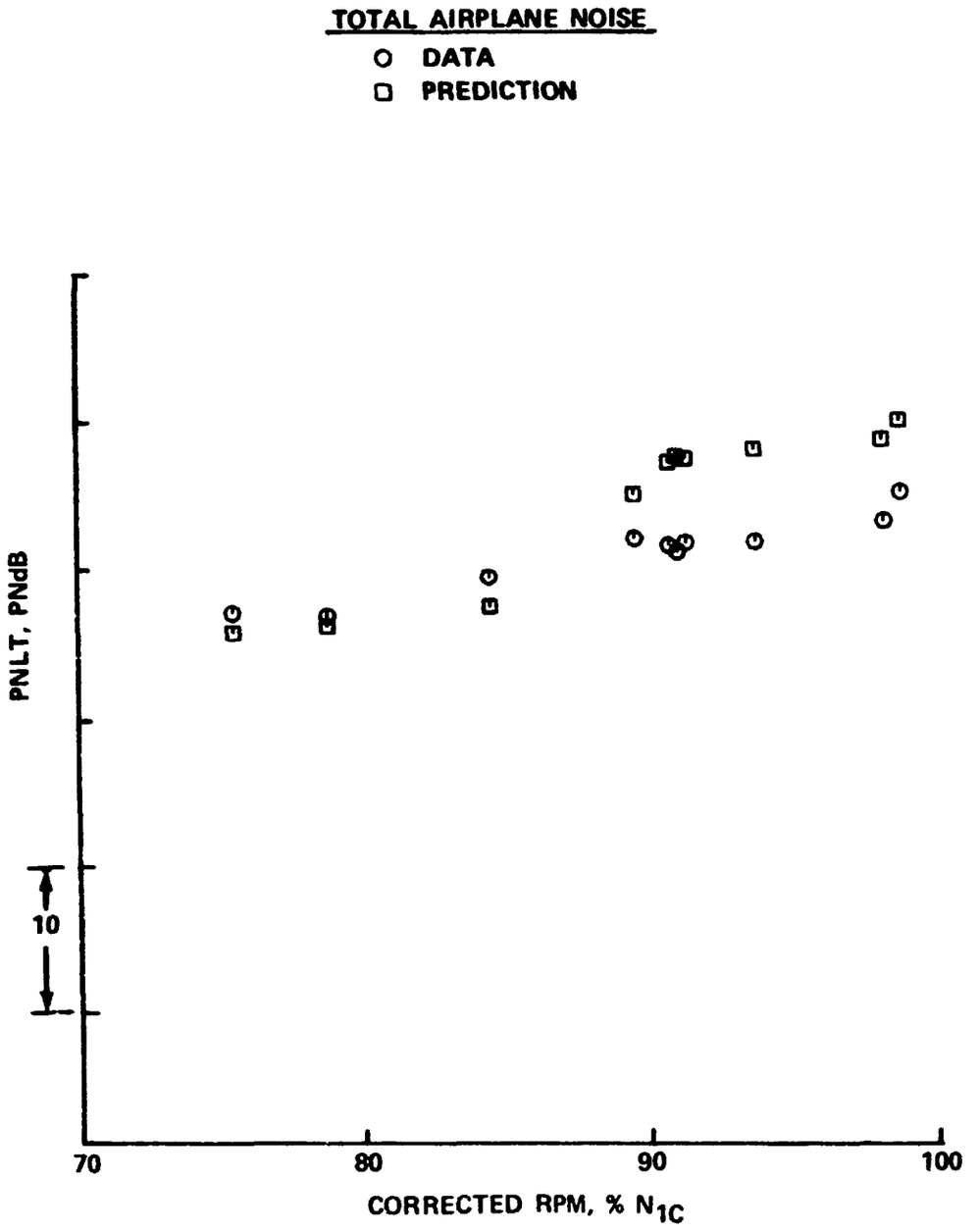

b) Directivity Angle 60°

Figure 22. – (Continued)

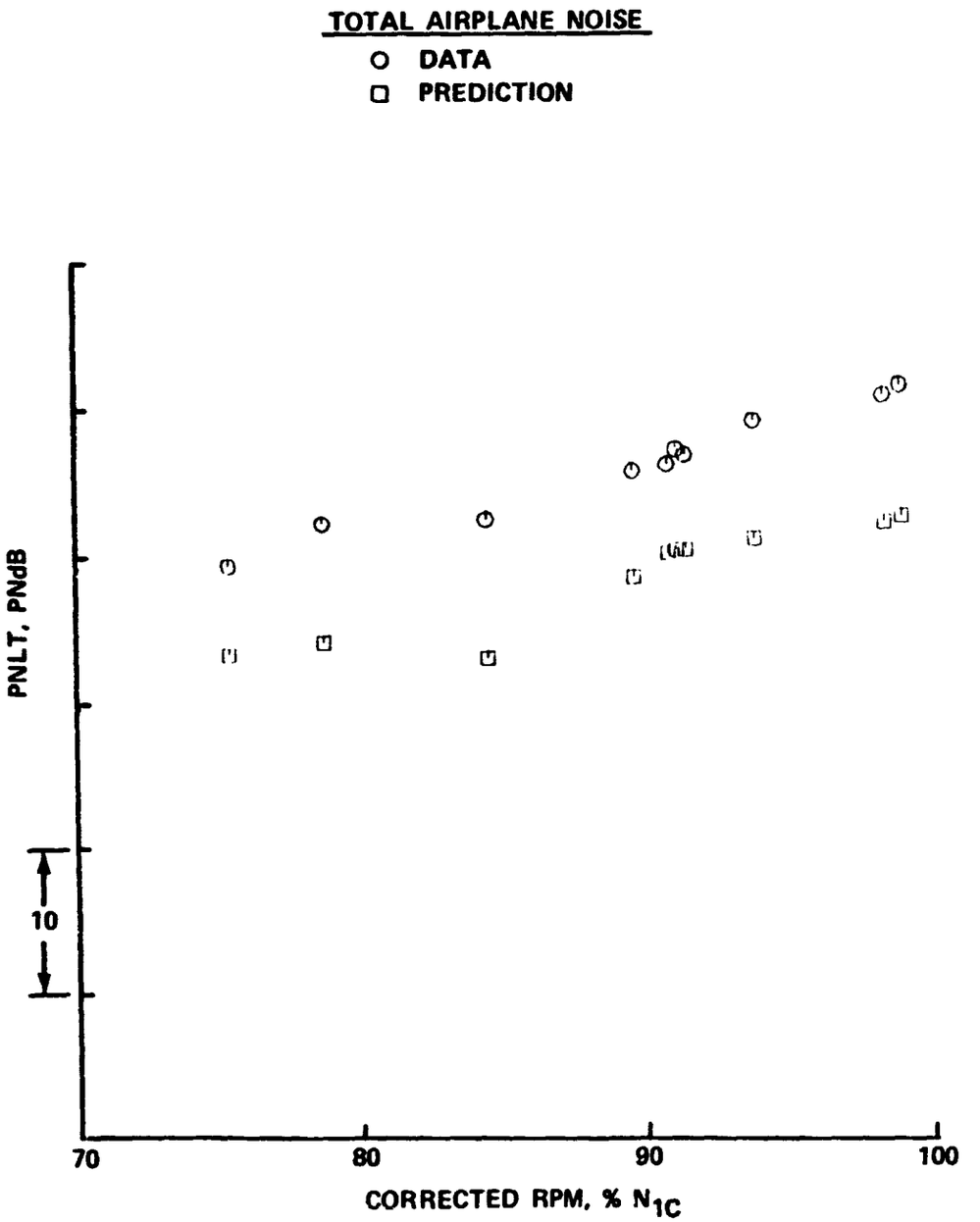

c) Directivity Angle 90°

Figure 22. – (Continued)

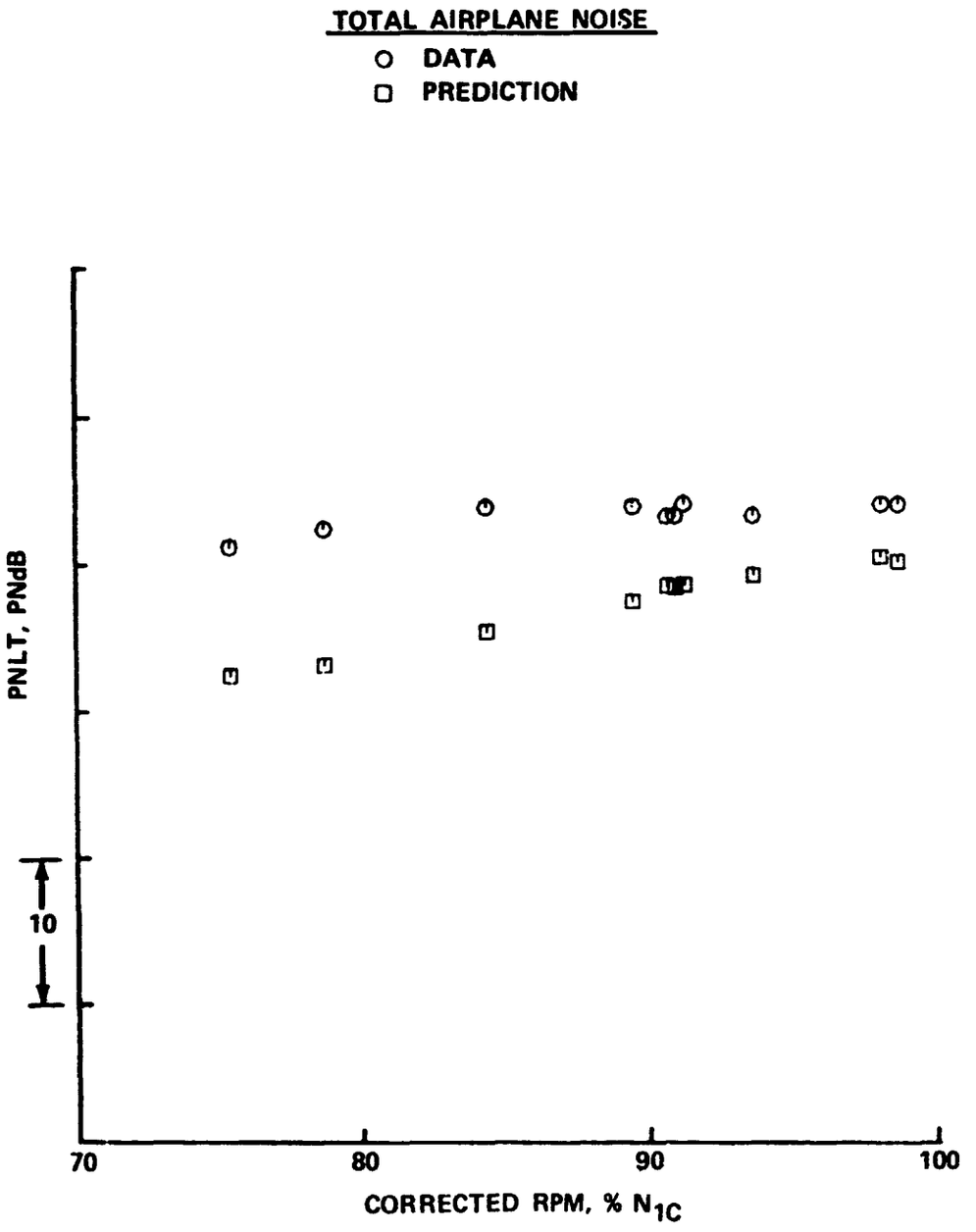

d) Directivity Angle 120°

Figure 22. – (Continued)

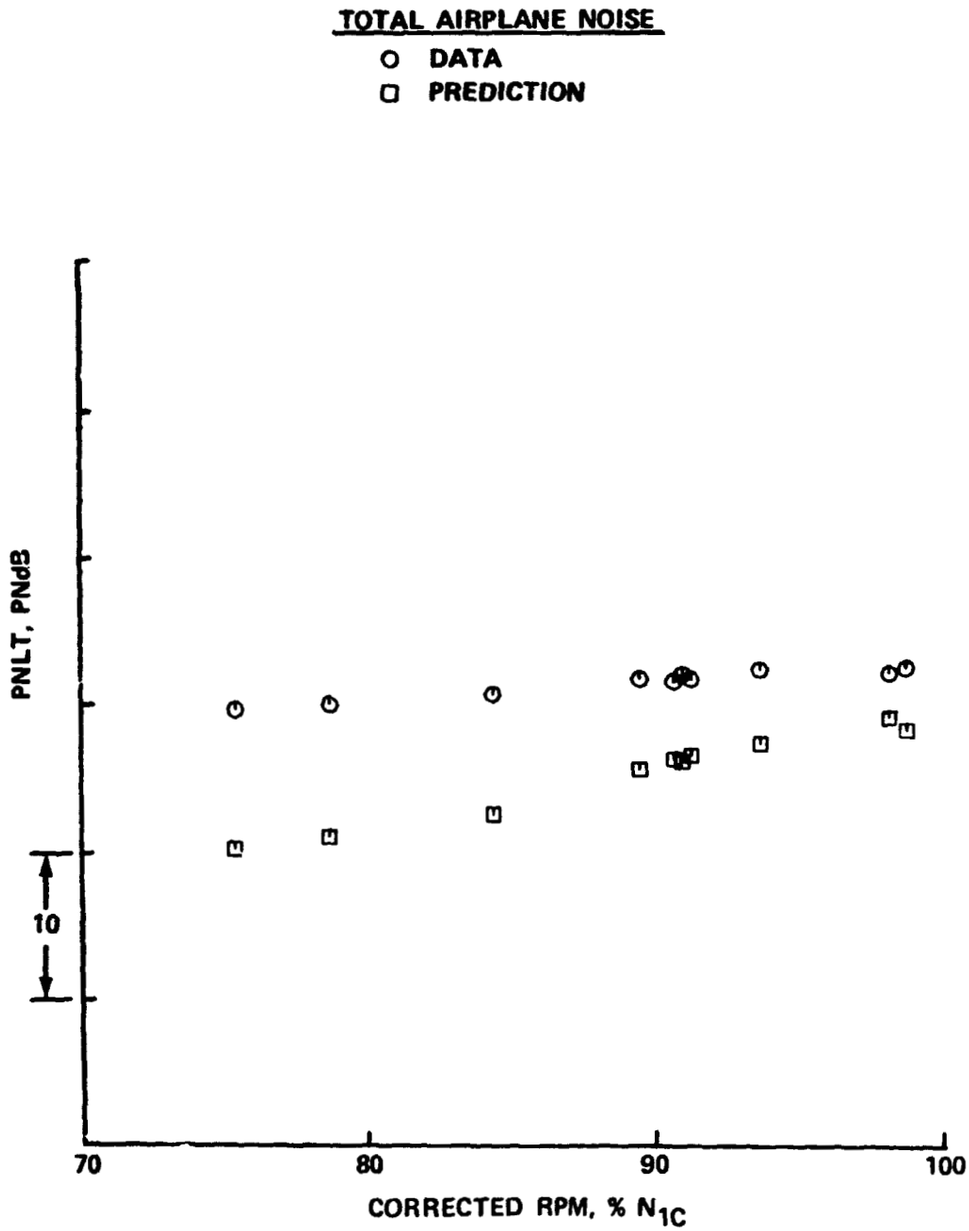

e) Directivity Angle 150°

Figure 22. – (Concluded)

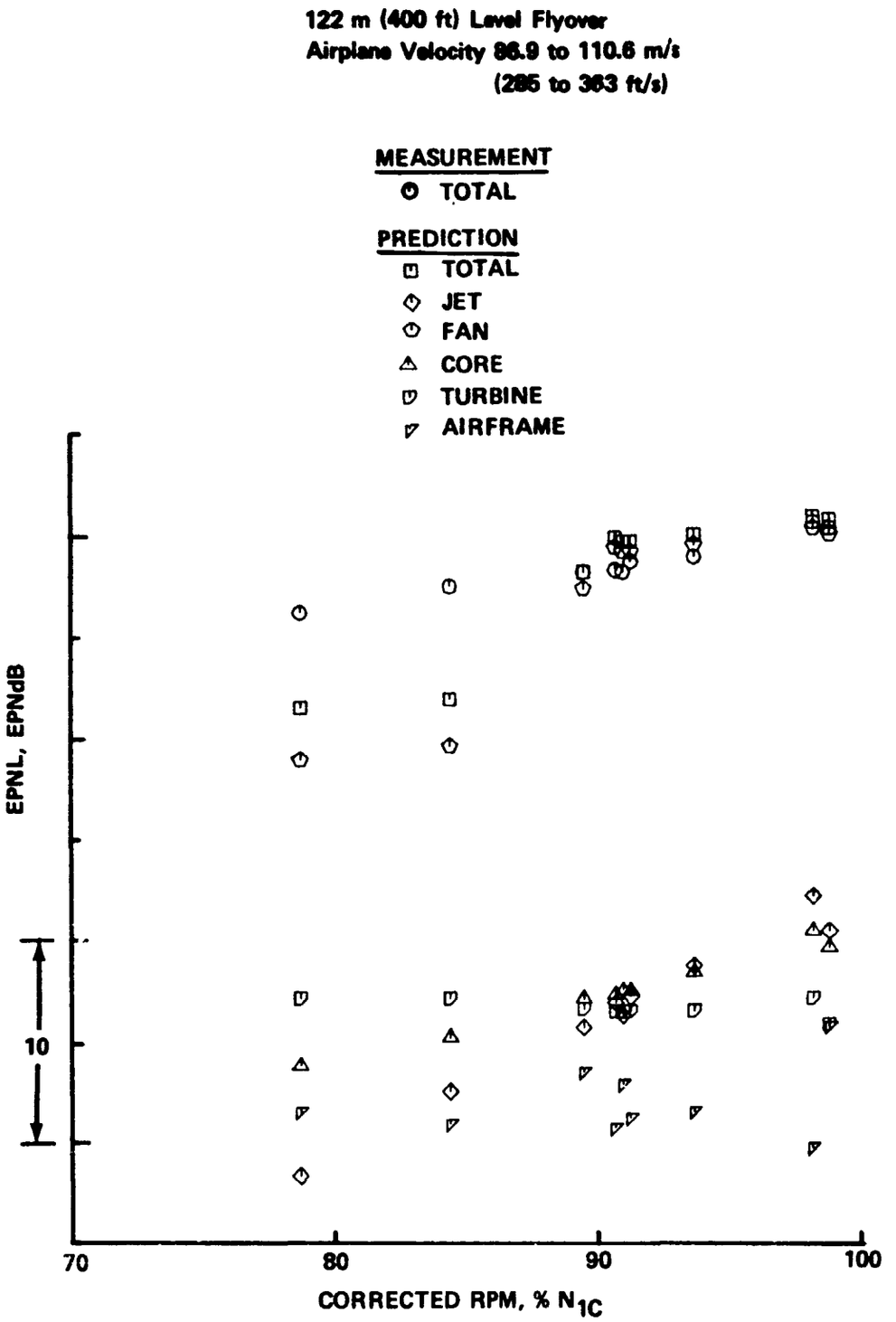

Figure 23. – EPNL Comparisons as a Function of Corrected RPM

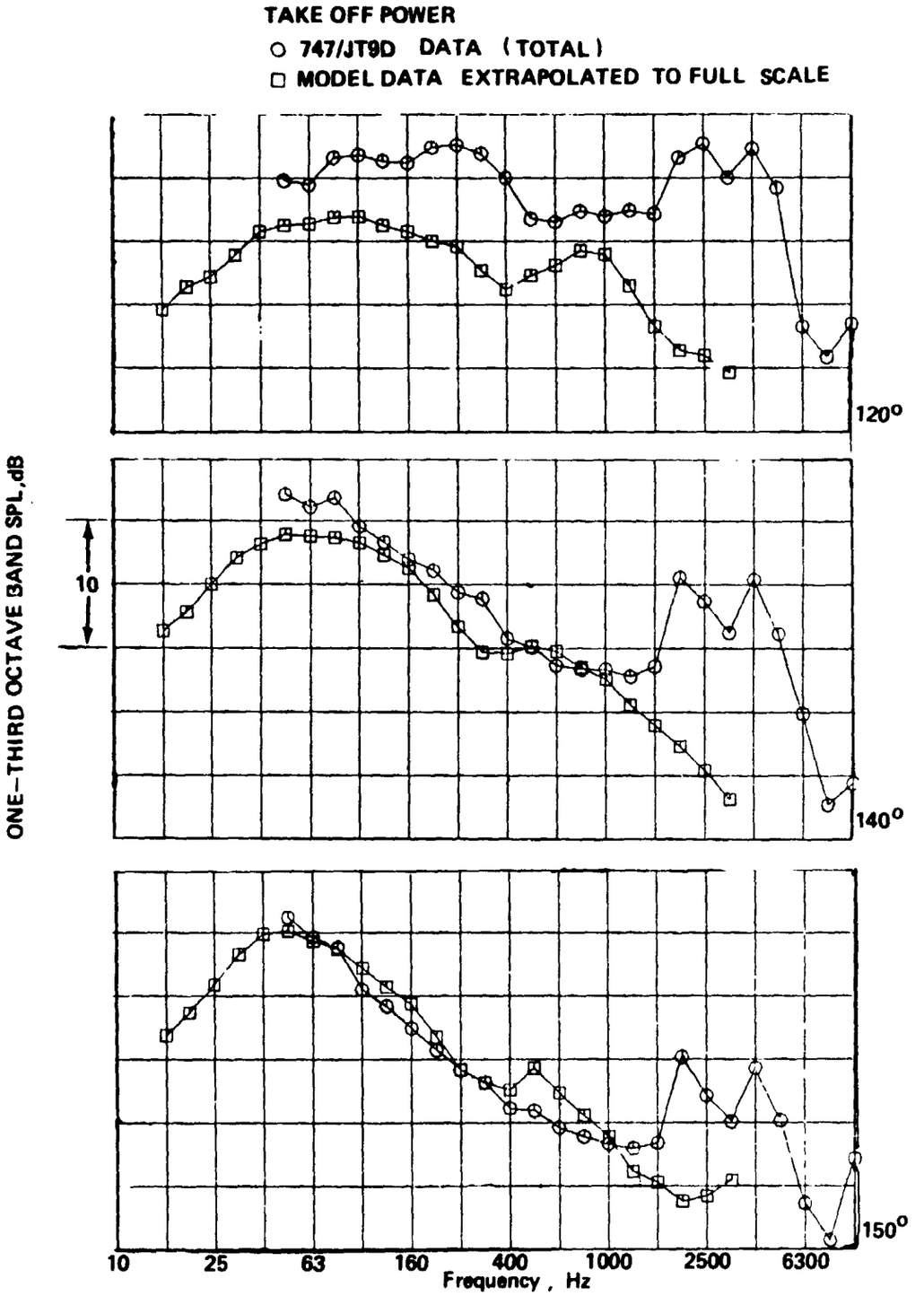

Figure 24.—Spectral Comparisons of 747/JT9D Flyover and Model Scale Jet Noise Data

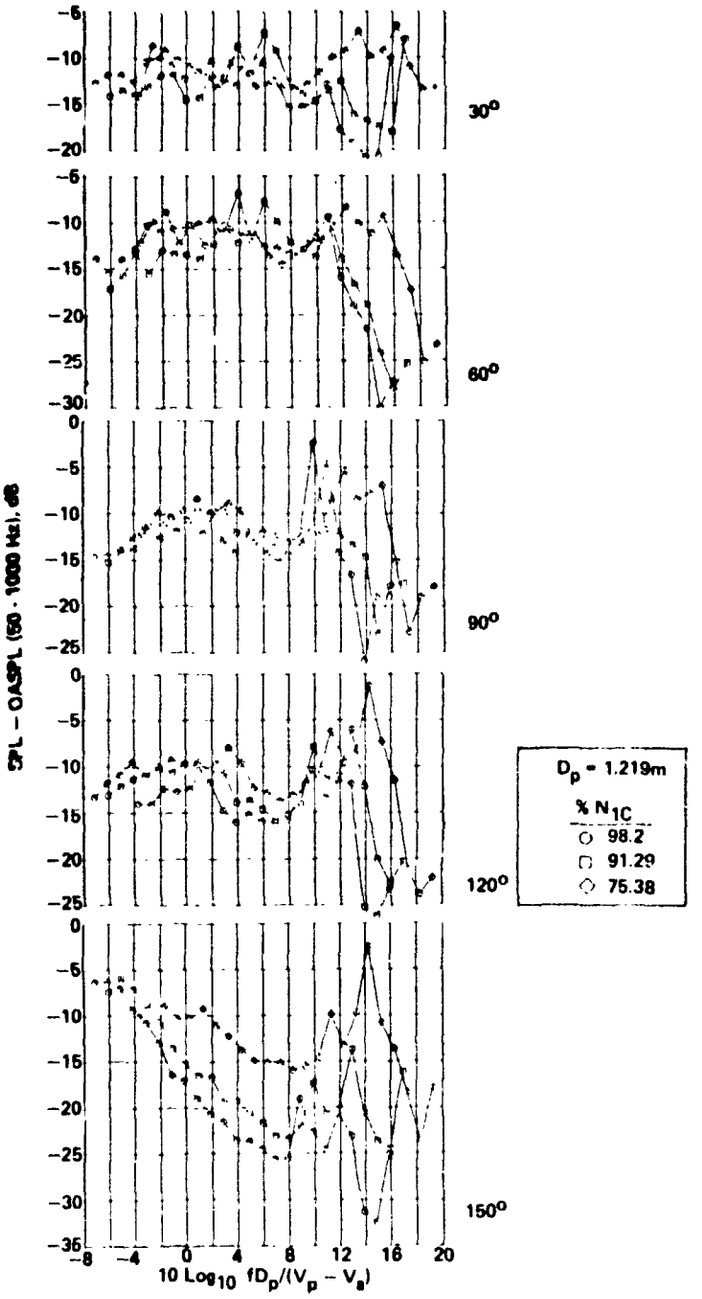

Figure 25.–Normalized Spectra for Jet Noise Component Separation

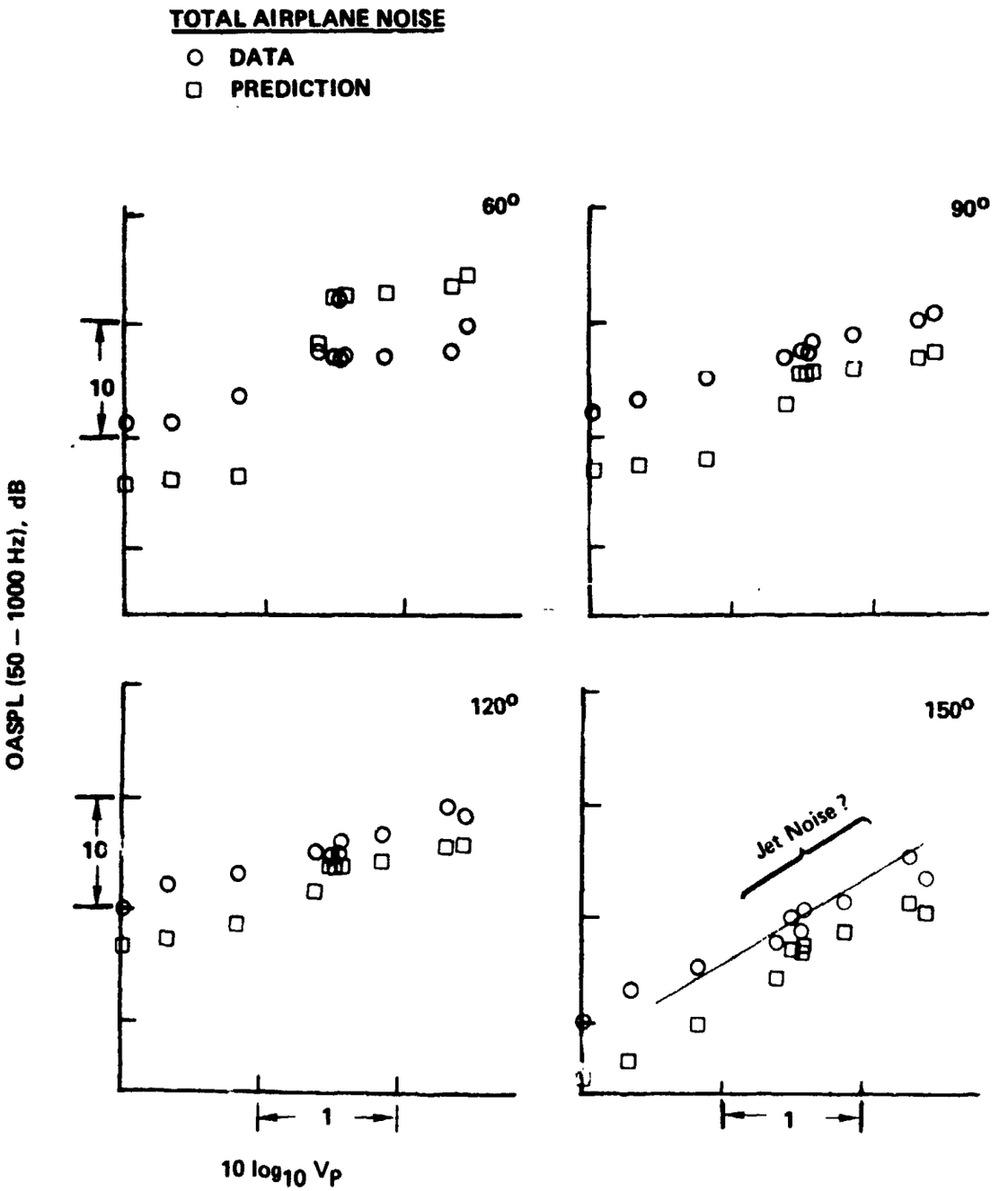

Figure 26. – Overall SPL Comparisons as a Function of Primary Jet Velocity

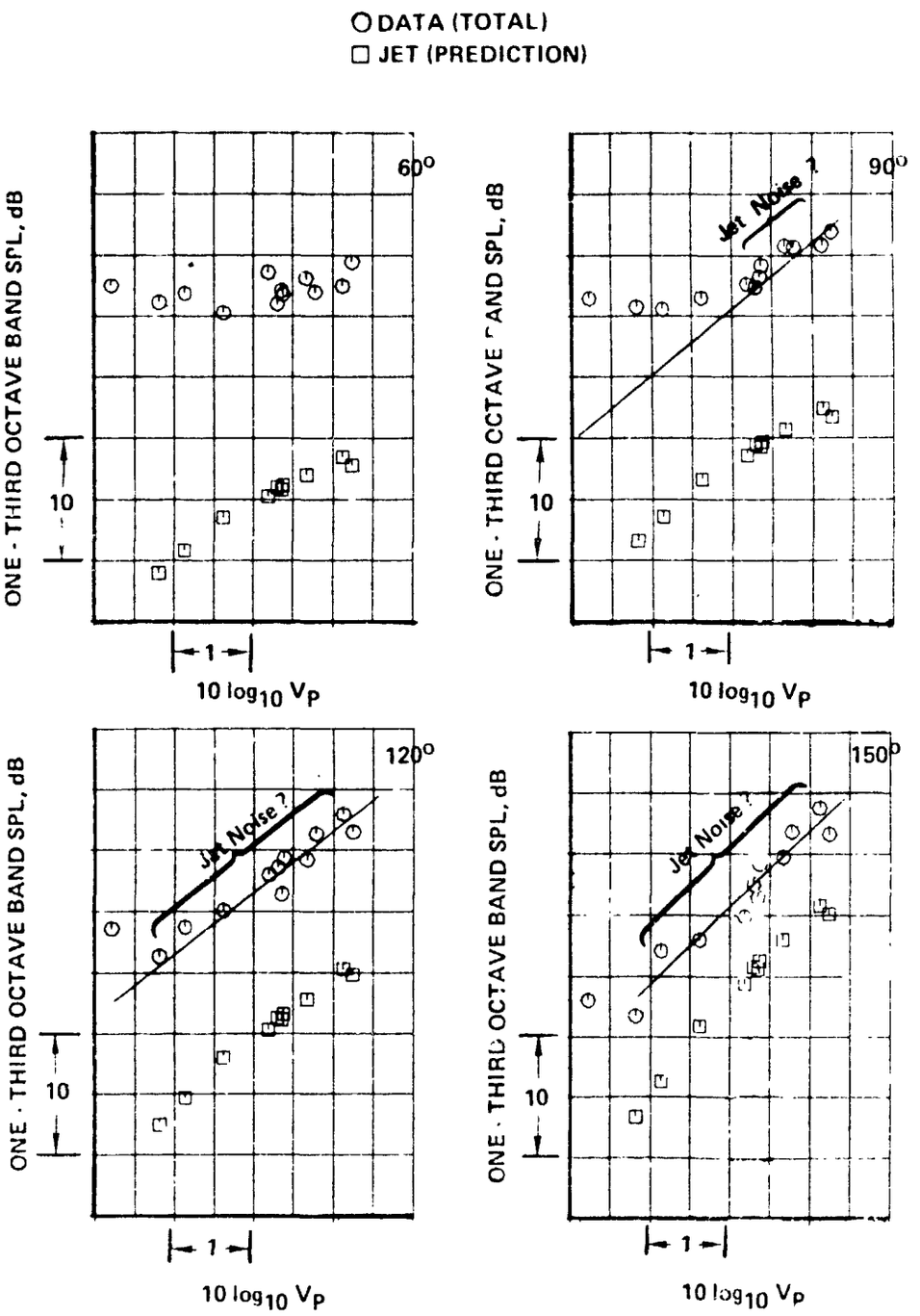

(a) 63 Hz

Figure 27.—SPL Comparisons as a Function of Primary Jet Velocity

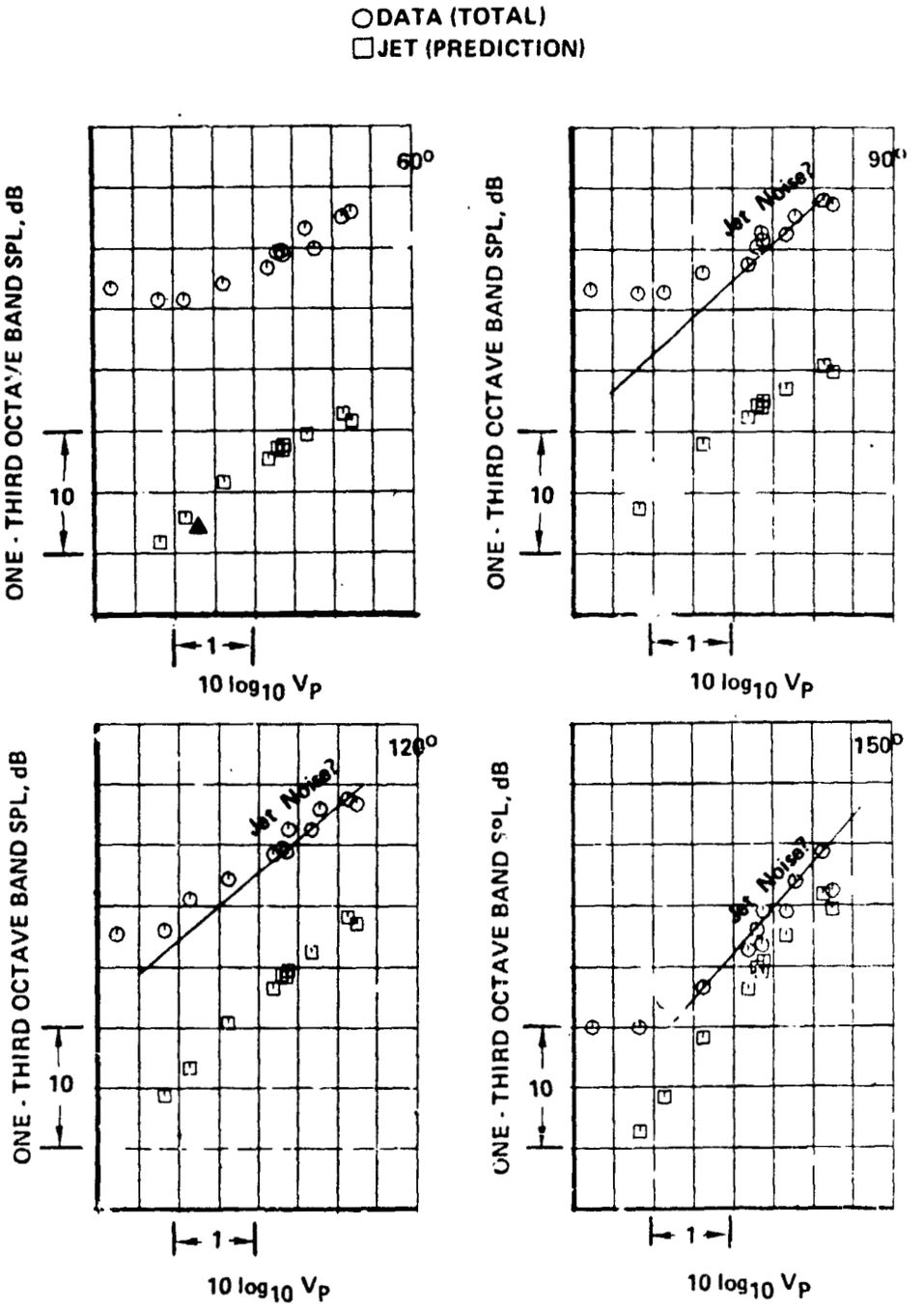

(b) 125 Hz

Figure 27.—(Continued)

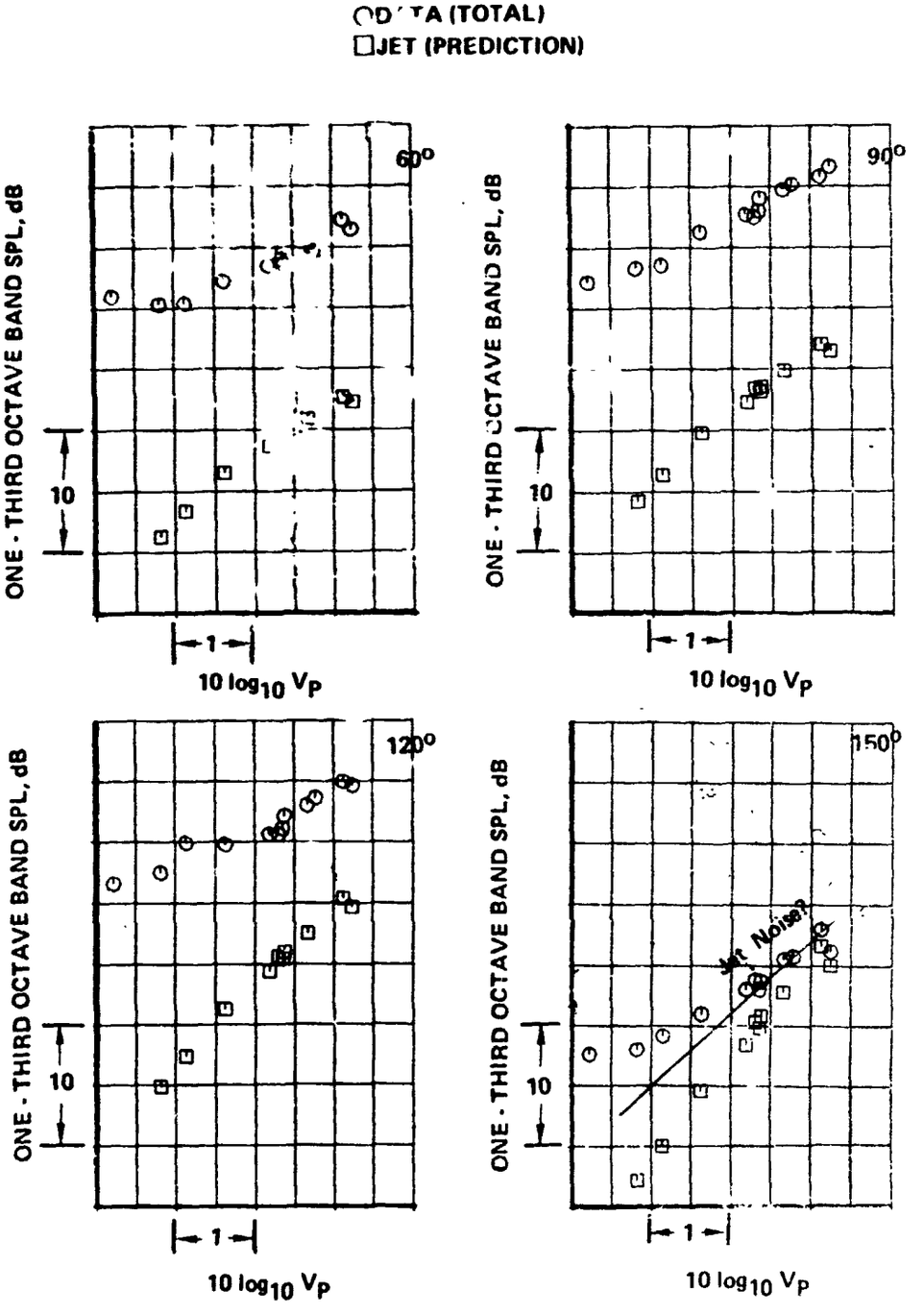

(c) 250 Hz

Figure 27.—(Concluded)

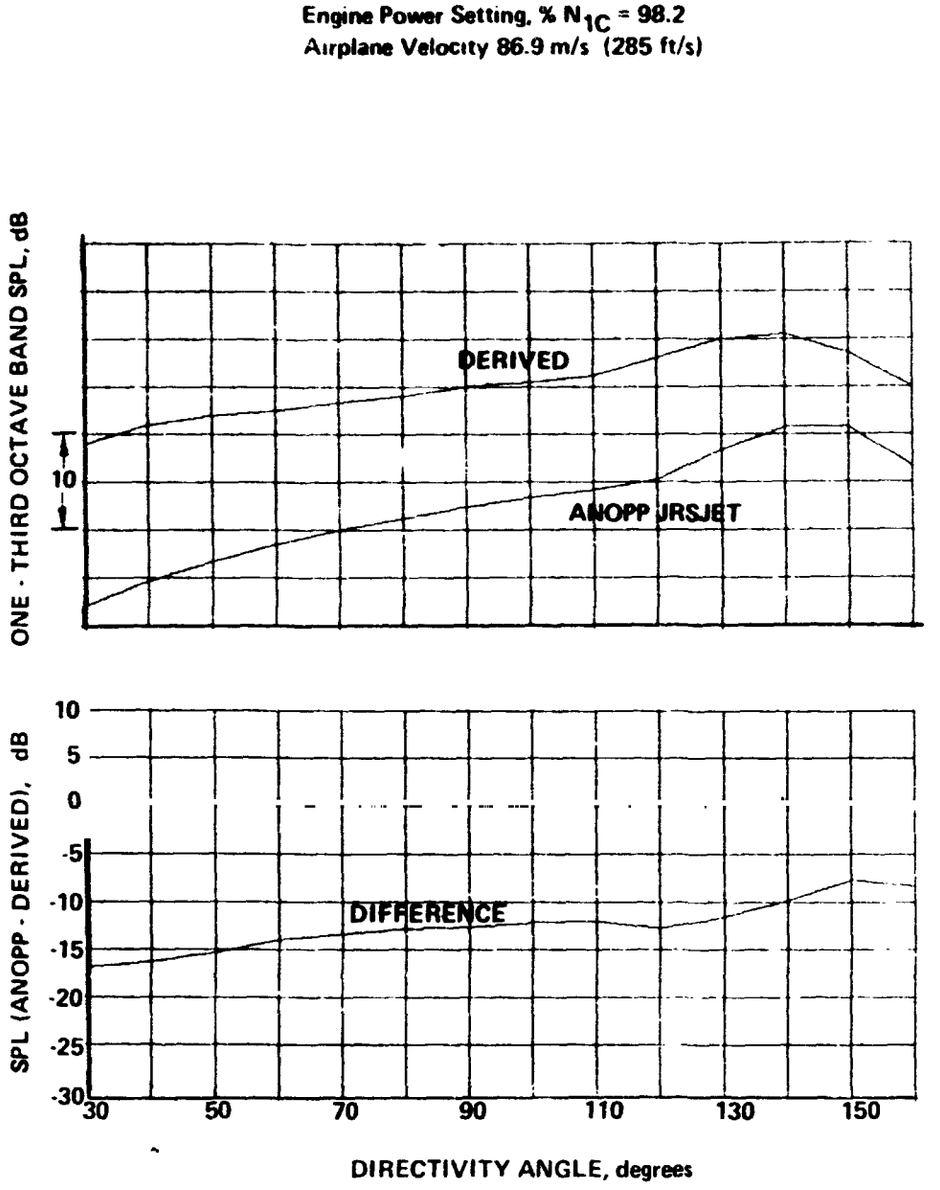

(a) 63 Hz

Figure 28.—SPL Directivity Comparisons of Predicted and Derived Flight Jet Noise

Engine Power Setting, % N_{1C} = 98.2
Airplane Velocity 86.9 m/s (285 ft/s)

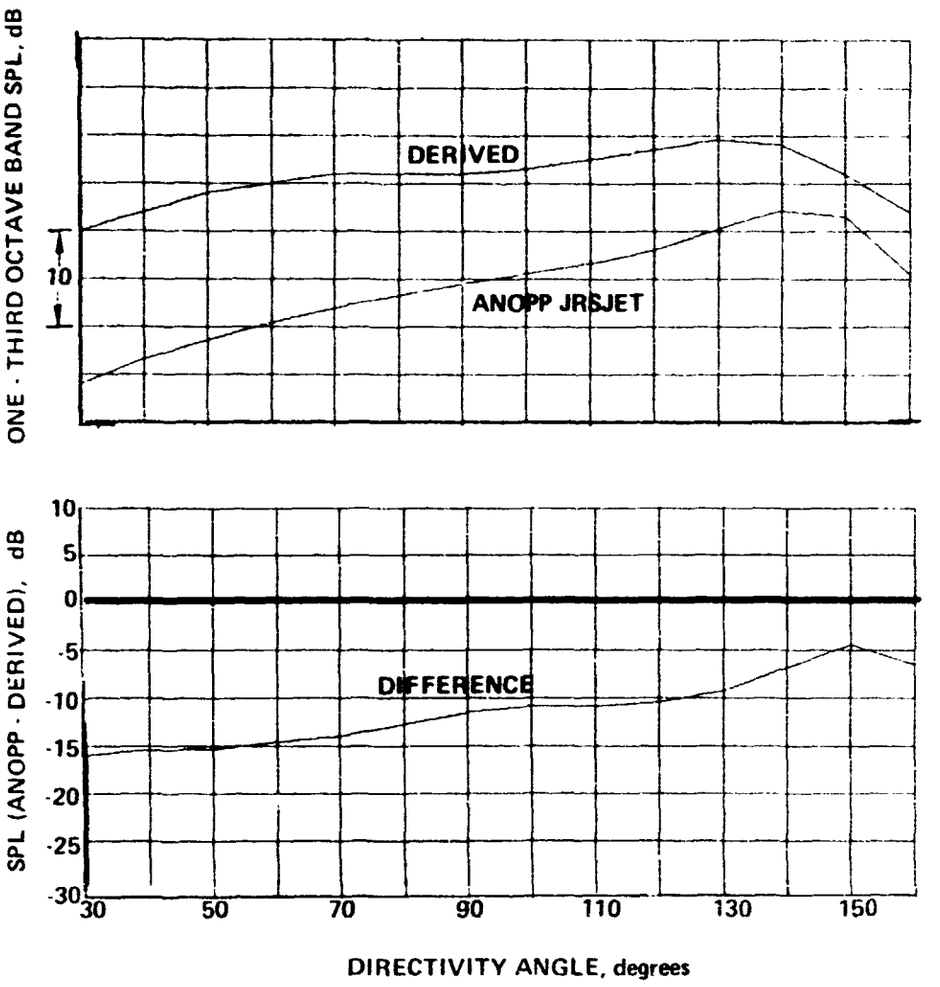

(b) 100 Hz

Figure 28.–(Continued)

Engine Power Setting, % N_{1C} = 98.2
Airplane Velocity 86.9 m/s (285 ft/s)

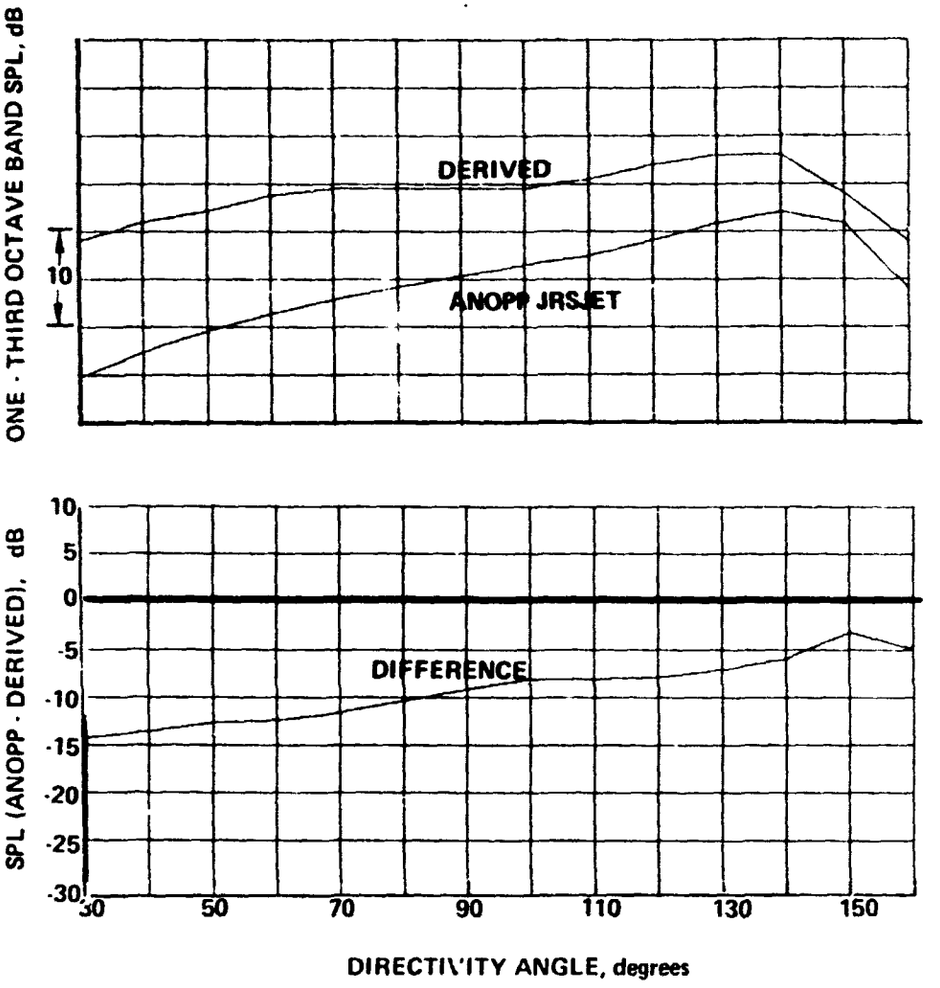

(c) 125 Hz

Figure 28.—(Continued)

Engine Power Setting, % N_{1C} = 98.2
Airplane Velocity 86.9 m/s (285 ft/s)

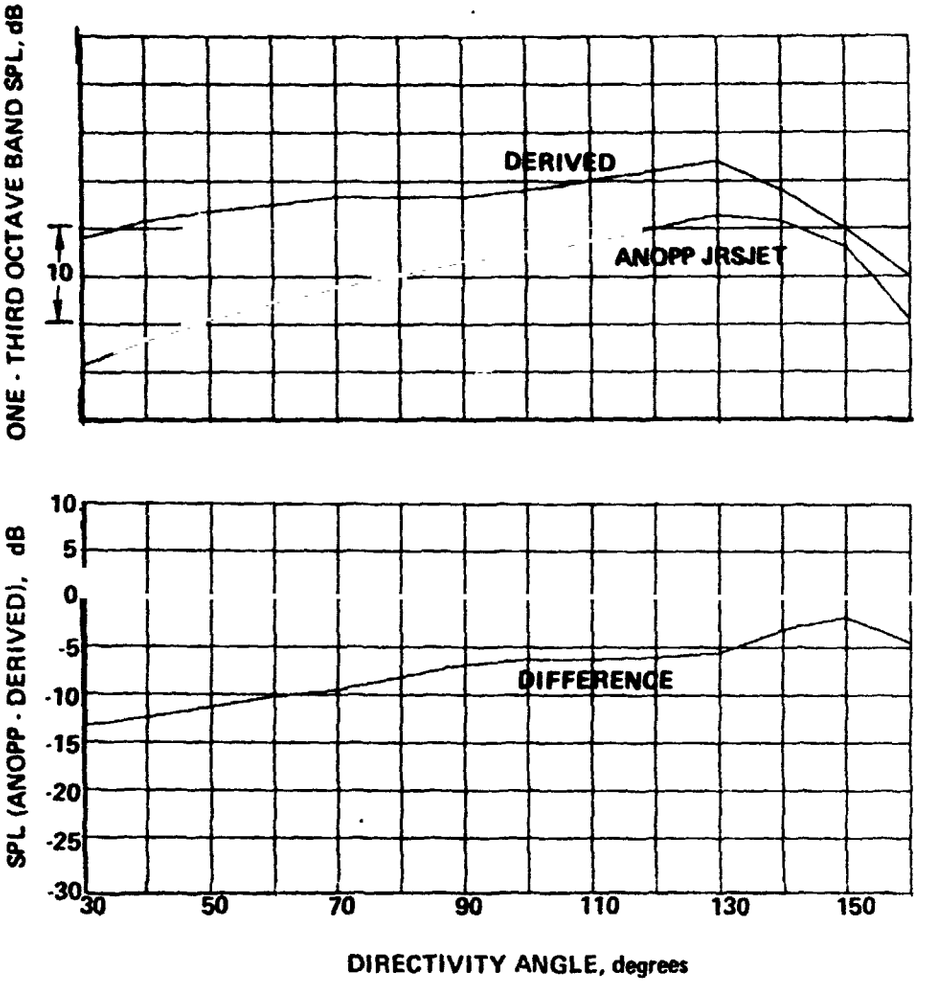

(d) 200 Hz

Figure 28.—(Concluded)

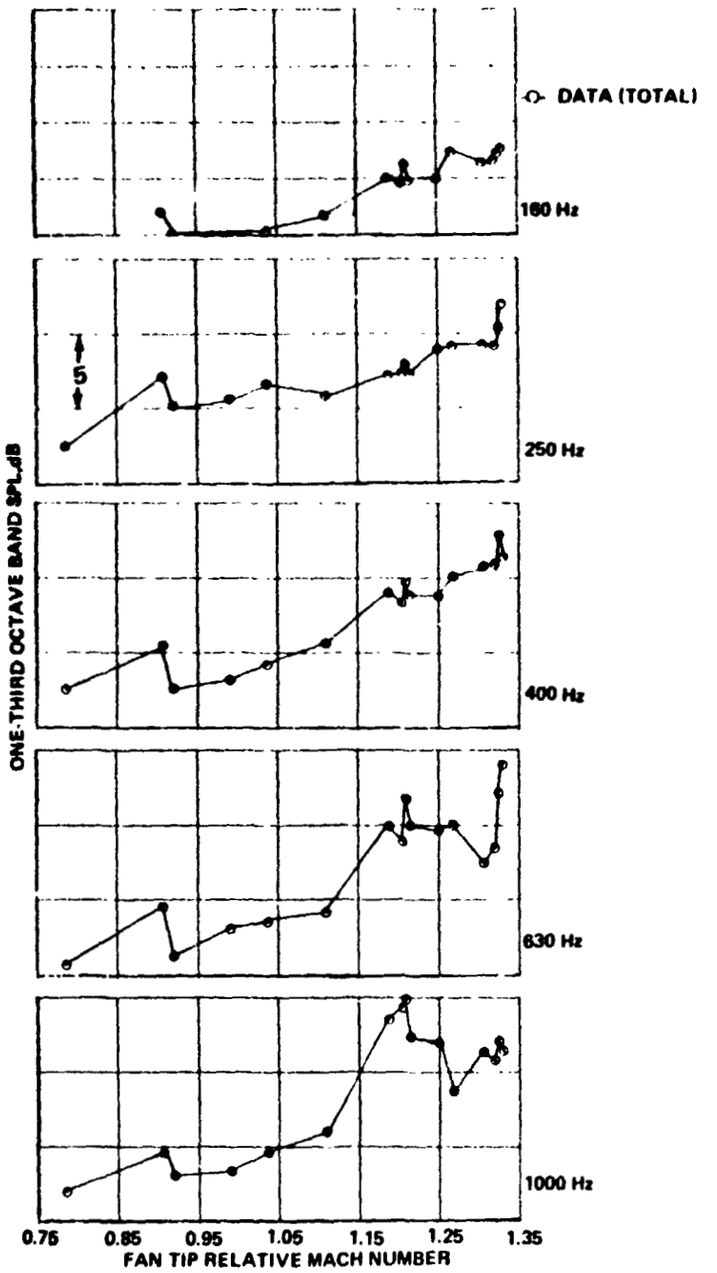

(a) DIRECTIVITY ANGLE 30°

Figure 29.–SPL as a Function of Fan Tip Relative Mach Number

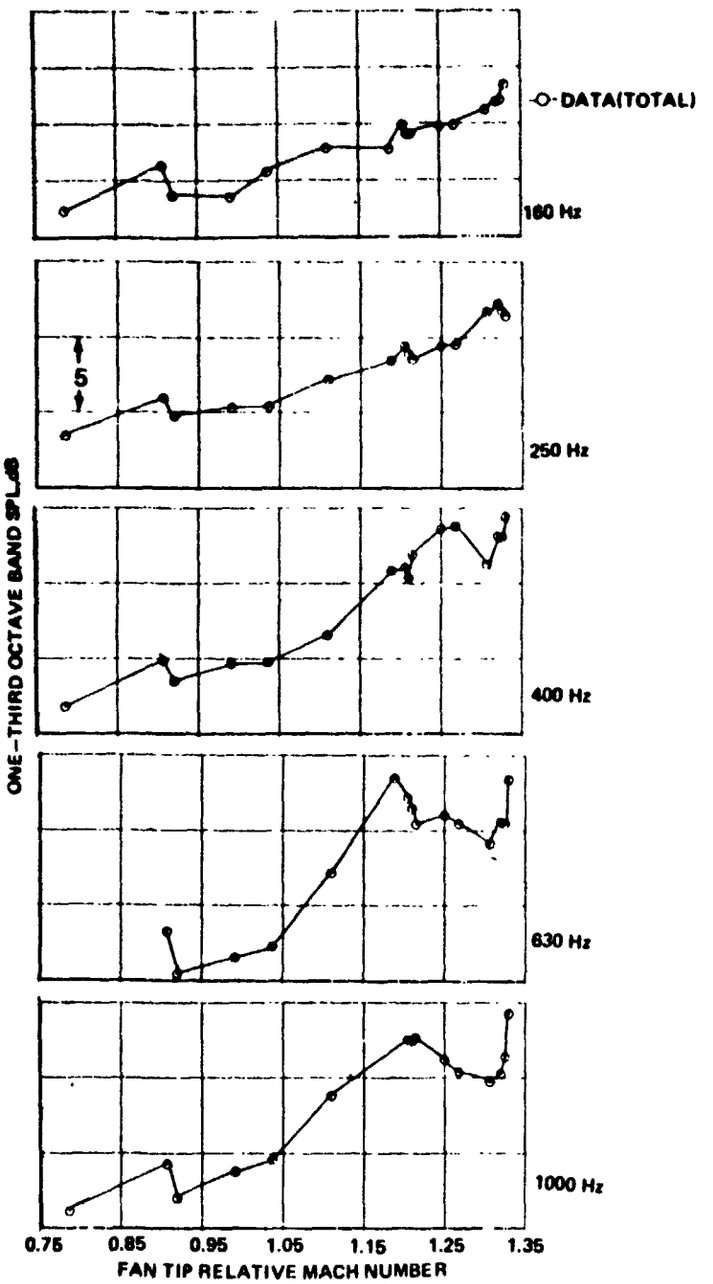

(b) DIRECTIVITY ANGLE 60°

Figure 29.—(Continued)

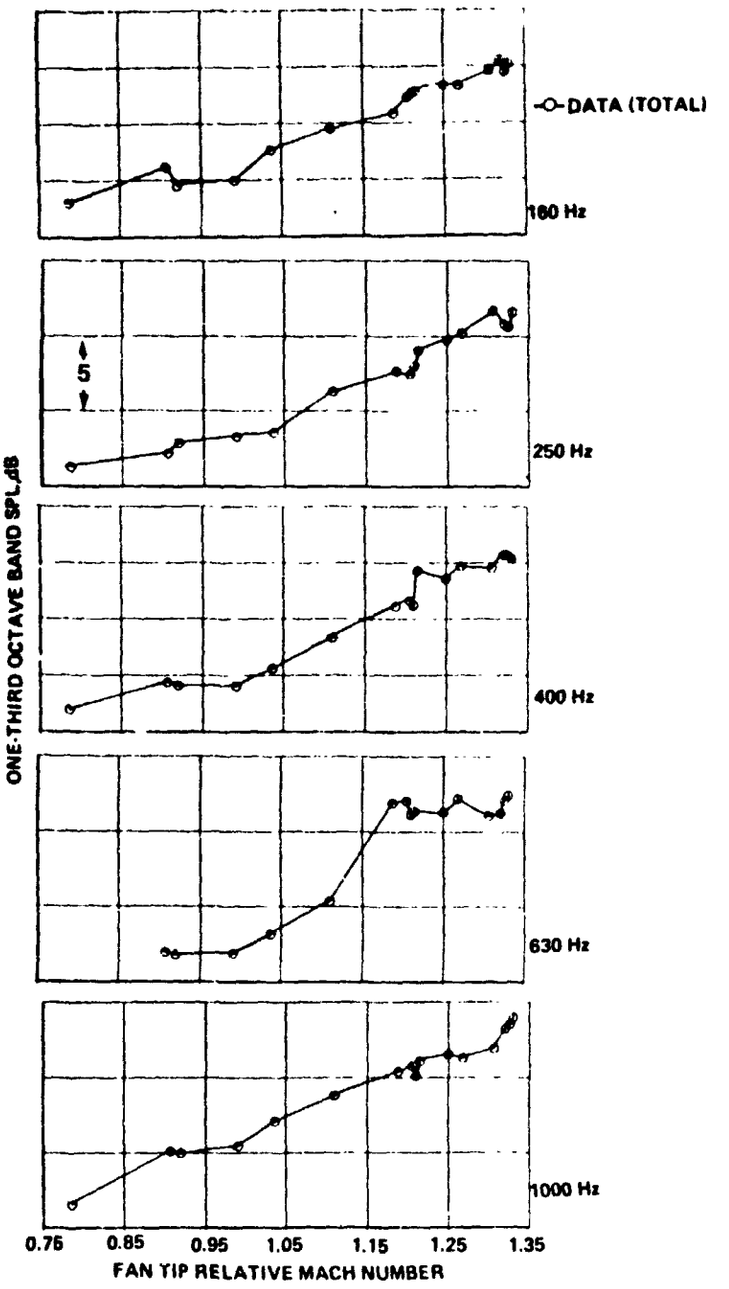

(c) DIRECTIVITY ANGLE 90°

Figure 29.—(Continued)

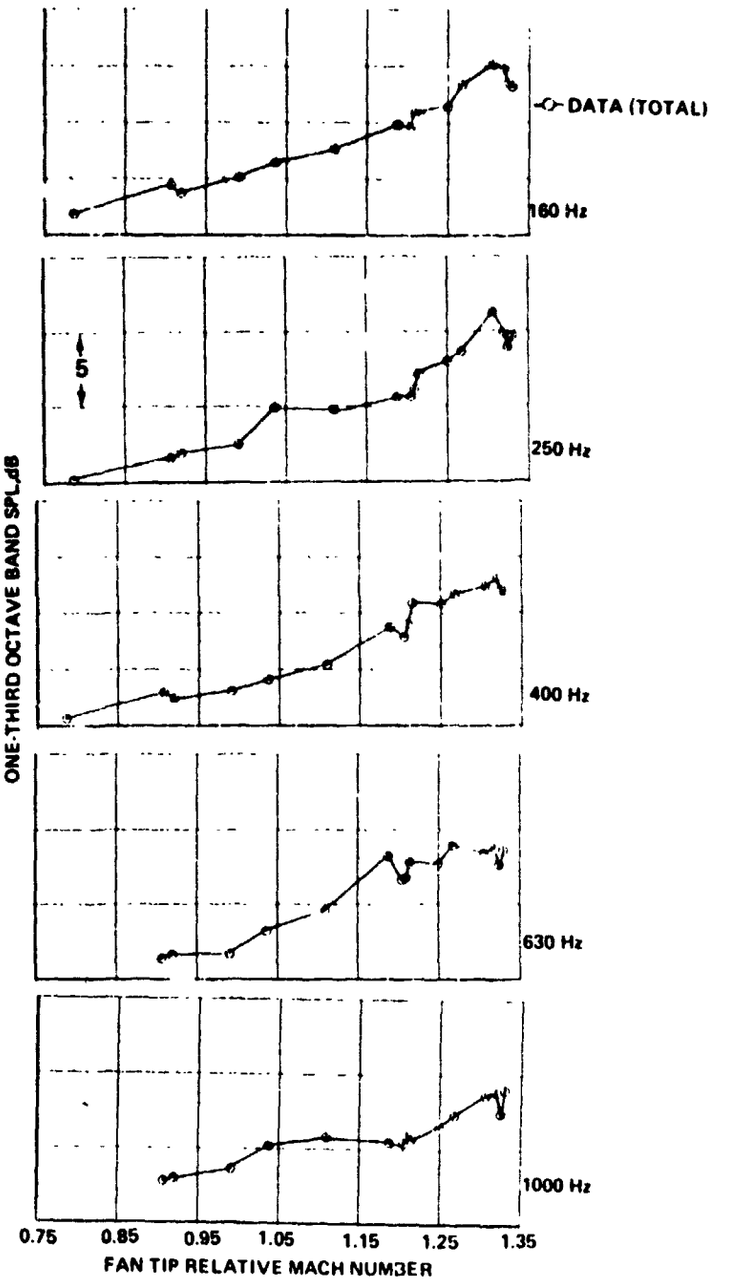

(d) DIRECTIVITY ANGLE 120°

Figure 29.—(Concluded)

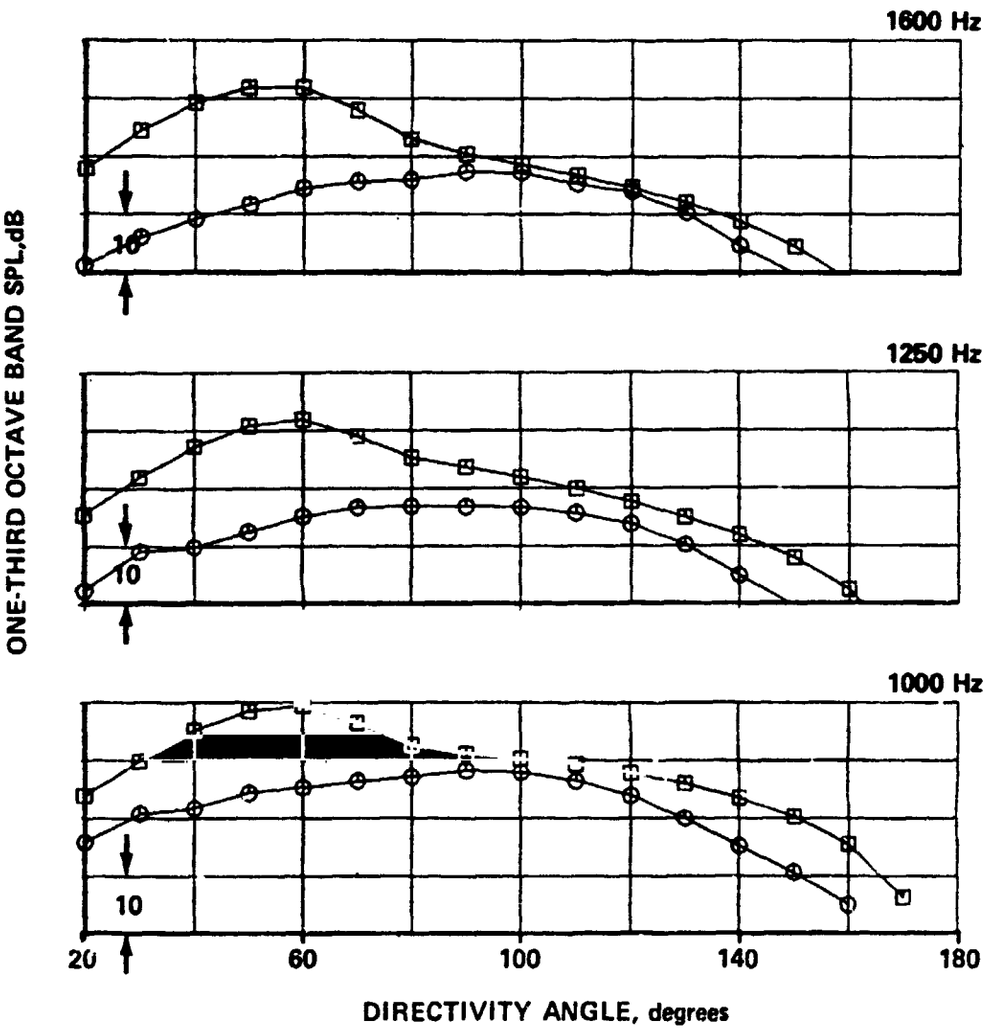

a) TAKEOFF POWER 1000-1600 Hz

Figure 30. – SPL Directivity Comparisons of Data and Prediction for Broadband Fan Noise and Buzzsaw Noise

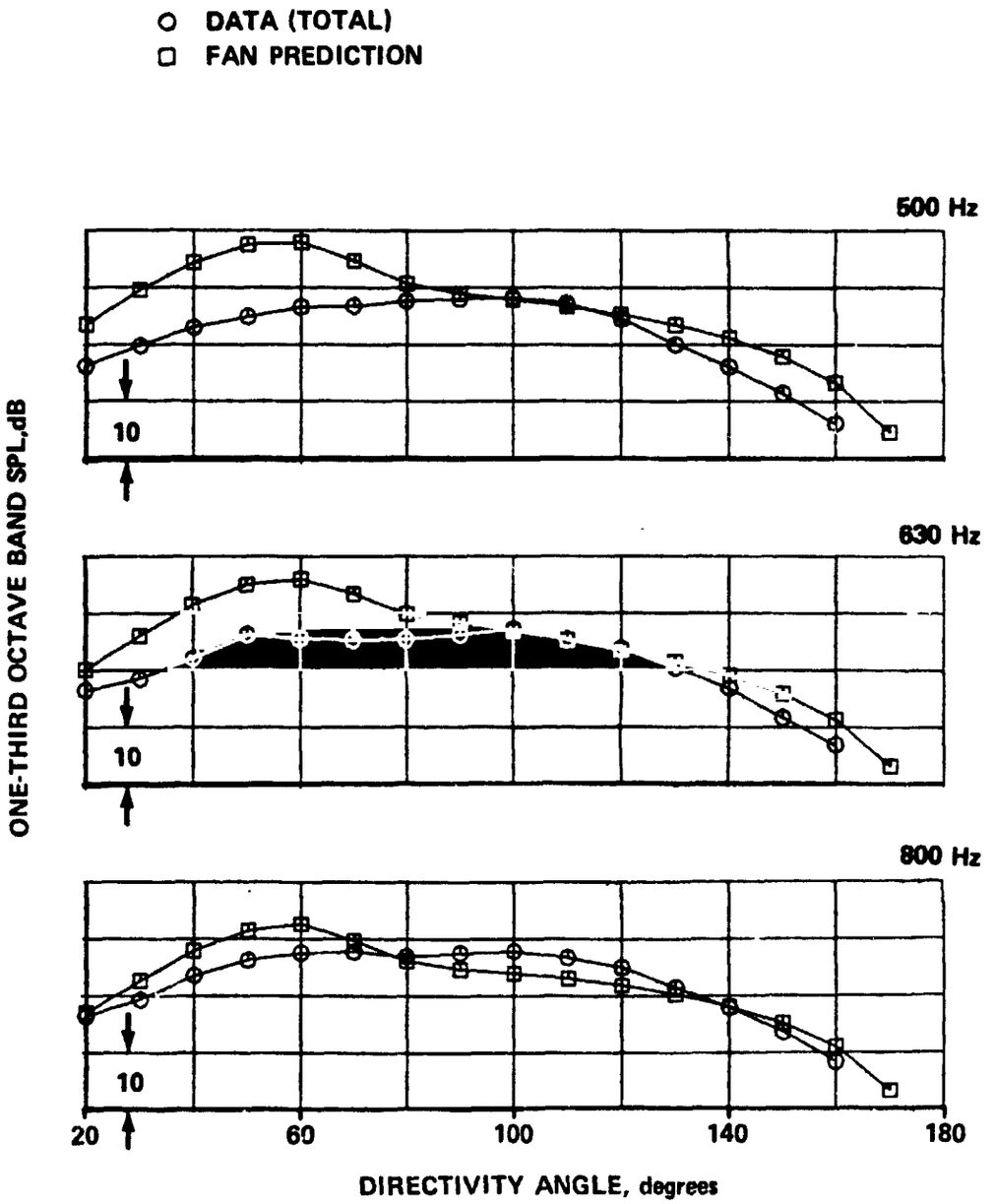

b) TAKEOFF POWER 500-800Hz

Figure 30. – (Continued)

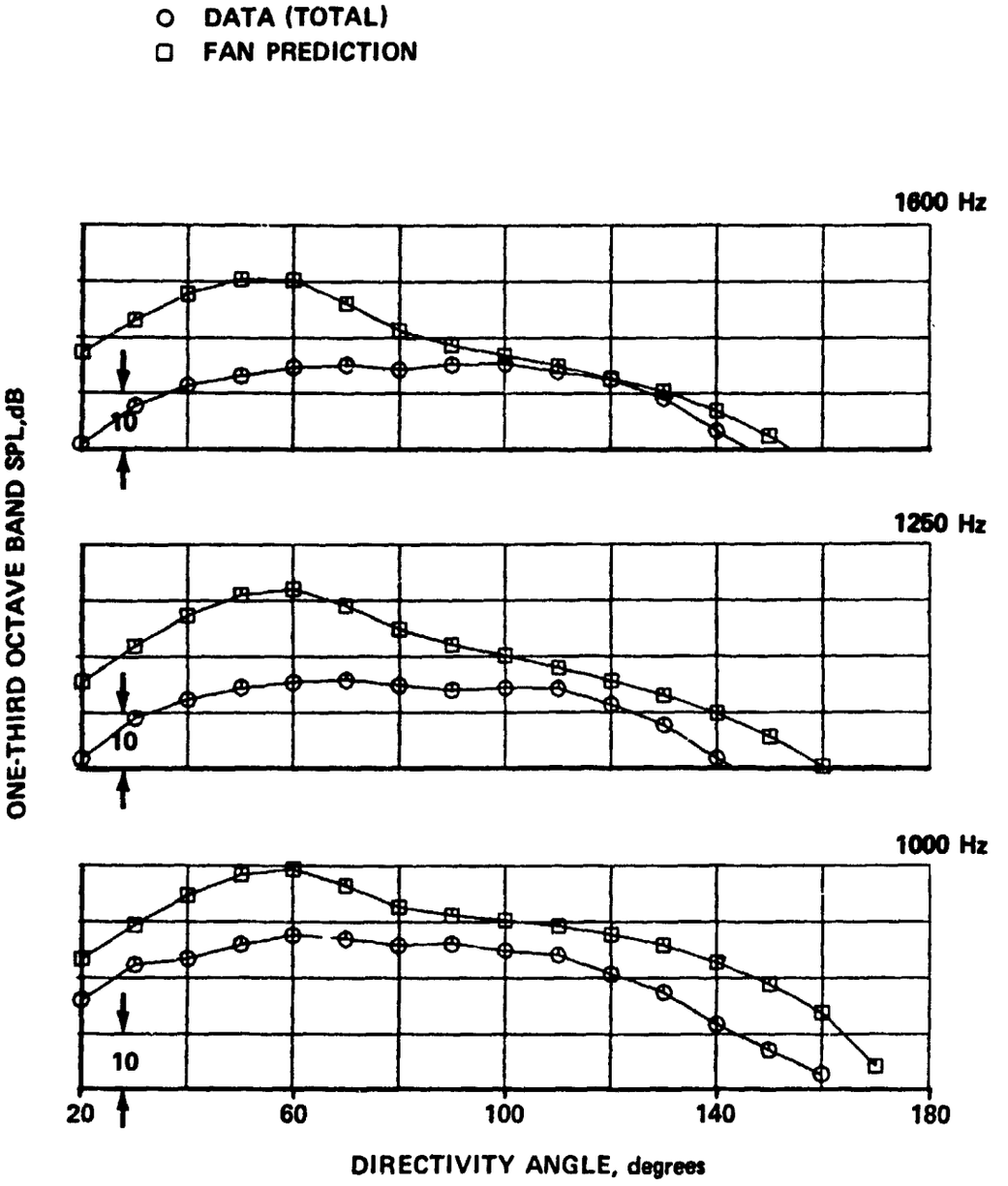

c) CUTBACK POWER 1000-1600 Hz

Figure 30. – (Continued)

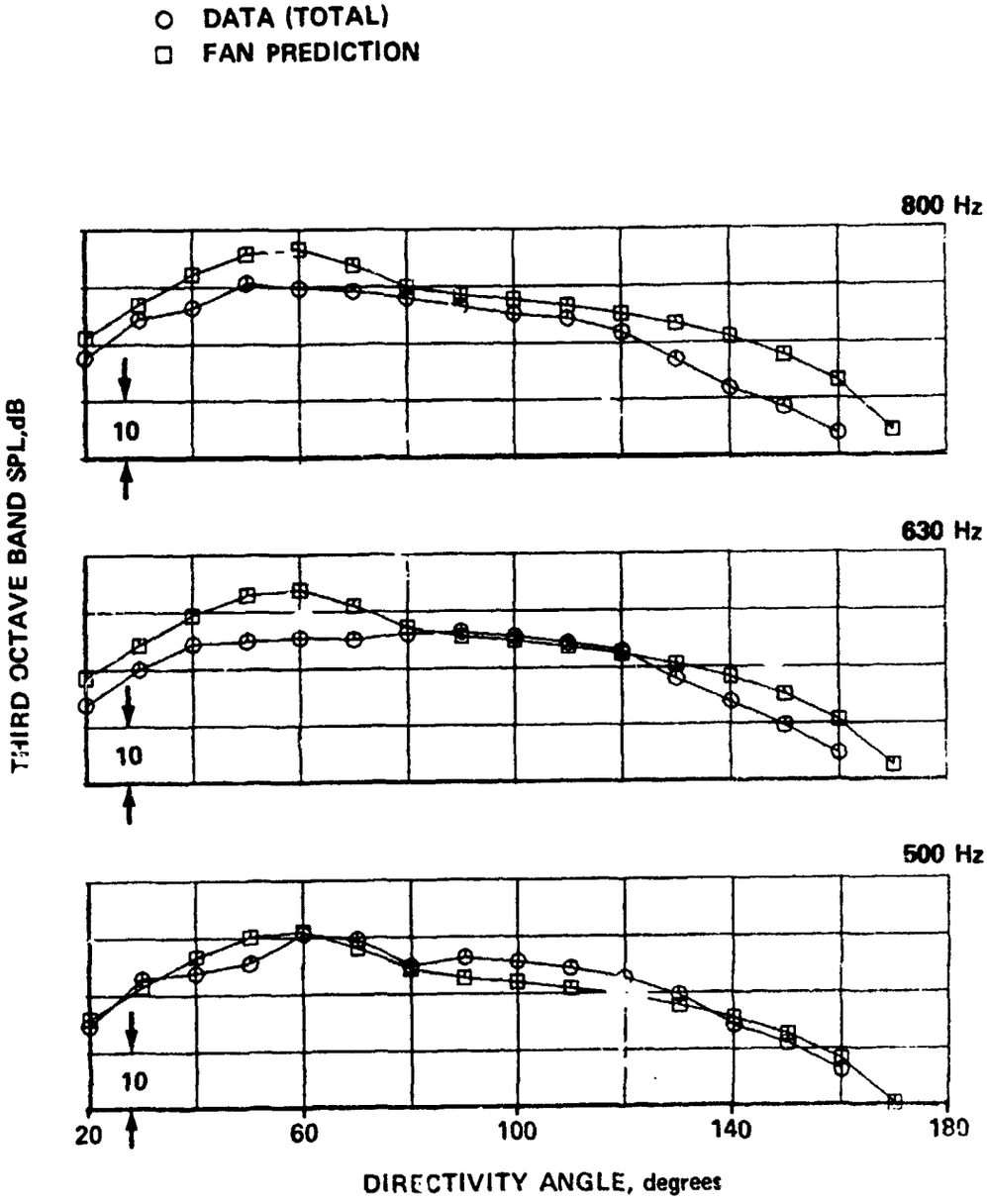

d) CUTBACK POWER 500-800 Hz

Figure 30. – (Continued)

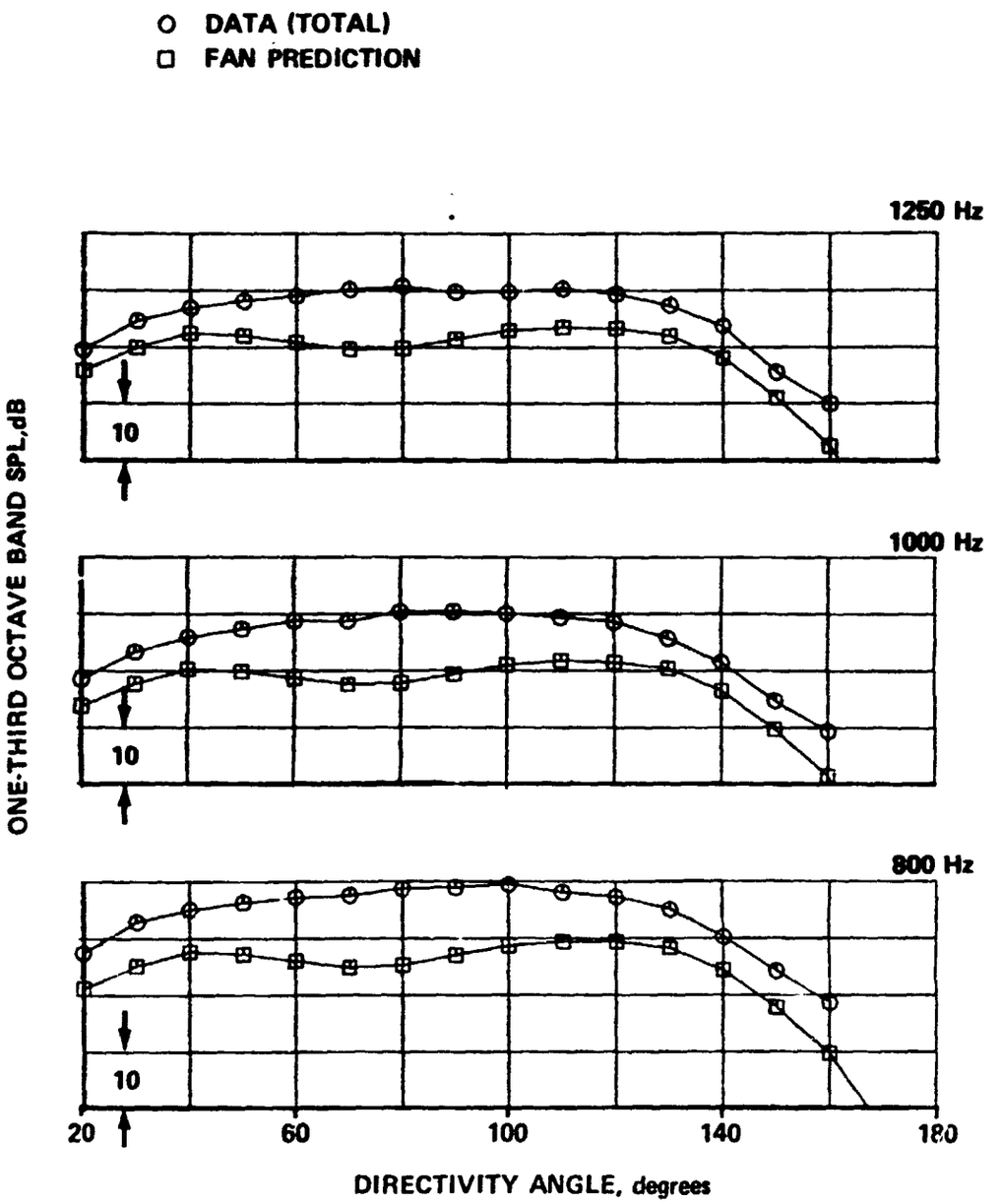

e) APPROACH POWER 800-1250 Hz

Figure 30. – (Continued)

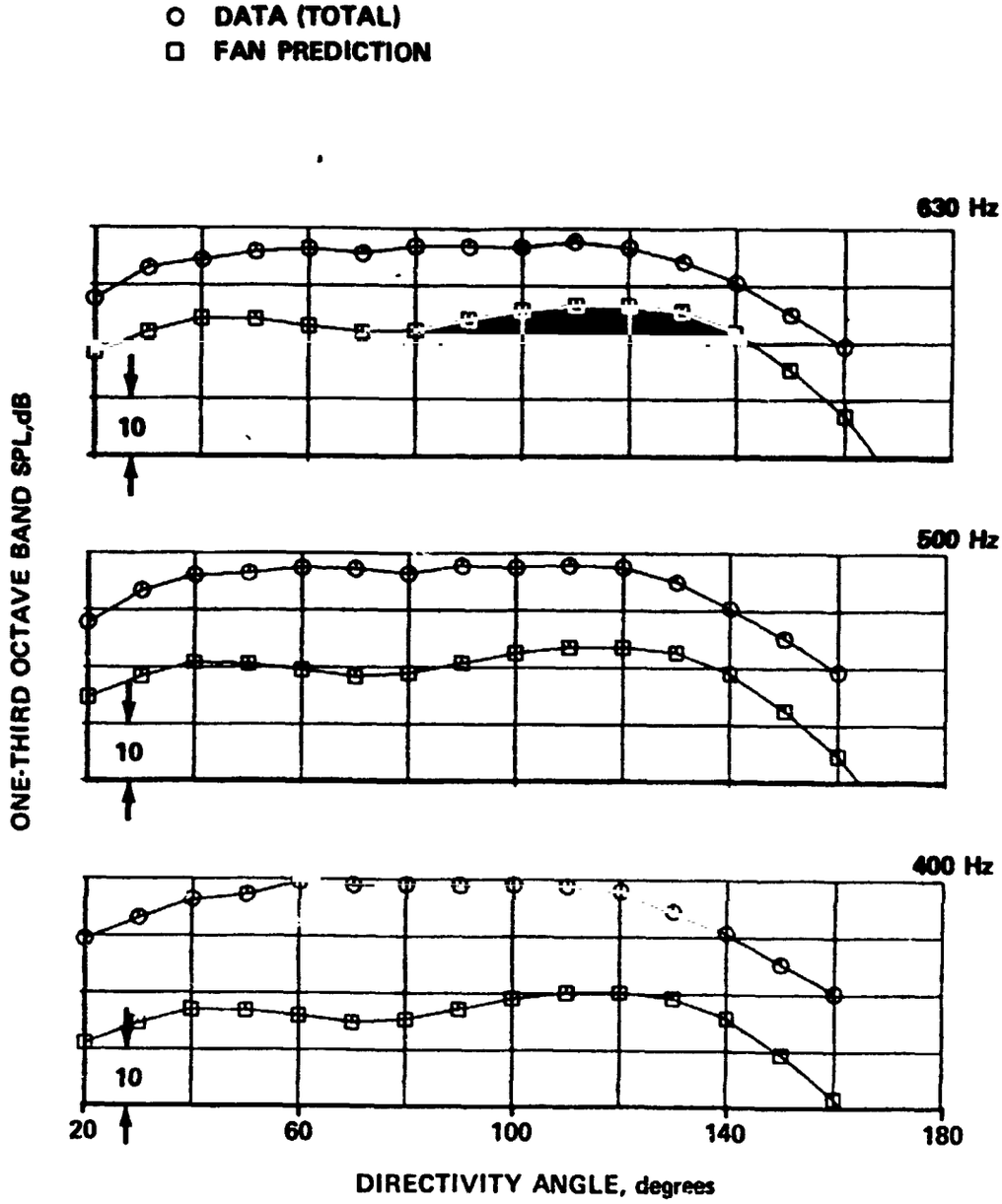

f) APPROACH POWER 400-630 Hz

Figure 30. – (Concluded)

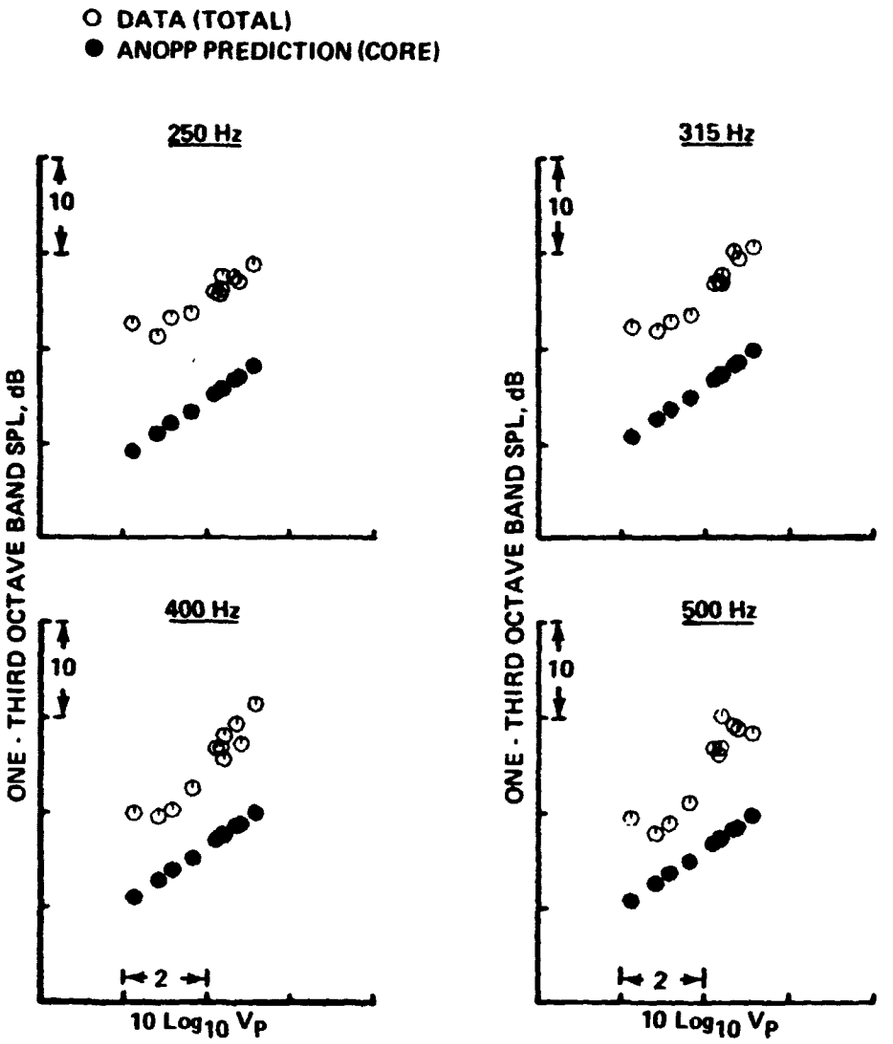

(a) DIRECTIVITY ANGLE 70°; 250 TO 500 Hz

Figure 31.—SPL as a Function of Primary Jet Velocity for Core Noise Component Separation

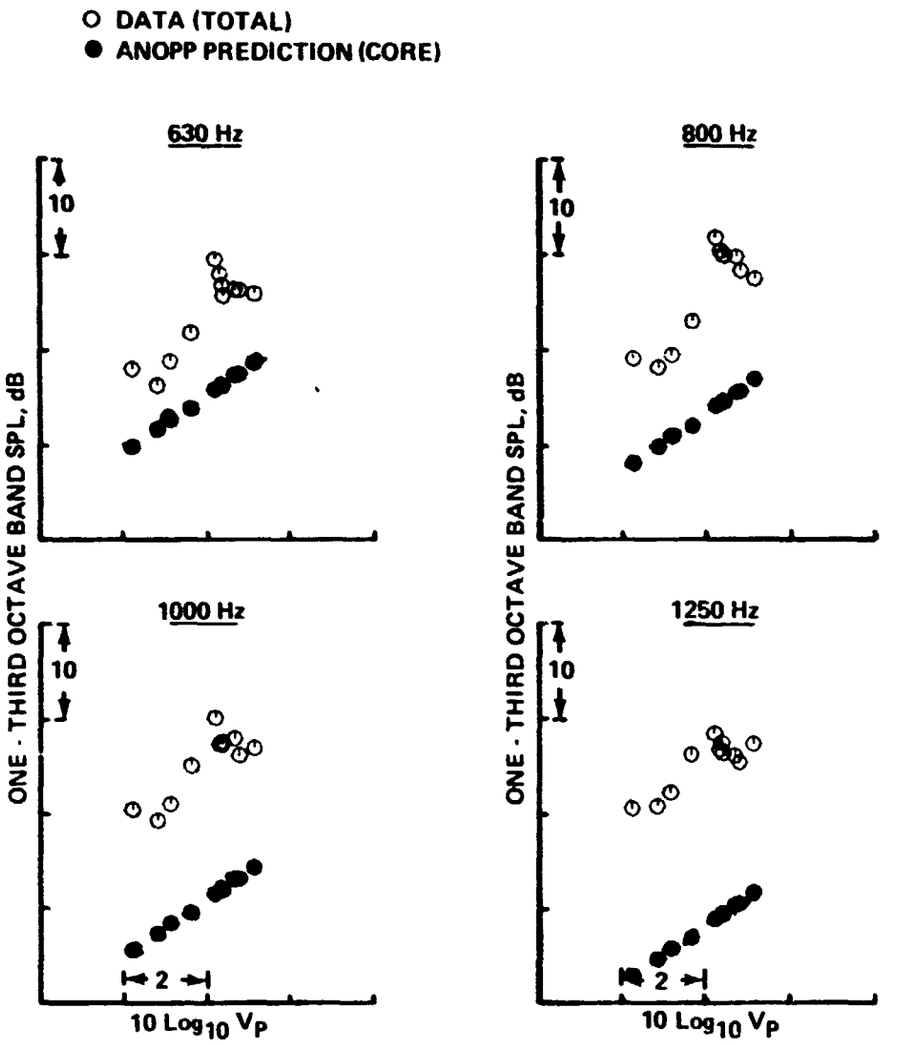

(b) DIRECTIVITY ANGLE 70°; 630 TO 1250 Hz

Figure 31.—(Continued)

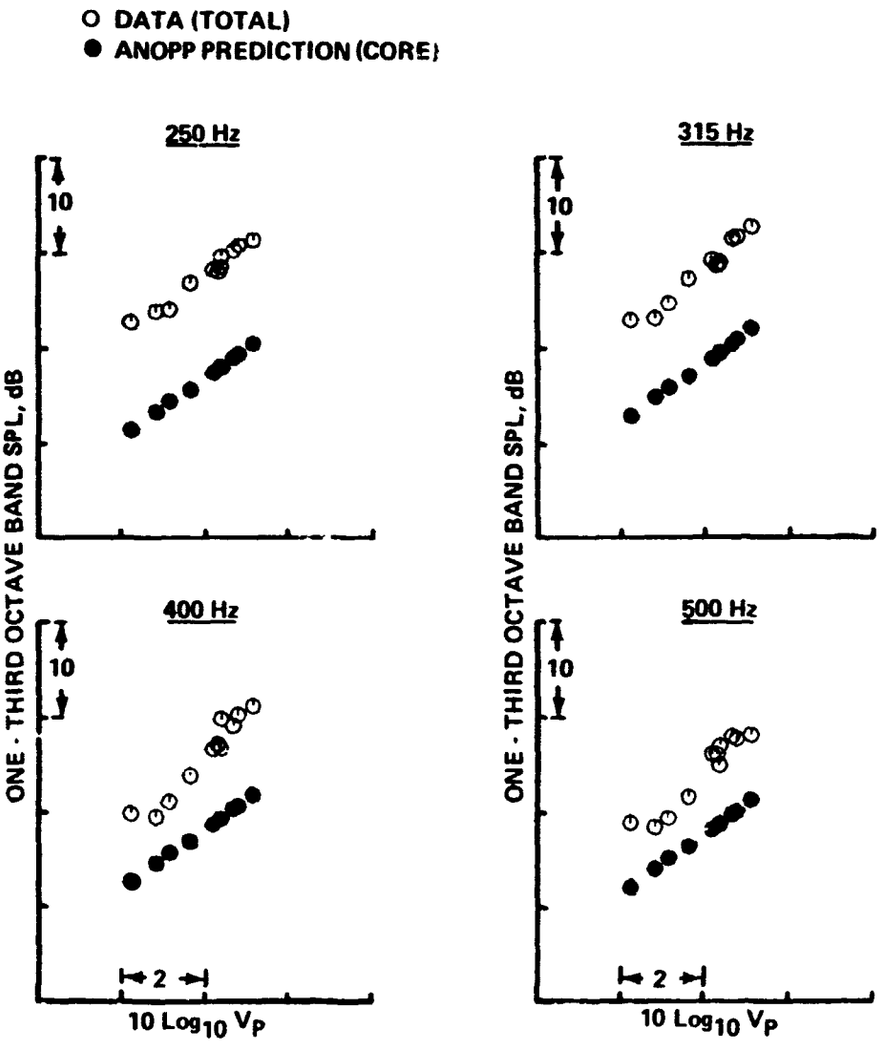

(c) DIRECTIVITY ANGLE 90°; 250 TO 500 Hz

Figure 31.—(Continued)

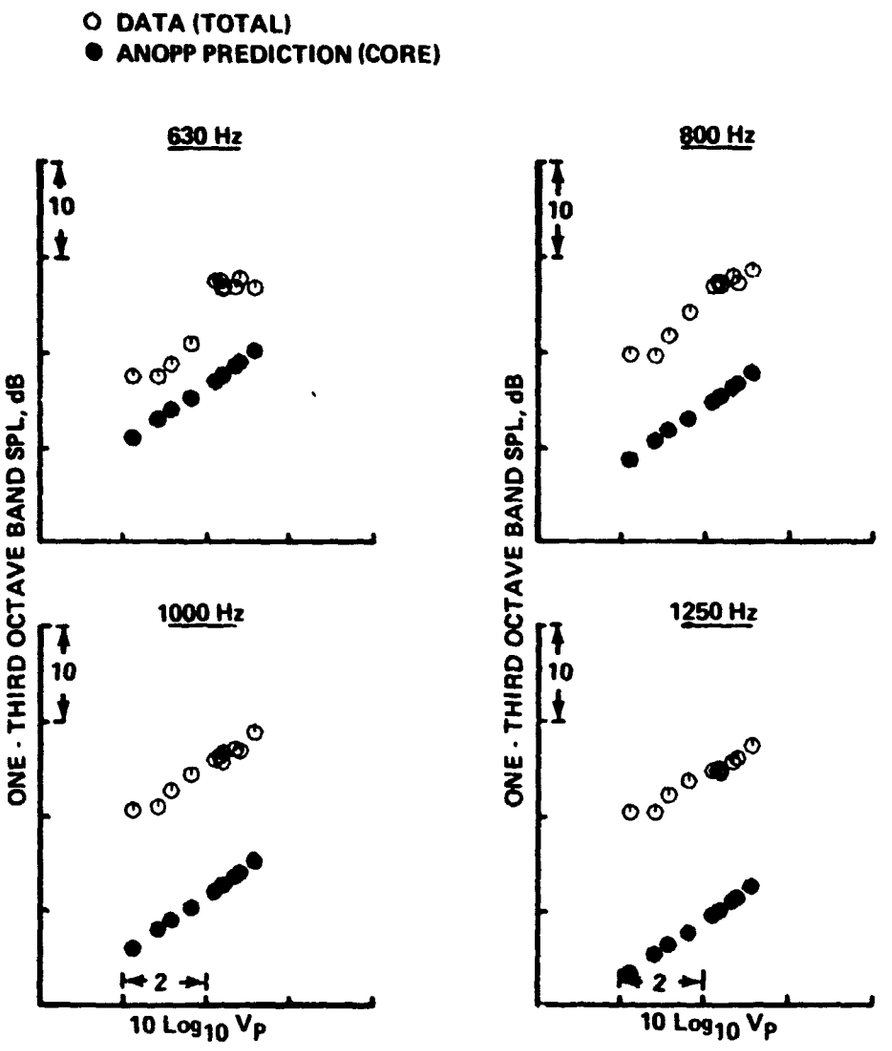

(d) DIRECTIVITY ANGLE 90°; 630 TO 1250 Hz

Figure 31.—(Continued)

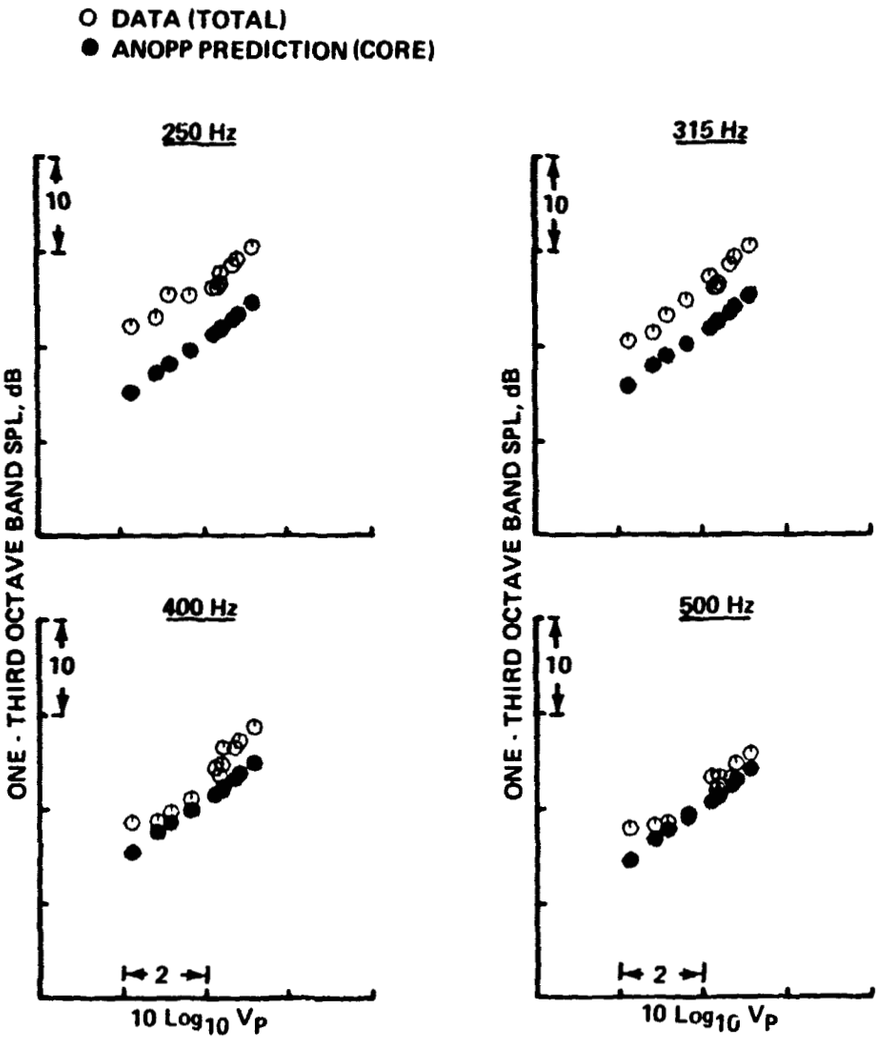

(e) DIRECTIVITY ANGLE 120°; 250 TO 500 Hz

Figure 31.—(Continued)

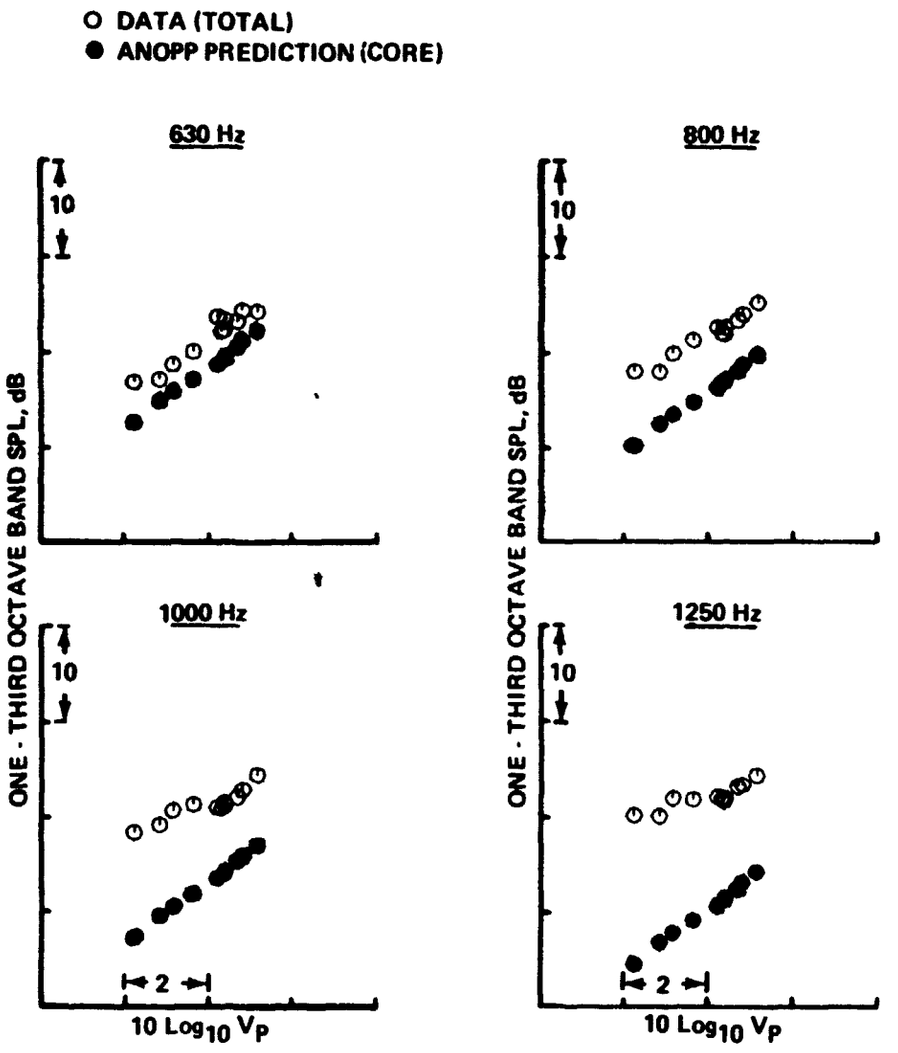

(f) DIRECTIVITY ANGLE 120°; 630 TO 1250 Hz

Figure 31.–(Continued)

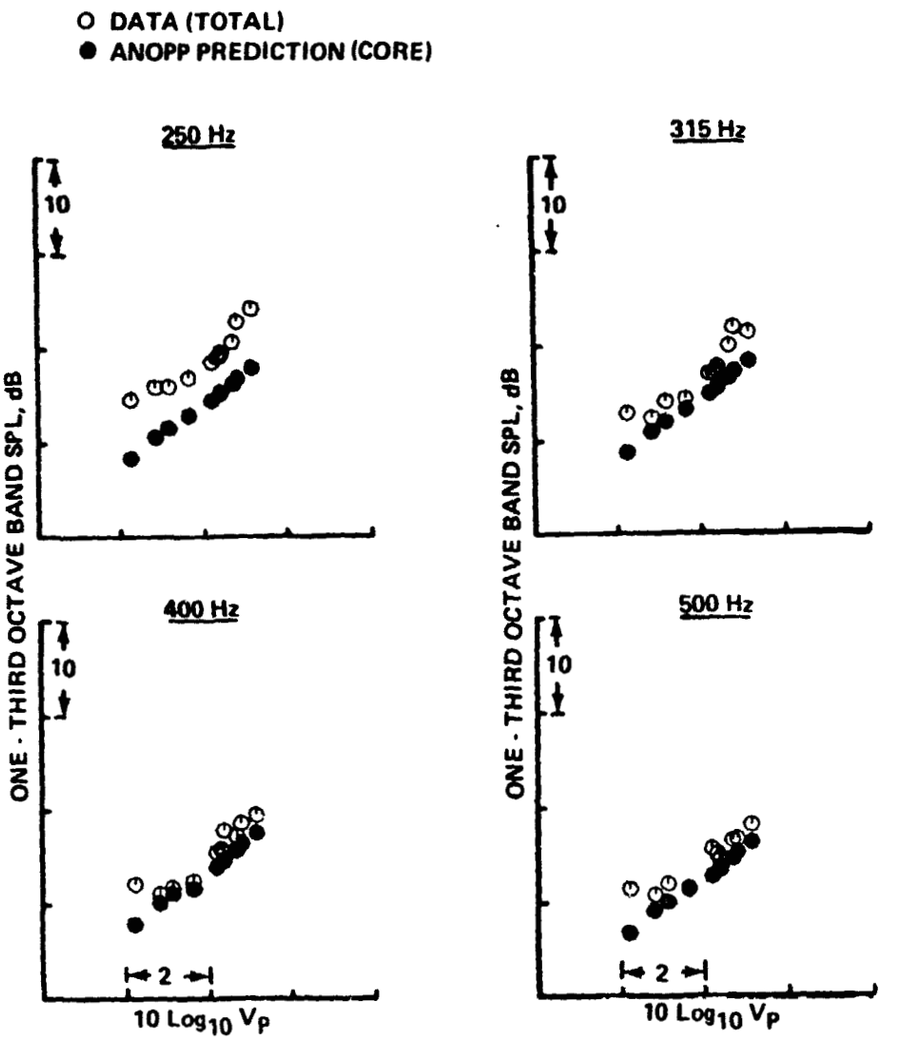

(g) DIRECTIVITY ANGLE 140°; 250 TO 500 Hz

Figure 31.—(Continued)

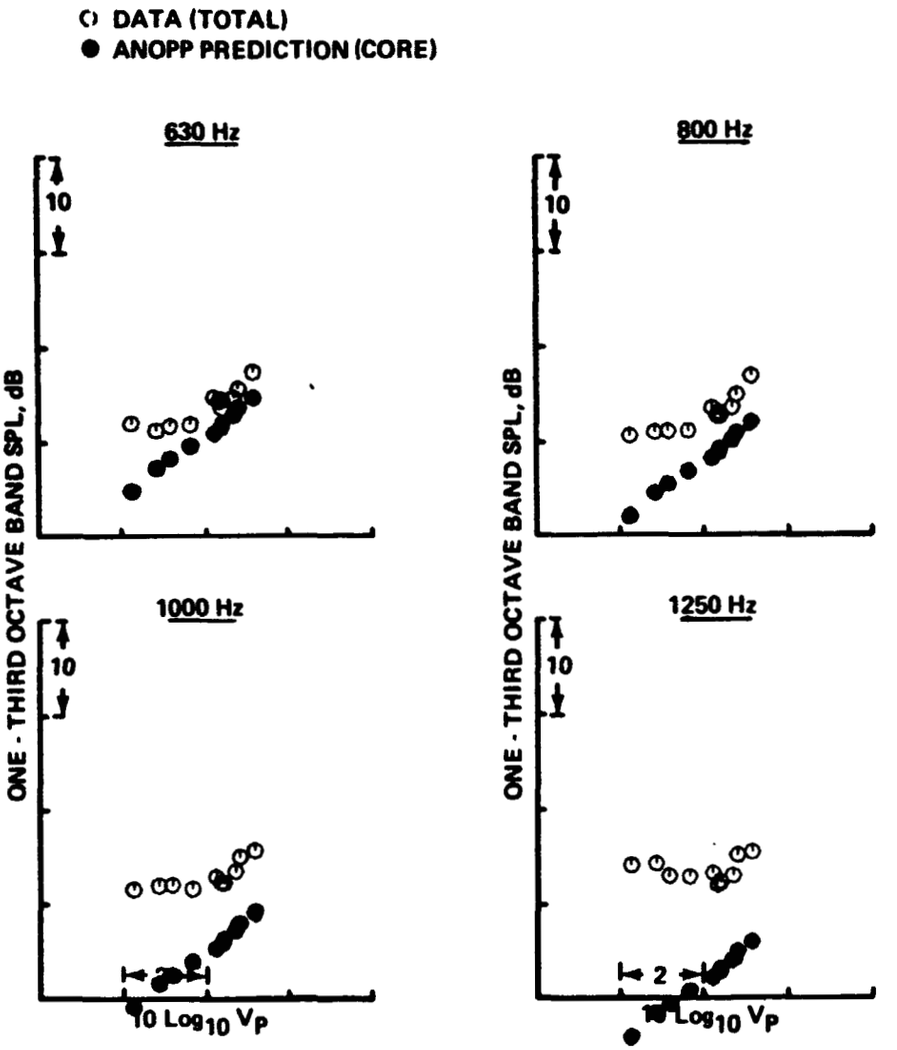

(h) DIRECTIVITY ANGLE 140°; 630 TO 1250 Hz

Figure 31.--(Concluded)

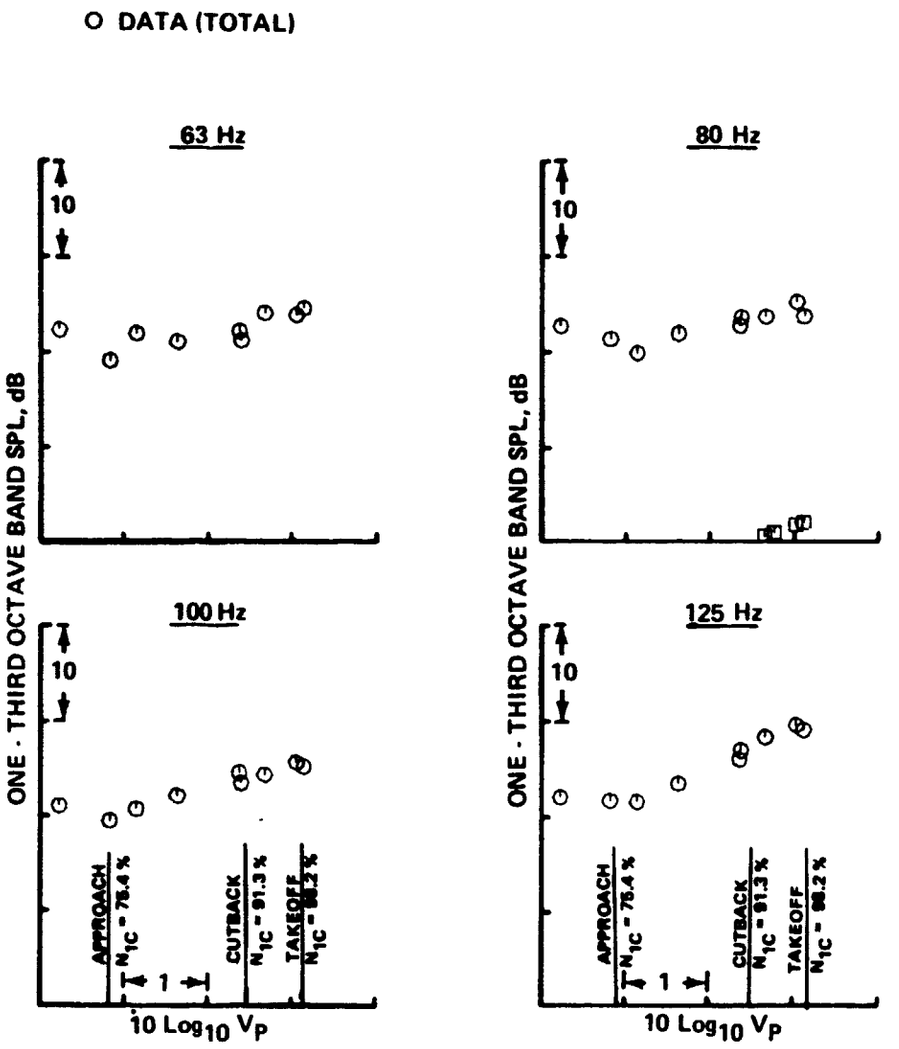

(a) DIRECTIVITY ANGLE 70°

Figure 32.--SPL as a Function of Primary Jet Velocity for Low Frequencies

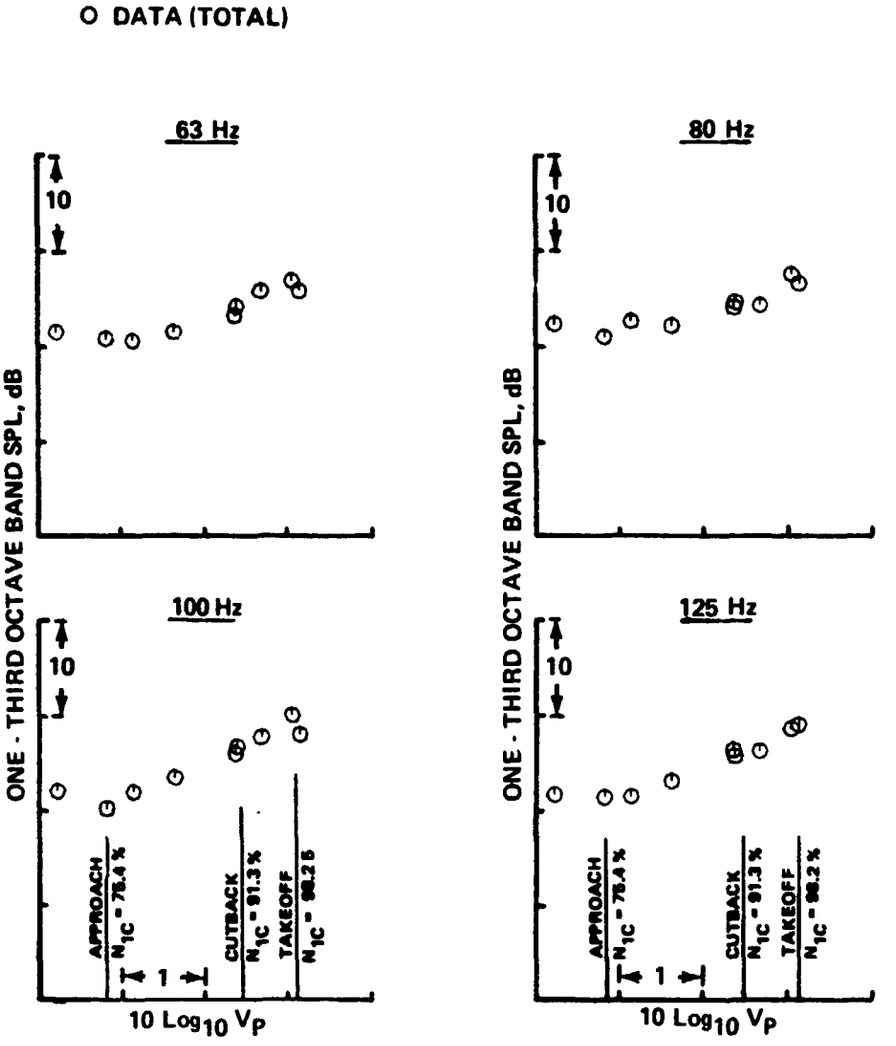

(b) DIRECTIVITY ANGLE 90°

Figure 32. -(Continued)

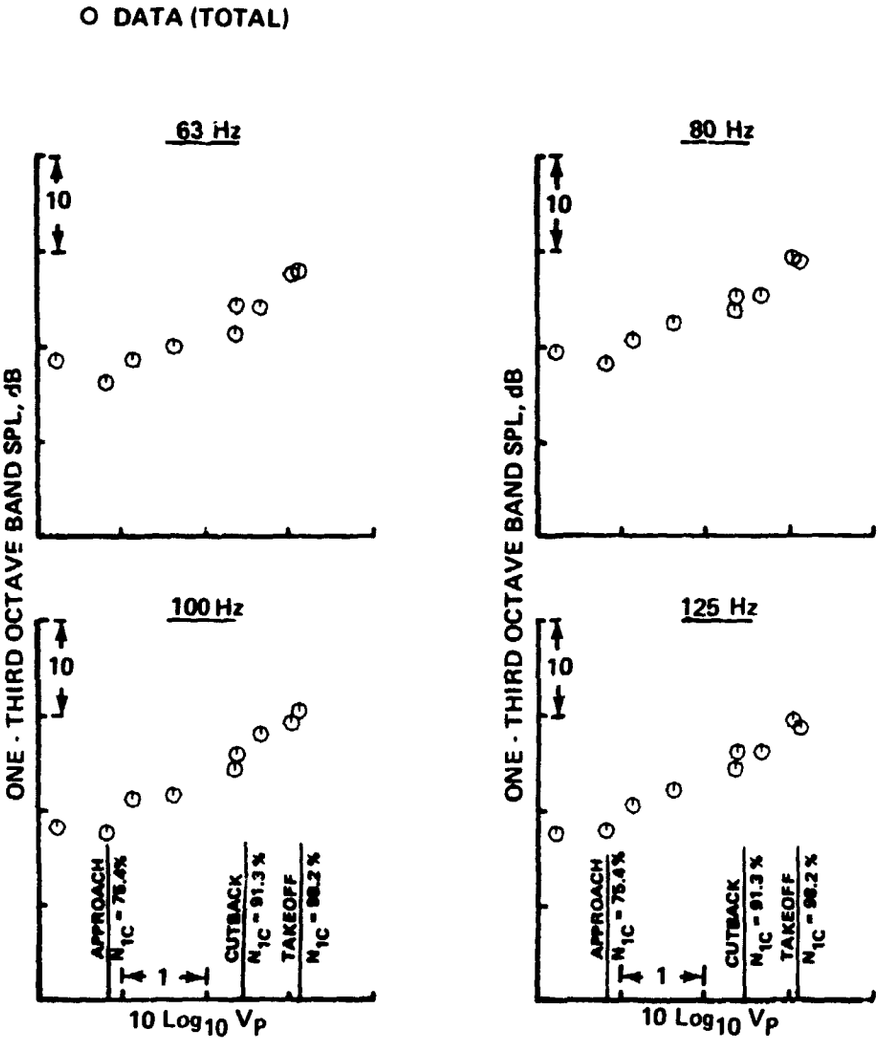

(c) DIRECTIVITY ANGLE 120°

Figure 32.—(Continued)

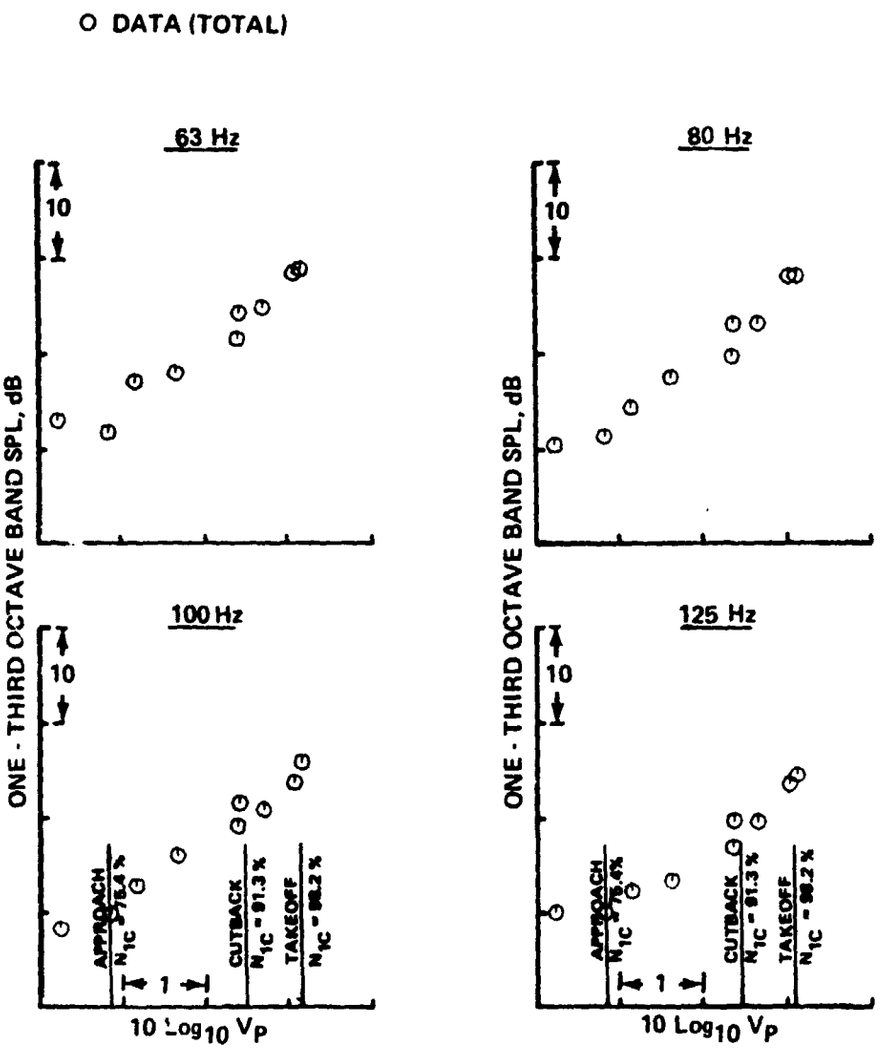

(d) DIRECTIVITY ANGLE 150°

Figure 32.–(Concluded)

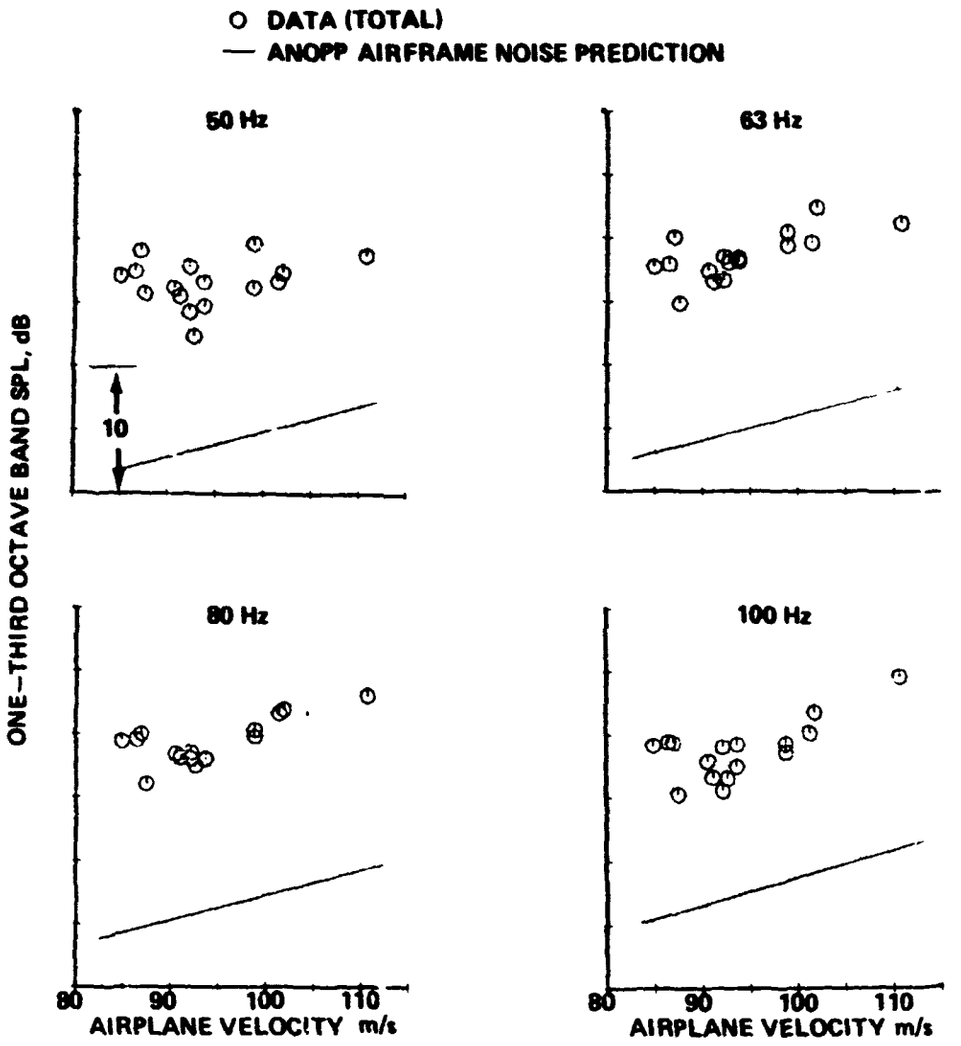

(a) DIRECTIVITY ANGLE 30°

Figure 33.—SPL as a Function of Airplane Velocity

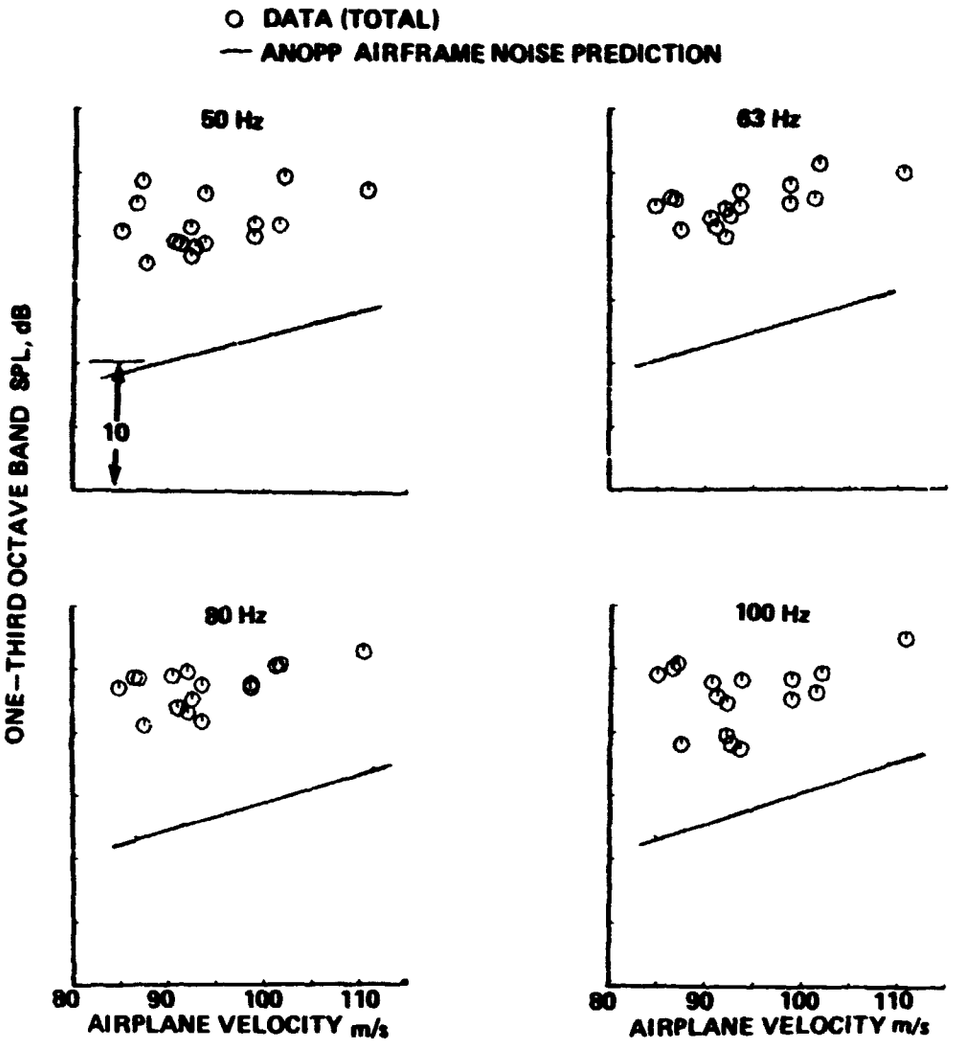

(b) DIRECTIVITY ANGLE 60°

Figure 33.—(Continued)

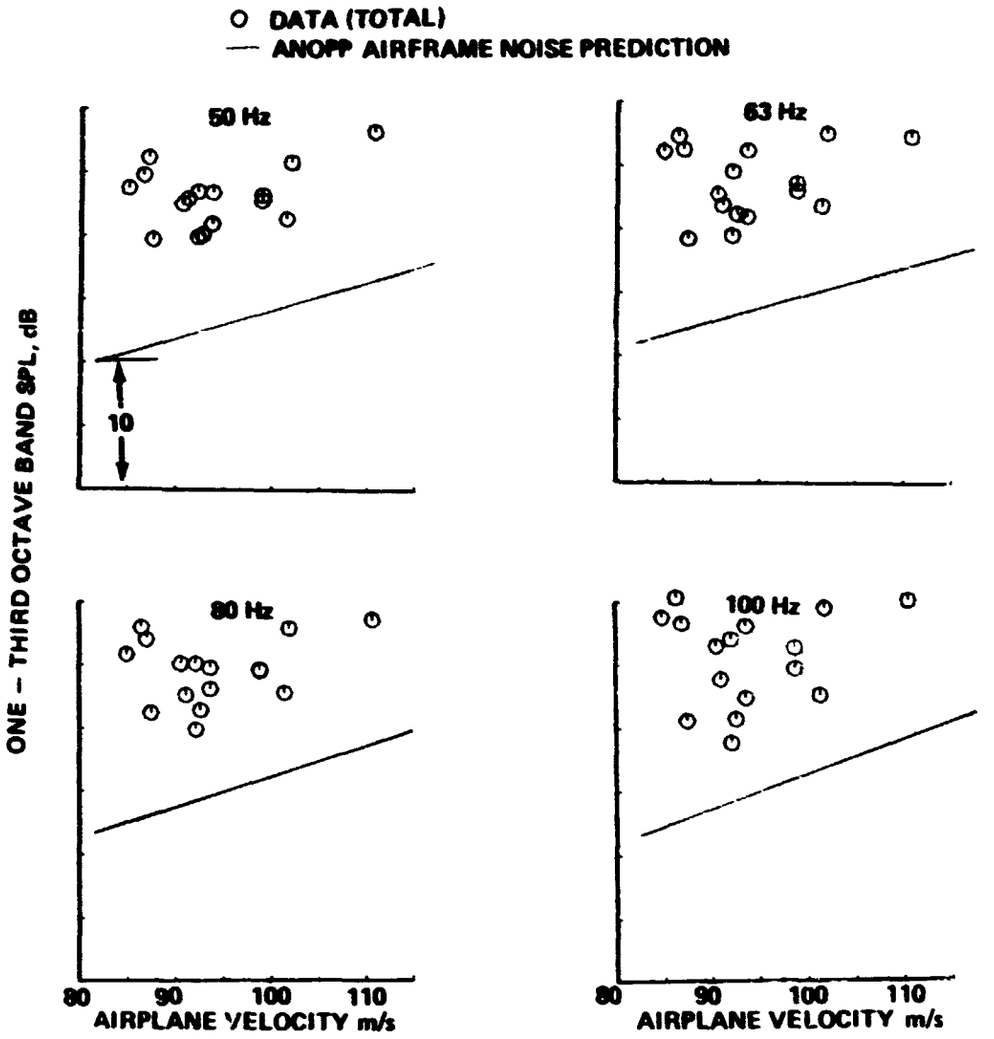

(c) DIRECTIVITY ANGLE 90°

Figure 33.—(Concluded)

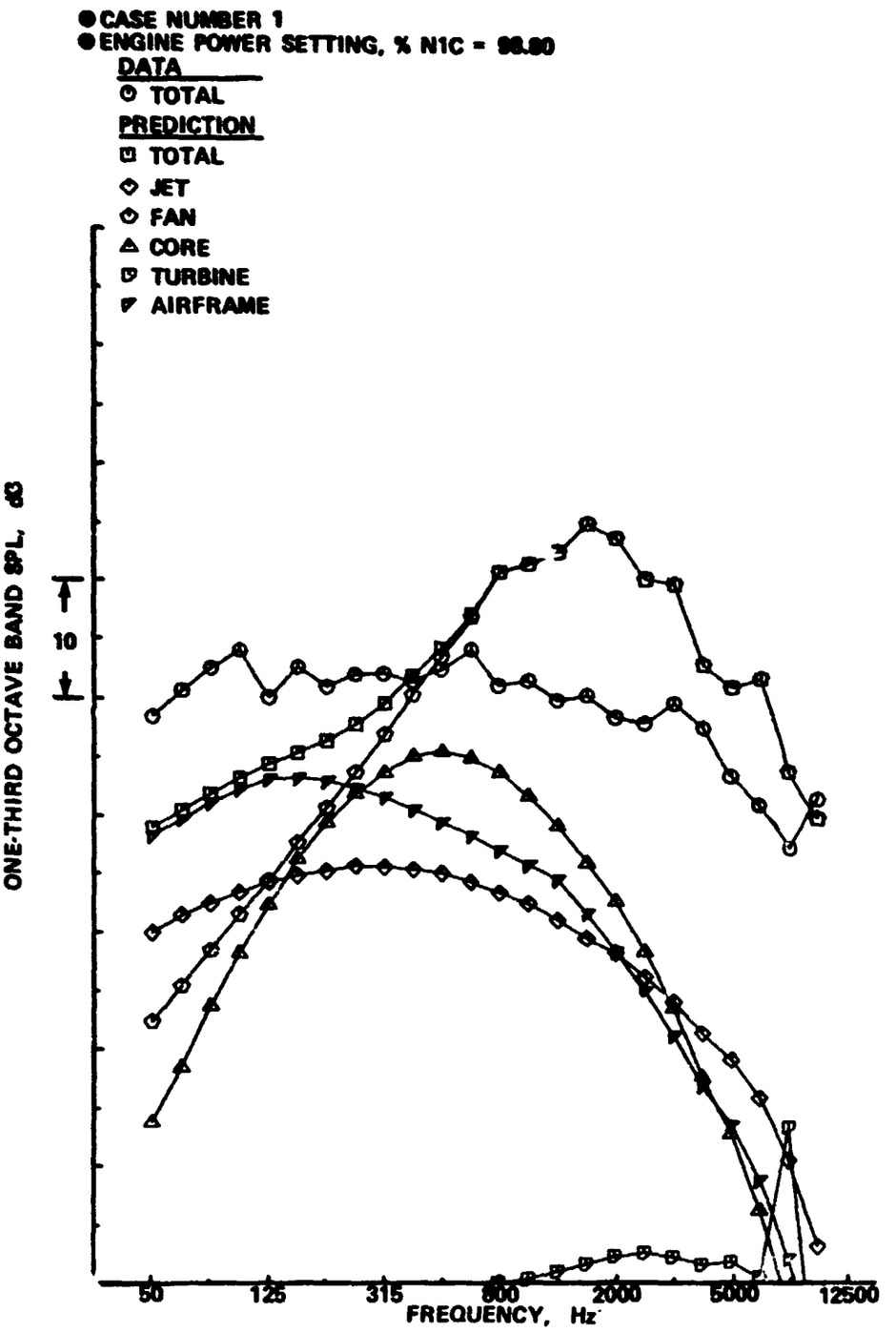

(a) DIRECTIVITY ANGLE = 30°

Figure A1. – Spectral Comparisons of Data and Prediction, Engine Power Setting % N_{1C} = 98.8

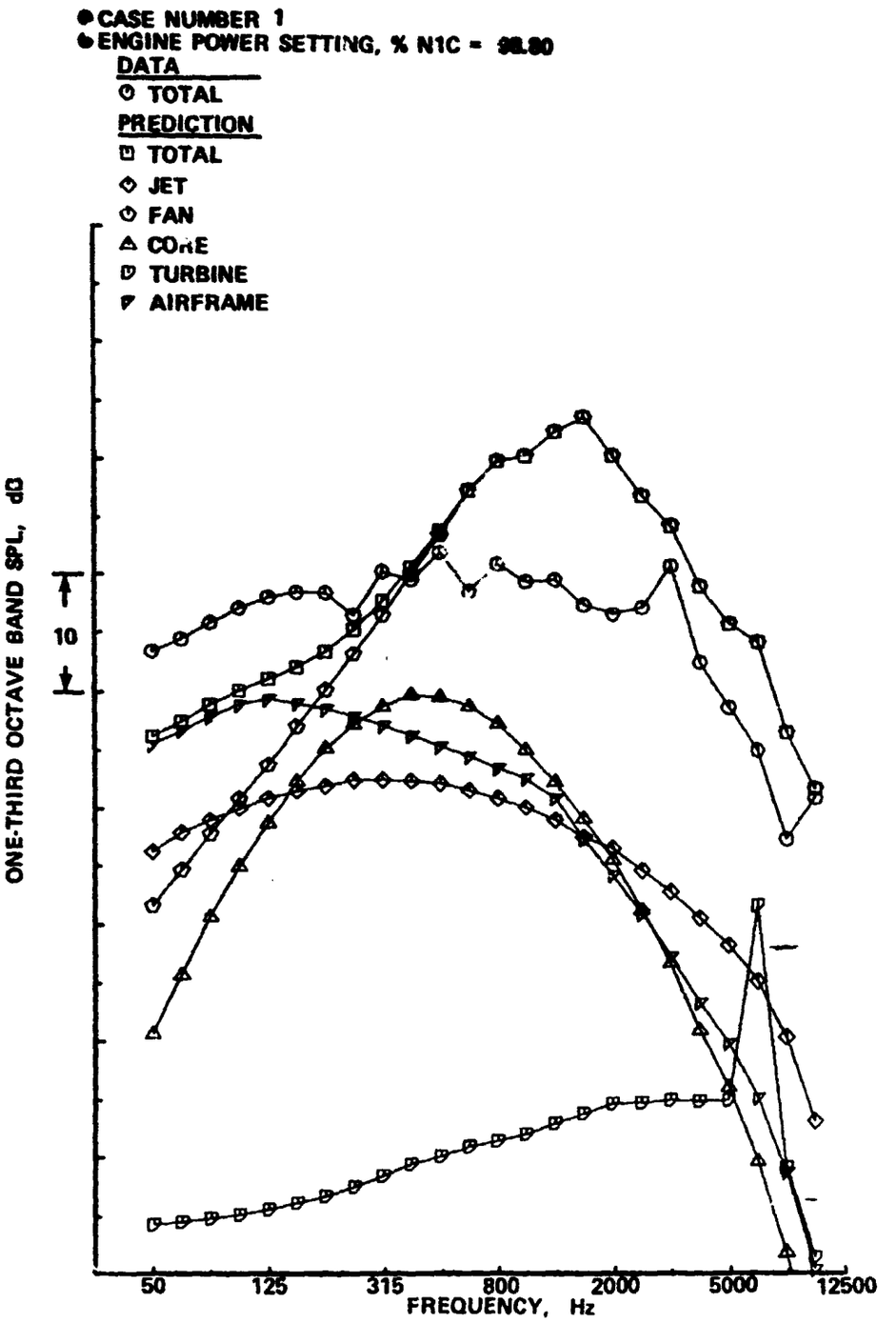

(b) DIRECTIVITY ANGLE = 60°

Figure A1. — (Continued)

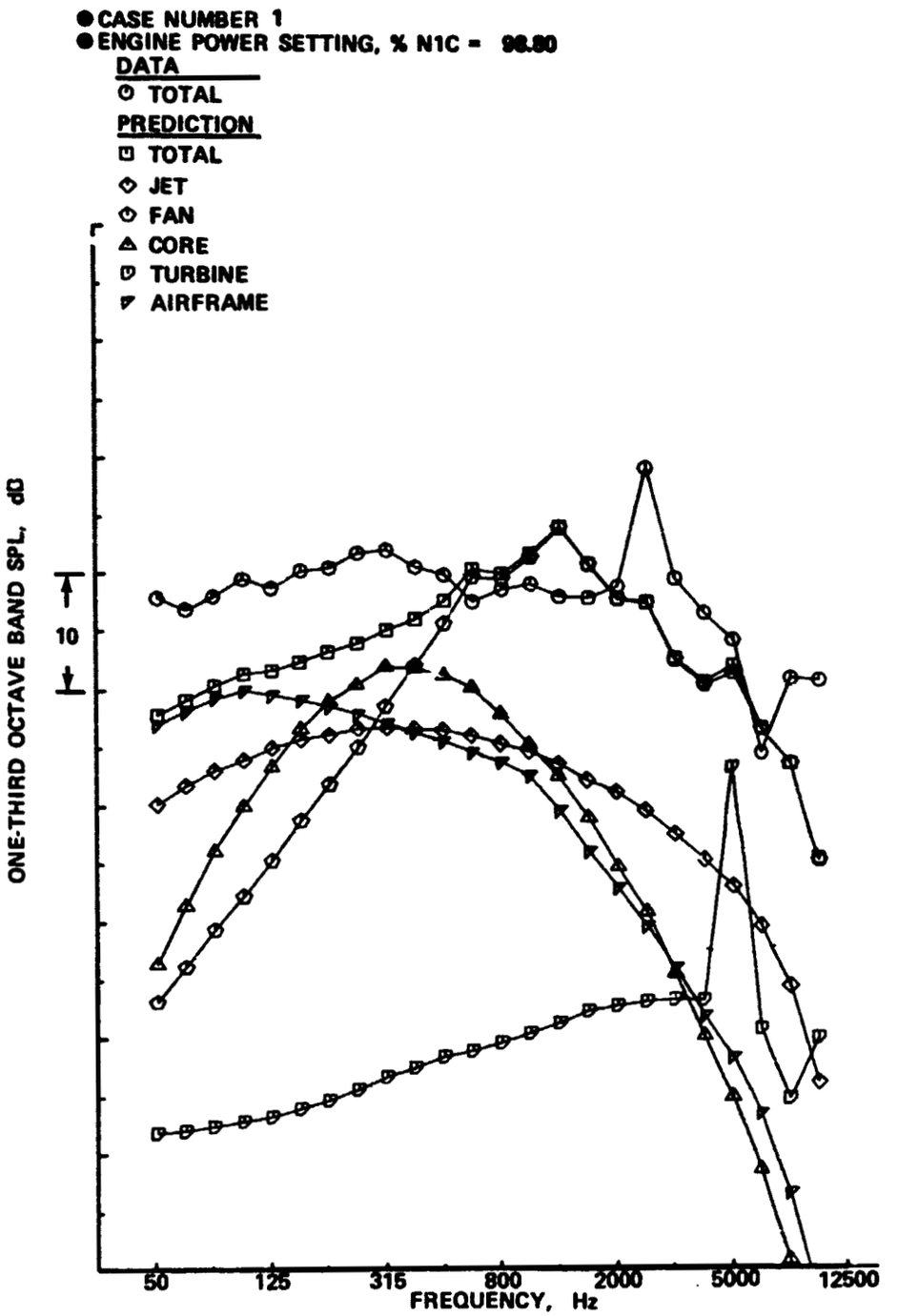

(c) DIRECTIVITY ANGLE = 90°

Figure A1. – (Continued)

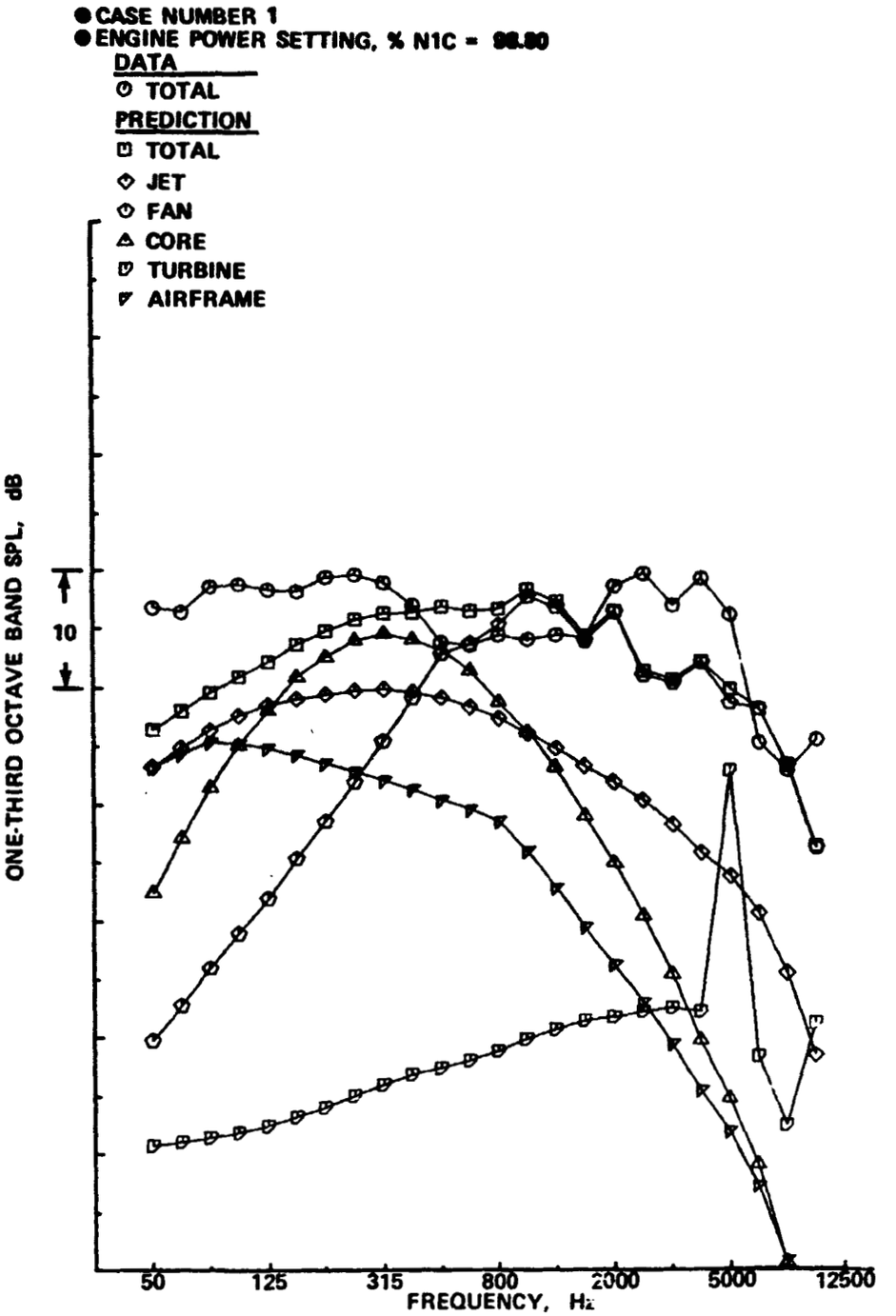

(d) DIRECTIVITY ANGLE = 120°

Figure A1. – (Continued)

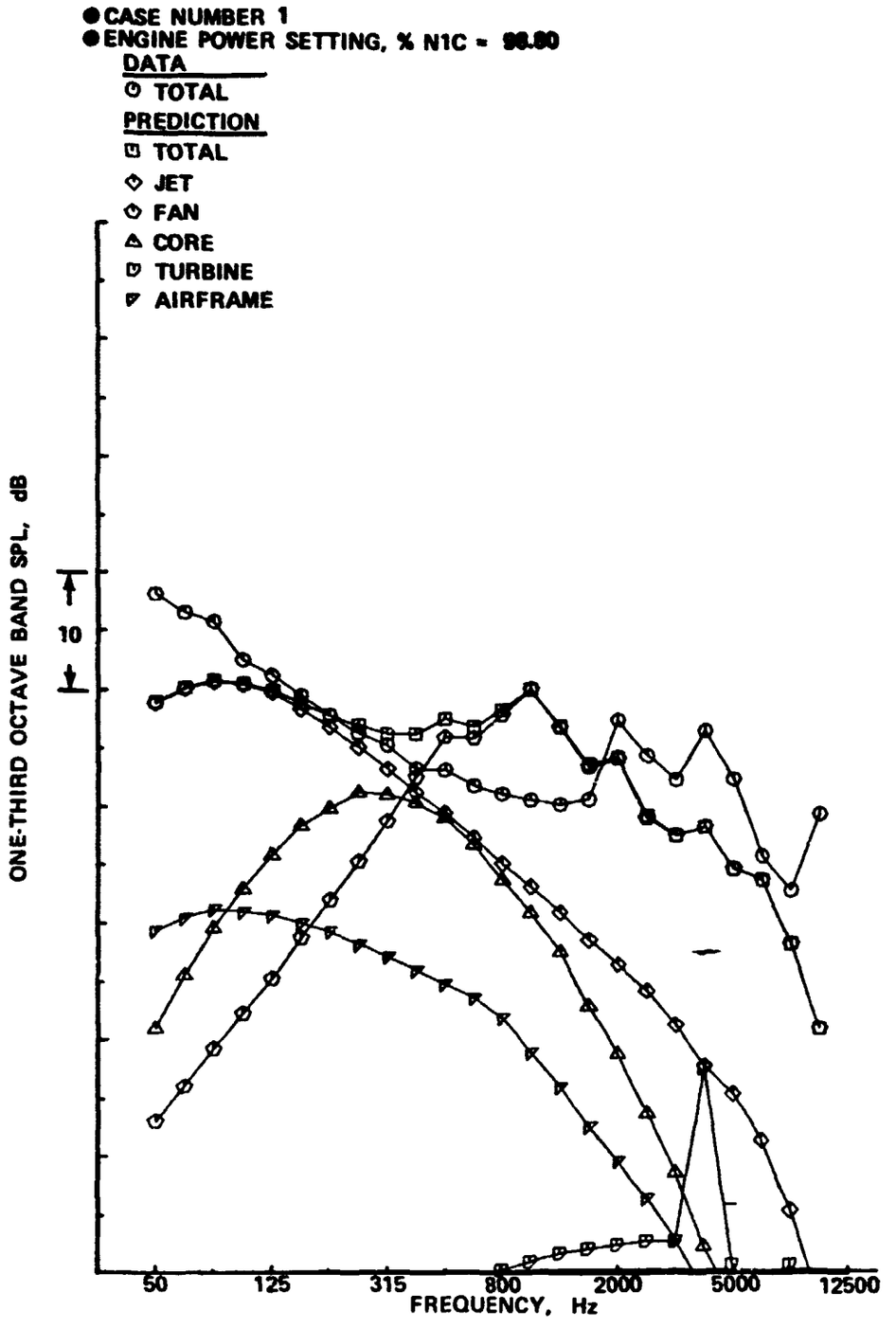

(e) DIRECTIVITY ANGLE = 150°

Figure A1. – (Concluded)

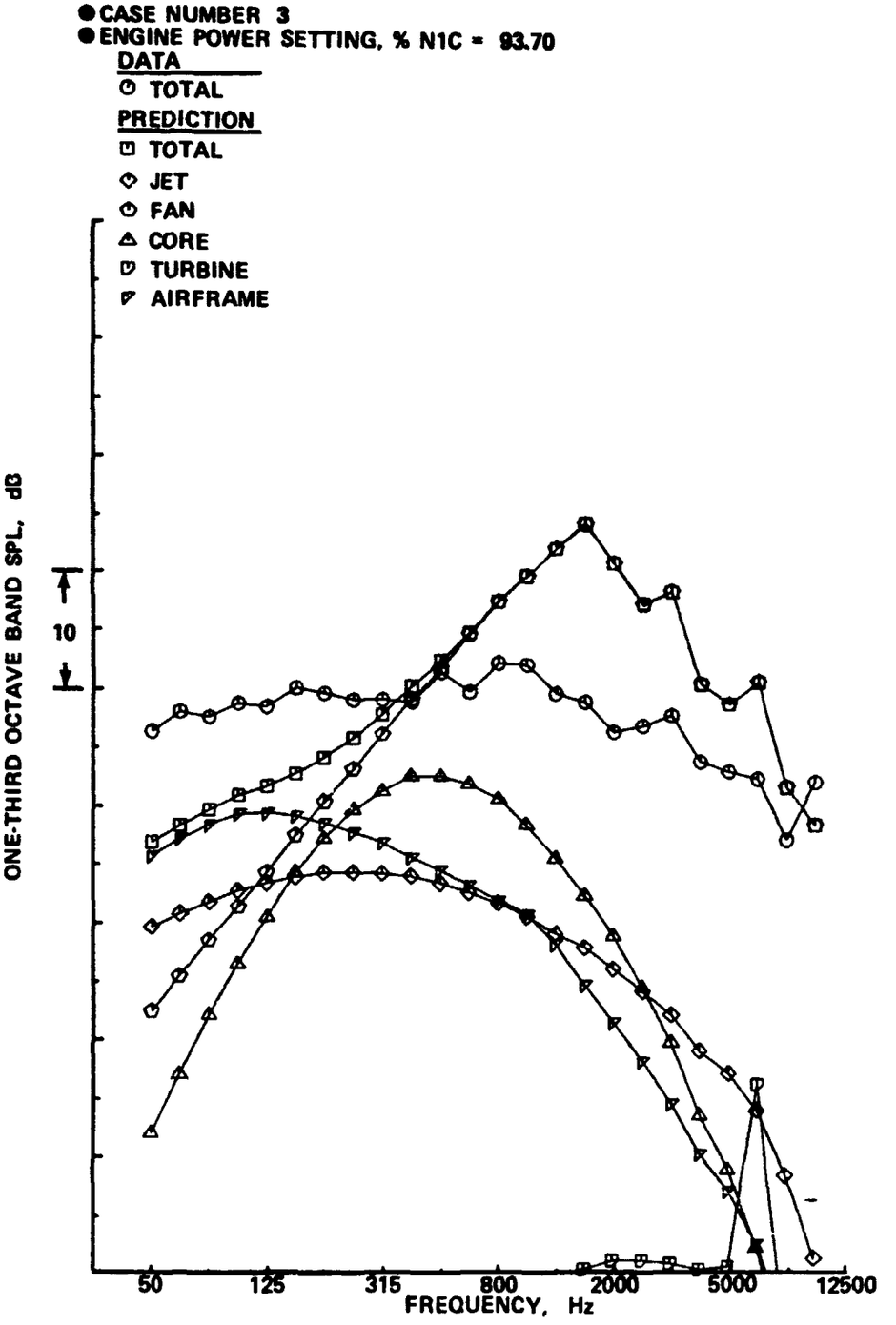

(a) DIRECTIVITY ANGLE = 30°

Figure A2. — Spectral Comparisons of Data and Prediction, Engine Power Setting % N_{1C} = 93.7

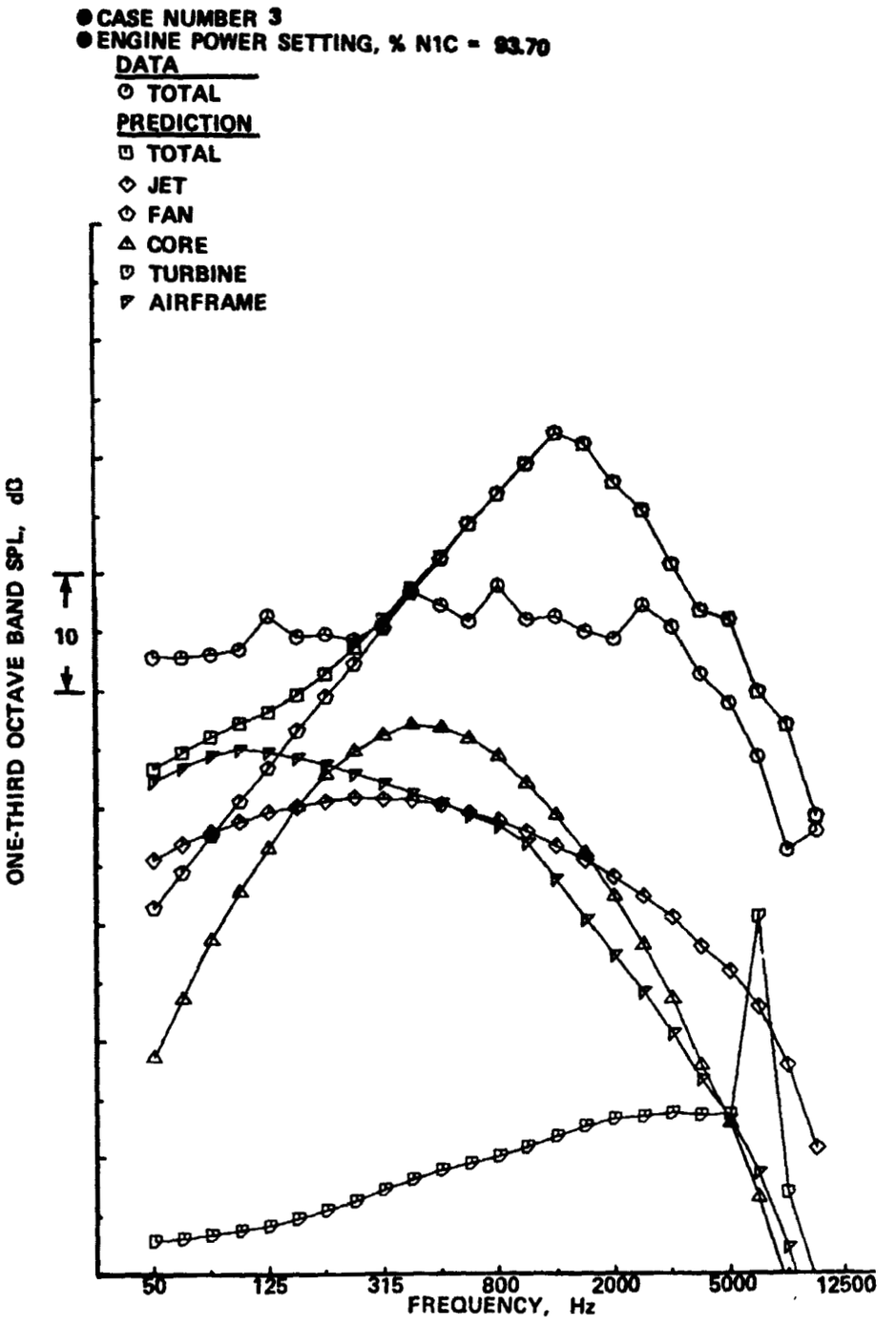

(b) DIRECTIVITY ANGLE = 60°

Figure A2. – (Continued)

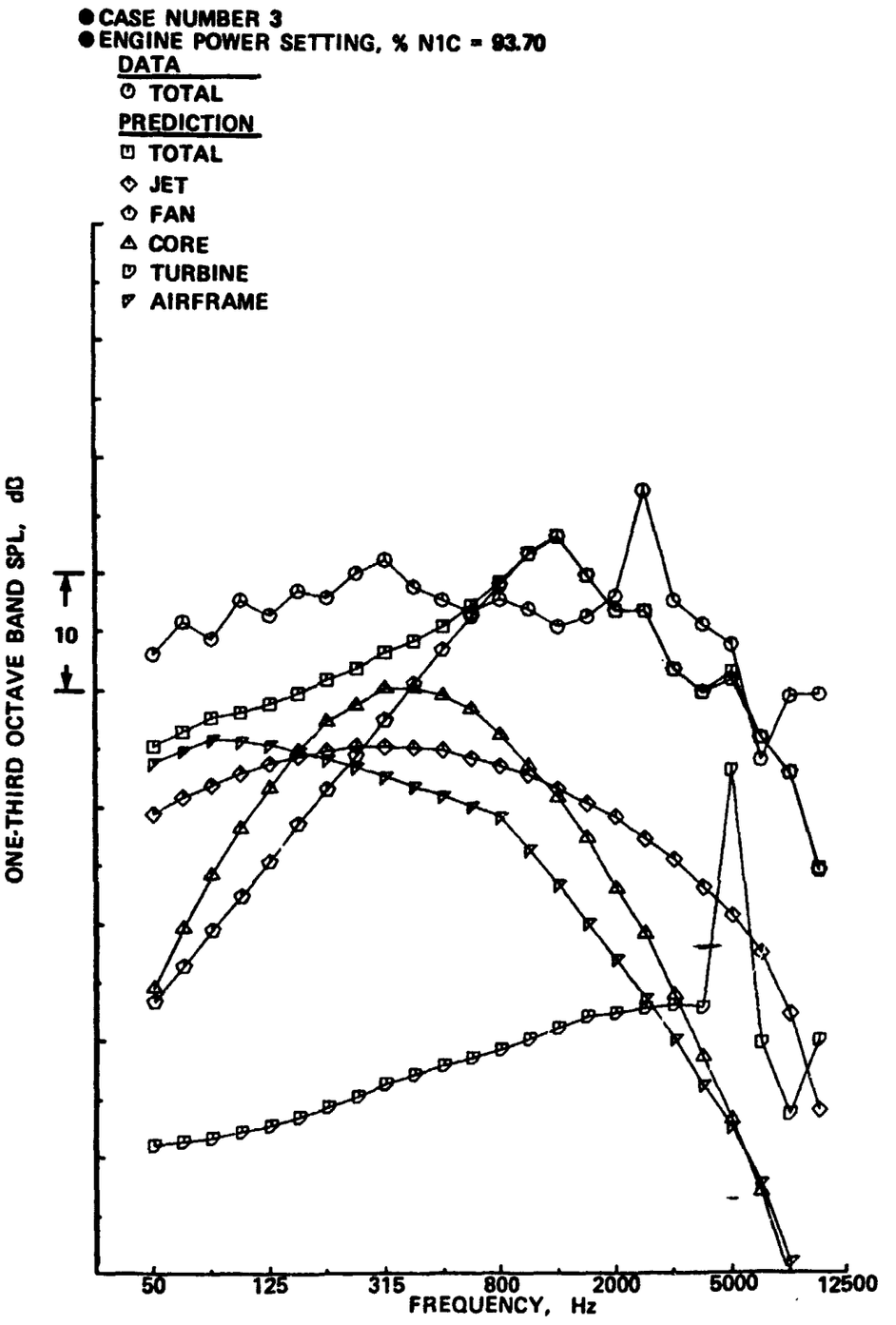

(c) DIRECTIVITY ANGLE = 90°

Figure A2. – (Continued)

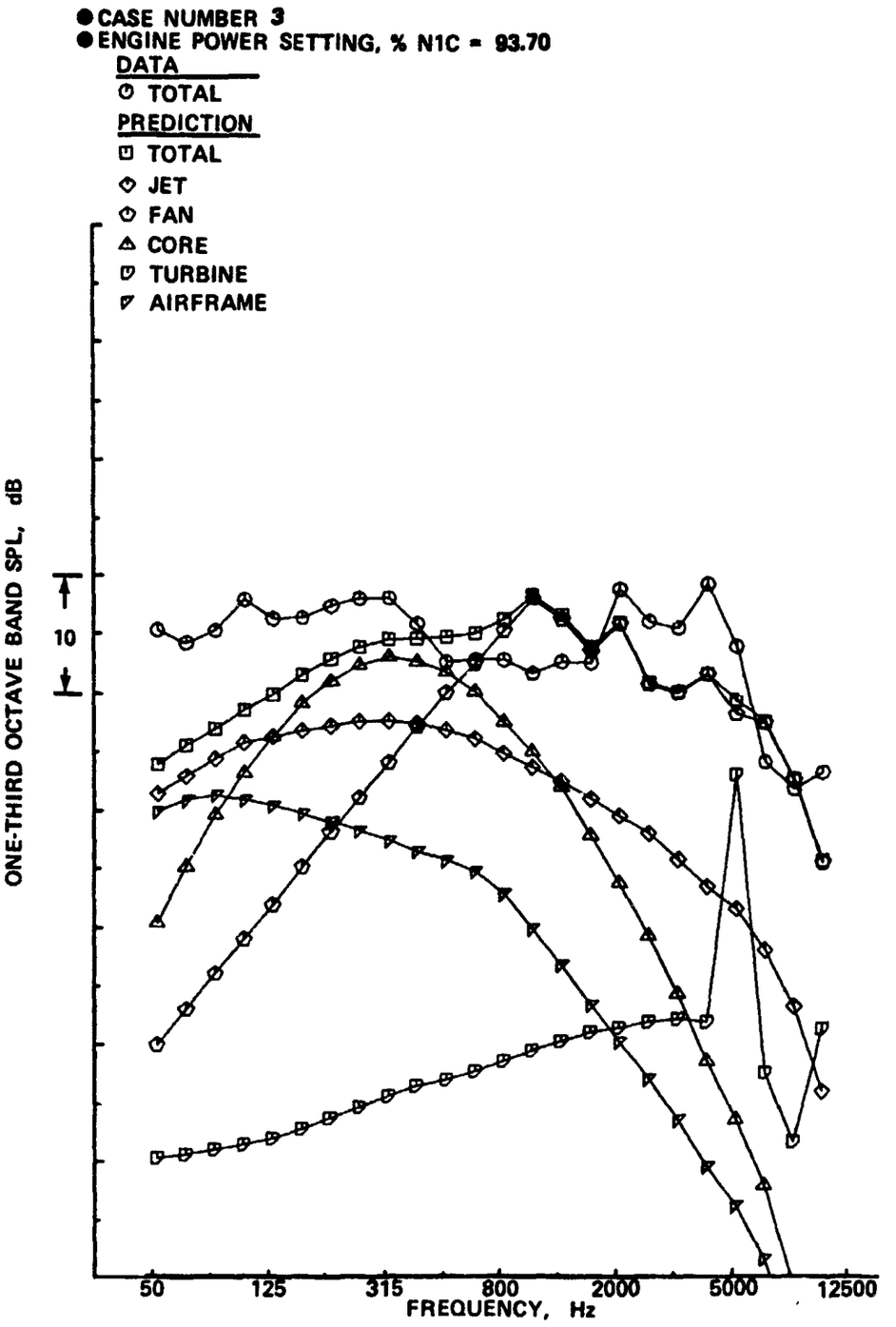

(d) DIRECTIVITY ANGLE = 120°

Figure A2. – (Continued)

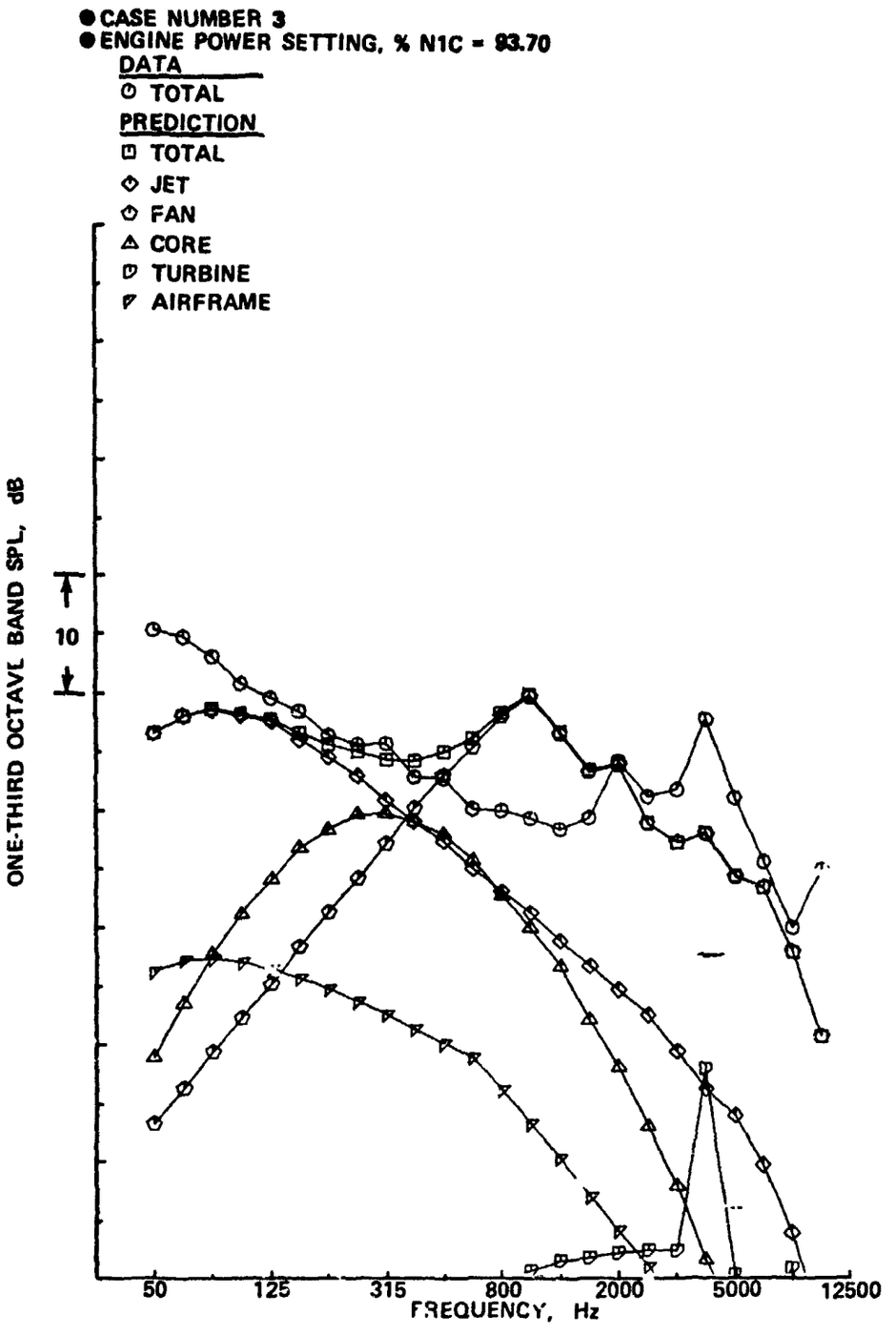

(e) DIRECTIVITY ANGLE = 150°

Figure A2. – (Concluded)

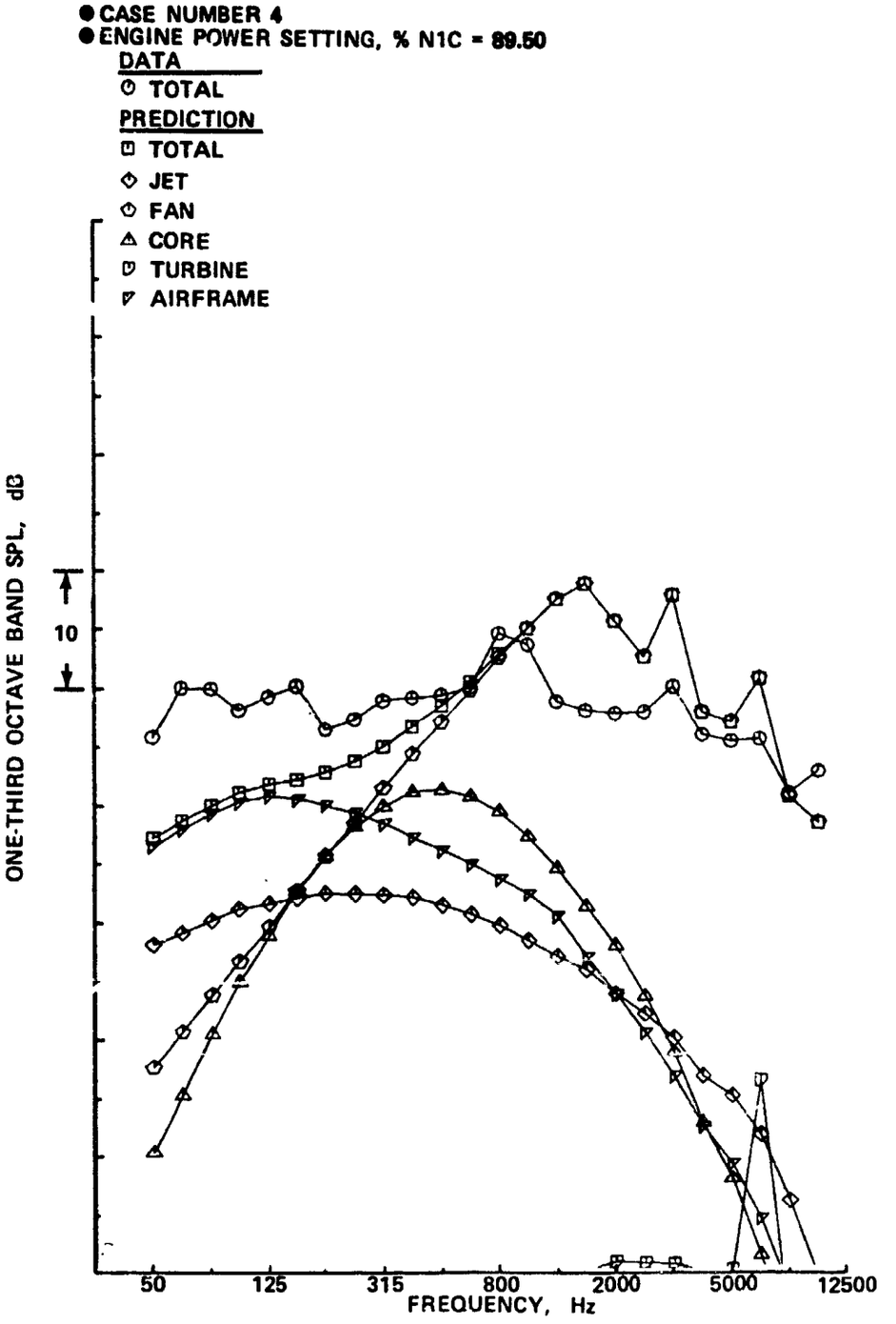

(a) DIRECTIVITY ANGLE = 30°

Figure A3. – Spectral Comparisons of Data and Prediction, Engine Power Setting % N_{1C} = 89.5

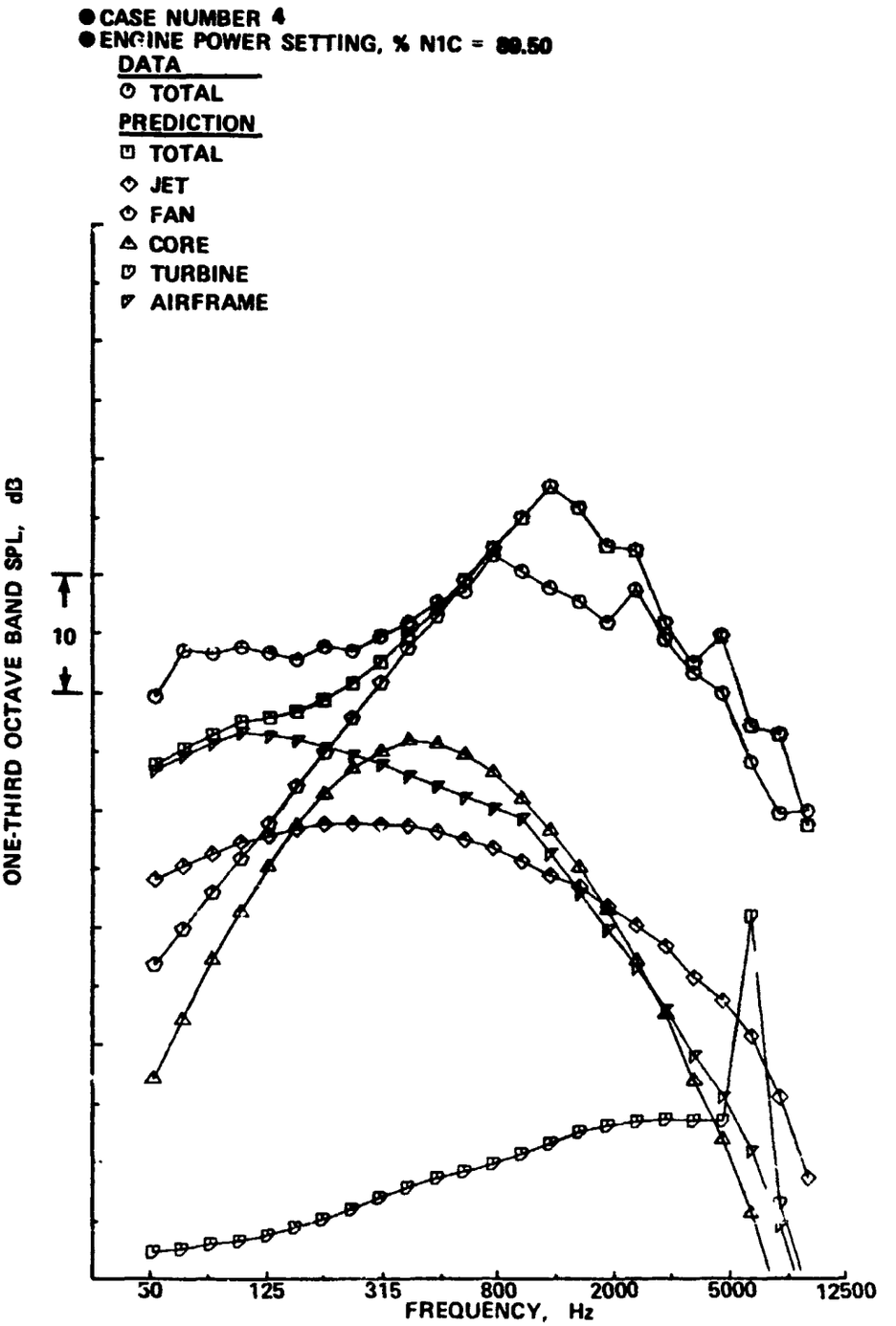

(b) DIRECTIVITY ANGLE = 60°

Figure A3. — (Continued)

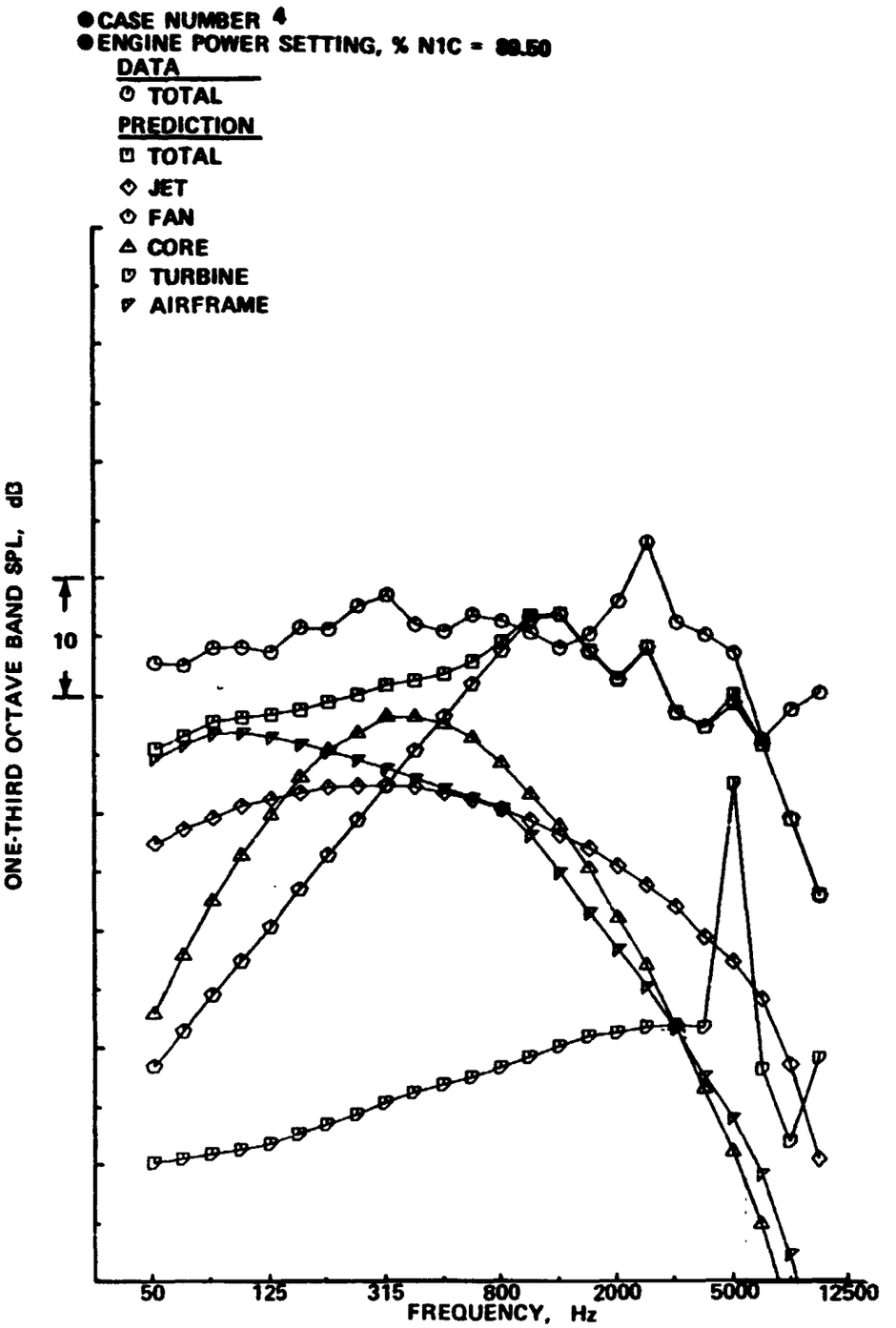

(c) DIRECTIVITY ANGLE = 90°

Figure A3. — (Continued)

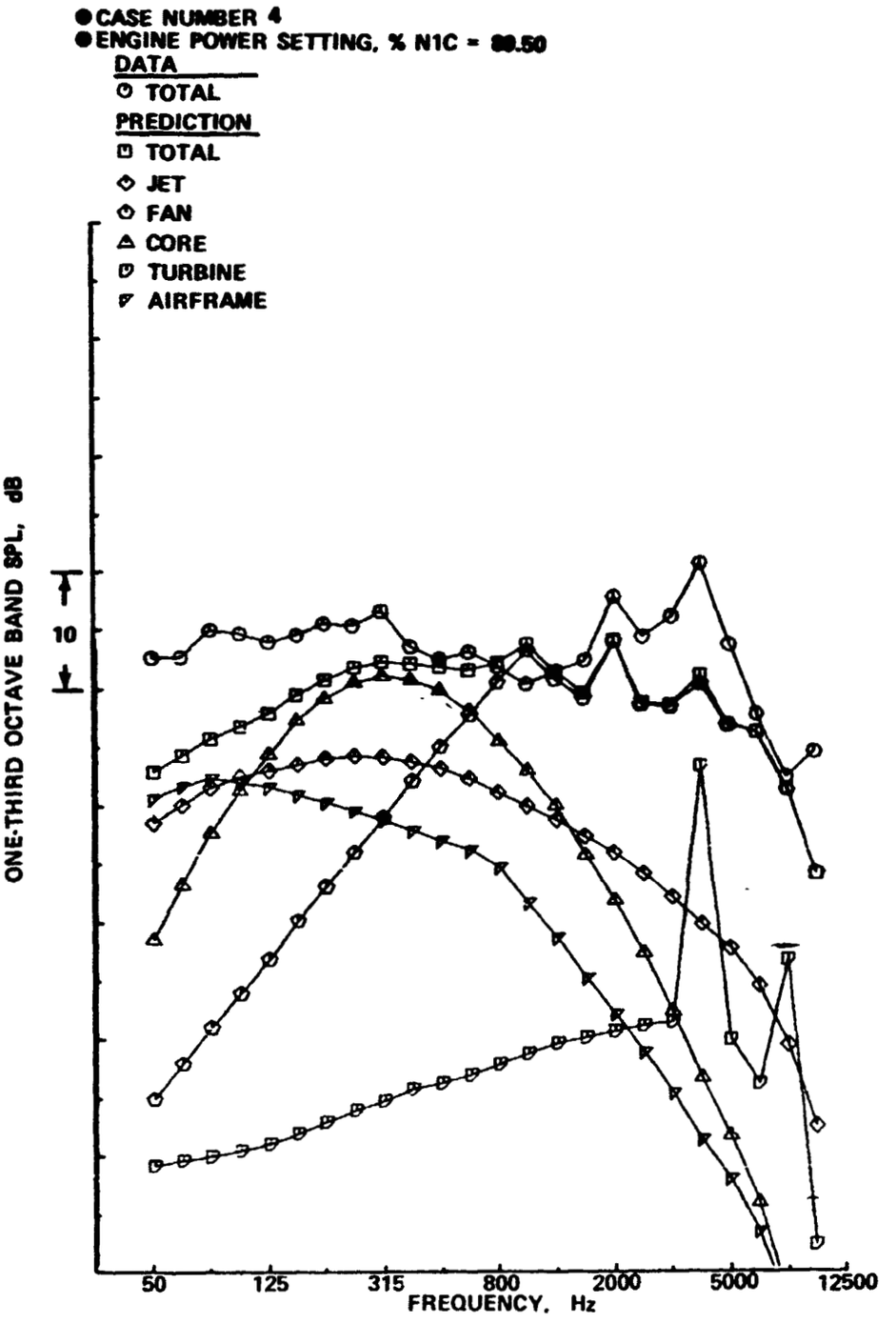

(d) DIRECTIVITY ANGLE = 120°

Figure A3. — (Continued)

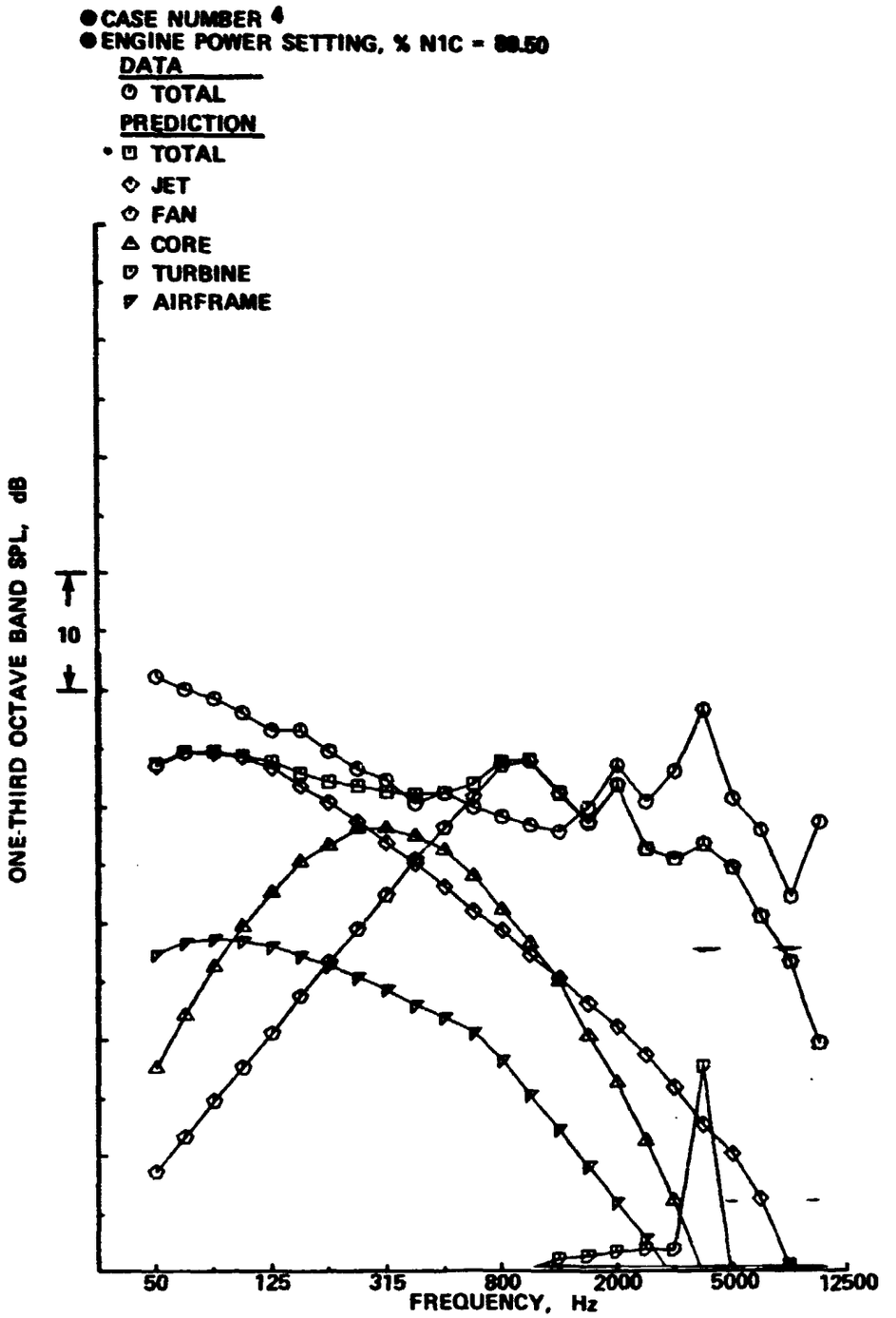

(e) DIRECTIVITY ANGLE = 150°

Figure A3. – (Concluded)

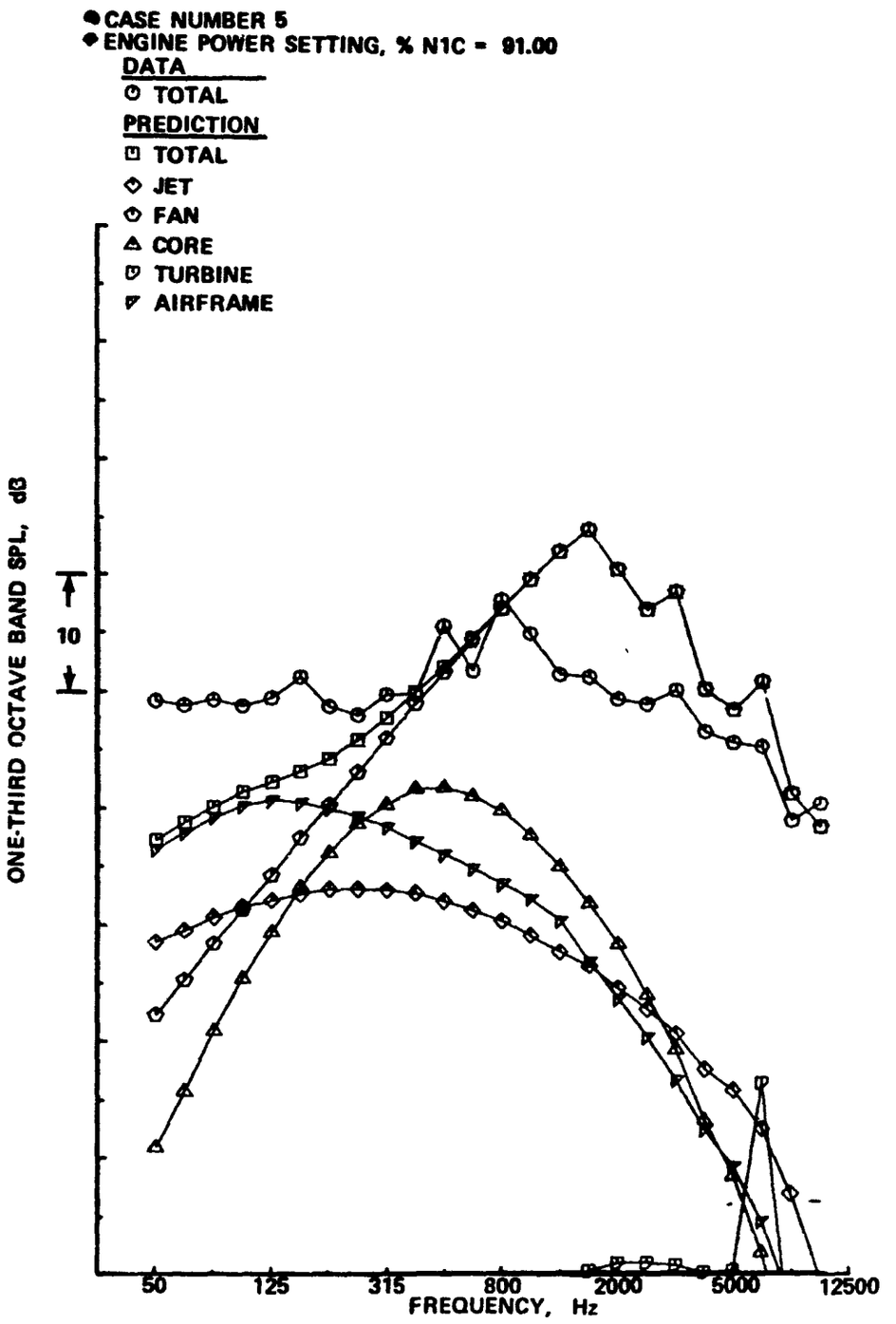

(a) DIRECTIVITY ANGLE = 30°

Figure A4. – Spectral Comparisons of Data and Prediction, Engine Power Setting $\%\ N_{1C} = 91.0$

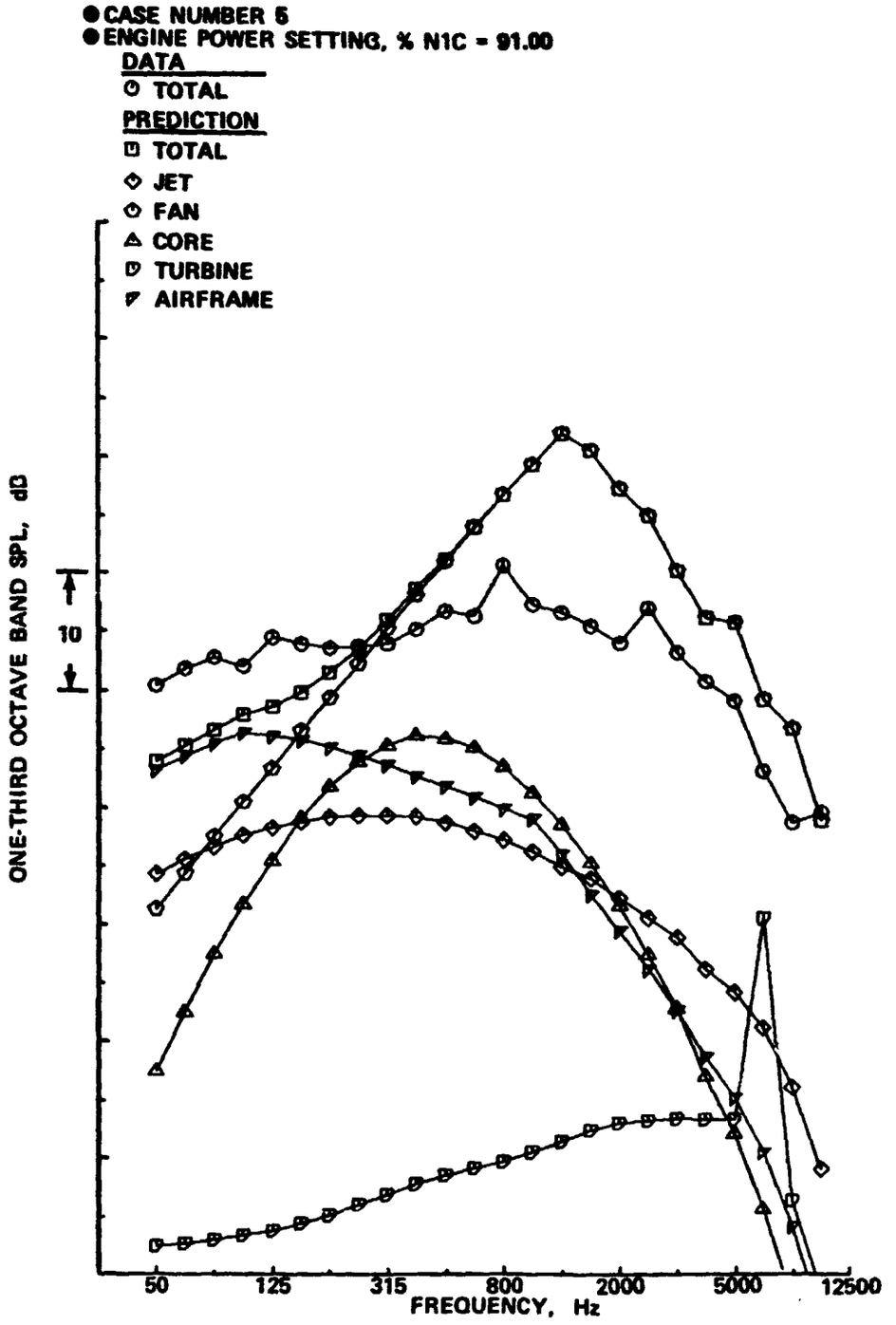

(b) DIRECTIVITY ANGLE = 60°

Figure A4. – (Continued)

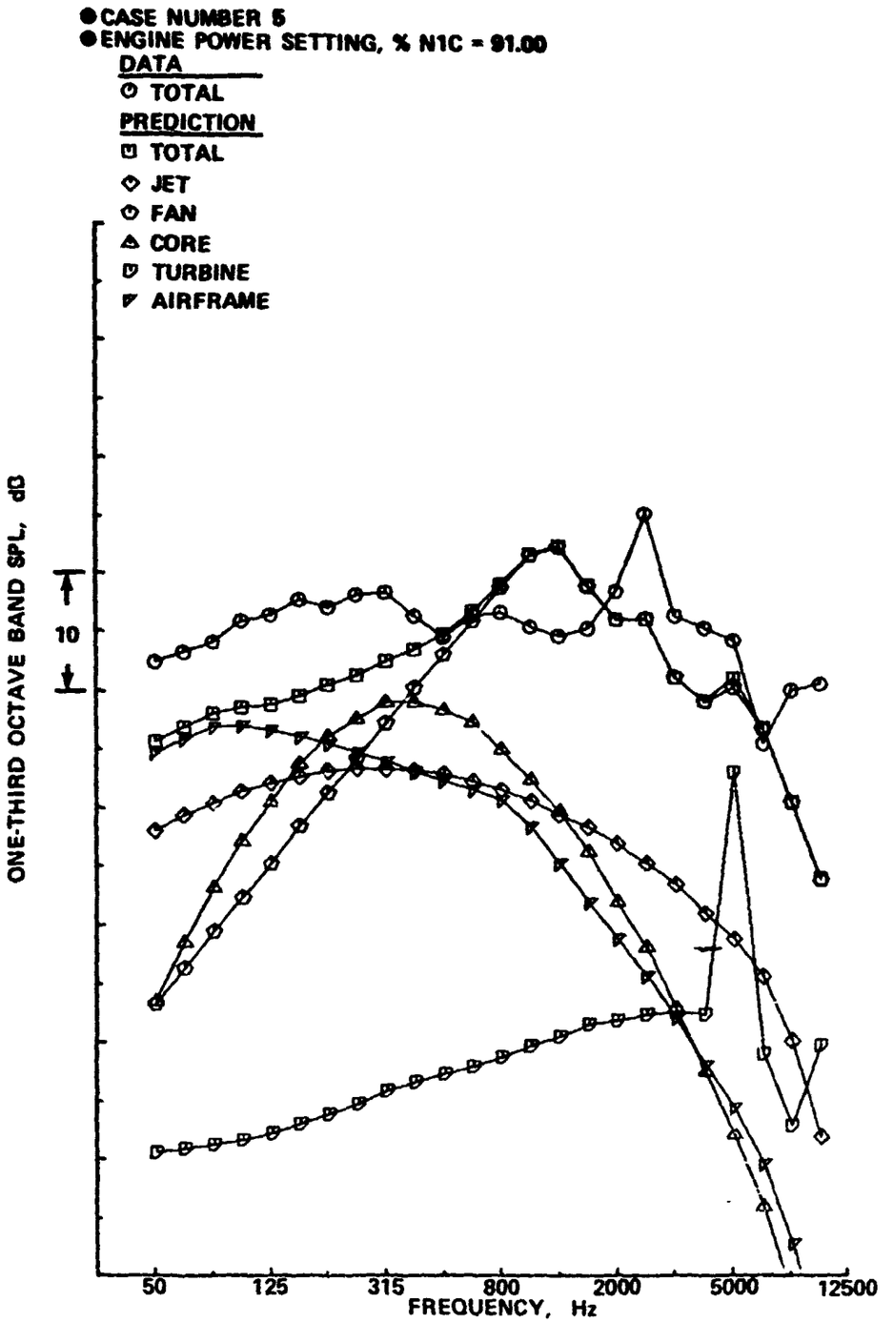

(c) DIRECTIVITY ANGLE = 90°

Figure A4. -- (Continued)

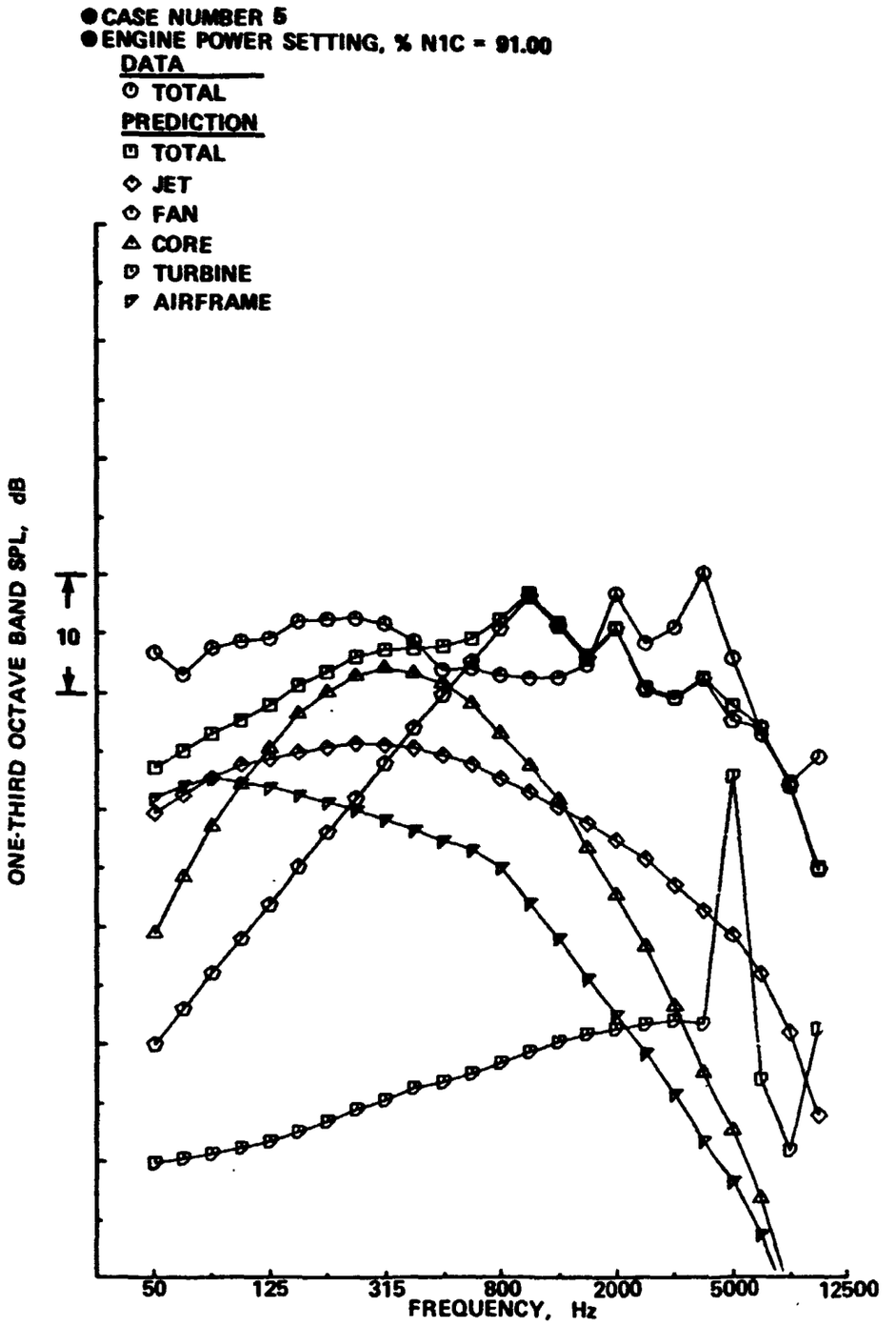

(d) DIRECTIVITY ANGLE = 120°

Figure A4. – (Continued)

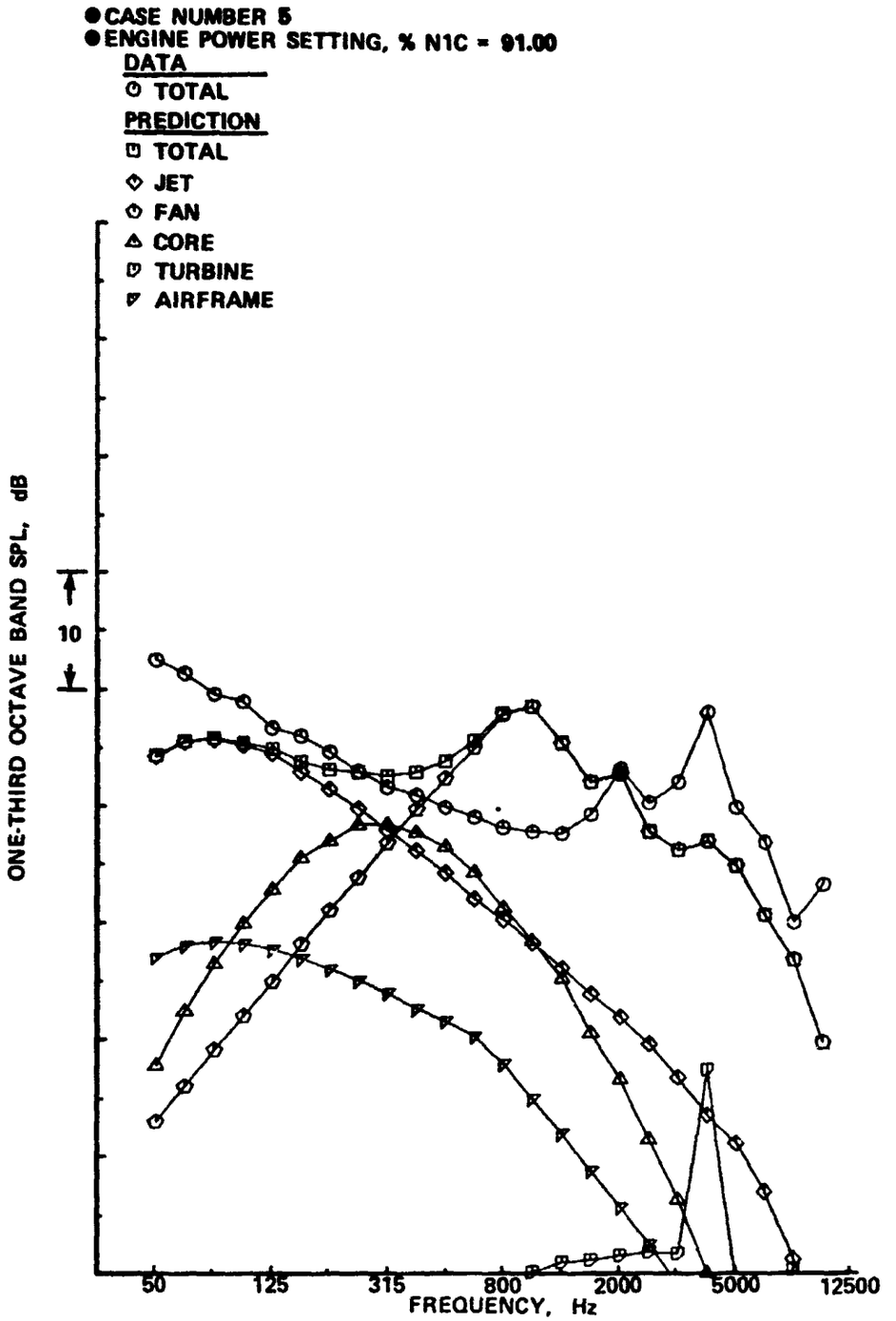

(e) DIRECTIVITY ANGLE = 150°

Figure A4. – (Concluded)

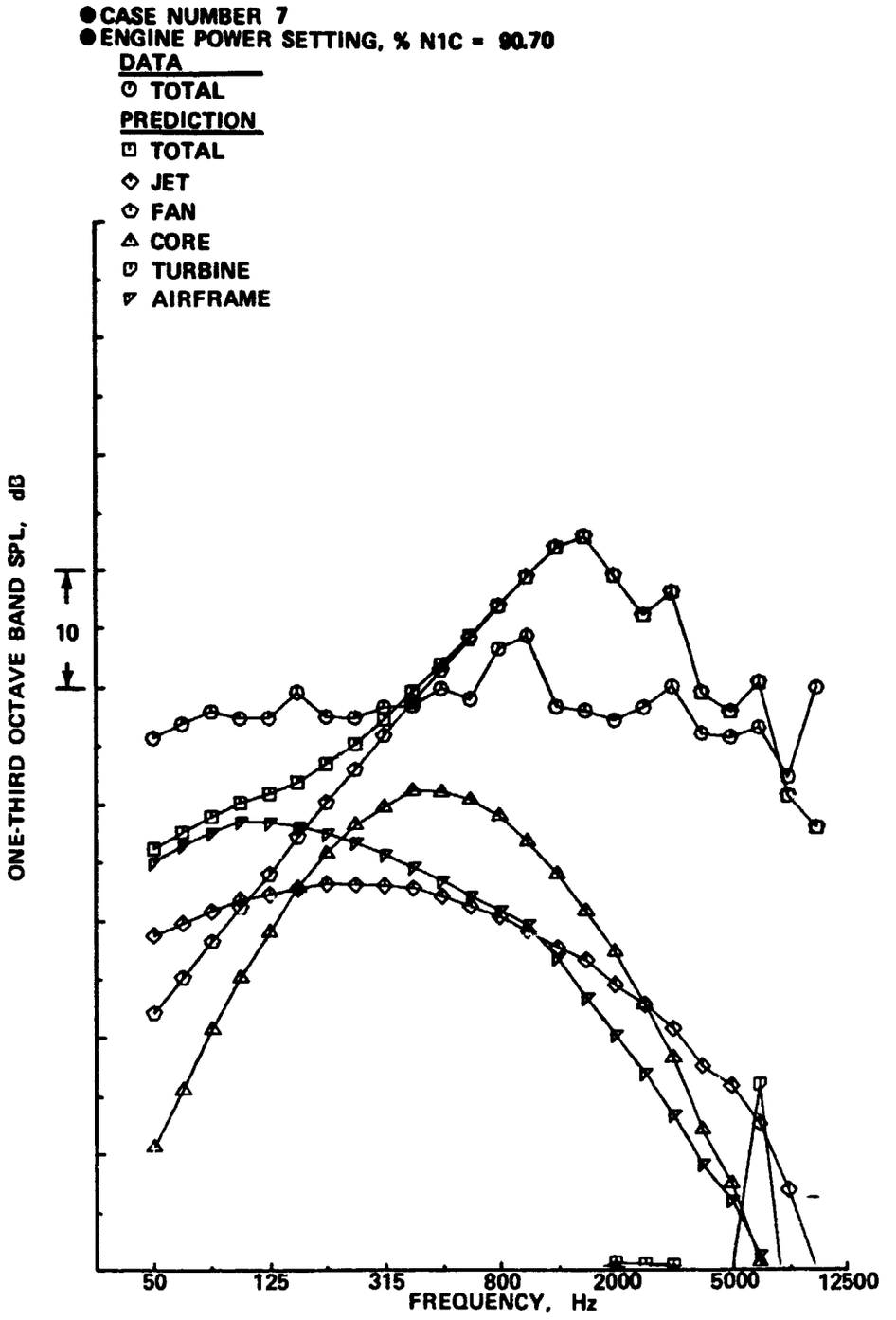

(a) DIRECTIVITY ANGLE = 30°

Figure A5. — Spectral Comparisons of Data and Prediction, Engine Power Setting % N_{1C} = 90.7

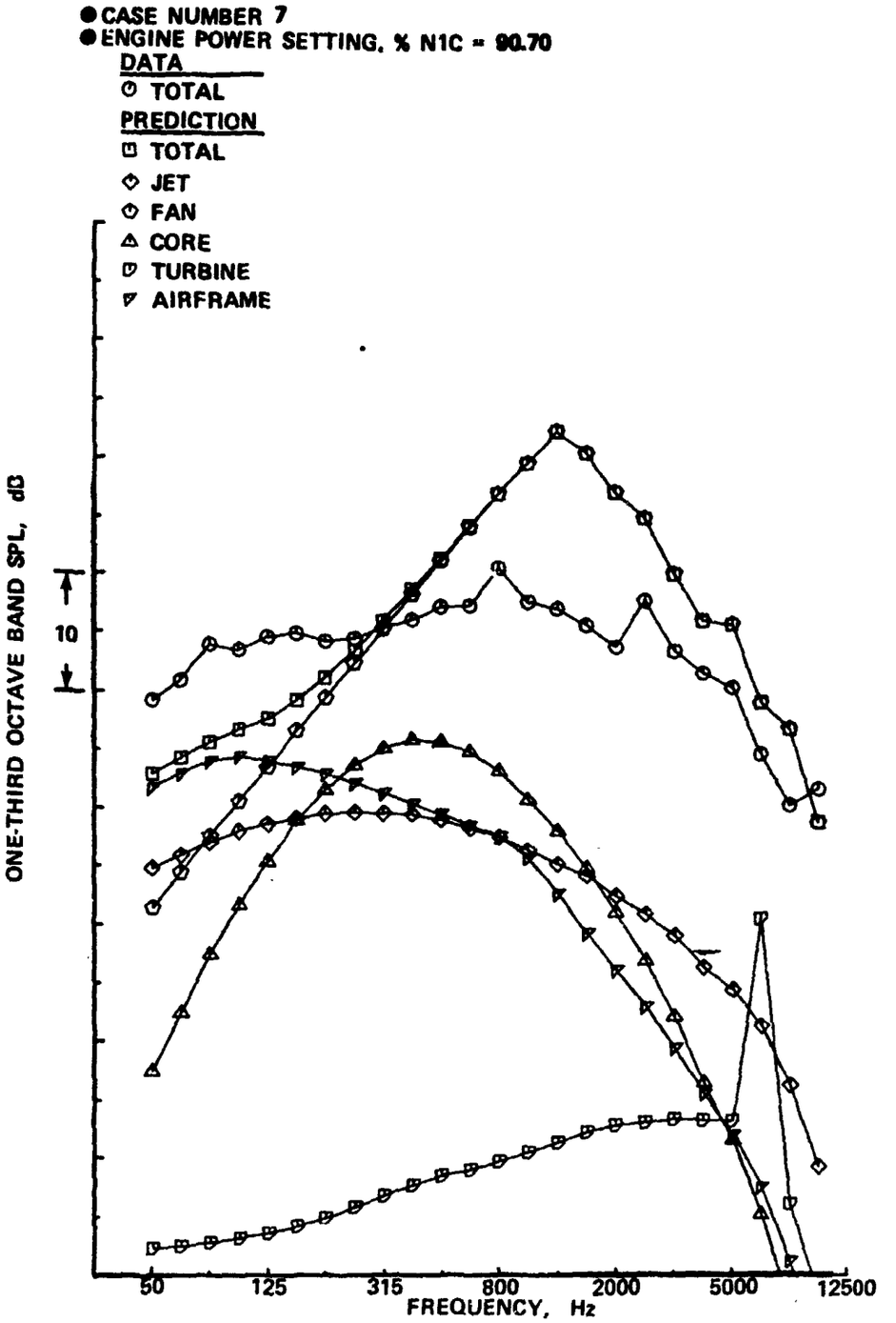

(b) DIRECTIVITY ANGLE = 60°

Figure A5. — (Continued)

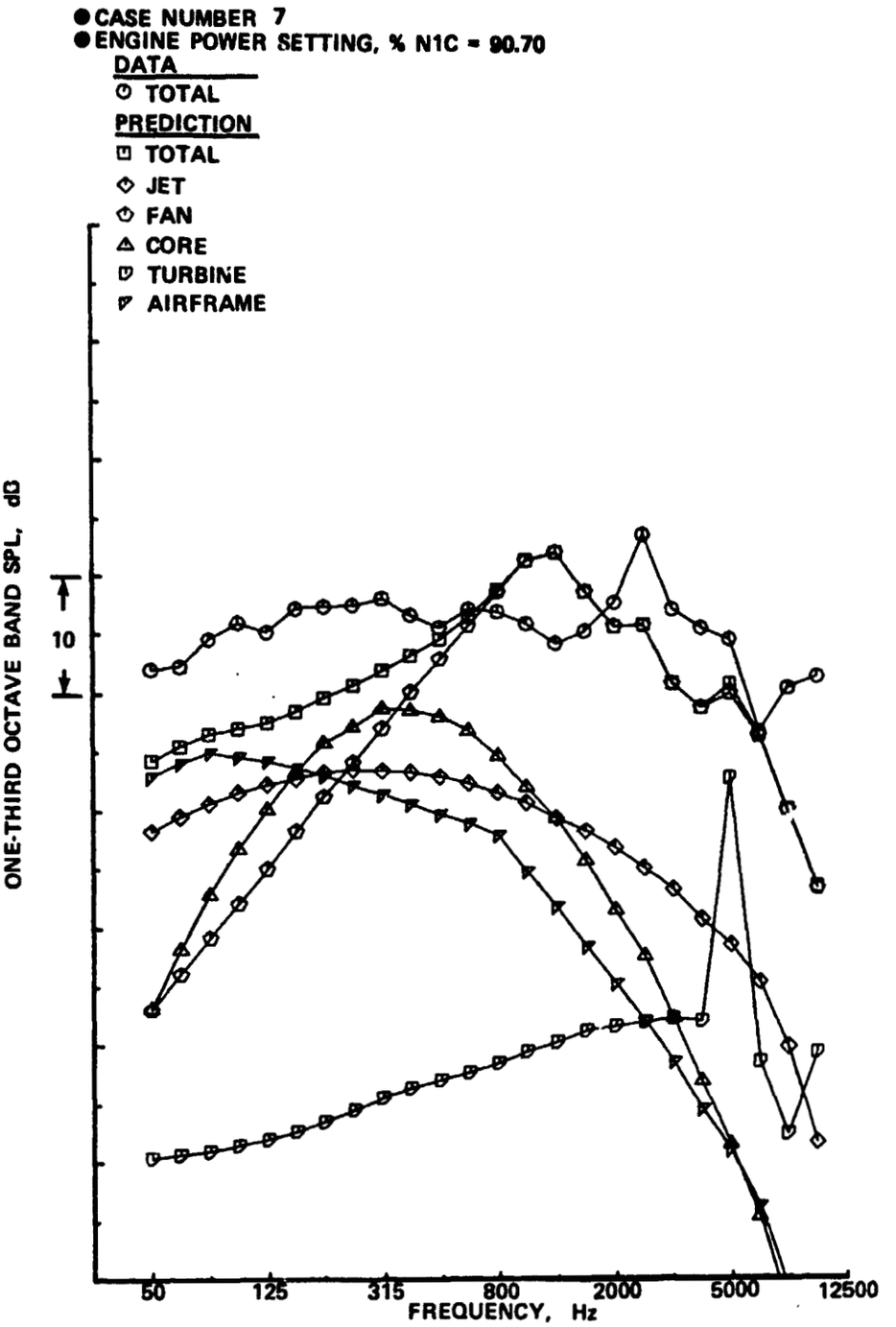

(c) DIRECTIVITY ANGLE = 90°

Figure A5. — (Continued)

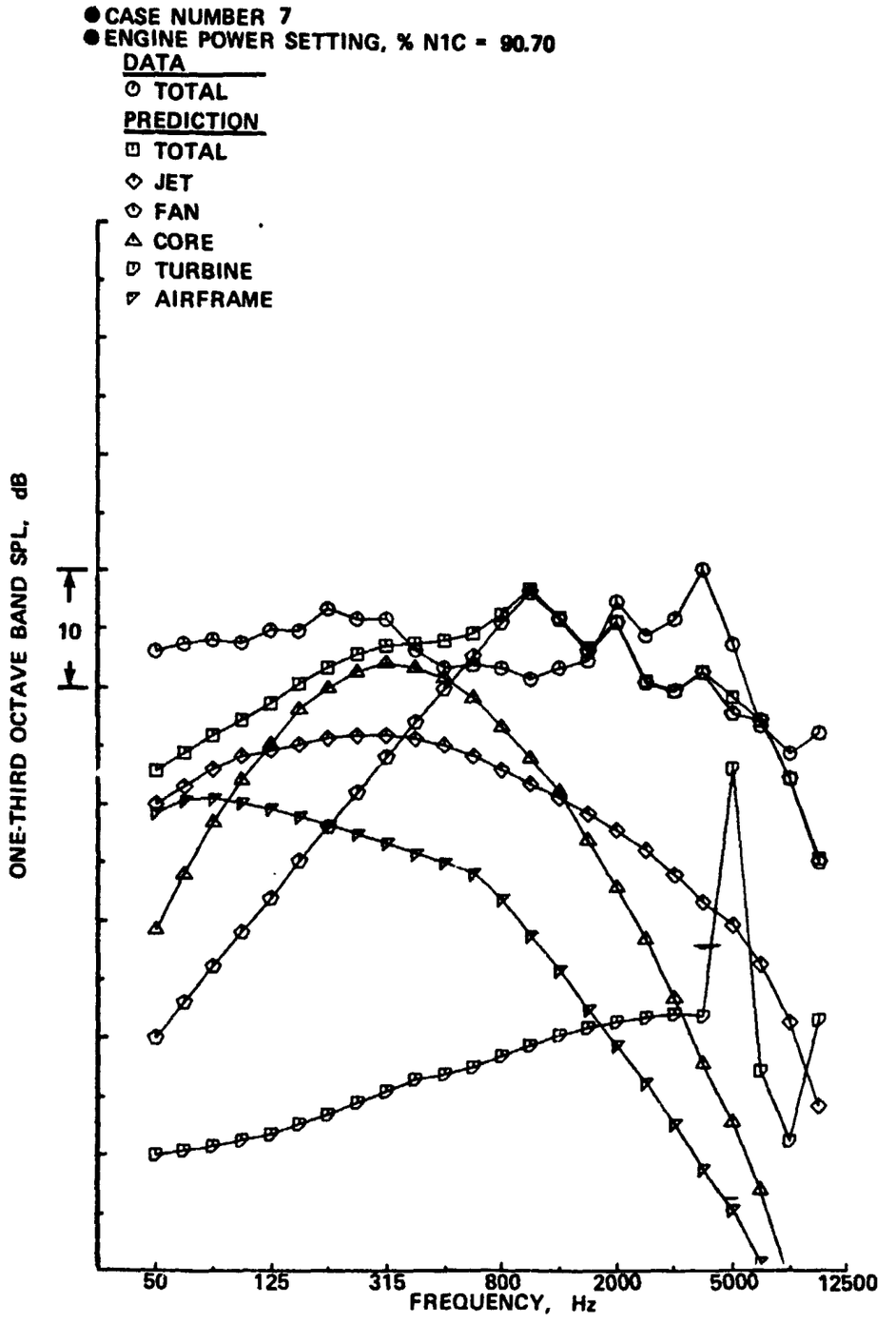

(d) DIRECTIVITY ANGLE = 120°

Figure A5. — (Continued)

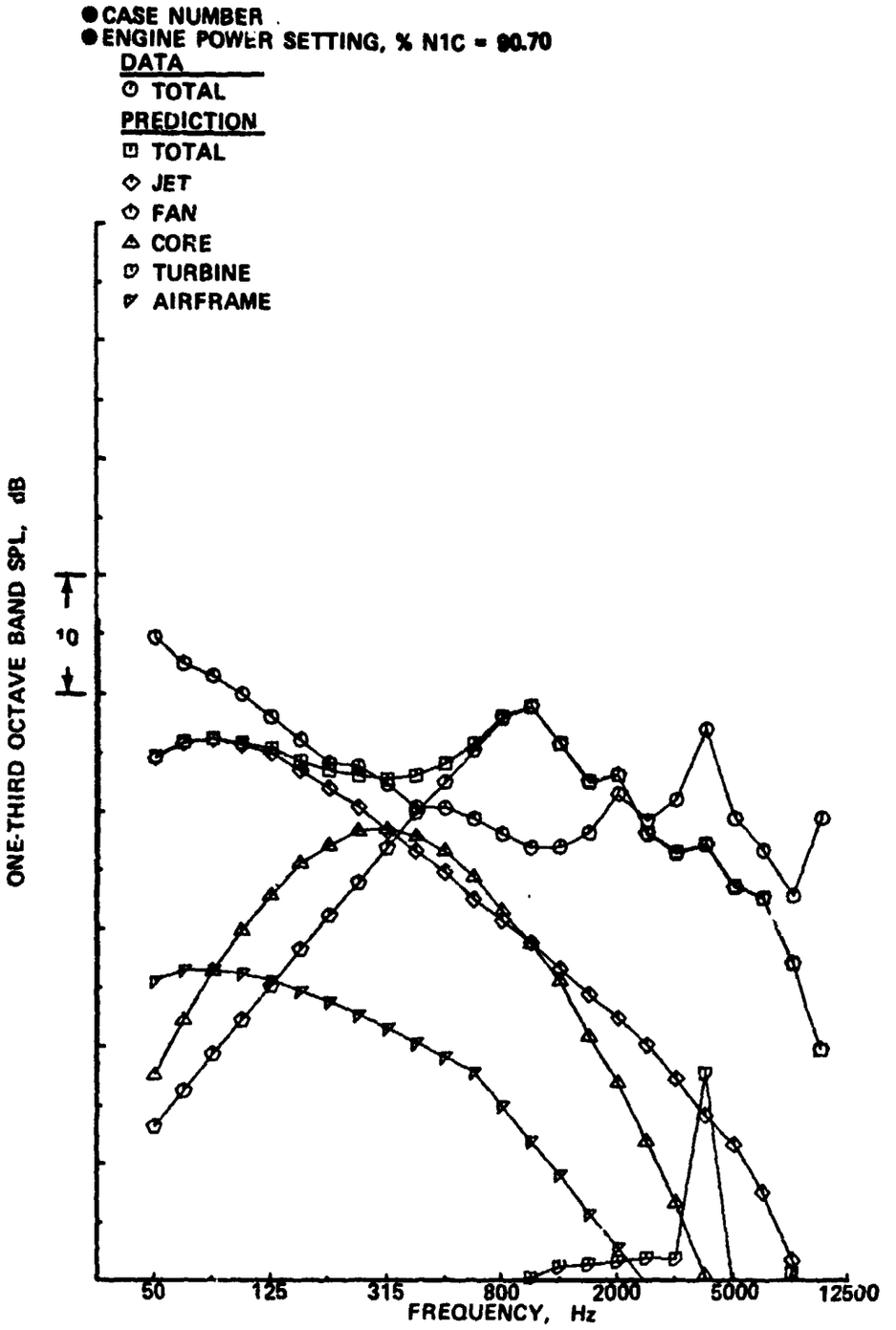

(c) DIRECTIVITY ANGLE = 150°

Figure A5. – (Concluded)

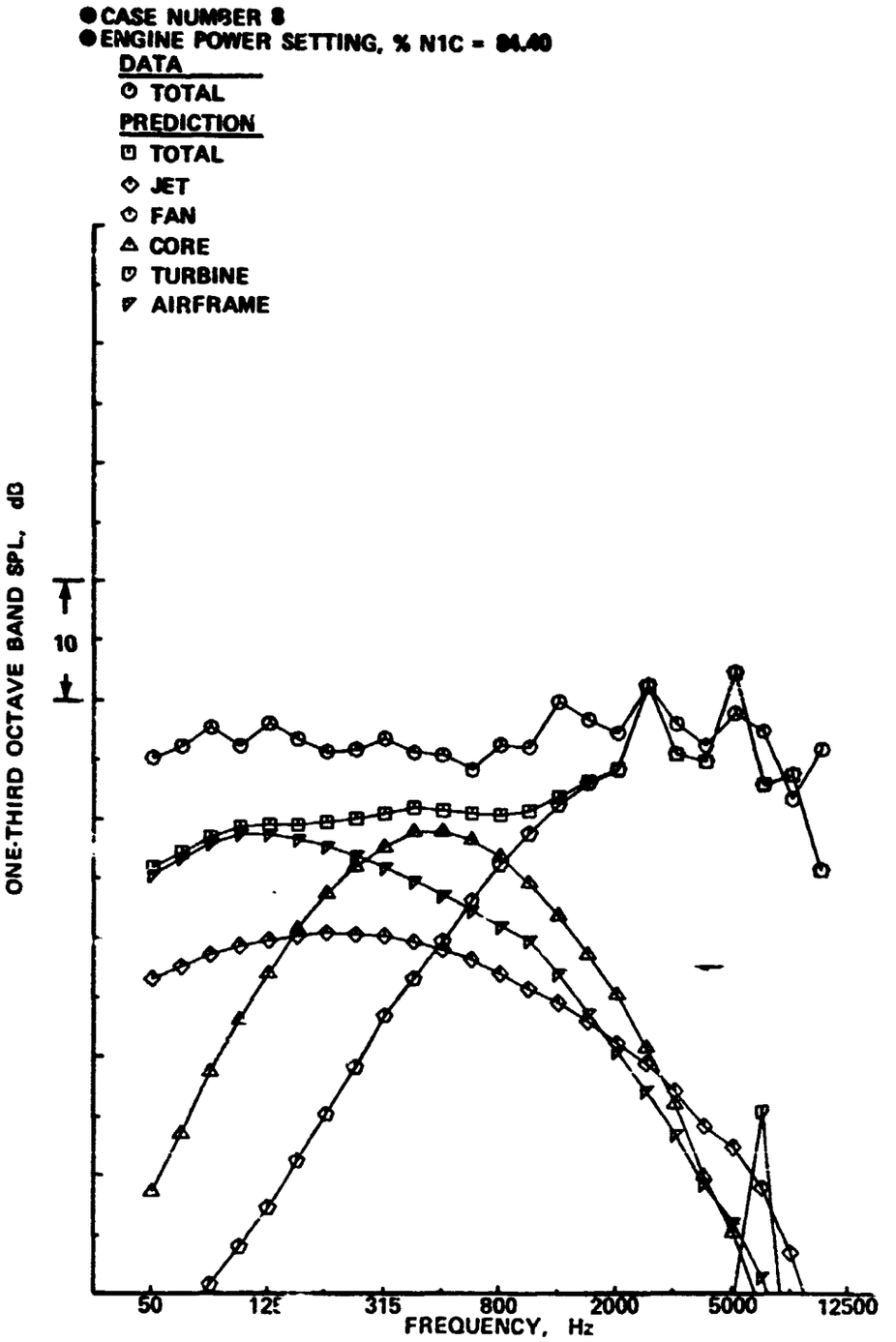

(a) DIRECTIVITY ANGLE = 30°

Figure A6. – Spectral Comparisons of Data and Prediction, Engine Power Setting $\%\ N_{1C} = 84.4$

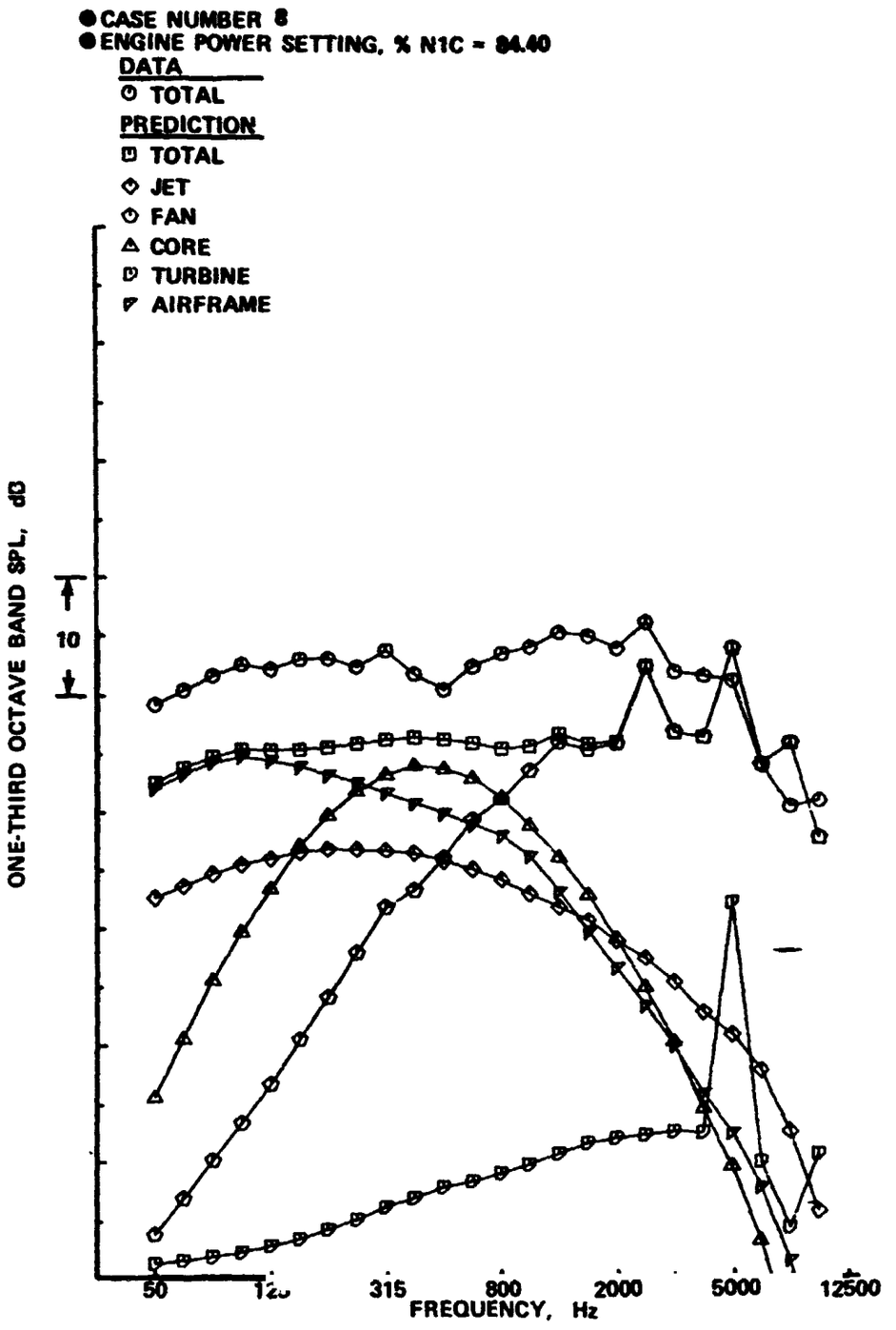

(b) DIRECTIVITY ANGLE = 60°

Figure A6. – (Continued)

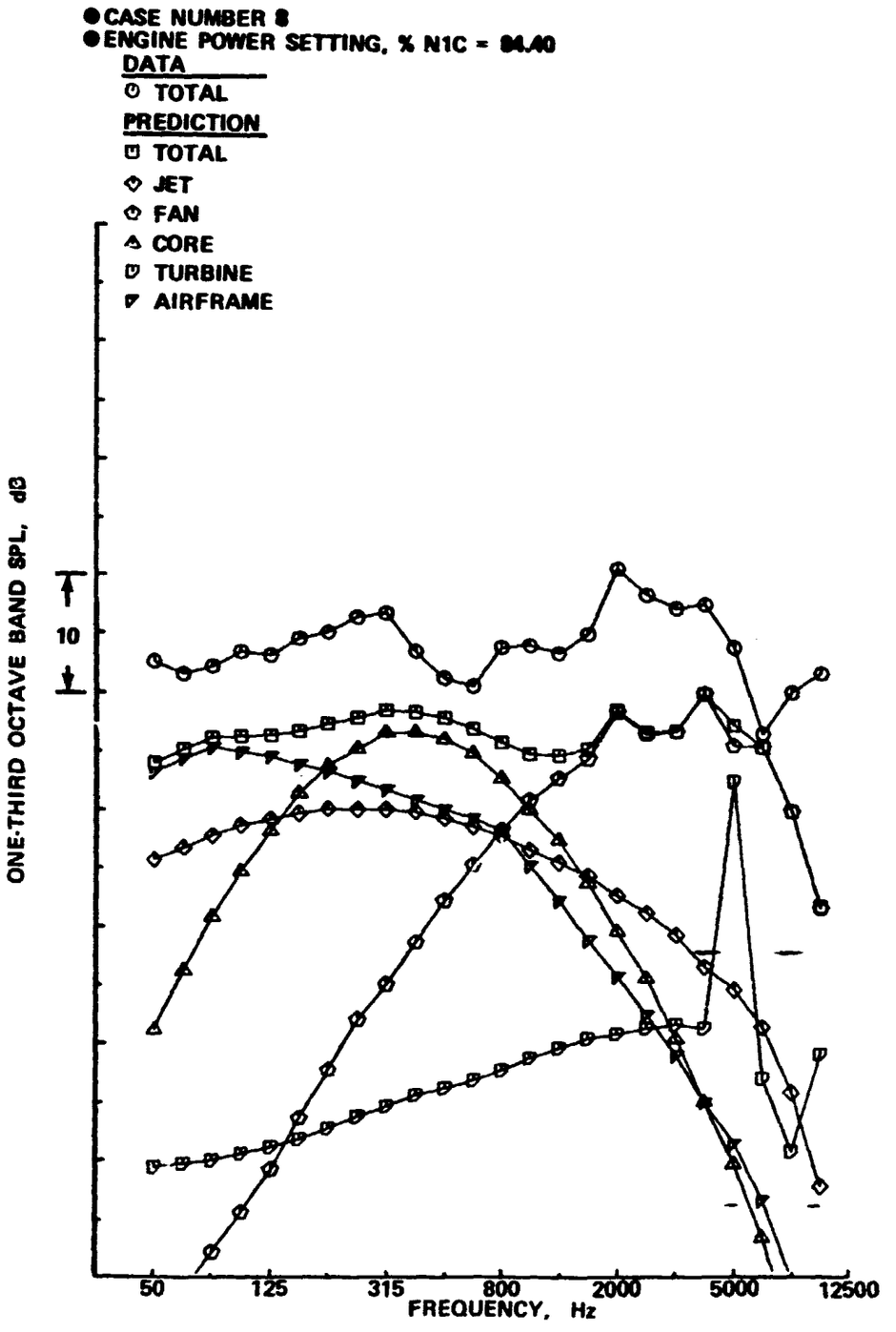

(c) DIRECTIVITY ANGLE = 90°

Figure A6. – (Continued)

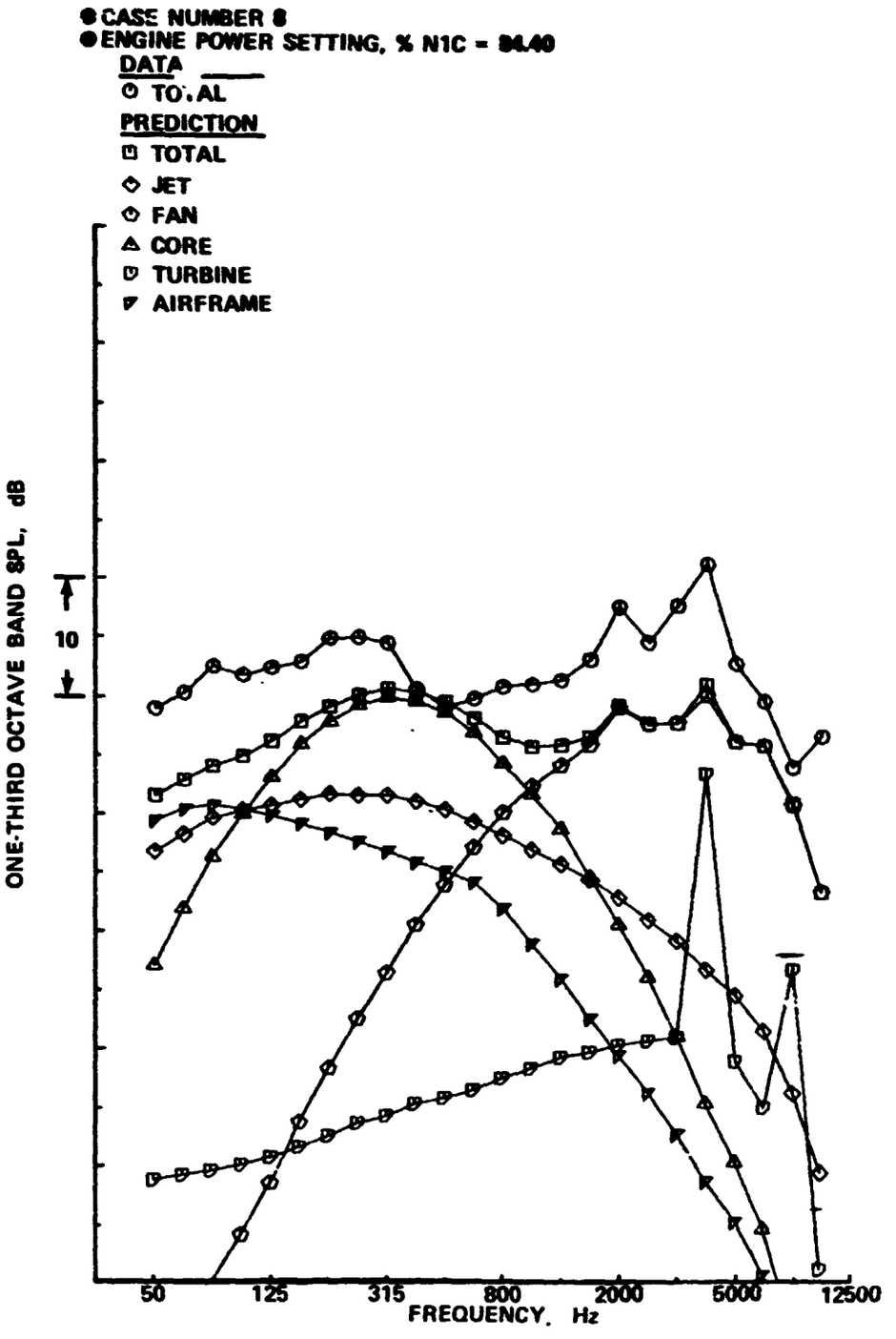

(d) DIRECTIVITY ANGLE = 120°

Figure A6. – (Continued)

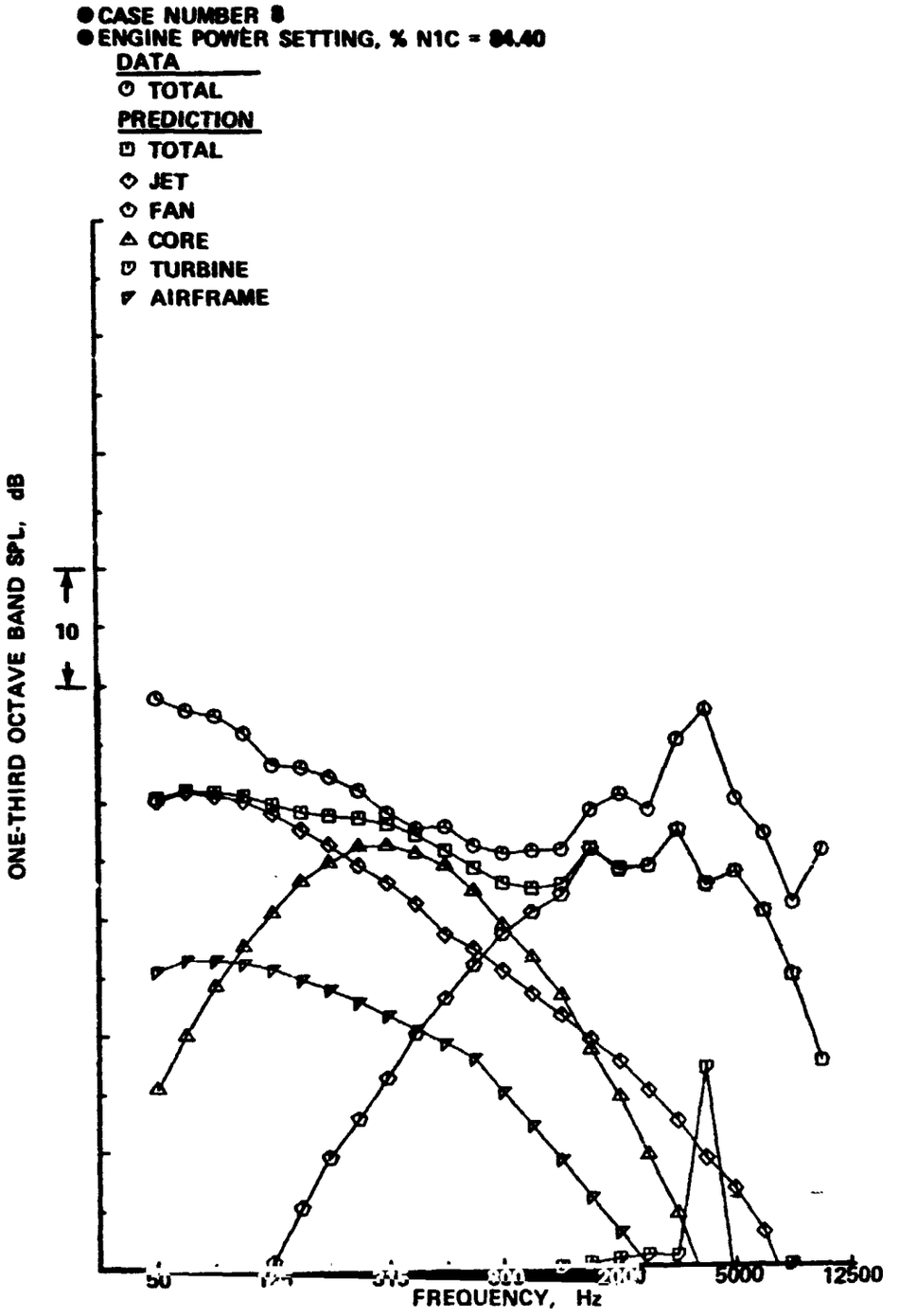

(e) DIRECTIVITY ANGLE = 150°

Figure A6. — (Concluded)

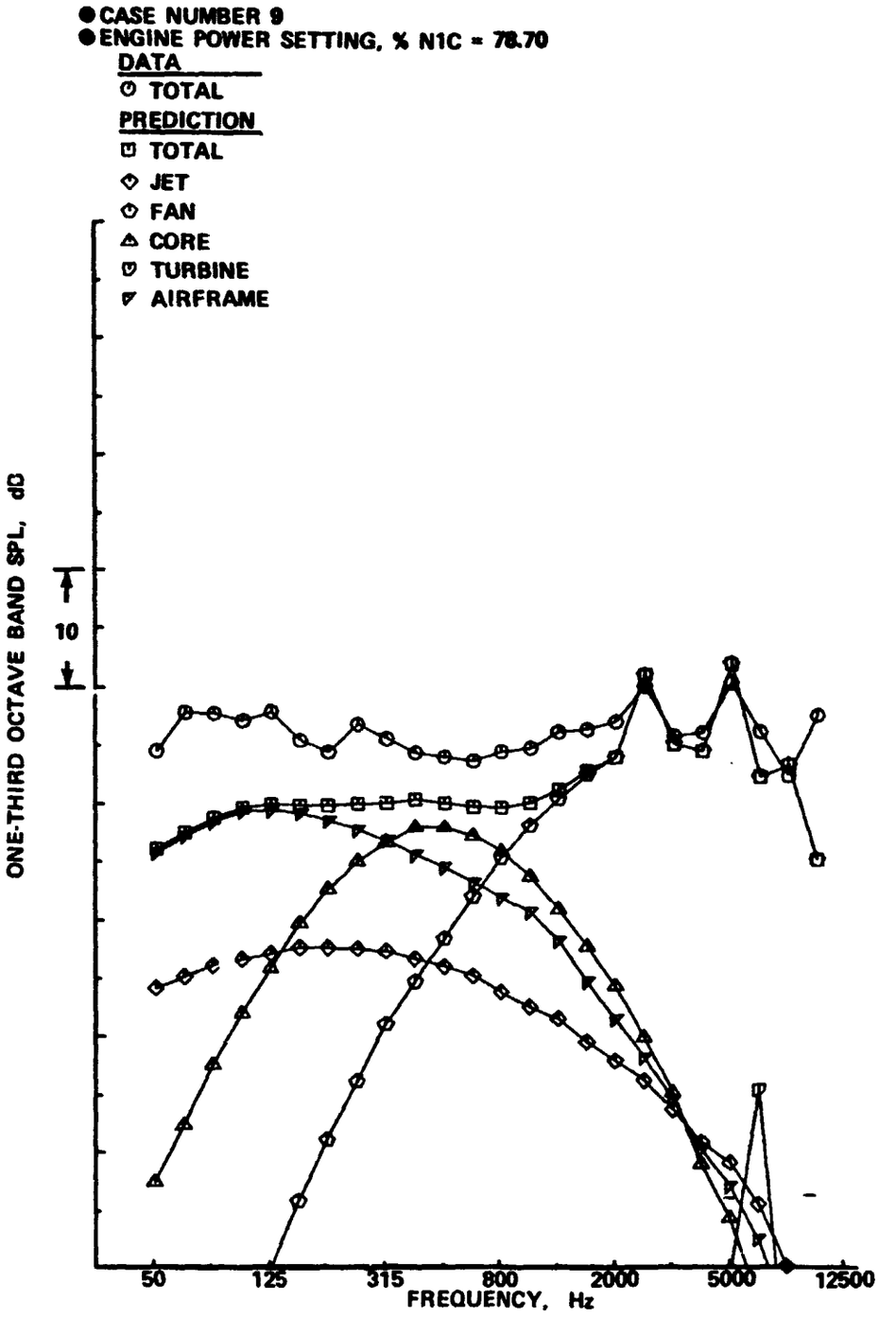

(a) DIRECTIVITY ANGLE = 30°

Figure A7. – Spectral Comparisons of Data and Prediction, Engine Power Setting % N_{1C} = 78.7

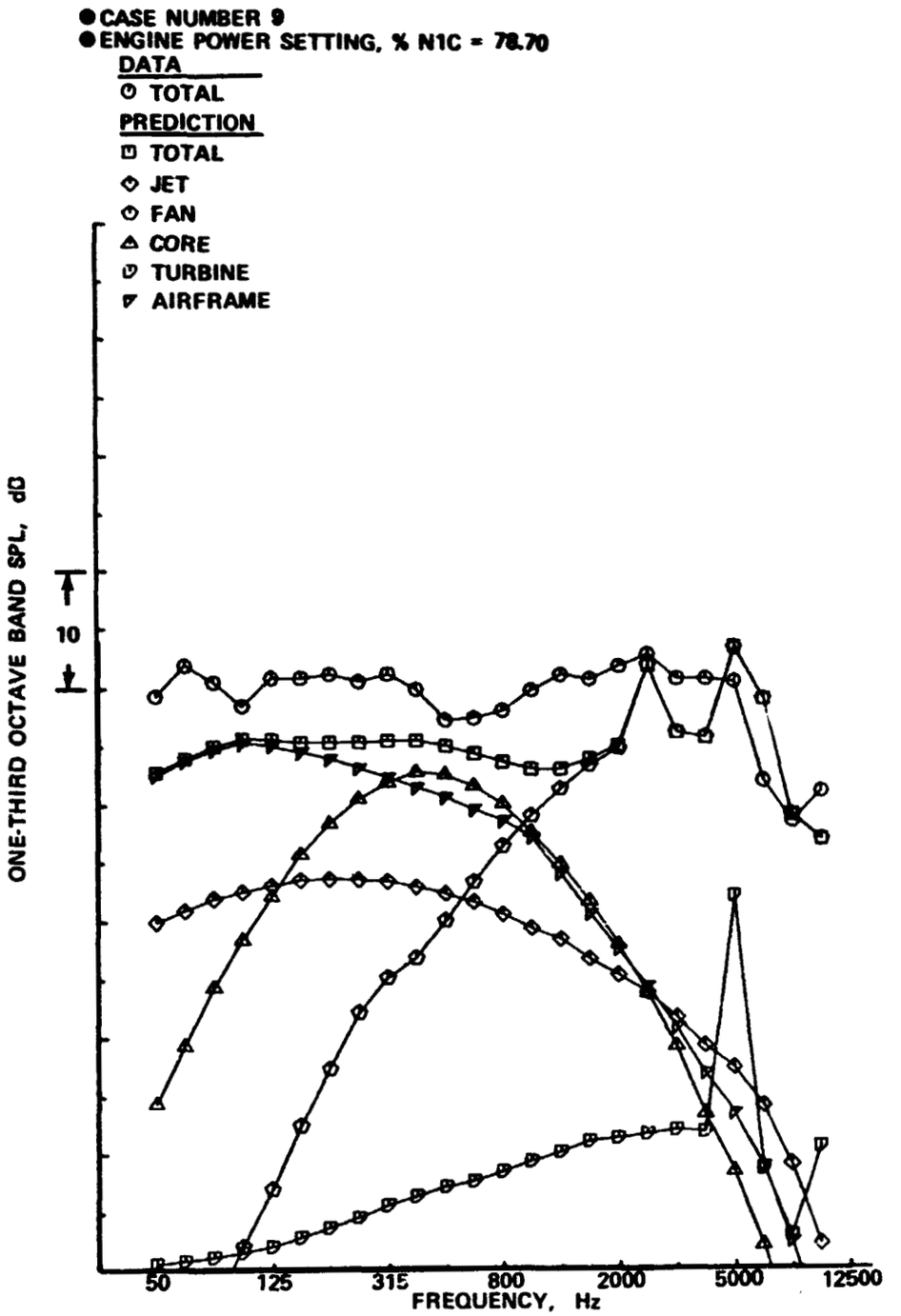

(b) DIRECTIVITY ANGLE = 60°

Figure A7. – (Continued)

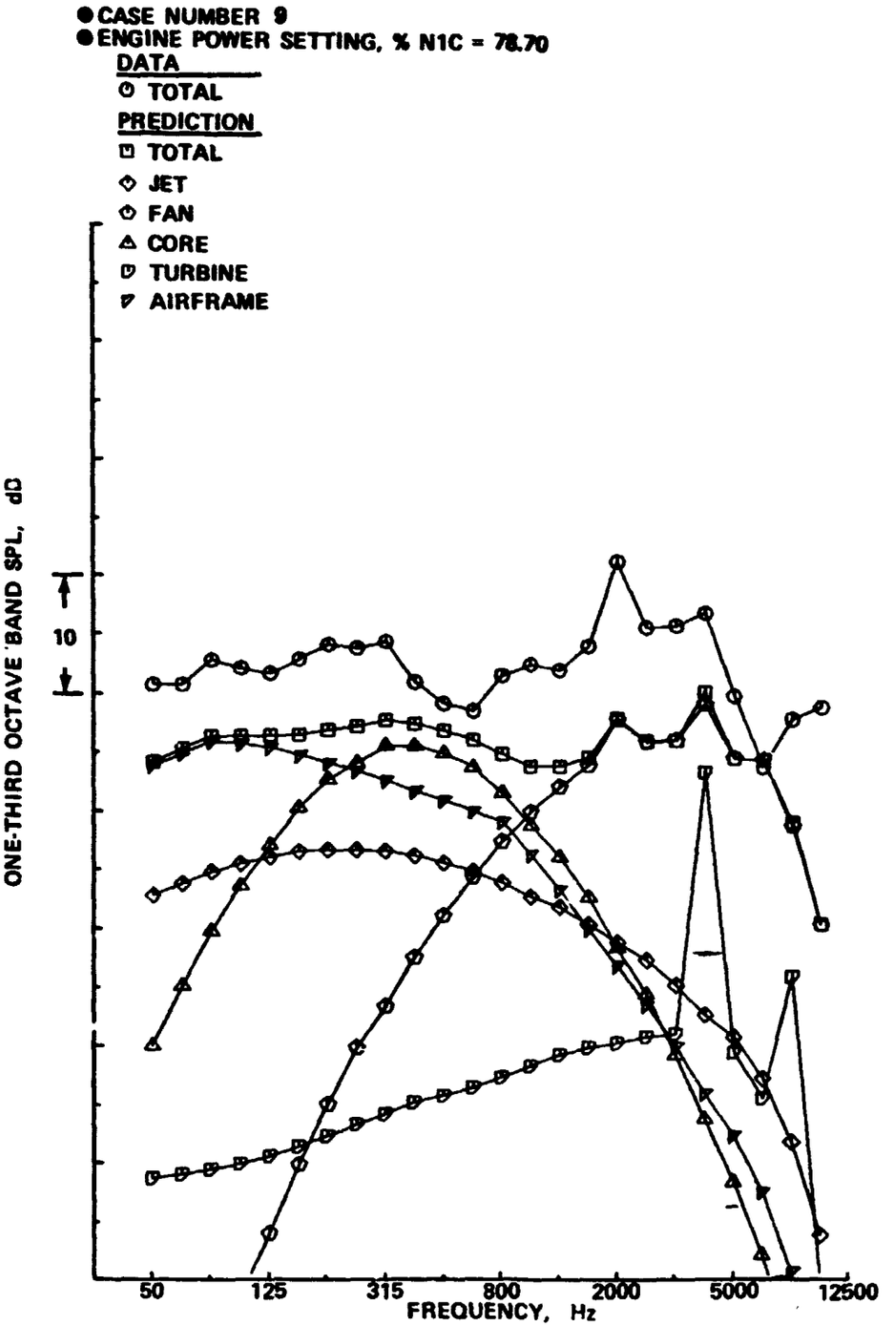

(c) DIRECTIVITY ANGLE = 90°

Figure A7. — (Continued)

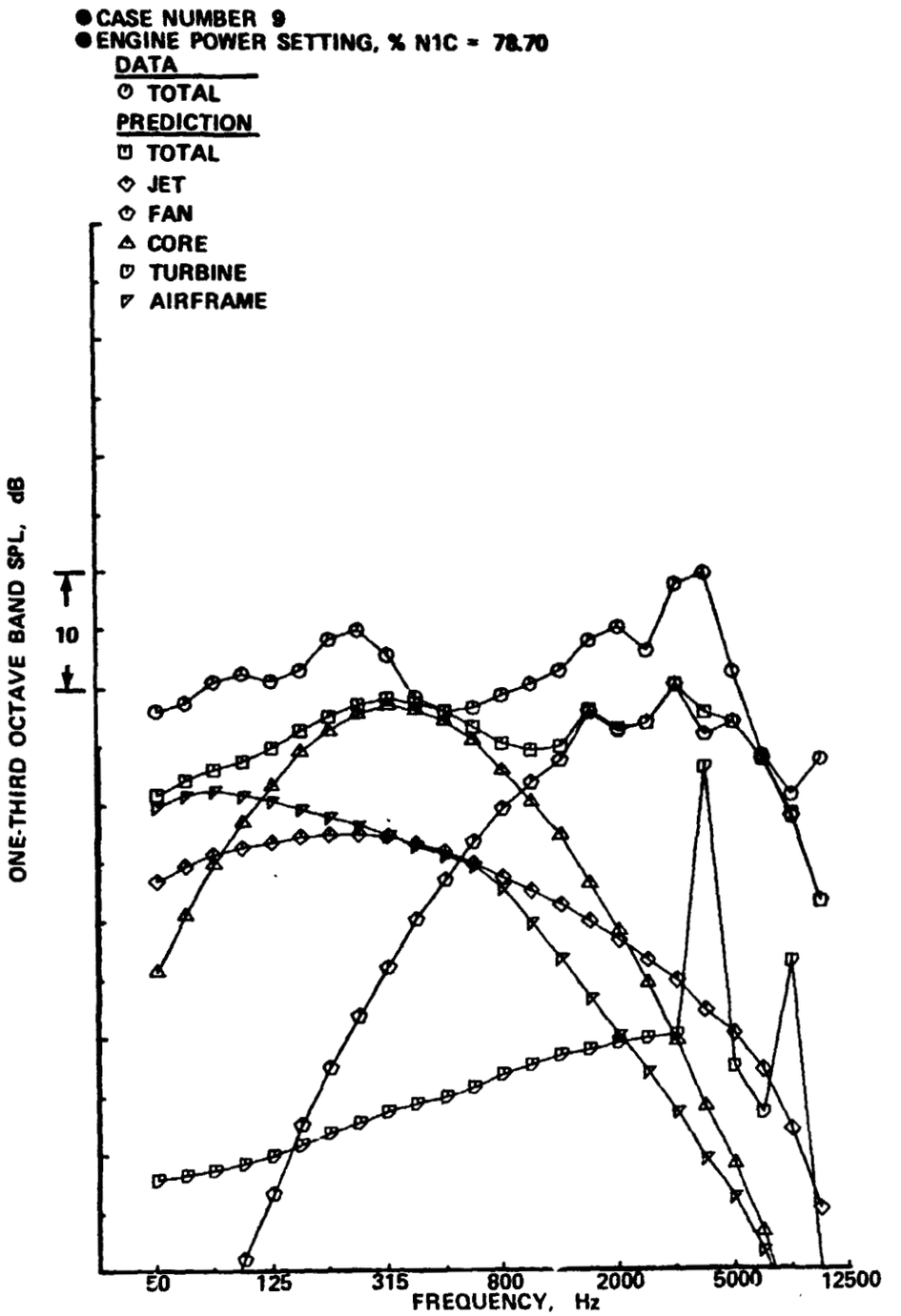

(d) DIRECTIVITY ANGLE = 120°

Figure A7. – (Continued)

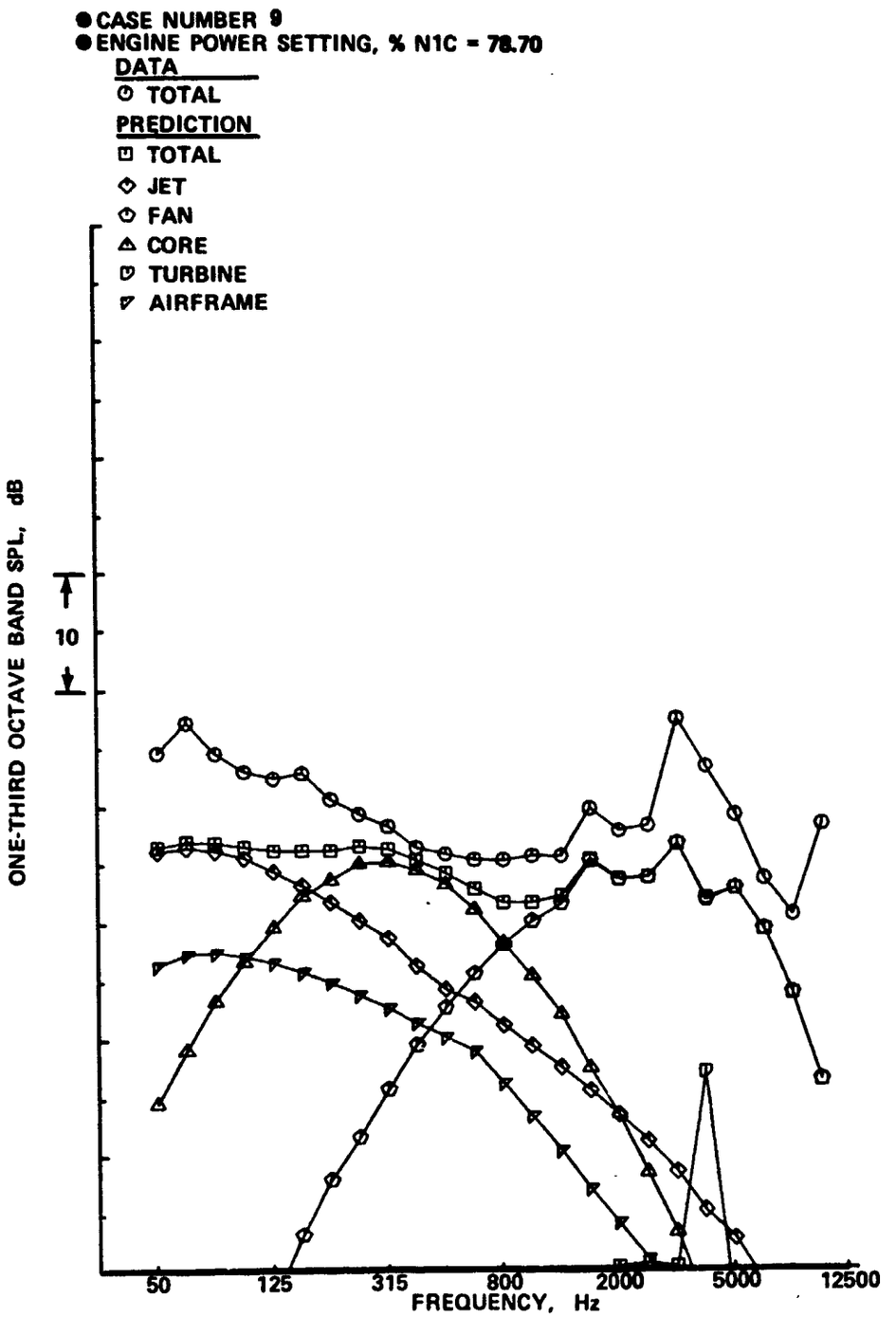

(e) DIRECTIVITY ANGLE = 150°

Figure A7. – (Concluded)

1. Report No.	2. Government Accession No.	3. Recipient's Catalog No.
NASA CR-159333		

4. Title and Subtitle	5. Report Date
AIRCRAFT NOISE PREDICTION PROGRAM VALIDATION	October 1980
	6. Performing Organization Code

7. Author(s)	8. Performing Organization Report No
Belur N. Shivashankara	D6-48727
	10. Work Unit No

9. Performing Organization Name and Address	11. Contract or Grant No
Boeing Commercial Airplane Company P.O. Box 3707 Seattle, Washington 98124	NAS1-15526
	13. Type of Report and Period Covered
12. Sponsoring Agency Name and Address	Contract report
Langley Research Center National Aeronautics and Space Administration Washington, D.C. 20546	14. Sponsoring Agency Code

15. Supplementary Notes

NASA Contract Monitor: W. E. Zorumski

16. Abstract

NASA has developed a modular program called Aircraft Noise Prediction Program (ANOPP) for predicting aircraft flyover and sideline noise. To evaluate its accuracy, the ANOPP predictions were compared with the flyover noise measurements of a Boeing 747 airplane fitted with four Pratt & Whitney JT9D engines with hardwall nacelles. In general, the predictions did not agree well with the data. At high powers, airplane perceived noise levels (PNLT s) were overpredicted in the forward arc and underpredicted in the aft arc. At low powers the PNLT s were underpredicted at all angles greater than 80°. Preliminary estimates of the various components indicate that significant modifications to the jet, fan, core, and turbine noise source modules may be required to improve the prediction-to-data match. Since the airplane was flown with flaps 20° and landing gear up, the airframe noise was not dominant and, therefore, evaluation of the accuracy of the airframe noise prediction was not possible.

17. Key Words (Suggested by Author(s))		18. Distribution Statement
Aircraft noise	Fan noise	Unclassified–unlimited
Jet noise	Engine noise	
Core noise	Airframe noise	
Turbine noise	Noise prediction	

19 Security Classif. (of this report)	20 Security Classif (of this page)	21. No. of Pages	22 Price*
Unclassified	Unclassified	162	